



## **University of Bradford eThesis**

This thesis is hosted in [Bradford Scholars](#) – The University of Bradford Open Access repository. Visit the repository for full metadata or to contact the repository team



© University of Bradford. This work is licenced for reuse under a [Creative Commons Licence](#).

DESIGN & SYNTHESIS OF NEW METALLO-ORGANIC  
COMPLEXES & THEIR EVALUATION AS ANTI-CANCER  
AGENTS

Synthesis, Characterisation and Biological Evaluation of Novel, Late First Row  
Transition Metal Schiff Base Complexes, as Anti-Cancer Metallopharmaceuticals

Jon LIDSTER

submitted for the degree  
of Doctor of Philosophy

Department of Chemical and Forensic Sciences

University of Bradford

2011

# DESIGN & SYNTHESIS OF NEW METALLO-ORGANIC COMPLEXES & THEIR EVALUATION AS ANTI-CANCER AGENTS

Synthesis, Characterisation and Biological Evaluation of Novel, Late First Row Transition Metal Schiff Base Complexes, as Anti-Cancer Metallopharmaceuticals.

Jon LIDSTER

## Abstract

This work is concerned with the design and synthesis of the cheap, late first row transition metal complexes of Schiff base ligand systems. The prepared complexes readily afford systematic variation in order to probe potency and understand the role of metal, chelating ligands and anionic ligands when carrying out their cytotoxic effect. This study has led to a better understanding of the action of these classes of complex and will be used to direct the design of new anti-cancer metallopharmaceuticals going forward.

This thesis details the synthesis of a library of Schiff base macroacyclic ligands and their novel late first row transition metal complexes with varying anionic counterparts. The creation of a library with several degrees of variability provides a wide array of parameters to afford subtle variation in structure and chemistry e.g. denticity, coordination mode, chelate hole size, metal centred redox potentials, hydrolysis rates, coordinative saturation, lipophilicity, solubility and more.

Complexation of the ligands was carried out by the free ligand and a novel macroacyclic metal template approach using the cheap late first row transition metal salts of Cobalt (II), Nickel (II), Copper (II) and Zinc (II) plus one Ru (III) complex. Structural studies of the 80 generated complexes was carried out by vibrational spectroscopy, elemental analysis, mass spectrometry, magnetic susceptibility and NMR.

Single crystal X-ray structures have been determined with 20 reported in this thesis. All ligands act as tridentate ligands in all except one case to form monomeric distorted trigonal-bipyramidal, square-pyramidal or octahedral structures. In the case of zinc nitrate, the ligand  $L^2PhMe$  acts as a tetradentate ligand to give a distorted octahedral structure. Paramagnetic NMR and solution magnetic susceptibility of paramagnetic complexes was achieved by the Evans NMR method and analysis of the solution NMR showed that  $L^2R$  and  $L^3R$  ligands display 2-fold symmetry and are likely either tetradentate in solution or a fast exchange between imine N-donor sites is occurring even down to  $-65^\circ C$ .

The majority of the resulting complexes of  $L^1R$  were screened against a panel of three cancer cell lines. Several categories of complex were able to afford structure activity relationships. It was discovered that the ligand is indeed essential for activity of the metal salts against the panel of cell lines and it was largely discovered that the variation in 'tail group' and anionic coordinating ligands played little role in providing a dramatic variation in activity of the metal salt. In general all  $L^1R$  complexes displayed moderate cytotoxicity showing a trend in activity with respect to the metal in the order  $Ru^{III} \approx Co^{II} > Cu^{II} \approx Zn^{II} > Ni^{II}$ , over a 6 day exposure to the three cell panel  $Ru^{III}$  was shown to be the most potent metal of the  $L^1R$  series providing  $IC_{50}$  values of 4.6 (0.7) and 7.5 (1.2)  $\mu M$  against the DLD-1 and H460 cell lines respectively, which is *Ca.* 4.6 and 15

times less potent than cisplatin to the same cell panel respectively. Ru<sup>III</sup> was also discovered to be the only metal to provide an IC<sub>50</sub> value from a 1 hour exposure to the DLD-1 cell panel. The value of 20.4 (3.5) μM is a moderate figure but again *Ca.* 10 fold less potent than cisplatin for the same test.

The L<sup>2</sup>R and L<sup>3</sup>R complexes could not be screened by the same comprehension due to their low solubilities. However the lone screen that was possible from the very sparingly soluble complex [CuCl<sub>2</sub>(L<sup>3</sup>Bu<sup>i</sup>)] gave the most exciting result and most potent complex of this thesis. After a 6 day exposure, [CuCl<sub>2</sub>(L<sup>3</sup>Bu<sup>i</sup>)] gave IC<sub>50</sub> values of 4.3 (0.1) and 2.9 (0.1) μM against the DLD-1 and H460 cell lines respectively. These values are merely 4 and 6 fold more than Cisplatin to the same cell lines respectively and demonstrates the potential of this class of complex as cytostatic agents.

Further studies utilising a semi-quantitative DNA damaging assay, demonstrated that all first row complexes can damage DNA when in the presence of hydrogen peroxide, with the exception of Zn<sup>II</sup> complexes. Co<sup>II</sup> appeared to afford the greatest DNA damage with the most intense bands for double strand breaks and the Cu<sup>II</sup> complex of the ligand L<sup>3</sup>Bu<sup>i</sup> also demonstrated a greater DNA damage as opposed to its L<sup>1</sup>Bu<sup>i</sup> analogue.

### **Key Words**

Schiff base, macrocycle, template synthesis, X-ray crystallography, cancer chemotherapy, metallopharmaceuticals.

## Contents

1. Introduction.....	1
1.1. Natural History of Cancer .....	1
1.1.1. Carcinogenesis .....	2
1.1.1.1. Tumour Viruses.....	5
1.1.1.2. Chemical Carcinogens .....	5
1.1.1.3. Radiation .....	8
1.1.1.4. Reactive Oxygen Species.....	9
1.1.2. Risk Factors Associated with an Increased Incidence of Cancer.....	9
1.1.2.1. Smoking .....	10
1.1.2.2. Diet.....	10
1.1.2.3. Sex Hormones .....	11
1.1.2.4. Familial Cancers.....	11
1.2. The Global Burden of Cancer.....	11
1.2.1. Cancer Management.....	12
1.2.1.1. Surgery .....	12
1.2.1.2. Radiotherapy .....	13
1.2.1.3. Chemotherapy .....	13
1.3. Development of new chemotherapeutic agents.....	16
1.4. Aim of Project .....	17
1.5. Review of Anticancer Metallodrugs.....	19
1.6. The Likely Fate of Metallodrugs on Entering the Body .....	29
1.6.1. Transport .....	29
1.6.2. Tumour cell Specificity.....	30
1.6.3. Metal complex activation.....	31
1.6.4. Cellular Targets.....	33
1.6.5. DNA Structure and Metal Binding Sites.....	34
1.6.6. Binding Modes of Cisplatin with DNA .....	37
1.7. Effects of Metallodrugs on DNA Functions.....	42
1.7.1. DNA Replication.....	42
1.7.2. DNA Transcription.....	43
1.7.3. Telomeres and Telomerase .....	43
1.7.4. DNA Damage and Apoptosis.....	44

1.8.	Likely Mechanism of Action of Cisplatin After Entering the Cell .....	45
1.9.	Design of Schiff Base Metallodrugs.....	47
2.	Experimental.....	54
2.1.	Chemical Methods.....	54
2.1.1.	Reagents .....	54
2.1.2.	Starting Materials .....	54
2.1.3.	Preparation of Raney Nickel .....	56
2.1.4.	Solvents .....	56
2.1.5.	Instrumental Methods.....	56
2.1.5.1.	Infrared Spectroscopy (IR).....	56
2.1.5.2.	Nuclear Magnetic Resonance Spectroscopy (NMR) .....	57
2.1.5.3.	Magnetic Susceptibility.....	57
2.1.5.4.	Mass Spectrometry (MS) .....	59
2.1.5.5.	Single Crystal X-Ray Diffraction.....	60
2.1.5.6.	CHN Microanalysis.....	60
2.1.5.7.	Melting Points .....	60
2.1.5.8.	Numbering Scheme for Precursor Compounds and Ligand Head and Tail Groups. ....	61
2.1.6.	Preparation of Precursor Compounds .....	62
2.1.6.1.	Preparation of pyridine-2,6-dicarbaldehyde, P <sup>1</sup> .....	62
2.1.6.2.	Preparation of 2-bromo-6-methyl pyridine .....	63
2.1.6.3.	Preparation of 6,6'-dimethyl-2,2'-bipyridine.....	65
2.1.6.4.	Attempted Preparation of 2,2'-bipyridine-6,6'-dicarbaldehyde, P <sup>2</sup> with Selenium Dioxide.....	67
2.1.6.5.	Preparation of 2,2'-bipyridine-6,6'-dicarbaldehyde, P <sup>2</sup> with DMSO and Iodine.....	68
2.1.6.6.	Preparation of 1,10-phenanthroline-2,9-dicarbaldehyde, P <sup>3</sup> .....	70
2.1.6.7.	Preparation of 1,10-phenanthroline-2,9-dicarbaldehyde, P <sup>3</sup> with DMSO and Iodine. ....	71
2.1.7.	Preparation of Ligands .....	73
2.1.7.1.	General Procedure for the Preparation of Schiff base Ligands L <sup>1</sup> R and L <sup>3</sup> R .....	73
2.1.8.	Preparation of Metal Complexes of L <sup>1</sup> R, L <sup>2</sup> R and L <sup>3</sup> R .....	78
2.1.8.1.	Preparation of [MX <sub>2</sub> L] complexes.....	78

2.1.8.2.	Preparation of $[ML_2]X_2$ Complexes of $L^1R$ .....	79
2.1.8.3.	Formation of $[Co(H_2O)_2(L^1Cy)][BF_4]_2$ .....	80
2.2.	Biological Methods .....	91
2.2.1.	<i>In vitro</i> Cell Culture and Chemosensitivity .....	91
2.2.1.1.	Routine Subculture of Cells .....	91
2.2.1.2.	Counting Cells in Suspension .....	92
2.2.1.3.	MTT Colorimetric Assay .....	93
2.2.1.3.1.	Validation of the MTT Assay.....	95
2.2.1.3.2.	MTT assay .....	96
2.2.2.	DNA Damaging Assay.....	97
2.2.2.1.	Harvesting and Lysis of Bacteria .....	98
2.2.2.1.1.	Harvesting .....	98
2.2.2.1.2.	Lysis by Alkali .....	98
2.2.2.2.	Treatments of Plasmid DNA for Assay .....	100
3.	Synthesis of Precursors and Ligands .....	102
3.1.	Oxidation to Dialdehydes .....	102
3.1.1.	Pyridine-2,6-dicarbaldehyde, $P^1$ .....	107
3.1.2.	2,2'-bipyridine-6,6'-dicarbaldehyde, $P^2$ .....	109
3.1.2.1.	Step 1 – 2-bromo-6-methylpyridine, $P^{2a}$ .....	109
3.1.2.2.	Step 2 – 6,6'-dimethyl-2,2'-bipyridine, $P^{2b}$ .....	110
3.1.2.3.	Step 3 – 2,2'-bipyridine-6,6'-dicarbaldehyde, $P^2$ .....	111
3.1.3.	1,10-phenanthroline-2,9- dicarbaldehyde, $P^3$ .....	112
3.2.	Schiff Base Ligands.....	113
3.2.1.	Characterisation of Ligands .....	121
3.2.1.1.	IR Spectroscopy .....	121
3.2.1.2.	$^1H$ NMR Spectroscopy.....	122
4.	Synthesis of Metal Complexes .....	125
4.1.	The Template Reaction .....	126
4.2.	Characterisation of Metal Complexes .....	130
4.3.	Complexes of the Ligand $L^1PhNO_2$ .....	131
4.4.	Vibrational Spectroscopy of Complexes .....	134
4.4.1.	Binding Modes of Parent Ligands.....	138
4.4.2.	Binding Modes of Anionic Ligands.....	139

4.4.2.1.	Nitrato complexes .....	139
4.4.2.2.	Acetato complexes .....	143
4.4.2.3.	Isothiocyanato Complexes .....	146
5.	Solution Studies of Metal Complexes .....	151
5.1.	Magnetic Susceptibility in Solution by NMR .....	151
5.2.	NMR Studies .....	155
5.2.1.	<sup>1</sup> H NMR Assignment of Complex [CoCl <sub>2</sub> (L <sup>1</sup> Ph)] .....	157
5.2.2.	<sup>1</sup> H NMR Assignment of Complex [CoCl <sub>2</sub> (L <sup>1</sup> Bu <sup>i</sup> )] .....	158
5.2.3.	<sup>1</sup> H NMR Assignment of Complex [CoCl <sub>2</sub> (L <sup>1</sup> Cy)] .....	158
5.2.4.	Co <sup>II</sup> Solution Chemistry .....	159
5.2.5.	NMR Spectra of Zinc Complexes of Bipyridine L <sup>2</sup> and Phenanthroline L <sup>3</sup> .....	162
6.	X-Ray Structural Studies of Metal Complexes .....	164
6.1.	Data Collection .....	164
6.2.	Structure Solution and Refinement for [Cu(NO <sub>3</sub> ) <sub>2</sub> (L <sup>1</sup> Pr <sup>n</sup> )] .....	167
6.3.	Structural Descriptions and Comparisons .....	173
6.3.1.	Cu <sup>II</sup> Complexes of L <sup>1</sup> R .....	173
6.3.2.	Ni <sup>II</sup> Complexes of L <sup>1</sup> R .....	191
6.3.3.	Zn <sup>II</sup> Complexes of L <sup>1</sup> R .....	198
6.3.4.	Co <sup>II</sup> Complexes of L <sup>1</sup> R .....	206
6.3.5.	Complexes of L <sup>2</sup> R and L <sup>3</sup> R .....	211
7.	Biological Evaluations .....	217
7.1.	Determination of <i>in vitro</i> Toxicity of Schiff Base Complexes Against a Panel of Human Tumour Cell Lines .....	217
7.1.1.	Variation of Ligand ‘Tail’ Group .....	219
7.1.1.1.	Cobalt <sup>II</sup> chloride Complexes of Ligand L <sup>1</sup> R .....	219
7.1.1.2.	Nickel <sup>II</sup> chloride Complexes of L <sup>1</sup> R .....	222
7.1.1.3.	Copper <sup>II</sup> chloride Complexes of L <sup>1</sup> R .....	224
7.1.1.4.	Zinc <sup>II</sup> chloride Complexes of L <sup>1</sup> R .....	227
7.1.1.5.	General Observations .....	229
7.1.2.	Variation of Metal .....	231
7.1.3.	Variation of Anion .....	236
7.1.4.	Variation of Ligand ‘Head’ Group .....	243
7.2.	DNA Damaging Assay .....	247



8. Conclusions.....	250
9. Further Work.....	258
10. References.....	259
11. Appendix.....	273
11.1. Madonna Model for the Simulation of Reaction Profiles.....	273
11.1.1. Stoichiometric Reaction .....	273
11.1.2. Stoichiometric Reaction with Simulated Molecular Sieves (Removal of Water).....	274
11.1.3. 0.1eq Excess of Amine and Simulated Water Removal .....	275
11.2. Tables of Bond lengths and Angles for Cu <sup>II</sup> Complexes of Ligand L <sup>1</sup> R....	277
11.3. Tables of Bond lengths and Angles for Ni <sup>II</sup> Complexes of Ligand L <sup>1</sup> R....	279
11.4. Tables of Bond lengths and Angles for Zn <sup>II</sup> Complexes of Ligand L <sup>1</sup> R. ...	282
11.5. Tables of Bond lengths and Angles for Co <sup>II</sup> Complexes of Ligand L <sup>1</sup> R....	284
11.6. Tables of Bond lengths and Angles for Complexes of Ligand L <sup>2</sup> R and L <sup>3</sup> R. ..	289

In loving memory of Grandad and Aunty Gillian.

## AKNOWLEDGEMENTS

I would like to thank the following for their assistance and encouragement.

Dr. Ian Scowen and Prof. Howell Edwards for their useful discussions and passing on their indepth knowledge of X-ray crystallography, vibrational spectroscopy and coordination chemistry and their advice during the preparation of this thesis.

Dr. Roger Phillips for his enthusiastic interest in my project, his useful discussions and giving me the opportunity to screen my library against an *in vitro* cancer cell panel. I would also like to give a big thank you to his PhD student Qasem Abdallah who passed on his practical skills in aseptic technique and cell culture and gave me some helpful ideas and tips.

Andrew Healey for obtaining mass spectra, Arthur Kershaw for making weird and wonderful glass items and Dr. Derek Maitland for his help and advice with NMR.

Dr. Scott Seville who was my PhD colleague at the time. His encouragement and humour made my life and time during my PhD much more enjoyable.

I would finally like to thank Laura Lidster for her support and encouragement throughout the whole of my academic life and Anne-Laure Hepp for providing me the motivation, and encouragement to finish off.

Thanks

## List of Abbreviations

<b>IR</b>	<b>Infra-red Spectroscopy</b>
<b>NMR</b>	<b>Nuclear Magnetic Resonance Spectroscopy</b>
<b>FT-IR</b>	<b>Fourier Transform Infra-red Spectroscopy</b>
<b>MS</b>	<b>Mass Spectroscopy</b>
<b>EI-MS</b>	<b>Electron Impact Mass Spectroscopy</b>
<b>ESI-MS</b>	<b>Electrospray Ionisation Mass Spectroscopy</b>
<b>ESI+</b>	<b>Positive Ion Electrospray Ionisation</b>
<b>LC/MS-MS</b>	<b>Liquid Chromatography Tandem Mass Spectroscopy</b>
<b>FAB-MS</b>	<b>Fast Atom Bombardment Mass Spectroscopy</b>
<b>BM or <math>\mu_B</math></b>	<b>Bohr Magnetron</b>
<b><math>\mu_{eff}</math></b>	<b>Observed Magnetic Susceptibility</b>
<b>CHN</b>	<b>Carbon, Hydrogen and Nitrogen Analysis</b>
<b>TLC</b>	<b>Thin Layer Chromatography</b>
<b>UV</b>	<b>Ultra Violet</b>
<b>R<sub>f</sub></b>	<b>Relative Retention factor</b>
<b>m.p.</b>	<b>Melting Point</b>
<b>m/z</b>	<b>Mass to Charge Ratio</b>
<b>h</b>	<b>Hours</b>
<b>min</b>	<b>Minutes</b>
<b>sec</b>	<b>seconds</b>
<b>TMS</b>	<b>tetramethylsilane</b>
<b>IMS</b>	<b>Industrial Methylated Spirits</b>
<b>DCM</b>	<b>Dichloromethane</b>

<b>AcOH</b>	<b>Acetic Acid</b>
<b>AcO</b>	<b>Acetate</b>
<b>DMSO</b>	<b>Dimethyl sulphoxide</b>
<b>DMF</b>	<b>N,N'-dimethylformamide</b>
<b>TFA</b>	<b>trifluoroacetic acid</b>
<b><i>t</i>-BuI</b>	<b>tertiarybutyl iodide</b>
<b>Pr<sup>n</sup>Amine</b>	<b><i>n</i>-propylamine</b>
<b>MeOH</b>	<b>Methanol</b>
<b>EtOH</b>	<b>Ethanol</b>
<b>Et<sub>2</sub>O</b>	<b>Diethyl ether</b>
<b>CH<sub>3</sub>CN</b>	<b>Acetonitrile</b>
<b>SDS</b>	<b>Sodium Dodecyl Sulphate</b>
<b>DNA</b>	<b>Deoxyribonucleic acid</b>
<b>RNA</b>	<b>Ribonucleic acid</b>
<b>BSA</b>	<b>Bovine Serum Albumin</b>
<b>pH</b>	<b>-log [H<sup>+</sup>]</b>
<b>ECACC</b>	<b>European Collection of Cell Cultures</b>
<b>RPMI</b>	<b>Roswell Park Memorial Institute</b>
<b>MTT</b>	<b>3-(4,5-dimethylthiazol-2-yl)-2,5-diphenyltetrazolium bromide</b>
<b>EDTA</b>	<b>Ethylenediamine tetraacetic acid</b>
<b>ELISA</b>	<b>Enzyme Linked Immunosorbent Assay</b>
<b>TE</b>	<b>Tris EDTA buffer</b>
<b>TBE</b>	<b>Tris Borate EDTA buffer</b>

## **1. Introduction**

### **1.1. Natural History of Cancer**

In the body, the birth and death of normal cells are carefully regulated: in a young animal, the rate of cell multiplication exceeds that of cell death; in adults, the rate of cell multiplication and death is balanced at a steady state. Occasionally, these controls breakdown and cells continue to grow when no longer needed. Descendants of these cells inherit the characteristics of uncontrolled growth, which results in a mass of cells that continues to grow indefinitely, forming a tumour.<sup>1</sup>

Benign tumours are localised and closely resemble the normal 'parent' cells from which they arose; such tumours are normally encased in a fibrous capsule and pose little threat to life.<sup>2</sup> In general, benign tumours can be surgically removed and will not spread to other tissues (by virtue of their encapsulation). Benign tumours are only problematic if their size hinders the function of normal tissue or if they secrete excess amounts of chemical (e.g. hormones), which the body becomes unable to cope with.<sup>3</sup>

Unlike benign tumours, malignant tumours are not localised or encapsulated. These tumours have the ability to spread (metastasise);<sup>4</sup> they can invade neighbouring tissue or enter the circulatory system and appear as new tumours at sites remote to the tissue of origin.

The term 'cancer' is generally used to describe a malignant growth and will be used in this thesis. It is rarely possible to determine exactly how a malignancy began, although

some cancer risk factors have been identified. For further information on cancer and its molecular features, refer to the excellent review by Hanahan *et al.*<sup>1</sup>

### **1.1.1. Carcinogenesis**

A normal cell can be transformed into a malignant cell by the expression of one or more oncogenes. Oncogenes are genes that encode proteins (oncoproteins) that are able to induce cancer in animals, or transform cells in culture, and are responsible for the breakdown of normal cell regulation. Most oncogenes are derived from normal genes; these precursors are known as proto-oncogenes and are often important for normal cell function. Oncogenes may give rise to mutant forms of the protein coded for by the proto-oncogene, leading to malignant transformation, or may code for the same protein as the proto-oncogene (here, malignancy occurs by virtue of an overexpression of the protein or expression where the protein is normally absent).<sup>1</sup>

Five classes of protein have been identified which are involved in the regulation of cell growth. These are growth factors, growth factor receptors, intracellular signal transducers, nuclear transcription factors and cell-cycle control proteins. Genes for each class of protein are known to give rise to one or more oncogenes, further demonstrating that regulation of cell growth is inherently linked to the initiation of malignancy. Oncogenes often act together to cause malignancy, no one oncogene has been shown to be capable of inducing malignant transformation on its own. It may take some time for a cell to acquire enough alterations to induce malignancy; this could account for the long periods of time that may pass between exposure to carcinogen and development of cancer.<sup>1</sup>

Oncogenes are transformed by, or carried into cells, by one of three main types of transforming agents: viruses, chemical carcinogens and radiation. Each transforming agent is briefly discussed in the following sections.

The other set of growth regulatory proteins are the tumour suppressor genes (anti-oncogenes), which can be deactivated. If DNA is damaged in a normal cell, there are cellular 'policemen' that can detect damage and block DNA replication. This gives the cell time to repair the damaged DNA before the next cell division. If repair does not prove possible, the cell commits suicide (apoptosis).<sup>5</sup> Tumour suppressor genes are genes which code for proteins that are involved in these processes of checking, repair and suicide. *TP53* is an important example of such a gene and codes for the protein of the same name (p53). If the *TP53* gene is damaged, the repair mechanisms become less efficient, defects are carried forward from one cell generation to another and as the damage increases, the chances of the cell becoming cancerous increase.

Genetic defects can lead to the following cellular defects, all of which are associated with cancer:

- Abnormal signalling pathways
- Insensitivity to growth-inhibitory signals
- Abnormalities in cell cycle regulation
- Evasion of programmed cell death (apoptosis)
- Limitless cell division (immortality)
- Ability to develop new blood vessels (angiogenesis)
- Tissue invasion and metastasis



It is thought that most, if not all, of these conditions have to be met before a defective cell can spawn life-threatening malignant growth. Thus, a single defect can be kept under control by a series of safeguards. This can explain why cancers may take many years to develop after exposure to a damaging mutagen such as asbestos or coal dust. That first exposure may have caused mutations in some cells, but cellular chemistry has the control systems in place to cope and to keep the cells in check. A lifetime's exposure to other damaging mutagens such as tobacco smoke, however, results in further genetic damage which overwhelm the safeguards one by one until the abnormal cell finally breaks free of its shackles and becomes cancerous.

The various hurdles and safeguards that a potential cancer cell has to overcome explain why cancers are relatively rare early on in life and are more common in later years. This also helps to explain why cancer is so difficult to treat once it does appear. Since so many cellular safeguards have already been overcome, it is unlikely that tackling one specific cellular defect is going to be totally effective. As a result, traditional anticancer drugs have tended to be highly toxic agents and act against a variety of cellular targets by different mechanisms.<sup>6</sup> Unfortunately, since they are potent cellular poisons, they also affect normal cells and produce serious side effects. Such agents are said to be cytotoxic, and dose levels have to be chosen which are high enough to affect the tumour but are bearable to the patient.<sup>7</sup>

In recent years, anticancer drugs have been developed which target specific abnormalities in a cancer cell, allowing them to be more selective and have less serious side effects. However, bearing in mind the number of defects in a cancer cell, it is unlikely that a single agent of this kind will be totally effective and it is more likely that

these new agents will be most effective when they are used in combination with other drugs having different mechanisms of action, or with surgery and radiotherapy.<sup>8</sup>

#### **1.1.1.1. Tumour Viruses**

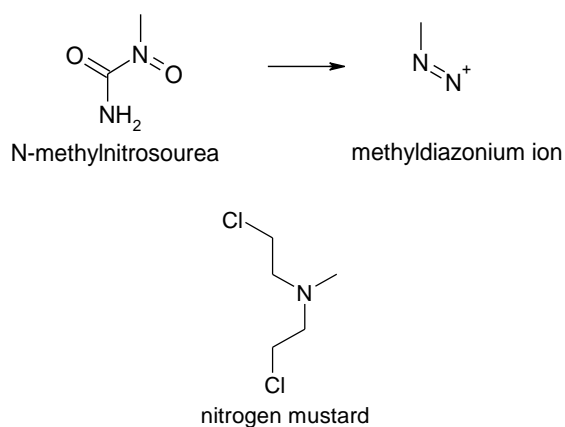
There are two types of tumour virus that can act as transforming agents: RNA-containing viruses (retroviruses) and DNA-containing viruses. The tumour viruses achieve malignancy by integrating their own genetic information into the DNA of the host cell. This can lead to chronic expression/over-expression of oncoproteins, which cause the cell to go out of control.

#### **1.1.1.2. Chemical Carcinogens**

Most of the known chemical carcinogens do not share a common chemical structure. However, there are two (very broad) categories of chemical carcinogens, direct-acting and indirect-acting.<sup>9</sup>

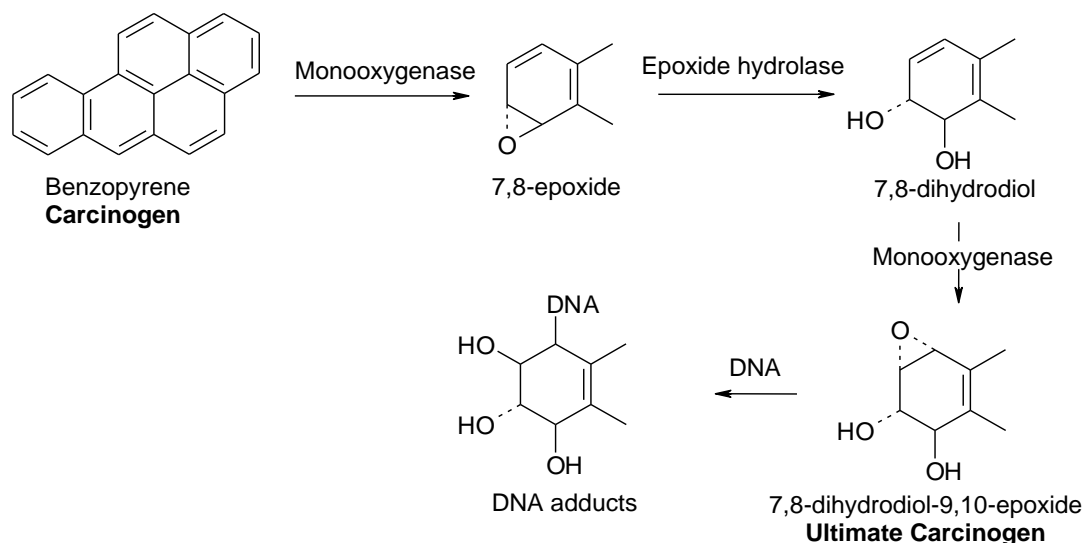
Direct-acting carcinogens are highly reactive electrophiles, of which there are only a few (e.g. some nitrosamines and certain alkylating agents). N-methylnitrosourea is a direct-acting carcinogen that can form the methyldiazonium ion (Figure 1), which can then form adducts with DNA causing malignancy. Other nitrosamines require metabolic activation to form the methyldiazonium ion and, therefore, cannot be classified as direct-acting. Nitrogen mustard is an example of an alkylating agent that can function as a direct-acting carcinogen. As nitrogen mustard is bifunctional (Figure 1), it can form inter- and intrastrand crosslinks with adjacent bases in DNA and is direct-acting because its chlorine groups are sufficiently electrophilic to interact with nucleophiles, without metabolic activation.<sup>10</sup>

**Figure 1.** Examples of direct-acting carcinogens.<sup>10</sup>



Indirect-acting carcinogens (e.g. polycyclic aromatic hydrocarbons, aromatic amines) require metabolic activation and the introduction of electrophilic centres, in order to become ultimate carcinogens and therefore carcinogenic. Enzymes in the body, particularly those in the liver, carry out metabolic activation. These activation processes serve to detoxify chemicals, adding hydrophilic groups to insoluble compounds and, thus, allowing them to be easily excreted by the body. The metabolic activation process is catalysed by the cytochrome P450 family of proteins and can lead to highly reactive electrophiles (e.g. epoxides) that are ultimate carcinogens. Figure 2 shows the activation of benzopyrene, an indirect-acting carcinogen.

**Figure 2.** Example of indirect-acting carcinogens – metabolic activation of benzopyrene.<sup>10</sup>



Thus, the ultimate carcinogens and the direct-acting carcinogens can form covalent bonds with many different negative charged centres, including DNA, RNA and proteins, by virtue of their electrophilic nature. However, it is only the DNA-adducts which are thought to be related to the development of malignancy; such adducts alter the sequence of the DNA and thus, are mutagens. This is not to say that all mutagens are carcinogens, sometimes, mutagenicity can result in immediate cell death, rather than an increased growth rate of cells.

The International Agency for Research on Cancer (IACR) has developed a classification system for describing the carcinogenic risk to humans of such agents, mixtures and exposure circumstances. Table 1 summarises the IACR classification system of chemical carcinogen.

**Table 1.** IACR classification of chemical carcinogens<sup>10, 11</sup>

Group	Risk	Chemicals (no. in group)	Exposure circumstances
1	Carcinogenic	Benzene, nitrogen mustard (28)	Tobacco smoking
2A	Probably carcinogenic	Benzo(a)pyrene, dimethylsulfoxide (63)	Petroleum industry
2B	Possibly carcinogenic	Aziridine, chloroform (235)	Dry cleaning
3	Unclassifiable	Aniline, bromoethane (483)	Leather goods manufacture
4	Probably not carcinogenic	Caprolactam (1)	

### 1.1.1.3. Radiation

Humans are exposed to radiation from many sources and several types of radiation are responsible for causing certain cancers, as summarised in Table 2.

**Table 2.** Types and sources of radiation that cause cancer in humans.<sup>10</sup>

Radiation type	Source	Related cancer
Ultraviolet	Exposure to sunlight	Skin
X-ray	Medical procedures	Leukaemia, thyroid
Atomic particle	Military weapons	All types
Radon	Mining, building materials	Lung

Ultraviolet (UV) radiation and ionising radiations (X-rays and atomic particles are particularly dangerous. UV radiation has only limited penetration and consequently, mainly affects the skin. UV radiation does not break chemical bonds in DNA; rather it excites other molecules and makes them more reactive. These excited species can then bond to DNA and once bound they can form covalent bonds between pyrimidine bases, producing dimers. These dimers interfere with DNA transcription and replication and if they are not quickly repaired, can cause carcinogenesis. Ionising radiation causes single-

and double-strand breaks in DNA, resulting in chromosome deletions and rearrangements.

#### **1.1.1.4. Reactive Oxygen Species**

Reactive free radicals are routinely generated during normal metabolic pathways. These reactive species are capable of oxidising nucleic acids and lipids, causing alterations in DNA, interfering with DNA repair mechanisms and activating signal transduction pathways. Cells come under oxidative attack numerous times a day, but mostly the damage is repaired. Occasionally, base changes are not repaired and can contribute to carcinogenesis. The main culprits here are reactive oxygen species, the major source of which is oxidative phosphorylation, although reactive nitrogen species can also cause problems.<sup>10</sup> The predominant forms of reactive oxygen are the superoxide radical and its conjugate acid the hydroperoxy radical (the most reactive and therefore most dangerous) and hydrogen peroxide (which, although is not an actual radical, is a precursor to the hydroxyl radical).<sup>12</sup> Cells contain various species capable of inactivating reactive oxygen species, such as proteins, glutathione and certain vitamins.<sup>13</sup>

#### **1.1.2. Risk Factors Associated with an Increased Incidence of Cancer**

The previous sections outlined agents that are known to promote carcinogenesis. However, there are certain lifestyle factors that are associated with an increased risk of developing cancers. Epidemiological analysis of the five main cancers in both men and women (see Table 3) has identified four factors (tobacco smoking, diet, sex hormones and family history) which were associated most frequently with the prevalent cancers and these are discussed in the proceeding sections.

**Table 3.** Incidence of the five main cancers in the USA and their risk factors.<sup>10</sup>

<b>Cancer</b>	<b>Percentage of all cases</b>	<b>Risk factors</b>
<b>Men</b>		
Prostate	36	Sex hormones Diet
Lung	13	Tobacco Smoking Diet
Colorectal	12	Family history
Urinary tract	9	Smoking
Leukaemia/lymphoma	7	Non identified
<b>Women</b>		
Breast	33	Sex hormones Family history Diet
Lung	13	Smoking Family history
Colorectal	12	Diet
Leukaemia/lymphoma	6	Non identified
Ovary	5	Ovulation Family history

#### **1.1.2.1. Smoking**

Tobacco smoking is widely known to be a risk factor in lung cancer, but it is also implicated in a number of other cancers, including those of the mouth, bladder and kidney. More than 40 potential carcinogens have been isolated from tobacco smoke and there is a clear close relationship between the number of cigarettes smoked and cancer risk.

#### **1.1.2.2. Diet**

Diet has the most effect in areas of the body that come into direct contact with food (e.g. the gastrointestinal tract); however, diet is also implicated in other areas, such as the breast and lung. It is difficult to conclude exactly which foods are ‘good’ and ‘bad’ in terms of cancer risk, as the modern diet is varied. A diet high in fruit and vegetables is

thought to be beneficial in terms of decreasing the risk of cancer, because of the presence of antioxidants that are able to counteract the DNA-damaging effects of reactive oxygen species. Saturated fat, meat, salt and alcohol are all considered to be dietary risk factors and are implicated in a number of cancers (stomach, colon and breast cancer).

#### **1.1.2.3. Sex Hormones**

Sex hormones are implicated in the most common smoking-unrelated cancers, in both men and women (prostate and breast cancer, respectively). Chemical or surgical castration of men dramatically reduces the incidence of prostate cancer, while removal of the ovaries reduces the risk of breast cancer. These hormones influence proliferation of their target cells and hence, increase the risk of cancer at these sites.

#### **1.1.2.4. Familial Cancers**

The majority of cancers (>90%) are sporadic and no evidence exists to suggest that the disease may be inherited from family members. A small percentage of cancers (5-10%) have some degree of familial involvement, including breast and colon cancer. A very small percentage of cancer (approximately 0.1%), have a strong familial link, including retinoblastoma and Wilm's tumour of the kidney.

### **1.2. The Global Burden of Cancer**

Cancer is an indiscriminate, collection of diseases, affecting millions of people worldwide. The global number of new cancer cases reported in 2000 was 10.1 million, (excluding cases of non-malignant skin cancer)<sup>14</sup> and in 2006 in the UK alone 293,601



people were diagnosed with cancer.<sup>15</sup> The most commonly occurring cancer in 2000 was that of the lung, with 1.2 million new cases and 1.1 million lung-cancer related deaths reported. Lung cancer was once rare, but today incidence of the disease has reached epidemic proportions.<sup>16</sup> North America and Europe have the highest incidence of lung cancer, with one of the highest rates occurring here in the UK. Clearly, there is an urgent need for new, effective treatments for this and many other cancers.

### **1.2.1. Cancer Management**

#### **1.2.1.1. Surgery**

The majority of patients with solid tumours will require surgical intervention at some point in their treatment programme. A large proportion of patients will undergo an initial diagnostic biopsy before treatment starts. Surgery and subsequent pathological examination of excised tissue, is used to determine the stage to which the disease has progressed, allowing suitable treatment to be chosen and defining the risk of relapse. If a tumour is localised and displays limited spread to the regional nodes or metastases, a complete surgical cure may be achieved. During surgery, the lymph nodes are often removed, providing information on disease progression and helping to prevent recurrence. Distant metastases are sometimes removed, although these are commonly dealt with by non-surgical means. Surgery alone is rarely able to provide a cure once the disease has metastasised, as there is a risk of recurrent disease at the primary site, in conjunction with the fact that micrometastases may continue to grow. In these cases, a cure is more likely to be achieved by a combination of surgery with chemotherapy and/or radiotherapy. Surgery is also used in palliative care, but careful consideration is given to whether the proposed benefits outweigh the possible trauma and discomfort of

a surgical procedure. Prophylactic surgeries are carried out, typically mastectomy on women with a family history of breast cancer.

#### **1.2.1.2. Radiotherapy**

Ionising radiation induces DNA damage in normal and tumour cells; if DNA damage is not repaired, apoptosis (programmed cell death) results. Radiotherapy can be administered as one single dose but it is more commonly given in multiple doses, with rest periods between treatments. This is because cells are only radiosensitive during certain phases of the cell cycle. Therefore, administering the treatment in cycles allows normal cells to recover from the effects of the radiation and allows tumour cells to become re-oxygenated. This is important, as hypoxic cells are resistant to ionising radiation.

Radiotherapy is routinely used to treat a number of cancers, including head and neck, cervical, bladder, lung, lymph and oesophageal. As with surgery, radiotherapy can be used effectively at a variety of stages in the treatment programme. Radiotherapy is commonly used as an adjuvant therapy (to help in local disease control) or in neoadjuvant therapy (to reduce tumour mass prior to surgery). Post-operative radiotherapy is also carried out, particularly when residual disease is present. Finally, radiotherapy can be used in palliative care to improve quality of life.

#### **1.2.1.3. Chemotherapy**

Chemical agents are used in a variety of ways, throughout the treatment programme. Cancers are rarely cured by chemotherapy alone, although there are a limited number of

malignancies that can be managed this way. More often, chemotherapy is used as part of a treatment regimen or to alleviate symptoms and improve quality of life.

The main ways that chemical agents are used in cancer treatment are: as neoadjuvant therapy prior to surgery; as adjuvant therapy following surgical removal of the tumour; as palliative therapy to improve quality of life; and as prophylactic treatment in high-risk groups (e.g. tamoxifen in women with a family history of breast cancer). Curative chemotherapy, in particular, tends to be aggressive and side effects are severe.

There are several groups of chemical agents used in cancer chemotherapy. Table 4 provides an overview of the types of drugs used, their mechanism of action, the tumours that they are used to treat and their major side effects. This list is not exhaustive but it serves to illustrate the major groups of chemotherapeutic agents that are available. The reader is referred to the textbook by Tannock and Hill,<sup>17</sup> for a more complete list of chemotherapeutic agents.

**Table 4.** The different groups of chemical agents used in cancer therapy.

Type of agent	Mechanism of action	Example	Target tumours	Major toxicity
Alkylating agents	Most bifunctional agents, which form inter- and intrastrand crosslinks with DNA double helix and cause disruption of DNA synthesis	Cisplatin	Ovarian Testicular	Nausea Renal dysfunction Neural effects
Antimetabolites	Inhibit the synthesis of nucleic acid	5-fluorouracil	Breast Stomach	Bone marrow effects
Natural products	Various mechanisms	Taxol	Leukaemia Ovarian Testicular	Bone marrow effects
Hormone therapy	Deprive tumour of the hormone required for proliferation	Tamoxifen	Breast	Gastrointestinal effects Menstrual irregularities

There are a number of problems with chemotherapeutic drugs, not least the many adverse events that are common to cytotoxic agents (including acute effects, such as nausea and vomiting, myelosuppression and alopecia, and long-term complications, such as secondary malignancies and infertility). Adverse events occur because these drugs are systemic therapies; they have potential to effect cells anywhere in the body. These adverse events can seriously impair quality of life and so there is a need for less toxic (i.e. tumour selective) drugs. The onset of structure-based drug design may help to increase tumour selectivity and, thus, reduce the severity of side effects. Another major problem with chemotherapy is drug resistance; a fraction of a tumour may become resistant to a drug (or class of drug) that it has previously responded to, causing relapse of the tumour.<sup>18</sup> The development of drugs that have a unique mode of action has been proposed as a possible route to overcome drug resistance.

There is clearly plenty of scope for major improvements on traditional chemotherapeutic agents, because:

- The common tumours, such as those of the colon, breast and lung, do not respond well to existing therapies
- The majority of drugs:-
  - Are toxic to normal cells
  - Have a low therapeutic index
  - Preferentially kill rapidly-dividing cells
- Drug resistance is a problem

There is an urgent need to develop cytotoxic drugs that are selective for malignant cells, thus reducing side effects, increasing the therapeutic index and removing the need for prolonged cycles of treatment (which can lead to drug resistance). The development of selective antitumour drugs is one of the main aims in current cancer research.

### **1.3. Development of new chemotherapeutic agents**

Historically new drugs were found by random screening of compounds against experimental models, in the hope that an effective agent would be found by chance. This empirical method of drug discovery is still valid, although it is usually restricted to the screening of natural products. The US National Cancer Institute (NCI) 60 human tumour cell line anticancer drug screen (NCI60) was developed in the late 1980s as an *in vitro* drug-discovery tool intended to supplant the use of transplantable animal tumours in anticancer drug screening. This screening model was rapidly recognized as a

rich source of information about the mechanisms of growth inhibition and tumour-cell kill. Recently, its role has changed to that of a service screen supporting the cancer research community. New methods, such as target orientated drug screening and rational drug design are rapidly superseding the traditional methods, fuelled by a growth in our understanding of tumour biology. As medicinal technology has advanced, new targets involved in carcinogenesis and cancer biology have been discovered. Identification of these new target molecules is one step towards broadening the type and range of chemotherapeutic agents, bringing new choices for treatment and helping to overcome resistance to the traditional chemotherapies. New approaches currently in development include: interfering with signal transduction pathways that are upregulated in cancer cells; preventing new tumour blood vessel formation (angiogenesis);<sup>18</sup> gene therapy;<sup>19</sup> and immunotherapy.<sup>20</sup>

Twenty-first century drug development (particularly in the pharmaceutical industry) focuses upon the development of therapeutic strategies designed to interfere with specific target molecules, with the aim of producing selective agents.

#### **1.4. Aim of Project**

As mentioned in the previous sections, in medicine new drugs are often sought to improve upon or find novel areas of application that previous drug developments could not manage. In many cases drug resistance can become a big issue and severe side effects triggered by less selective drugs can cause drugs to fail or serious discomfort in the patient. To try and improve upon the drugs on the market, novel compounds with novel modes of action or PKPD profiles are most likely to give results. However even

by a rational drug design approach, this discovery is not a guarantee and serendipity finds its way into finding new leads.

Our interest in the Schiff base complexes in this study has been brought about by the desire to discover new generations of anticancer metallopharmaceuticals, which have been eagerly sought since that of cisplatin as described by many books and reviews.<sup>21-24</sup> The particular Schiff base systems of this study were initially developed as polymerisation precatalysts,<sup>25</sup> and show similar chemistry in many respects to known anticancer metallopharmaceuticals, cisplatin and the metallocene dihalides and have yet to be investigated in anticancer drug applications or any other medicinal application. The initial investigation into this class of complex focused on the Schiff base complexes  $[\text{CoCl}_2(\text{L}^1\text{Ph})]$  and  $[\text{CuCl}_2(\text{L}^3\text{Ph})]$ . These were prepared and tested for their ability to bind to calf thymus DNA by measuring DNA melting temperatures in the presence of such compounds.<sup>26</sup> These particular complexes showed very promising results and so it is from those discoveries which this research stems.

The aim of this research was to identify the potential and to understand the role these systems would play as cytostatic agents. Possible model experiments were also an area of interest and would provide an opportunity in identifying biomolecular targets and their drug binding sites and modes, with the prospect of identifying an initial mechanism of action for these potential anticancer metallopharmaceuticals.

Since our initial lead stems from pure speculative insight and some promising results arising from it, there was no real rationale other than the compound similarities to known anti-cancer metallopharmaceuticals. It has also been discovered in the following

review that besides cisplatin, antiproliferative activity has been detected during the past 30 years for numerous other non-platinum group metal compounds. This means that anti-tumour activity is not limited to platinum complexes, but includes numerous other organometallic and inorganic compounds of transition metals and main group elements. In fact it turns out to be most advantageous that the spectrum of activity and pattern of toxicity of most non-platinum group metal anti-tumour agents do not resemble those induced by cytostatic platinum drugs. This observation qualifies non-platinum group metal antitumour compounds to be independent groups of antiproliferative agents and justifies the hope the class of complex and their metal salts in this study may actually improve the prognosis of patients suffering from certain cancer diseases in the future.

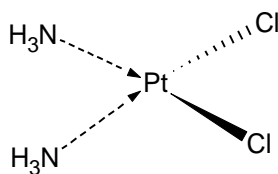
In order to design complexes in a study such as this, it is always sensible to have a fundamental understanding of the role such agents play in carrying out their task. Knowledge of potential modes of action can give good ideas as to what chemistry should be probed or tuned within a compound to provide the desired affect. The following section provides a review of anti-cancer metallopharmaceuticals, their coordination chemistry and provides the proposed mechanisms of action on which the later drug design in this thesis is based.

### **1.5. Review of Anticancer Metallodrugs**

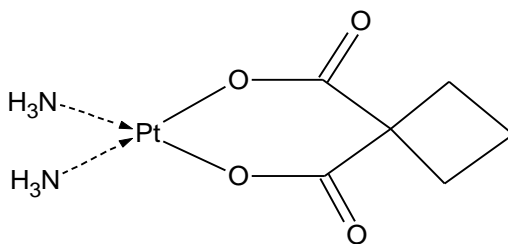
After the discovery and success of cisplatin **1**, as an anticancer agent, many investigations have been driven towards finding more metallodrugs with improved anticancer properties. Although the progression has been rather slow a handful of anticancer metallodrugs have made it through the rigorous clinical trials to be used in clinical treatments of cancer today. Numerous platinum complexes of the second



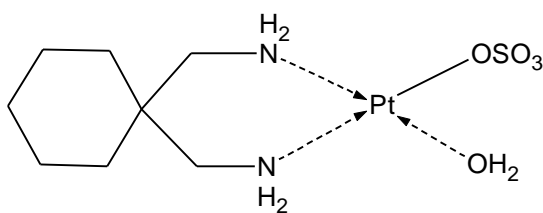
generation have been developed; about 10 of them entered clinical studies in the late 1970's.<sup>27</sup> The main compounds that represent these second generation platinum complexes are diammine(cyclobutane-1,1-dicarboxylato)platinum<sup>II</sup> (carboplatin, **2**) and aquo {1,1-bis(aminomethyl)cyclohexane}(sulfato)-platinum<sup>II</sup> (spiroplatin,**3**), which like cisplatin are four-coordinate, planar complexes, and bis(isopropylamine)-*cis*-dichloro-*trans*-dihydroxoplatinum<sup>IV</sup> (iproplatin, **4**), which in contrast contains platinum<sup>IV</sup> in an octahedral coordination sphere.<sup>28</sup>



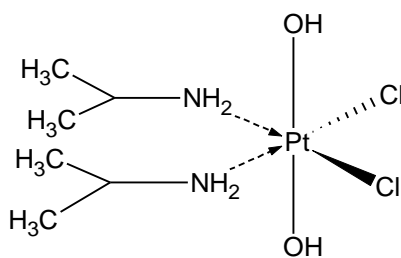
**1**



**2**

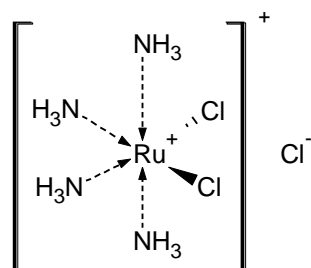


**3**

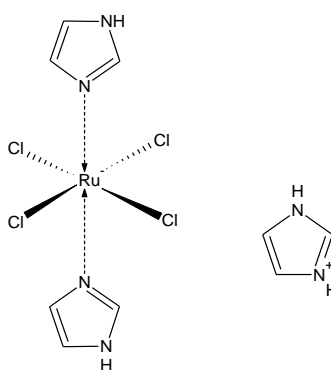


4

Not only platinum complexes exhibit antitumour properties; many complexes containing platinum group metals such as ruthenium, rhodium, or palladium are characterised by cytostatic activity. The problem with the rhodium and palladium complexes being their toxicity. Keppler and co-workers have shown amine and imine complexes of Ru<sup>III</sup>, to have antitumour properties, namely *cis*-[Cl<sub>2</sub>(NH<sub>3</sub>)<sub>4</sub>Ru]Cl, **5** and (HIm)[*trans*-[(Im)<sub>2</sub>Cl<sub>4</sub>Ru] (NAMI-A), **6** which are both octahedral complexes with *cis* chloro ligands and are highly water soluble. In addition Mestroni and co-workers have shown DMSO analogues to have activity against certain tumours.<sup>29</sup> These complexes and their analogues have shown inhibition of DNA replication and transcription along with inhibition of cellular DNA repair mechanisms. The complexes have too shown a direct correlation between cytotoxicity along with DNA binding, the binding has been shown to be primarily single and double stranded binding to the N7 of guanine bases as with cisplatin, but in the case of the octahedral Ru complexes with *trans* chloro ligands, interstrand binding is more of a possibility.

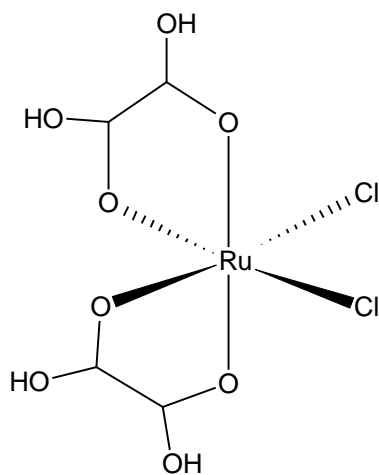


5



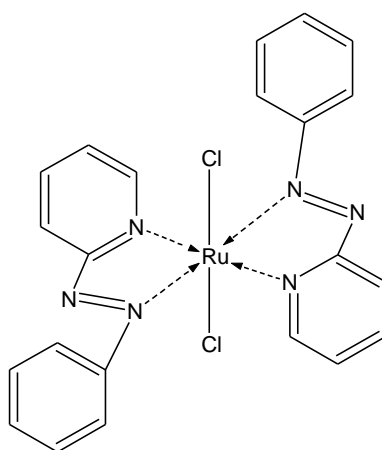
6

Other Ruthenium complexes to have shown promise are the polyamino and polycarboxylates, which are six coordinate, octahedral and highly water soluble. One example is the Ru<sup>IV</sup> complex [Cl<sub>2</sub>(cdta)Ru<sup>IV</sup>], **7** where the chlorides are *cis*- to one another and the carboxylates appear to be labile. The Ru centre has a high reduction potential for these complexes and the compound is expected to be reduced to the Ru<sup>II</sup> compound *in vivo*. The Ru<sup>III</sup> metal ion has a high affinity for transferrin (Tf), and has been proposed to be transported to cells by this iron transport protein. The active species *in vivo* has also been proposed to be the Ru<sup>II</sup> metal (*vide infra*).



7

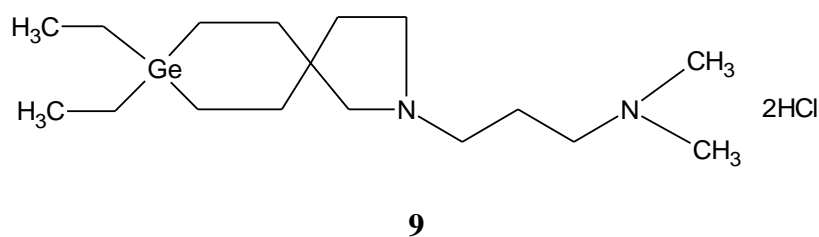
The isomer of *cis*-[Cl<sub>2</sub>(azpy)<sub>2</sub>Ru] (azpy = 2-(phenylazo)pyridine), **8** with C<sub>2</sub> symmetry exhibits substantial activity against several cell lines.<sup>30</sup> Possible reasons for this are, (1) the decrease in the rate of chloride aquation due to the π-acceptor effect of the imine ligands increasing the effective charge on the metal ion so that the hydrolysis rates are in the range of cisplatin; (2) increased hydrophobic or intercalative interactions with DNA, which may facilitate covalent binding; (3) geometric effects exerted by the ligands, which may facilitate (or inhibit) protein binding to the nucleic acid.

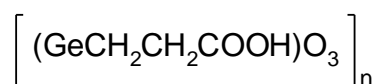


8

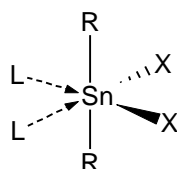
Gallium salts were the first main-group compounds for which antiproliferative activity was described (in 1975).<sup>31</sup> Gallium trinitrate is one metallodrug that has shown good

anticancer properties and it is used against some soft tissue cancers and bone cancers.<sup>31</sup> Ga(NO<sub>3</sub>)<sub>3</sub> is a salt and not a metal complex and possibly for that reason it is not considered to kill tumour cells by binding to DNA. But it has been proposed that the compound binds to transferrin and therefore inhibits the incorporation of iron into tumour cells, which is an essential metal; used in DNA replication. Other important main group cytostatics contain metals neighbouring gallium, i.e. germanium and tin. Presently there are two main representatives of antitumour germanium compounds: the monomeric 8,8-diethyl-2-[3-(N-dimethylamino)-propyl]-2-aza-8-germaspiro[4.5]decane (spirogermanium, **9**),<sup>32</sup> and the polymeric bis[(carboxyethyl)germanium] trioxide (germanium sesquioxide, Ge-132, **10**),<sup>28</sup> and the third group of antitumour main-group metal complexes detected so far is represented by diorganotin<sup>IV</sup> derivatives such as octahedral diorganotin dihalide complexes R<sub>2</sub>SnX<sub>2</sub>L<sup>2</sup> [R=alkyl, phenyl; X= F, Cl, Br, I, NCS; L= unidentate ligand (e.g. pyridine); L<sup>2</sup>= bidentate chelating ligand (e.g. 2,2'-bipy), **11** and di- and triorganotin complexes of nitrogenous bases and amino acids, e.g. R<sub>2</sub>Sn [adeninate(1-)]<sub>2</sub> and R<sub>2</sub>Sn[L-cysteinate(2-)].<sup>33</sup> Their antiproliferative activity was detected in 1980 and later against p388 leukaemia. Though this activity is strong comparable to that of **1**, further studies showed that there is obviously no activity against other experimental tumour systems.<sup>28</sup>





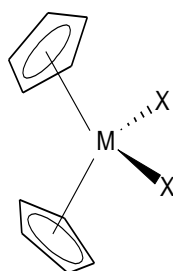
**10**



**11**

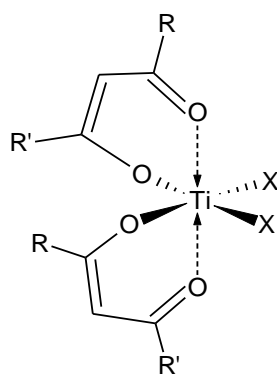
Antitumour compounds of transition metals other than platinum-group metals either contain early transition metals like titanium and vanadium, medium transition metals like iron, or late transition metals like copper and gold. Early transition metal compounds showing tumour inhibiting efficacy are mainly represented by metallocene complexes of type **12** ( $M = \text{Ti, V, Nb, Mo}$ ; e.g.,  $X = \text{Cl}$ ). These are organometallic complexes, the cyclopentadienyl ring ligands being bound to the central metal ion  $M$  by carbon-metal bonds. Metallocene complexes **12** have shown antiproliferative activity against experimental tumours. The antitumour activity of metallocene dihalide complexes is dependent upon the metal ion with  $M = \text{Ti, V, Nb, Mo}$ , showing marked activity, Ta and W, exhibiting marginal effectiveness and Zr and Hf, being inactive. The diagonal relationship between the active metal ions (Ti-Nb and V-Mo) suggests that active complexes fall within a window of size and substitution reactivity of the metal ion. The most successful of these agents being  $\text{Cl}_2\text{Cp}_2\text{Ti}$  which subsequently made phase II clinical trials. Whilst these compounds were initially tested as possible analogues of cisplatin, the effectiveness of  $\text{Cl}_2\text{Cp}_2\text{Ti}$  against platinum-resistant cell lines indicates a different mechanism of action.<sup>34</sup> The metal ion has been shown to

accumulate in cellular regions rich in nucleic acids with highest concentrations in the chromatin. The compound  $\text{Cl}_2\text{Cp}_2\text{Ti}$  has also been shown to bind strongly to the  $\text{Fe}^{\text{III}}$  binding sites in Tf, which may provide a transport mechanism into the tumours.<sup>35</sup> Later studies indicated that metallocene dihalides do not bind strongly to DNA at neutral pH and do not suppress DNA-processing enzymes, so that it is unlikely that their activity involves nucleic acids.<sup>36</sup>



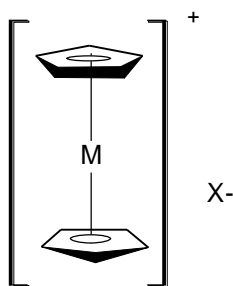
**12**

Other antitumour titanium complexes are the six co-ordinate bis(benzylacetonato)titanium<sup>IV</sup> dihalides and bis(alkoxides), **13** ( $\text{R} = \text{CH}_3$ ,  $\text{R}' = \text{C}_6\text{H}_5$ ,  $\text{X} = \text{F}, \text{Cl}, \text{Br}, \text{OC}_2\text{H}_5$ ) and some similar zirconium and hafnium complexes have also been found to show activity. Budotitane an example of this class of compound *cis*- $[(\text{CH}_3\text{CH}_2\text{O})_2(\text{bzac})_2\text{Ti}^{\text{IV}}]$ , where bzac = 1-phenylbutane-1,3-diketonate, was the first non-platinum transition-metal anticancer agent to be tested in clinical trials.<sup>37</sup> In the series *cis*- $[\text{X}_2(\text{bzac})_2\text{Ti}^{\text{IV}}]$ , activity varies in the order  $\text{Ti} \sim \text{Zr} > \text{Hf} > \text{Mo} > \text{Sn} > \text{Ge}$ ,<sup>37</sup> which is roughly inverse to the rates of X dissociating from the metal ion. Little is known about the mechanism of budotitane except that it is distinct from that of cisplatin.<sup>38</sup>



**13**

Whereas the antitumour metallocene dihalides, **12** are neutral compounds, the cytostatically active medium transition metal agents are saltlike metallocenium complexes, **14** ( $M = \text{Fe}, \text{Co}$ ; e.g.,  $X = \text{FeCl}_4^-$ ), containing in the cation the coordinatively saturated central metal atom interposed between two parallel cyclopentadienyl ring ligands. Thus, metallocenium compounds are also organometallic complexes. Their antitumour activity was detected in 1984 against Ehrlich ascites tumour.<sup>39</sup>

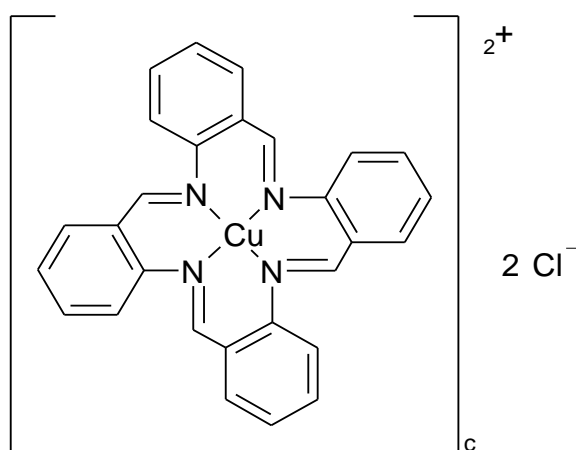


**14**

Regarding late transition metal antitumour agents, numerous compounds of copper are known that contain organic ligands exhibiting antiproliferative activity by themselves. Prominent examples of this type of cytostatic compounds are bleomycin- and

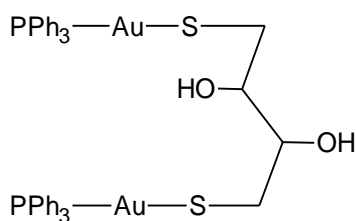


thiosemicarbazone-copper complexes. Besides these, many other copper complexes containing e.g. ligands of the Schiff base type have shown antiproliferative activity. Thus, efficacy against experimental animal tumours was revealed for the neutral complex trans-bis(salicylaldoximato)copper<sup>II</sup> as well as for copper<sup>II</sup> complex salt **15** of the macrocyclic ligand tetrabenzo[b,f,j,n]-1,5,9,13-tetraazacyclohexadecene.

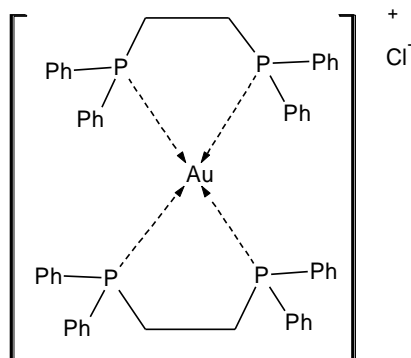


**15**

From certain gold<sup>I</sup> complexes like auranofin it is known that they are clinically well approved therapeutic drugs against rheumatoid arthritis. Reports of *in vivo* antitumour activity of gold complexes, however are comparably rare. Complexes for which *in vivo* antitumour activity has been described are gold<sup>I</sup> phosphine complexes such as the neutral binuclear **16**, containing a bridging dithiolate ligand and the saltlike, mononuclear, tetrahedral chelate complex, **17** comprised of two bidentate 1,2-bis(diphenylphosphino)ethane ligands. They effected antiproliferative activity against P388 leukemia, M5076 reticulum cell sarcoma, and mammary adenocarcinoma 16 / c.



**16**



**17**

## 1.6. The Likely Fate of Metallo drugs on Entering the Body

As mentioned before the majority of research into anti cancer metallopharmaceuticals is undoubtedly for that of cisplatin and some of the proposed concepts are therefore based on the findings of cisplatin research. Some concepts maybe based on research into other metallopharmaceuticals, but to a lesser extent.

### 1.6.1. Transport

It has been proposed that following injection into the bloodstream cisplatin encounters a relatively high concentration of chloride ions (100 mM) that suppress hydrolysis and maintains the compound in the neutral state. The limiting factor for accumulating platinum in cells is its concentration, and the uptake of cisplatin is not saturable.<sup>40, 41</sup>

Cisplatin uptake does not have a pH optimum nor is it inhibited by structural analogues such as carboplatin, suggesting that the transport is not carrier-mediated.<sup>42</sup> These results suggest that cisplatin enters cells by passive diffusion, although there is some evidence that uptake may in part occur by an active transport mechanism.<sup>43</sup>

Other metal ion complexes are similar in size to iron<sup>III</sup> and mimic some of the chemistry of iron in that they bind to transferrin (Tf) and can enter cells through transferrin receptors (TfR), as well as by routes that do not require transferrin. This also depends on the affinity of the metal ions for binding to Tf. For instance  $\text{Ga}(\text{NO}_3)_3$  a non platinum chemotherapeutic agent has a similar size and a high affinity for binding to Tf.<sup>44</sup> The uptake of the metal ions into cells is largely dependent on the TfR density on the exterior of cells, and cellular iron deprivation results in enhanced sensitivity of the cells to gallium.<sup>45</sup> As the enhanced requirements for nutrients of neoplastic cells from their generally higher metabolism compared to normal healthy cells, leads to higher TfR densities, the uptake of gallium into the tumour cells is generally higher than in other tissues. This can account for the selectivity of the metal ion for tumour cells over normal healthy cells. It is also thought that other metal complexes are transported in the same way, such as titanocene dichloride<sup>46</sup> and other metallodrugs may even be transported by other serum proteins such as albumins.<sup>47-49</sup>

### **1.6.2. Tumour cell Specificity**

Because tumour cells are highly proliferating their elevated requirements for nutrients coupled with their higher membrane permeability results in both specific and non-specific uptake of metallodrugs. But for cisplatin and many other cytotoxic

chemotherapeutics this still results in healthy cells being affected and many unwanted side effects.

### 1.6.3. Metal complex activation

The reaction mechanism of many anticancer metallodrugs with DNA has been shown to involve activation of the metallodrug by aquation.<sup>50</sup> For platinum<sup>II</sup> complexes the tendency of a ligand to leave the complex correlates with the affinity for binding to platinum<sup>II</sup>, decreasing in the order:

$\text{CN}^- > \text{NH}_3 \sim \text{Guo}, \text{Ado}, \text{OH}^- > \text{I}^- > \text{SCN}^- > \text{Br}^- > \text{Cl}^- \sim \text{phosphate}, \text{carboxylate} > \text{H}_2\text{O} > \text{NO}_3^-, \text{SO}_4^{2-}, \text{ClO}_4^-$ .

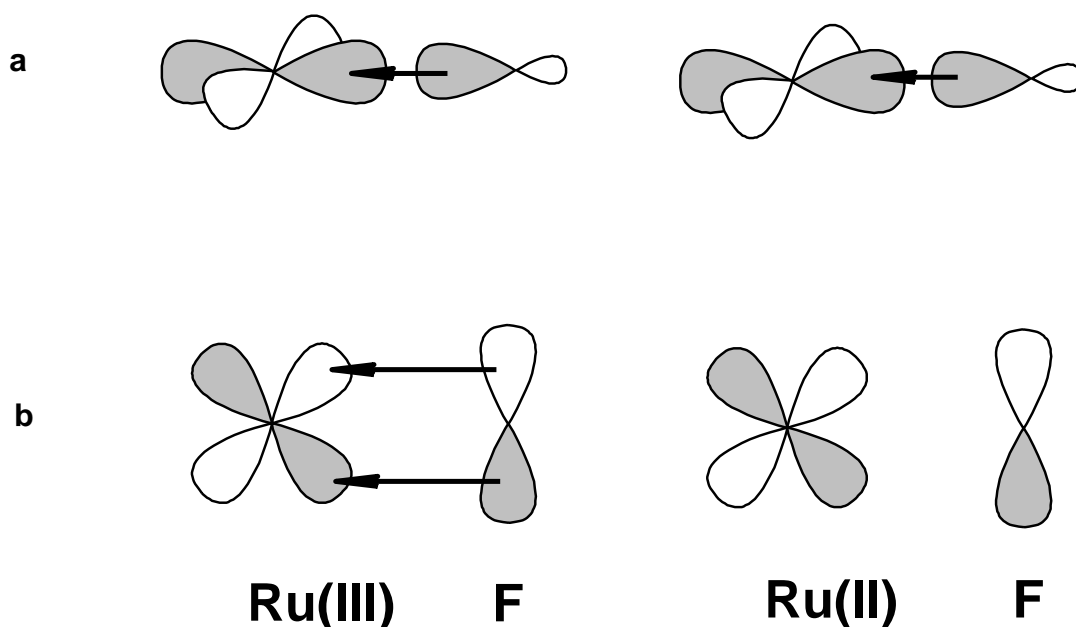
A platinum<sup>II</sup> complex co-ordinated with water or any ligand beyond water in this series may be called “activated”. The drug administered is not the active drug and is actually a prodrug since it is activated to a different compound *in vivo*. For cisplatin which is thought to be transported to the cell by passive diffusion it experiences a drop of chloride ion concentration from 100 mM to ~20 mM in the cell, which facilitates activation. Activation in biological reactions occurs by hydrolysis. For different complexes, rate constants of hydrolysis depend on the geometry of co-ordination and on the chemistry of the conserved ligands.

Another method of activation of metallodrugs is by reduction, a hypothesis that came to light more than two decades ago. It has been suggested that Ru<sup>III</sup> complexes may serve as prodrugs, which are activated by reduction *in vivo* to co-ordinate more rapidly to biomolecules.<sup>51, 52</sup> Indeed, glutathione and a number of redox proteins are capable of

reducing Ru<sup>III</sup> complexes *in vivo*.<sup>53</sup> The low dioxygen content (hypoxia) and lower pH should favour Ru<sup>II</sup>, which is generally more actively binding than Ru<sup>III</sup>, and thus provide for selective toxicity. It has also been suggested that octahedral platinum<sup>IV</sup> complexes are reduced to the square planar platinum<sup>II</sup> compound before binding to DNA *in vivo*.<sup>54</sup>

As reduction of Ru<sup>III</sup> to Ru<sup>II</sup> fills the dπ orbitals, those ligands that π-donate are no longer able to do so and bind less strongly (Figure 3). In the case of Ru (II) am(m)ine complexes, acido ligands are lost fairly rapidly.

**Figure 3.** a) Shows σ bonding between the filled sp hybrid orbital of F<sup>-</sup> and the empty e<sub>g</sub> orbitals of Ru(II) and (III). b) Shows π bonding between the filled p<sub>y</sub> orbital of F<sup>-</sup> and the empty t<sub>2g</sub> dπ orbitals of Ru(III), whereas Ru(II) has no empty dπ orbitals to form π bonds with the π donor F<sup>-</sup> (acido ligand).<sup>55</sup>



#### 1.6.4. Cellular Targets

Once the metal complex is activated it can then form adducts with biomolecular targets forming lesions and altering various ways in which these biomolecules function. Because there are many biomolecules in the body, there are numerous targets for metallodrugs, namely, DNA, RNA, nucleotides, nucleosides, amino acids, proteins, oligopeptides, phospholipids and others, all which contain donor functions for the metallodrugs, O, N, P, S donors and charged species which can bind co-valently or electrostatically or through weaker hydrogen bonding to the metal centres or to ligands in the primary co-ordination sphere.

From work carried out on cisplatin there is some evidence to suggest that non-DNA targets may be involved, and this topic has been reviewed.<sup>56</sup> Cisplatin interacts with phospholipids and phosphatidylserine in membranes,<sup>57, 58</sup> disrupts the cytoskeleton,<sup>59</sup> and affects the polymerisation of actin, presumably because of conformational changes resulting from the formation of Pt-S bonds.<sup>60</sup> The preference for Pt-N bond formation in the presence of S-donor ligands in cells has also been reviewed.<sup>61</sup> Thus although there is some evidence to suggest that other biological targets may be important in the cisplatin mechanism, it is generally accepted that DNA is the primary target, and research in this area has predominated. The theory that DNA is the target was corroborated by experiments measuring the rates of synthesis of DNA, RNA and proteins in cells treated with cisplatin by monitoring the incorporation of radiolabeled precursors. At therapeutic doses of cisplatin, DNA synthesis was preferentially inhibited over RNA and protein synthesis in both human AV<sub>3</sub> cells in culture and in Ehrlich ascites cells *in vivo*.<sup>41, 62</sup>

The inactive *trans* isomer inhibited DNA synthesis to only a minor extent at similar doses.<sup>62</sup>

### 1.6.5. DNA Structure and Metal Binding Sites

The surface of the DNA double helix is characterised by major and minor groves (Figure 4). The backbone of each DNA strand is composed of deoxyribose phosphodiester units. In Figure 5, is displayed a schematic of the backbone containing the numbering of the deoxyribose rings. The DNA backbone has polarity; the 5'-end of the molecule is at the top and the 3'-end is at the bottom.

**Figure 4.** Wireframe representation of the side view of B-DNA, arrows near the top and bottom of the helix point to major and minor grooves respectively, red dots represent waters of crystallisation.<sup>63</sup>

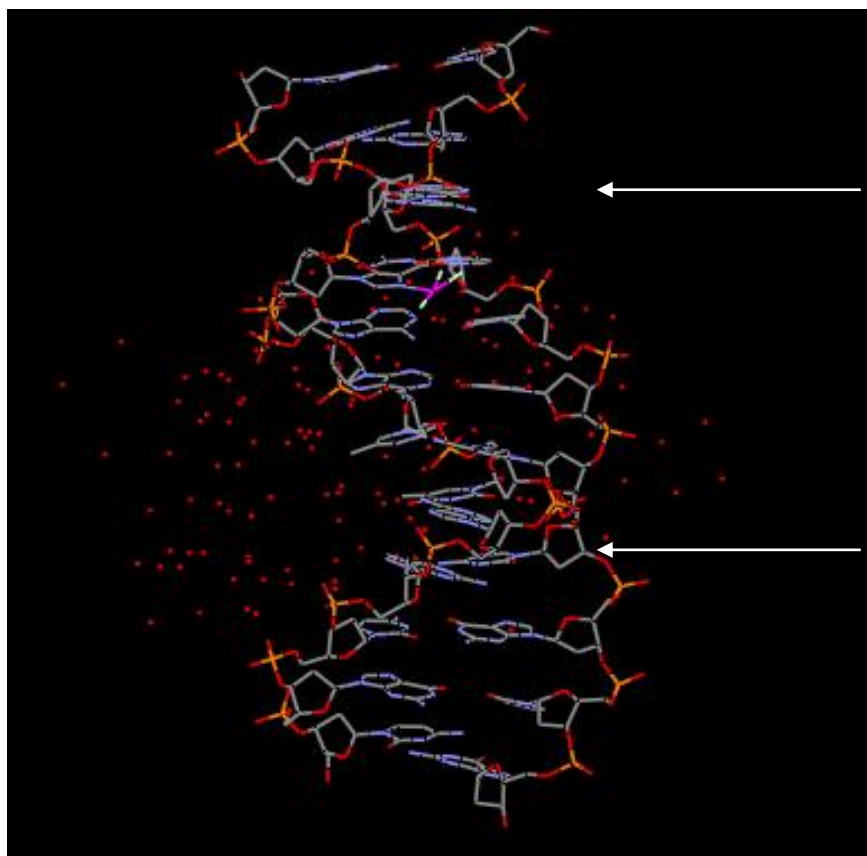
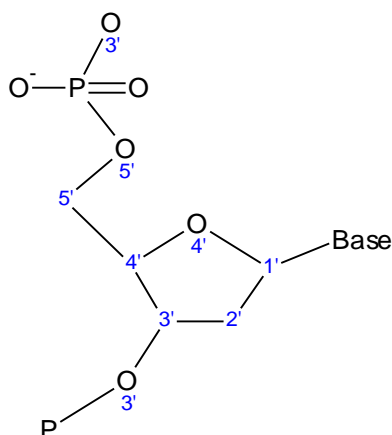


**Figure 5.** Schematic of the DNA backbone, showing deoxyribose ring numbering schemes.

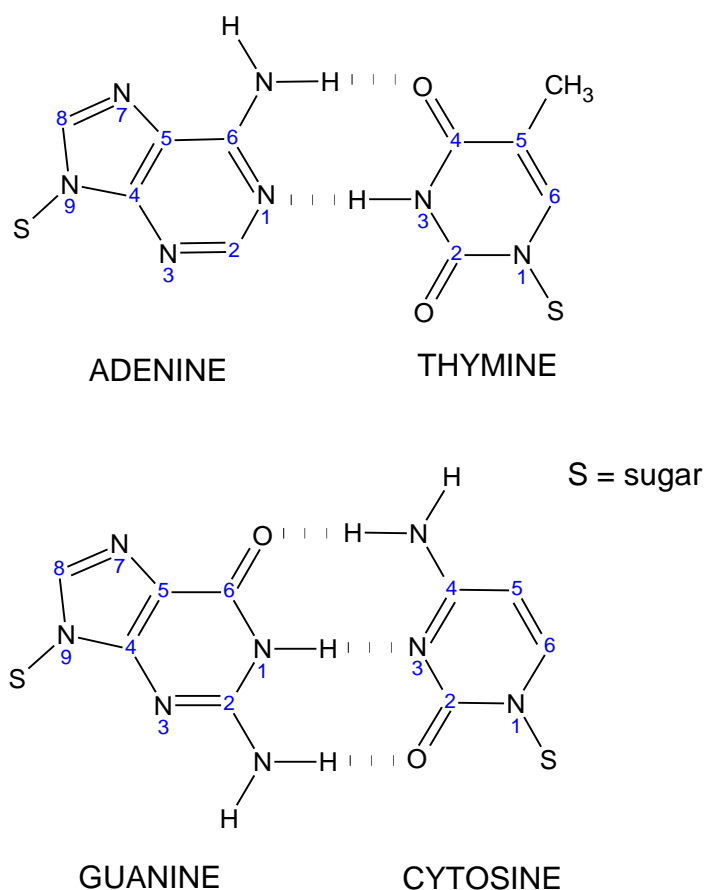


The N9 atoms of the purine bases, adenine and guanine (Figure 5), are attached via the glycosyl bond to the 1'-carbon atoms of the DNA backbone. The pyrimidine bases, cytosine and thymine, bond to C1' through their N1 atoms.

The double helix is stabilised by hydrogen bonds between guanine and cytosine and between thymine and adenine of opposite strands and by stacking interactions between parallel bases perpendicular to the helix axis. Figure 6 depicts the most common hydrogen bonding interactions between paired bases and their numbering schemes. Looking down the helix axes in Figure 4, the major groove of DNA is at the top of each base pair and the minor groove is at the bottom.



**Figure 6.** Schematic of Watson-Crick A-T and G-C base pairs, showing the atom numbering schemes. In these views down the helix axes, the major grooves of DNA are pointed toward the top of the figure and the minor grooves are pointing toward the bottom of the figure.



There are a variety of binding sites available to heavy metals on DNA.<sup>64</sup> Metals may covalently bind to the negatively charged phosphate oxygen atoms and to the nitrogen and oxygen atoms of the purine and pyrimidine bases. Planar molecules can intercalate between DNA base pairs.<sup>65</sup>

Early experiments revealed a shift of the absorbance maximum of DNA from 259 to 264 nm upon reaction with platinum compounds, indicating platinum association with

the bases.<sup>66</sup> Moreover, cisplatin noncompetitively inhibits the binding of the intercalator, ethidium bromide, to DNA. The platinum complex therefore binds covalently and not by intercalation.<sup>67, 68</sup> Although the platinum can bind to the phosphates of mononucleotides,<sup>69,70</sup> the pyridine-like and imidazole-like nitrogen atoms have a greater affinity for the polarisable Pt<sup>II</sup> atom,<sup>71</sup> and it is therefore less likely that phosphate coordination will occur in a competitive binding situation.<sup>72</sup>

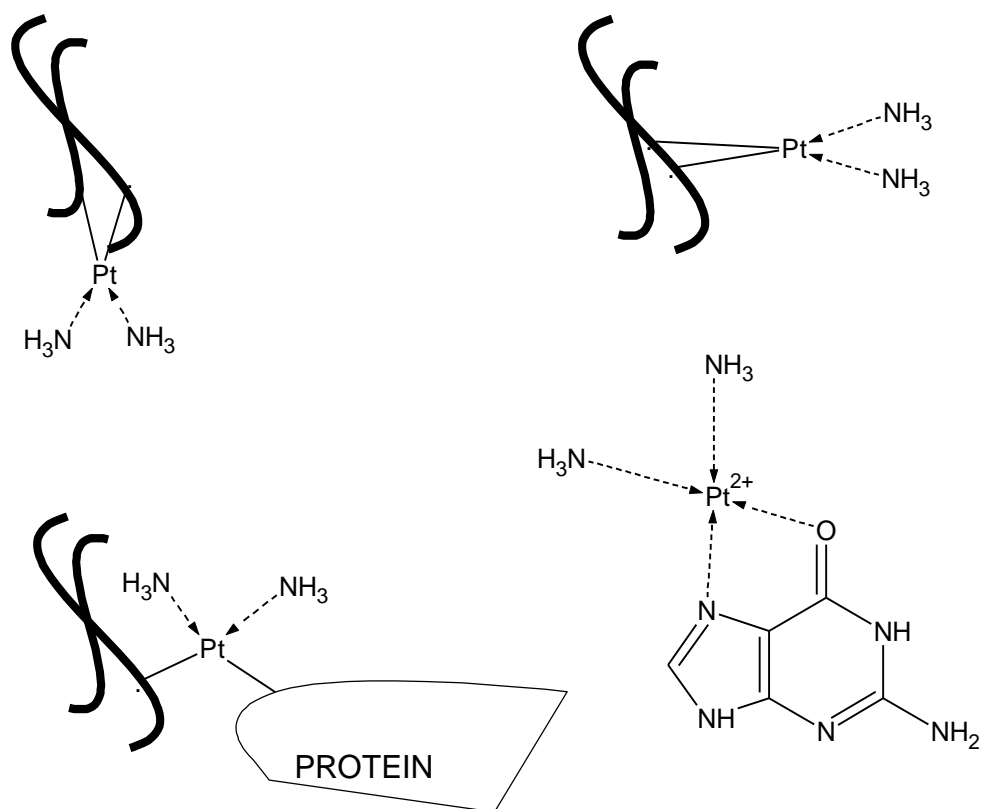
X-ray diffraction and NMR studies of complexes formed between platinum and N9-alkylated purines, N1-alkylated pyrimidines, nucleosides and nucleotides have been used to elucidate platinum binding sites.<sup>73</sup> Under neutral conditions, platinum binds to the N7 atom of guanine, the N7 and N1 atoms of adenine and the N3 atom of cytosine. In DNA, atoms involved in base pairing, i.e. N1 of adenine and N3 of cytosine, are less available for metal binding than the more exposed sites in the grooves. By Raman difference spectrophotometry, the order of reactivity in competitive reactions of four nucleoside monophosphates with *cis*- and *trans*-platin was established as GMP > AMP >> CMP > UMP, confirming that N7 of GMP is the preferred binding site.<sup>74</sup> Electrostatic potential calculations indicate that the guanine carbonyl group enhances the basicity of N7, while the amino group in adenine reduces the relative basicity of N7.<sup>75</sup> In DNA, N7 of guanine is exposed on the surface of the major groove (Figure 6), making it very accessible to metal binding.

#### **1.6.6. Binding Modes of Cisplatin with DNA**

Various possible bifunctional binding modes of cisplatin with DNA are represented in Figure 7. Since *cis*- and *trans*-platin are expected to form similar monofunctional

adducts, and because platinum complexes such as  $[\text{Pt}(\text{dien})\text{Cl}]^+$  are inactive as antitumour drugs and ineffective at blocking DNA replication *in vitro*,<sup>76</sup> monofunctional adducts are unlikely to be responsible for the biological activity of cisplatin. Instead, cross-links between two bases on opposite strands of the DNA helix, DNA-protein cross-links and intrastrand cross-links between two bases on the same DNA strand have all been proposed as being responsible for the antitumour activity of cisplatin.

**Figure 7.** Four DNA adducts a) Interstrand, b) Intrastrand, c) DNA-Protein crosslink, d) N7-O6 chelate with guanine.



Some of the earliest proposed binding modes involved platinum coordination to two sites on a single base.<sup>77</sup> Among these, the most popular was an N7-O6 chelate on guanine, which would alter the normal Watson-Crick hydrogen bonding of the G-C base pair in duplex DNA.<sup>78, 79</sup> To date there is no X-ray crystallographic or NMR support for

such a structure,<sup>80</sup> and the N7-O6 chelate has been generally rejected on geometric grounds.<sup>64</sup> It is also unlikely that such a binding mode would compete with other, more favourable binding interactions under normal conditions.<sup>81</sup>

Interstrand cross-linking of DNA *in vivo* and *in vitro*<sup>82</sup> has been measured by both denaturing gradient centrifugation and alkaline elution techniques. By analogy to bifunctional DNA alkylating agents,<sup>83</sup> which display many of the same biological properties of cisplatin, such crosslinks have been postulated to be responsible for the activity of platinum anticancer drugs. Later estimates indicate that DNA interstrand cross-links formed in mammalian cells constitute less than 1% of total Pt-DNA adducts shortly after treatment.<sup>84</sup> Statistically this percentage is too low to account for the cytotoxicity of cisplatin.<sup>85</sup>

From experiments carried out to identify the adducts produced by binding cisplatin to DNA, it has been demonstrated that interstrand cross-linking occurs predominantly between two guanine N7 atoms on opposite strands.<sup>86</sup>

Cross-links between DNA and proteins also comprise only a small fraction (0.15%) of the total Pt-DNA adducts formed in mammalian cells.<sup>84</sup> Both cis- and trans-platin cross-link nuclear DNA and non histone chromosomal proteins<sup>87</sup> transplatin forms more such cross-links than cisplatin at equivalent D / N ratios. There is no correlation between inhibition of DNA synthesis and DNA-protein cross-linking,<sup>87</sup> which along with their low frequency, indicates that DNA-protein cross-links are unlikely to be responsible for the antitumour activity of cisplatin. As yet, nothing is known about the identities of donor atoms on proteins involved in DNA-protein cross-links. Intrastrand binding of

cisplatin to the N7 atoms of two adjacent guanosine nucleosides occurs more frequently *in vitro* and *in vivo* than any other binding mode. The notion that cisplatin preferentially binds to guanosine was supported by experiments using both spectrophotometry and  $^{195}\text{Pt}$ -labeled cisplatin to monitor its reaction with DNA.<sup>88, 89</sup> Conclusions were drawn from buoyant density measurements that both cis- and trans-platin bind equally well to individual guanine bases but that only cisplatin is selective for adjacent guanosines.<sup>90</sup>

Not only are the site and mode of bidentate platinum binding to DNA dictated by local helix structure, but the resulting platinum adducts, in turn distort the structure of the double helix. There has been much conflicting information, however, concerning the extent of the distortions caused by cisplatin, transplatin and even  $[\text{Pt}(\text{dien})\text{Cl}]^+$  on DNA structure.

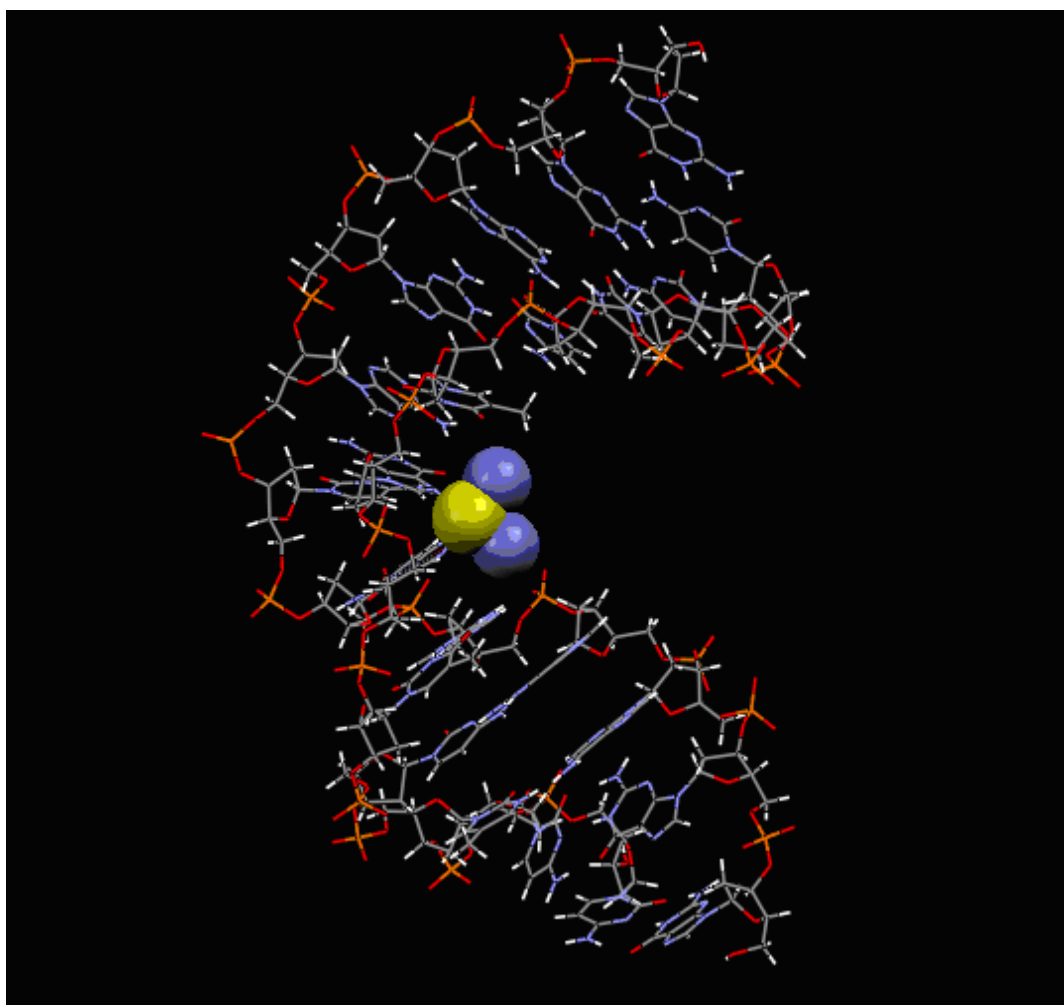
Changes in both the UV and circular dichroism spectra upon binding of cis- and transplatin to DNA reflect a loss in normal base stacking within the helix.  $[\text{Pt}(\text{dien})\text{Cl}]^+$  does not seem to affect base stacking as measured by these techniques.<sup>88, 91</sup> Increasing amounts of bound cis- $[\text{Pt}(\text{NH}_3)_2]^{2+}$  destabilise the DNA double helix resulting in a decrease in melting temperature.

High resolution X-ray and NMR structure studies of various cisplatin-DNA adducts have been carried out previously and revealed their propensity to distort DNA in very different ways. The major 1,2-intrastrand cross-links afford a bent, unwound duplex with a widened, shallow minor groove unlike that displayed by the minor cisplatin adducts. Their contrasting structural features suggest different roles for these various adducts in mediating the antitumour properties of cisplatin. This is also a suggestion for

other anticancer metallodrugs, that they interact with DNA to form different adducts, to those of cisplatin and their antitumour mechanism is therefore slightly different.

Figure 8 shows the NMR solution of a cis-GG cross-link on a platinated DNA dodecamer and here the overall helix bend is  $78^\circ$ , and the dihedral angle between adjacent guanine bases is  $47^\circ$ . These values are larger than observed for the X-ray crystal structure, reflecting the influence of crystal packing in the latter study. The base pairing at the site of platination is also more distorted in the NMR solution structure.<sup>84</sup>

**Figure 8.** The NMR solution of a DNA dodecamer with a cisplatin adduct at d(GpG).<sup>84</sup>



## **1.7. Effects of Metallodrugs on DNA Functions**

The ability of anticancer metallodrugs to bind to DNA and distort its structure suggest that they could interfere with the normal functioning of this important cellular component. DNA replication and transcription are essential for cell division and protein production; any disruption in these processes would be cytotoxic.

### **1.7.1. DNA Replication**

When a cell is going to divide, each DNA molecule replicates itself; this is an essential molecular process that involves unravelling of double stranded DNA from chromatin, separation of the duplex strands, and the synthesis of a new DNA using the original strands as templates. DNA polymerases are integrally involved in this process. It has been proposed that metallodrugs can inhibit the process of DNA replication by blocking the enzymes needed for this process. The metal-DNA lesions alter the conformation of the DNA helix by distorting the DNA base pairs at the site of metallation, which was suggested to alter the alignment of DNA in the binding site of the DNA polymerases, slowing the protein conformational change necessary for polymerisation. The binding of the next correct nucleotide would then also be affected by the presence of the metal adduct. The inhibition of replication by the metallodrugs suggests that they might kill cancer cells by blocking their ability to synthesise new DNA required for division.

### **1.7.2. DNA Transcription**

Transcription is the essential cellular process whereby mRNA is produced from a DNA template, a critical step in protein synthesis. Again it has been proposed that anticancer metallodrugs may inhibit this essential process by blocking RNA polymerase enzymes due to metal-DNA lesions and therefore inhibiting gene expression, which means the inability to synthesise some of the essential proteins required for cell function. This would lead to the cell cycle being arrested and ultimately cell death.

### **1.7.3. Telomeres and Telomerase**

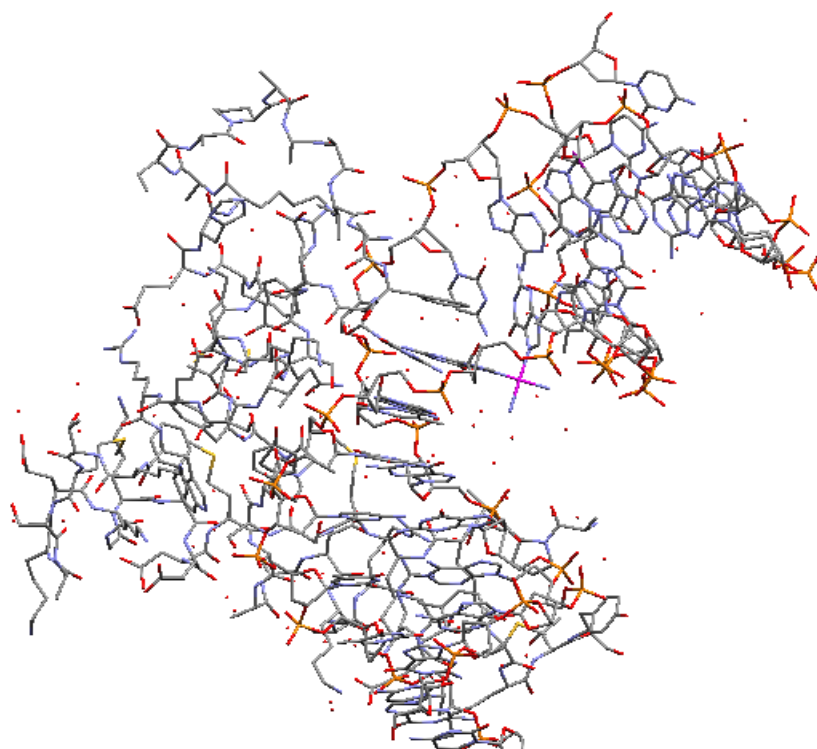
The telomeric regions of DNA represent a very appealing target for cisplatin and may interfere with normal DNA function. Telomeres occur at the ends of eukaryotic chromosomes and consist of a tandem, G-rich repeat sequence. In humans, the sequence is 5'-TTAGGG-3'.<sup>92</sup> Part of their function is to protect the ends of the chromosomes from degradation and to ensure that the genetic information is properly inherited at each cell division.<sup>93</sup> During one cell division, telomeres are shortened by 50-200 bp.<sup>94</sup> When they become critically shortened, cells become senescent and die. One way cells can become immortalised is to counteract the shortening of the telomeres with the ribonucleoprotein telomerase. Telomerase synthesises these repeat sequences at the ends of chromosomes and is postulated to play a role in the growth of malignant tumours.<sup>95</sup> Since the telomere-repeat sequences contain many guanosine residues, they represent a promising potential target for cisplatin.



#### 1.7.4. DNA Damage and Apoptosis

Another mechanism by which cell death may occur and is the mechanism that has been widely accepted as the most probable (for cisplatin at least), is by recognition of the distortion of DNA by a variety of proteins which leads to cell apoptosis (programmed cell death). This mechanism is thought to be the most probable mechanism of cisplatin induced cell death. An important aspect of this process is believed to be high-mobility group (HMG), domain protein recognition of and binding to DNA bent by the metal adduct (Figure 9). HMG domain protein binding is believed to interfere with the repair and removal of the metallated site by the normal repair mechanisms and this interference probably initiates the apoptosis process.

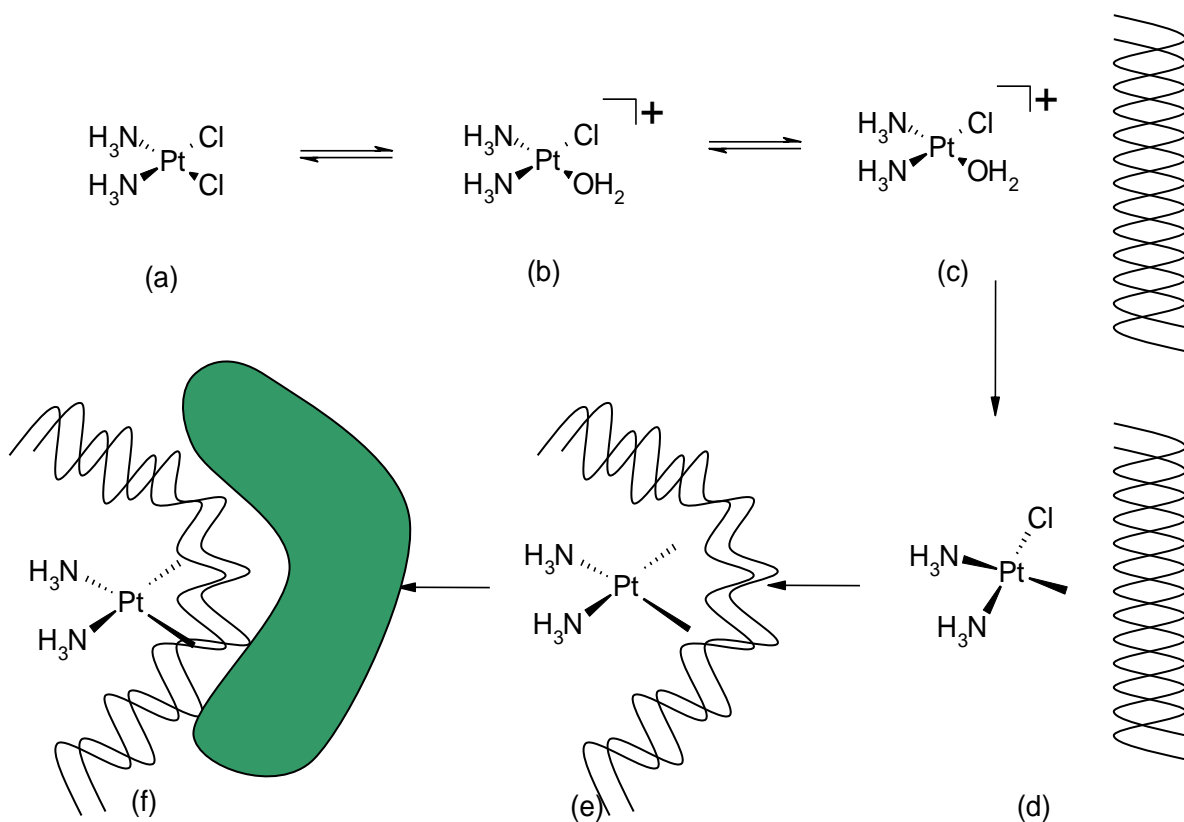
**Figure 9.** The Crystal structure of HMG1 domain A bound to a cisplatin modified DNA duplex.<sup>96</sup>



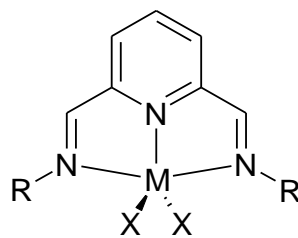
### 1.8. Likely Mechanism of Action of Cisplatin After Entering the Cell

Experiments have shown that cisplatin binding to DNA is kinetically rather than thermodynamically controlled. As mentioned previously, once inside the cell cisplatin experiences a diminished chloride concentration compared to the blood stream, which facilitates hydrolysis. This results in an activated, mono-aquated form,  $cis[Pt(NH_3)_2Cl(H_2O)]^+$ , which can react more readily with cellular targets. This hydrolysis reaction is the rate limiting step for DNA binding, the half life being ~2 h. Aquated cisplatin subsequently binds to an N7 atom of a guanine base in DNA, which displaces the water molecule in a relatively fast reaction step ( $t_{1/2} \sim 0.1$  h), forming a monofunctional adduct. Closure of the monofunctional adduct to form the bifunctional adduct involves hydrolysis of the second chloride ligand, with a half life of ~2 h. The distortion of the DNA is recognised by the HMG-domain A protein which ultimately signals apoptosis and cell death results (Figure 10).<sup>97</sup>

**Figure 10.** The sequence of events in cisplatin binding to DNA involves at least, (b) aquation, (c) preassociation, (d) monofunctional adduct formation, (e) closure to a bifunctional adduct (perhaps preceded by aquation), (f) distortion of DNA and recognition of this distortion by a variety of proteins.<sup>97</sup>



## 1.9. Design of Schiff Base Metallo drugs



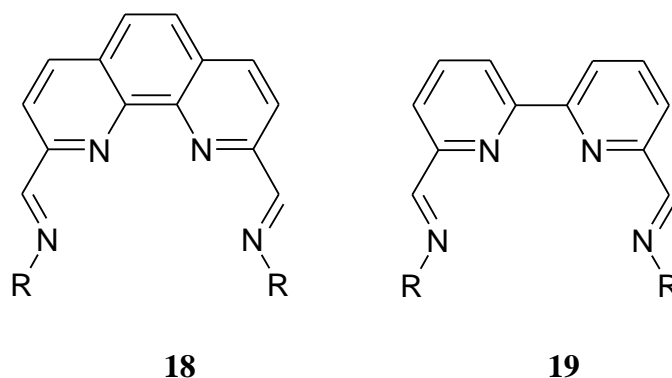
**17**

The use of metals in drug design provides new opportunities in the development of next generation anti-tumour drugs. Recently several classes of organometallic complexes (species that contain metal-carbon bonds) have been found to show anti-tumour properties. Of these, the metallocene dihalides and diacido complexes, **12** [ $\text{Cp}_2\text{MX}_2$  ( $\text{Cp} = \eta^5 - \text{C}_5\text{H}_5$ ;  $\text{M} = \text{Ti}, \text{V}, \text{Nb}, \text{Mo}, \text{Re}$ ;  $\text{X} = \text{halide or acido ligand}$ ), have been most widely studied and show activity against a range of tumour models in mice and several xenografted human tumours transplanted into athymic mice.<sup>98</sup> Titanocene dichloride ( $\text{Cp}_2\text{TiCl}_2$ ) made phase-II clinical trials<sup>99</sup> and more recently functionalised titanium metallocene compounds have been discovered to show promise as new antitumour drugs.<sup>100-102</sup> The metallocene type complexes have also found important applications in polymerisation catalysis.<sup>103-105</sup> The schiff base metal complexes of diformylpyridine, ( $\text{X} = \text{halide}$ ,  $\text{R} = \text{aryl group}$ ), developed by the Brookhart group in 1995, have shown high potential as effective polymerisation pre-catalysts.<sup>25, 104, 105</sup> The Schiff base complexes **17**, show very similar chemistry in many respects to the metallocenes **12**, but have yet to be investigated in anti-cancer drug applications.

Previously new generations of catalyst with similar ligand and co-ordination chemistry have been desired and are the next step in producing new and possibly improved

catalyst complexes. This would also be an interesting step to be taken in terms of drug design.

When systematically changing the ligand design of the complexes, obvious ligands with similar chemistry are the bidentate 1,10-phenanthroline **18** and 2,2'-bipyridine **19** ligands with diformyl groups to form the schiff base ligands, by condensation with primary amines (R = alkyl, aryl).



In order to generate a matrix of ligands that could be easily compared against activity results to present structure activity relationships, subtle variations in the ligand head and tail groups had to be devised along with variation in the central metal atom and labile ligands. The ligand 'head groups' used were three dicarbaldehydes, their structures shown in Table 5. As previously mentioned pyridine-2,6-dicarbaldehyde and 2,9-dicarbaldehyde-1,10-phenanthroline compounds have been used previously as precursors for polymerisation precatalysts and the 6,6'-dicarbaldehyde-2,2'-bipyridine being very much a novel precursor, again its application as a polymerisation precatalyst. These three 'head groups' provide subtle variations which can give varying metal cavity dimensions, denticity, electronic effects on the metal centre and also as we go from pyridine, bipyridine to phenanthroline, provide an extra domain that may afford intercalating abilities into the DNA structure, to supply a foothold for covalent binding

of the metal centre to donor atoms of nucleobases and also a possibility of inducing local modifications in DNA structure that may influence the sequence specificity of metallation. The ligand ‘tail groups’ can then be added to these precursors by condensation of 2 equivalents of primary amine with the dicarbaldehyde to form open macrocycles. Such variation of the ‘tail groups’ include degree of unsaturation, aromaticity, flexibility and functional groups. These variations in ‘tail groups’ can provide the ability to tune ligand affinities, electron transfer and substitution rates, and in the case of redox active metals reduction potentials and also the opportunity to provide secondary binding. The metal salts used in this program are the chlorides of  $\text{Co}^{\text{II}}$ ,  $\text{Ni}^{\text{II}}$ ,  $\text{Cu}^{\text{II}}$ ,  $\text{Zn}^{\text{II}}$ , and  $\text{Ru}^{\text{III}}$ . The reasons why these metals have been chosen is the fact that they are cheap, readily available, relatively air stable and have been used previously with these ligand systems as polymerisation precatalysts and have yet to be deeply studied in drug applications, with the exception of Ru which has shown great promise as a metal centre in anticancer drug applications with imine ligands.<sup>106</sup> However Co, Ni, Cu and Zn have shown activity against cancer cell lines with various other ligands previously,<sup>107-110</sup> notably  $\text{Co}^{\text{III}}$  compounds have shown considerable promise as bioreductive drugs offering a selective strategy.<sup>111-117</sup> The chloride anion was chosen initially as these metal salts are readily available and cisplatin and titanocene dichloride both contain *cis*- chloride ligands along with many of the afore mentioned metallodrugs. The chloride ligands could also provide stability for transport *in vivo* where a chloride ion concentration gradient exists between the systemic system and the cell, facilitating hydrolysis and consequently activation at the desired site. Other labile ligands that were of interest and subsequently used in this study were the acetate, nitrate, isothiocyanate and other halide ligands. Varying the anionic coordinating

ligand potentially provided variation and tuning of metal-ligand substitution rates (particularly hydrolysis), to values that can improve potency.

The rationale behind changing the ligand ‘tail’ group was to create subtle variations in chemical and physical properties of the complexes to affect the way these complexes could effectively carry out their role as cytotoxic agents *in vivo*.

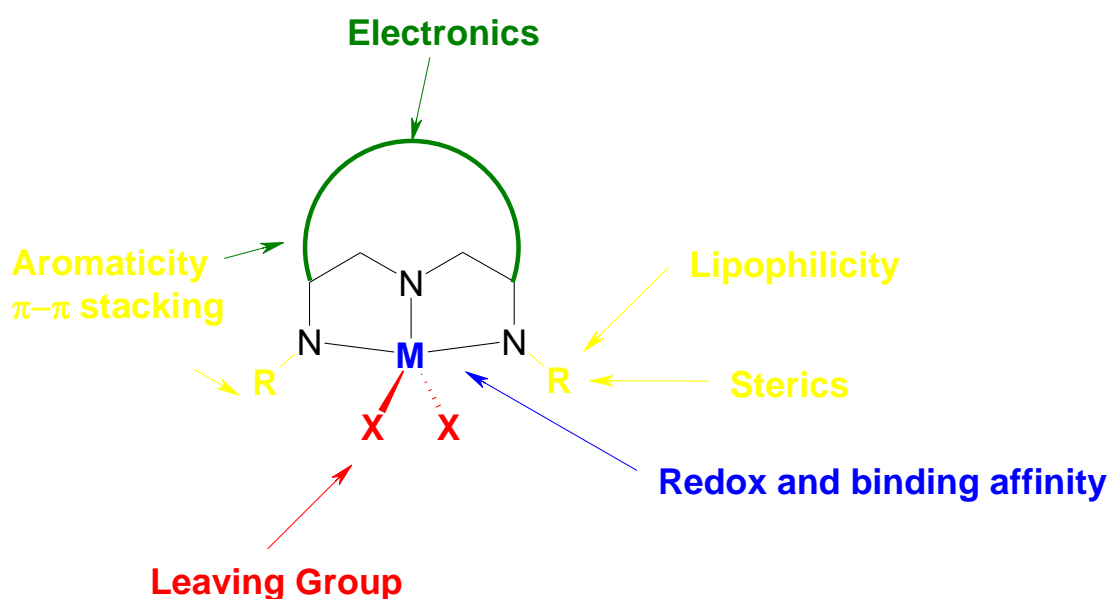
The subtle variation consisted of several parts. The first was by starting with a short chain aliphatic tail group and increasing the length and degree of branching of these groups (Table 5). These changes can impose several variations in electronic properties of the ligand on the metal centre through the inductive effect, this could effectively tune several properties of the metal centre, namely the solvolysis rates (in particular hydrolysis), of any labile coordinating ligands thereby effectively altering the activation process for metallation of DNA, that is if the complexes work analogously to cisplatin. The second effect would be that on the metal centred redox properties. The +I variation could tune the redox profiles to biologically accessible values whereby altering the complex’s cytotoxic effect if they are at all working via a redox mechanism or potentially both redox and DNA binding.

The degree of branching could also affect steric properties of the complexes. The bulkiness of the tail groups could aid or hinder the complexes binding to donor sites on biomolecular targets, thereby affecting the mode of action of these complexes and therefore their cytotoxic effect. Also the increase in carbon chain length and degree of branching can effect the lipophilicities of the ligands and therefore potentially the complexes. These physical chemical differences can be expressed numerically in terms

of their LogP values. In the case of the complexes of this study, the experimental LogP values of the complexes were not determined, but the calculated LogP (cLogP), values have been calculated of the free ligands using Chem Draw software. Generally the larger the LogP value the greater the lipophilicity of the compound. A list of cLogP values for the free ligands can be seen in Table 6.

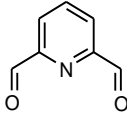
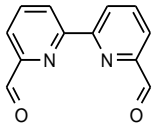
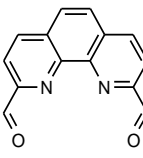
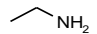
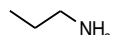
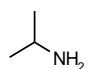
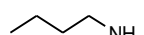
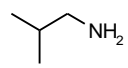
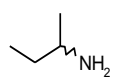
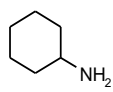
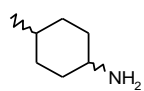
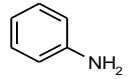
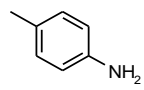
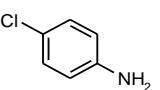
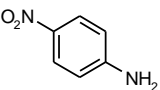
The second part of the subtle structural changes was by making the tail groups aromatic and changing different substituents on the aromatic ring to alter both steric and electronic properties of the ligands and again to impose the same effects as those designed for the aliphatic tail groups. The steric, electronic and solubility properties of the ligands could be altered by simply placing various groups in different positions of the rings and also perhaps adding multiple groups to the rings. In this study only *p*-monofunctionalised anilines were utilised and therefore a systematic series was obtained. All these structural changes are also depicted in Figure 11.

**Figure 11.** Influence of Structural Changes on Complex Chemistry

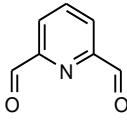
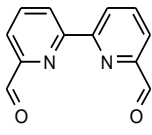
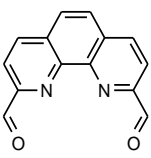
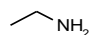
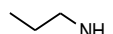
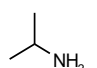
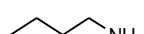
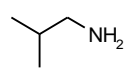
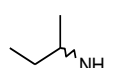
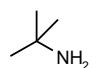
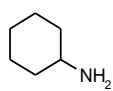
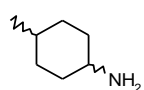
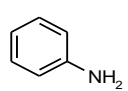
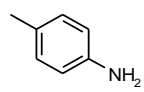
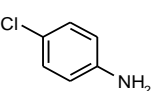
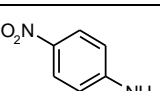




**Table 5.** Matrix of ‘Head’ and ‘Tail’ groups with ligand abbreviations.

			
	<b>L<sup>1</sup>Et</b>	<b>L<sup>2</sup>Et</b>	<b>L<sup>3</sup>Et</b>
	<b>L<sup>1</sup>Pr<sup>n</sup></b>	<b>L<sup>2</sup>Pr<sup>n</sup></b>	<b>L<sup>3</sup>Pr<sup>n</sup></b>
	<b>L<sup>1</sup>Pr<sup>i</sup></b>	<b>L<sup>2</sup>Pr<sup>i</sup></b>	<b>L<sup>3</sup>Pr<sup>i</sup></b>
	<b>L<sup>1</sup>Bu<sup>n</sup></b>	<b>L<sup>2</sup>Bu<sup>n</sup></b>	<b>L<sup>3</sup>Bu<sup>n</sup></b>
	<b>L<sup>1</sup>Bu<sup>i</sup></b>	<b>L<sup>2</sup>Bu<sup>i</sup></b>	<b>L<sup>3</sup>Bu<sup>i</sup></b>
	<b>L<sup>1</sup>Bu<sup>t</sup></b>	<b>L<sup>2</sup>Bu<sup>t</sup></b>	<b>L<sup>3</sup>Bu<sup>t</sup></b>
	<b>L<sup>1</sup>Cy</b>	<b>L<sup>2</sup>Cy</b>	<b>L<sup>3</sup>Cy</b>
	<b>L<sup>1</sup>CyMe</b>	<b>L<sup>2</sup>CyMe</b>	<b>L<sup>3</sup>CyMe</b>
	<b>L<sup>1</sup>Ph</b>	<b>L<sup>2</sup>Ph</b>	<b>L<sup>3</sup>Ph</b>
	<b>L<sup>1</sup>PhMe</b>	<b>L<sup>2</sup>PhMe</b>	<b>L<sup>3</sup>PhMe</b>
	<b>L<sup>1</sup>PhCl</b>	<b>L<sup>2</sup>PhCl</b>	<b>L<sup>3</sup>PhCl</b>
	<b>L<sup>1</sup>PhNO<sub>2</sub></b>	<b>L<sup>2</sup>PhNO<sub>2</sub></b>	<b>L<sup>3</sup>PhNO<sub>2</sub></b>

**Table 6.** List of cLogP values for the designed ligands obtained using an algorithm in ChemDraw Ultra 9.0. <sup>118</sup>

			
	<b>1.73</b>	<b>2.01</b>	<b>2.51</b>
	<b>2.79</b>	<b>2.71</b>	<b>3.57</b>
	<b>2.43</b>	<b>3.07</b>	<b>3.2</b>
	<b>3.86</b>	<b>4.14</b>	<b>4.63</b>
	<b>3.49</b>	<b>3.77</b>	<b>4.26</b>
	<b>3.49</b>	<b>3.77</b>	<b>4.26</b>
	<b>3.13</b>	<b>3.4</b>	<b>3.9</b>
	<b>4.79</b>	<b>5.07</b>	<b>5.56</b>
	<b>5.77</b>	<b>6.05</b>	<b>6.55</b>
	<b>3.19</b>	<b>3.46</b>	<b>3.96</b>
	<b>4.11</b>	<b>4.38</b>	<b>4.88</b>
	<b>4.86</b>	<b>5.14</b>	<b>5.64</b>
	<b>3.95</b>	<b>4.23</b>	<b>4.72</b>

## 2. Experimental

### 2.1. Chemical Methods

#### 2.1.1. Reagents

Reagents employed were used as supplied, unless otherwise stated and were of general purpose reagent (GPR) grade. Aniline and cyclohexylamine were distilled prior to use.

#### 2.1.2. Starting Materials

Origins and purities of reagents used in the synthesis of organic precursor compounds are summarised in Table 7.

**Table 7.** Origin and estimated purity of reagents used in synthesis of compounds.

<b>Compound</b>	<b>Source</b>	<b>Purity/Concentration</b>
Ni : Al alloy	Avocado	50:50
2-amino-6-methylpyridine	Aldrich	98 %
Neocuproine hemihydrate	Avocado	98 %
Pyridine-2,6-dimethanol	Avocado	98 %
Ethylamine	Aldrich	98 %
<i>n</i> -propylamine	Aldrich	98 %
<i>i</i> -propylamine	Aldrich	98 %
<i>n</i> -butylamine	Aldrich	98 %
<i>i</i> -butylamine	Aldrich	98 %
R/S <i>sec</i> -butylamine	Aldrich	98 %
<i>t</i> -butylamine	Aldrich	98 %

Cyclohexylamine	Aldrich	98 %
<i>cis/trans-p</i> -methylcyclohexylamine	Aldrich	98 %
aniline	Aldrich	98 %
<i>p</i> -methylaniline	Aldrich	98 %
<i>p</i> -chloroaniline	Aldrich	98 %
<i>p</i> -nitroaniline	Aldrich	98 %
2-aminobenzimidazole	Aldrich	98%
RuCl <sub>3</sub> .x H <sub>2</sub> O	Aldrich	97%
CoCl <sub>2</sub> .6H <sub>2</sub> O	Aldrich	98 %
CoBr <sub>2</sub>	Aldrich	98%
Co(NCS) <sub>2</sub> .xH <sub>2</sub> O	Aldrich	96%
Co(NO <sub>3</sub> ) <sub>2</sub> .6H <sub>2</sub> O	Aldrich	98%
Co(AcO) <sub>2</sub> .4H <sub>2</sub> O	Aldrich	98%
Co(BF <sub>4</sub> ) <sub>2</sub> .6H <sub>2</sub> O	Aldrich	99%
NiCl <sub>2</sub> .6H <sub>2</sub> O	Aldrich	98 %
Ni(AcO) <sub>2</sub> .4H <sub>2</sub> O	Aldrich	98%
CuCl <sub>2</sub> .2H <sub>2</sub> O	Aldrich	98 %
Cu(NO <sub>3</sub> ) <sub>2</sub> .3H <sub>2</sub> O	Aldrich	98%
CuBr <sub>2</sub> .2H <sub>2</sub> O	Aldrich	98 %
Cu(BF <sub>4</sub> ) <sub>2</sub>	Aldrich	98 %
ZnCl <sub>2</sub>	Aldrich	98 %
Zn(NO <sub>3</sub> ) <sub>2</sub> .6H <sub>2</sub> O	Aldrich	98%
Zn(AcO) <sub>2</sub> .2H <sub>2</sub> O	Aldrich	98%
AgBF <sub>4</sub>	Aldrich	98%

### 2.1.3. Preparation of Raney Nickel

Raney-nickel was prepared by dissolution of aluminium in a nickel-aluminium alloy (50:50), with aqueous sodium hydroxide. The method was carried out by a developed procedure as written in Vogle's, 'Textbook of Practical Organic Chemistry'.<sup>119</sup>

### 2.1.4. Solvents

General purpose grade solvents were used as supplied in most cases unless otherwise stated. Toluene was dried by standing over activated 5 Å molecular sieves.<sup>120</sup> 1,4-dioxane was predried over CaH<sub>2</sub> and then distilled from sodium/benzophenone under dry nitrogen and used within one week.<sup>121</sup> Ethanol was dried by distilling over magnesium and iodine under nitrogen, used immediately or stored over 3 Å molecular sieves under nitrogen.<sup>121</sup> Acetonitrile was dried by distilling over P<sub>2</sub>O<sub>5</sub> under nitrogen used immediately or stored under nitrogen.<sup>122</sup> In all cases the initial forerun (*ca.* 5 %) was rejected.

### 2.1.5. Instrumental Methods

#### 2.1.5.1. Infrared Spectroscopy (IR)

IR spectra of solid samples were recorded as KBr plates and spectra of liquids were obtained as capillary films using NaCl plates. Spectra were recorded with a Nicolet 140 FTIR spectrophotometer in the range 4000 - 400 cm<sup>-1</sup>.

### 2.1.5.2. Nuclear Magnetic Resonance Spectroscopy (NMR)

$^1\text{H}$  and  $^{13}\text{C}$ [ $^1\text{H}$ ] NMR spectra were recorded at 270 and 68 MHz, respectively, on a JEOL GX270 spectrometer, or at 600 and 170 MHz, respectively, on a JEOL ECA600 spectrometer. Chemical shifts were referenced to tetramethylsilane (TMS), as an internal standard (0 ppm), or via the residual proton impurity of the deuterated solvent. Deuterated solvents were obtained from Goss Scientific Instruments. For all spectra  $^1\text{H}$  and  $^{13}\text{C}$  typically 10-20 mg of sample was dissolved in 0.7 ml of the appropriate deuterated solvent, the solution was filtered if dissolution was incomplete. The spectra were recorded at ambient probe temperature (293 K) unless otherwise stated.

For diamagnetic compounds standard JEOL Delta  $^1\text{H}$  and  $^{13}\text{C}$  experiments and processing was employed. For paramagnetic compounds,  $^1\text{H}$  spectra were obtained with a scan range between -50 – 250 ppm, 64 K datapoints, 16 scans, and a relaxation delay of 100 ms.

The following notation is used for the  $^1\text{H}$  NMR spectral splitting patterns: singlet (s), doublet (d), triplet (t), multiplet (m), broad (b).

### 2.1.5.3. Magnetic Susceptibility

Magnetic susceptibilities were obtained according to the NMR method described by Evans.<sup>123</sup> A solution of the compound (ca. 3 mg), in a mixture of a suitable deuterated solvent (in our case methanol- $d_4$  or  $\text{D}_2\text{O}$  was used), and *t*-butylalcohol (95/5 v/v) as reference was prepared in a 1.0 ml volumetric flask. A portion of this solution was transferred into a Wilmad 517-insert co-axial NMR tube and was placed into a Wilmad

517 (5 mm) NMR tube containing the deuterated solvent / *t*-butylalcohol (95/5) mixture. The chemical shift difference of the *t*-butylalcohol signal between the inner and the outer tubes was measured at ambient probe temperature. From this difference in the chemical shift the molar susceptibility ( $\chi_M$ ) and the magnetic moment ( $\mu_{eff}$ ) can be calculated with Equation 1 and Equation 2 (given in S.I. units).

**Equation 1**

$$\chi_M = \frac{3\Delta f}{1000fc}$$

**Equation 2**

$$\mu_{eff} = \sqrt{\frac{3k}{N_0\mu_0\mu_B} T \chi_M} = 798\sqrt{T \chi_M}$$

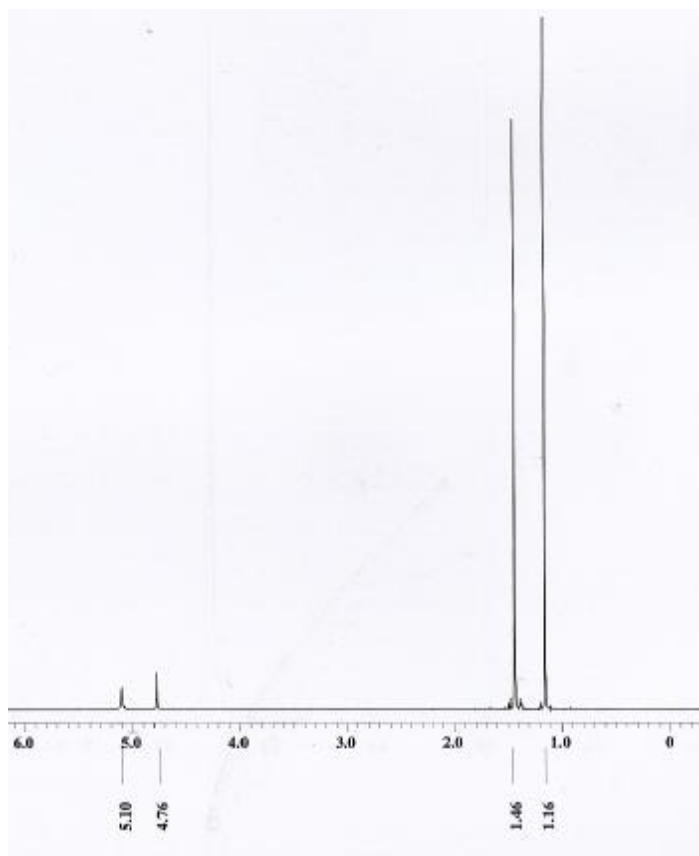
Where  $\chi_M$ : is the molar susceptibility of the sample in  $\text{m}^3 \text{mol}^{-1}$ ,  $\Delta f$ : is the difference in the chemical shift of the reference protons in Hz,  $c$ : is the concentration of the sample in  $\text{mol dm}^{-3}$ ,  $f$ : is the magnetic frequency of the spectrometer in Hz,  $T$ : is the temperature in K,  $k$ : is the Boltzman constant,  $N_0$ : is Avagadros number,  $\mu_0$ : is the magnetic constant and  $\mu_B$ : is the Bohr magneton.

As an example the magnetic susceptibility determination of  $[\text{CoCl}_2(\text{L}^1\text{Ph})]$  is described below:

A solution of  $[\text{CoCl}_2(\text{L}^1\text{Ph})]$  (3.53mg, 8.5mM), in  $\text{D}_2\text{O}/t\text{BuOH}$  (95:5), was placed into the co-axial insert which was then placed inside the NMR tube containing  $\text{D}_2\text{O}/t\text{BuOH}$

(95:5). The  $^1\text{H}$  NMR spectrum was obtained at a frequency,  $f$  of 270 MHz, and a probe temperature,  $T$  of 15.9 °C (288.9 K) and afforded a shift,  $\Delta f$  between methyl signals of *t*BuOH of 75.645 Hz (See Figure 12). After inputting the data into equation 1 to give the molar susceptibility,  $\chi_M$  ( $9.89 \times 10^{-8} \text{ m}^3 \text{ mol}^{-1}$ ). After applying  $\chi_M$  to equation 2, the magnetic susceptibility,  $\mu_{\text{eff}}$  is thus obtained ( $4.27 \mu_B$ ).

**Figure 12.**  $^1\text{H}$  NMR spectrum (270 MHz) of *t*BuOH observed when running the magnetic susceptibility determination of  $[\text{CoCl}_2(\text{L}^1\text{Ph})]$ .



#### 2.1.5.4. Mass Spectrometry (MS)

Electron impact mass spectra (EI-MS), were obtained for organic compounds using a AEI MS902 operated by Andrew Healey at the University of Bradford. Electrospray



ionisation mass spectra (ESI-MS), obtained for inorganic compounds, were recorded on a Waters, Quadrupole LC/MS-MS by Andrew Healey at the University of Bradford.

#### **2.1.5.5. Single Crystal X-Ray Diffraction**

Single crystals of compounds were generally grown by slow vapour diffusion of diethyl ether into a saturated acetonitrile solution of the complex, unless otherwise stated. The crystals were mounted and reflection data was recorded on a STOE STADI-4 diffractometer or Bruker Apex X8 diffractometer. X-ray data collection, structure solution and refinement is described in section 6.2.

#### **2.1.5.6. CHN Microanalysis**

Analysis for carbon, hydrogen and nitrogen content of samples was carried out in duplicate at the School of Pharmacy, University of London.

#### **2.1.5.7. Melting Points**

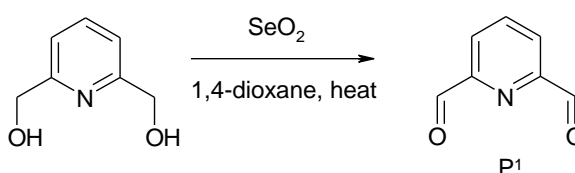
Melting points of solid products were recorded on a Kopfler hotstage microscope between glass slides and are uncorrected.



## 2.1.6. Preparation of Precursor Compounds

### 2.1.6.1. Preparation of pyridine-2,6-dicarbaldehyde, P<sup>1</sup>

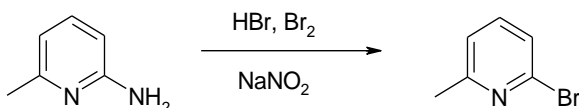
Pyridine-2,6-dicarbaldehyde was prepared through an adaptation of a method developed by Jerchel *et al.*,<sup>124</sup> utilising selenium dioxide to controllably oxidise pyridine-2,6-dimethanol to the desired dicarbaldehyde.



Pyridine-2,6-dimethanol (5.3 g, 38.0 mmol), and dry 1,4-dioxane (80ml), were placed in a 250 ml round bottomed flask along with selenium dioxide (5.7 g, 50.6 mmol), and the mixture was refluxed for 4 hours, during which time the colour of the mixture changed to a brick red solution and finally to a green/yellow solution, with a solid black selenium precipitate. The hot solution was filtered under gravity to remove the precipitated selenium and solvent was removed from the filtrate with a rotary evaporator to leave a green solid residue. The solid was recrystallised from chloroform / petroleum ether (bp 40-60). The product was isolated at the pump and dried in vacuo to give off white crystals of P<sup>1</sup> (3.74 g, 72 %), mp 132-134 °C (lit.,<sup>124</sup> 132-134 °C), m/z 135 (M)<sup>+</sup>, 107 (M-CO)<sup>+</sup>, 78 (M-(CO)(CHO))<sup>+</sup>,  $\nu_{\max}$  cm<sup>-1</sup> 3150, 3100, 3025 (aromatic C-H), 2875 (aldehyde C-H), 1720 (C=O), 1695 (C=N);  $\delta_{\text{H}}$  (270 MHz, CDCl<sub>3</sub>) 10.19 (HC=O, 2H, s); 8.17 (H<sup>3/5</sup>, 2H, d, J = 8.1 Hz); 8.07 (H<sup>4</sup>, 1H, t, J = 8.1 Hz).

### 2.1.6.2. Preparation of 2-bromo-6-methyl pyridine

2-bromo-6-methyl pyridine was prepared from 2-amino-6-methyl pyridine by a Sandmeyer reaction adapted from the method given by Vogtle *et al.*<sup>125</sup>

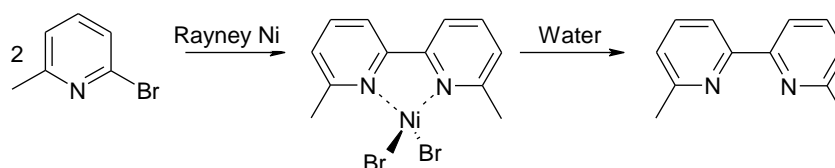


To a three necked flask fitted with mechanical stirrer and dropping funnel was added hydrobromic acid (80 ml), and then crushed 2-amino-6-methyl pyridine (15.1 g, 0.14 mmol), was added with care. The solution was stirred and cooled to below  $-15^\circ\text{C}$  with an IMS / dry ice bath. Bromine (24 ml, 0.15 mol) was added dropwise over *Ca.* 45 mins, during which time the reaction mixture became increasingly viscous and deep orange in colour. After the addition of bromine was complete, sodium nitrite (27 g, 0.47 mmol), in water (40 ml), was added dropwise whilst the temperature was maintained below  $-10^\circ\text{C}$ . During the addition, bromine gas was evolved, and the reaction mixture became a dark brown colour. Once the evolution of bromine gas had ceased (*Ca.* 30 mins), sodium hydroxide (60 g, 1.5 mol), in water (100 ml) was added over 1 h, whilst maintaining the temperature of the mixture below  $0^\circ\text{C}$ . At this stage the mixture became a darker orange colour. The orange solution was allowed to warm to room temperature and the product was then extracted from the mixture with diethyl ether (3 x 200 ml), the organic extracts were combined and washed with water (2 x 100 ml), then dried over magnesium sulphate and the solvent was removed using a rotary evaporator at  $40^\circ\text{C}$ , to yield an orange / brown liquid. The resulting liquid was vacuum distilled to leave a colourless free flowing liquid (16.46 g, 68 %), bp (1.6-1.7 mmHg)  $50-54^\circ\text{C}$  (lit.,<sup>125</sup> 91

mmHg 46-49 °C),  $m/z$  171 ( $M$ )<sup>+</sup>, 173 ( $M+2$ )<sup>+</sup>, 92 ( $M-Br$ )<sup>+</sup>,  $\nu_{\max}$   $\text{cm}^{-1}$  3150, 3100 (aromatic C-H), 2990, 2950, 2900 (methyl C-H), 1650 (Ring breathing), 1595, 1560 (C=C),  $\delta_{\text{H}}$  (270 MHz,  $\text{CDCl}_3$ ) 7.41 ( $\text{H}^4$ , 1H, t,  $J = 8.1$  Hz); 7.27 ( $\text{H}^3$ , 1H, d,  $J = 8.1$  Hz); 7.08 ( $\text{H}^5$ , 1H, d,  $J = 8.1$  Hz); 2.52 ( $\text{CH}_3$ , 3H, s).

### 2.1.6.3. Preparation of 6,6'-dimethyl-2,2'-bipyridine

This preparation was developed by Breitmer and Rode.<sup>126</sup> and utilises finely divided nickel to complex to and displace bromine from 2-bromo-6-methyl pyridine, to form the 6,6'-dimethyl-2,2'-bipyridine nickel(II)bromide complex. The resulting nickel bromide complex is then hydrolysed to give the free bipyridine.

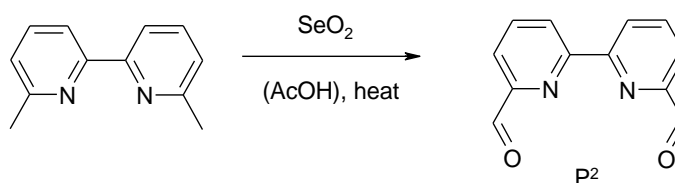


2-bromo-6-methyl pyridine (16.46 g, 95.7 mmol) was added dropwise over half an hour to a refluxing suspension of rayney-nickel (Ca. 8g), in dry toluene (100 ml). The mixture was refluxed for 22 hours whereupon a dark purple solid precipitated in a bright blue solution. The mixture was allowed to cool to room temperature and was then filtered under suction and washed with dry toluene (2 x 10 ml). The purple solid (6.7 g), was then added to water (200 ml), and was stirred and maintained at ca. 60 °C for 24 hours, after 2 hours of that time, the purple suspension turned to a dark green/ turquoise colour. The green suspension was then filtered at the pump to afford a very pale green filtrate. The solid was washed with DCM (3 x 30 ml), and the filtrate was extracted into DCM (3 x 75 ml) to give a beige coloured organic layer. The organic layer was dried over magnesium sulphate and the solvent removed on the rotary evaporator to leave a pale beige solid. The solid was recrystallised from petroleum spirit (bp 40-60 °C). The desired product was isolated at the pump as off white crystals (1.70 g, 19 %) mp 92-94 °C (lit.,<sup>125, 126</sup> 88-89 °C), m/z 184 (M)<sup>+</sup>, 169 (M-CH<sub>3</sub>)<sup>+</sup>,  $\nu_{\max}$  cm<sup>-1</sup> 3067 (aromatic C-H),

2975, 2969, 2932 (methyl C-H), 1573 (C=C), 1437, 1375 (methyl C-H bend),  $\delta_{\text{H}}$  (270 MHz,  $\text{CDCl}_3$ ) 8.17 ( $\text{H}^{3/3'}$ , 2H, d,  $J = 8.1$  Hz) 7.64 ( $\text{H}^{4/4'}$ , 2H, t,  $J = 8.1$  Hz) 7.11 ( $\text{H}^{5/5'}$ , 2H, d,  $J = 8.1$  Hz) 2.61 ( $\text{CH}_3$ , 6H, s).

#### 2.1.6.4. Attempted Preparation of 2,2'-bipyridine-6,6'-dicarbaldehyde, P<sup>2</sup> with Selenium Dioxide.

This procedure was carried out by a method previously developed by Newkome *et al*,<sup>127</sup> via a controlled oxidation with selenium dioxide, to the dicarbaldehyde.

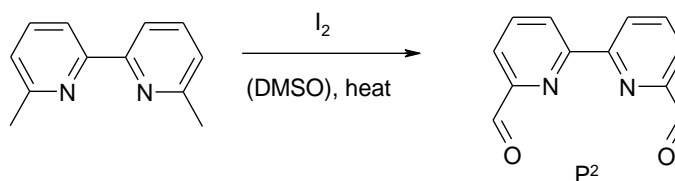


Selenium dioxide (2.6 g, 23.5 mmol), was placed in a 250 ml round bottomed flask with glacial acetic acid (100 ml). To the suspension was added 6,6'-dimethyl-2,2'-bipyridine (1.1 g, 5.7 mmol), and the mixture was refluxed for 24 hours, during which time the clear solution formed a green solution, with precipitated selenium in suspension. The hot mixture was filtered and the solvent was removed from the filtrate with a rotary evaporator, to leave an off-white powder. The powder was washed with cold methanol and treated by Soxhlet extraction with xylene to give a yellow solution. The solution was left to cool in the fridge overnight and crystals formed. The product was isolated at the pump as off white crystals (0.20 g, 20%), mp >230 °C (lit.,<sup>127</sup> 233-237 °C) m/z 212 (M)<sup>+</sup>, 184 (M-CO)<sup>+</sup>, 155 (M-(CO)(CHO))<sup>+</sup>,  $\nu_{\max}$  cm<sup>-1</sup> 3073 (aromatic C-H), 2855 (aldehyde C-H), 1703 (C=O); 1634 (C=N),  $\delta_{\text{H}}$  (600 MHz, CDCl<sub>3</sub>) 10.18 (2H, s, HC=O); 8.81 (H<sup>3/5</sup>, 2H, d, J = 6.2 Hz); 8.05 (H<sup>4</sup>, 2H, t, J = 6.2 Hz); 8.03 (H, 2H, d, J = 6.2 Hz).



### 2.1.6.5. Preparation of 2,2'-bipyridine-6,6'-dicarbaldehyde, P<sup>2</sup> with DMSO and Iodine.

This method was adapted from a general method for oxidation of methyl pyridines and picolines to the corresponding aldehydes.<sup>128</sup>



6,6'-dimethyl-2,2'-bipyridine (0.5 g, 2.8 mmol); was dissolved in DMSO ( 5 ml), in a 25 ml beaker. Iodine (1.42 g, 5.6 mmol) was added to the solution. The solution was then dropped into DMSO (50 ml), preheated to 130 °C. The mixture was then refluxed and stirred, where a vigorous exothermic reaction occurred with evolution of dimethyl sulphide. The mixture was held at reflux for 24 hours and left to cool to room temperature. Excess iodine was then destroyed by addition of a saturated aqueous sodium thiosulphate solution, until a pale yellow solution was obtained. Water was added to the solution to give a total volume of 250 ml and the solution was then extracted with dichloromethane (3 x 200 ml), washed with water (2 x 100 ml), dried over magnesium sulphate, filtered and finally the solvent removed on the rotary evaporator to yield a beige solid. The crude product was then crystallised by dichloromethane / petroleum ether bp 40-60°C to afford beige plates of P<sup>2</sup> ( 0.42 g, 71 %). mp >230 °C (lit.,<sup>127</sup> 233-237 °), m/z 212 (M)<sup>+</sup>; 184 (M-CO)<sup>+</sup>; 155 (M-(CO)(CHO))<sup>+</sup>, v<sub>max</sub> cm<sup>-1</sup> 3073 (aromatic C-H), 2855 (aldehyde C-H), 1703 (C=O), 1634

(C=N),  $\delta_{\text{H}}$  (600 MHz,  $\text{CDCl}_3$ ) 10.18 (2H, s, HC=O); 8.81 ( $\text{H}^{3/5}$ , 2H, d,  $J = 6.2$  Hz); 8.05 ( $\text{H}^4$ , 2H, t,  $J = 6.2$  Hz); 8.03 (H, 2H, d,  $J = 6.2$  Hz).

**Figure 13.** Crystal structure of 2,2'-bipyridine-6,6'-dicarbaldehyde,  $\text{P}^2$ .

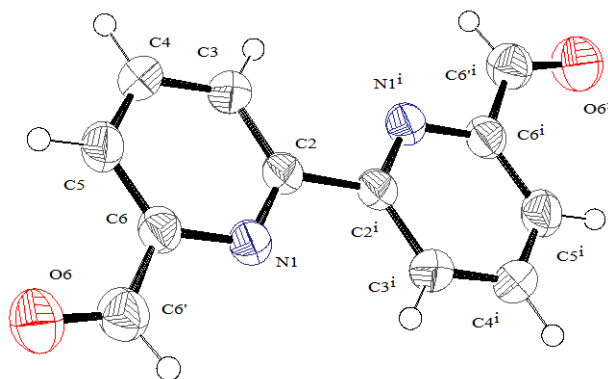
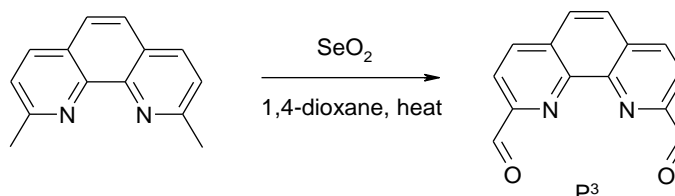


**Table 8.** X-ray structure and refinement parameters for  $\text{P}^2$ .

Compound	2,2'-bipyridine-6,6'-dicarbaldehyde
Chemical Formula	$\text{C}_{12}\text{H}_8\text{N}_2\text{O}_2$
Formula Weight	212.20
Crystal System	Monoclinic
Space Group	$P2_1/c_1$
$a / \text{\AA}$	8.2199 (4)
$b / \text{\AA}$	11.4334 (7)
$c / \text{\AA}$	5.5947 (3)
$\alpha / ^\circ$	90
$\beta / ^\circ$	109.896 (0)
$\gamma / ^\circ$	90
$V / \text{\AA}^3$	494.41 (0)
$T / \text{K}$	273 (2)
$Z$	2
$S$	0.760
No. unique data ( $R_{\text{int}}$ )	1476
No. measured reflections	17704

### 2.1.6.6. Preparation of 1,10-phenanthroline-2,9-dicarbaldehyde, P<sup>3</sup>

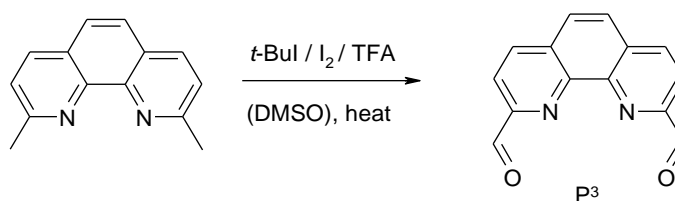
This method is an adaptation of a method described by Masood *et al.*<sup>129</sup>



Selenium dioxide (5.0 g, 45 mmol), was placed in a 500 ml round bottomed flask with 2,9-dimethyl-1,10-phenanthroline (2.50 g, 11.5 mmol), and 1,4-dioxane (200 ml). The mixture was stirred and refluxed for 4 hours, during which time the solution went through a series of colour changes, from a white precipitate to orangey pink and finally to a yellow solution with a suspended black precipitate of selenium. The mixture was filtered whilst hot to remove any selenium and the solvent was removed from the filtrate on the rotary evaporator to leave a green residue. The residue was dissolved in a minimum amount of DMF and left in the fridge for ~ 16 hours to precipitate any residual selenium. The cold solution was filtered and then crystallised from the DMF solution and water. The product was isolated at the pump as very fine needle-like, pale yellow crystals (1.90 g, 70 %). mp decomposes >230 °C (lit., 253 °C), *m/z* 236 (M)<sup>+</sup>; 208 (M-CO)<sup>+</sup>; 180 (M-2(CO))<sup>+</sup>.  $\nu_{\max}$  cm<sup>-1</sup> 3100, 3050, 3042 (aromatic C-H), 2852 (aldehyde C-H), 1702 (C=O),  $\delta_{\text{H}}$  (600 MHz, CDCl<sub>3</sub>) 10.55 (HC=O, 2H, s); 8.49 (H<sup>3/8</sup>, 2H, d, J = 8.1 Hz); 8.39 (H<sup>4/7</sup>, 2H, d, J = 8.1 Hz); 8.04 (H<sup>5/6</sup>, 2H, s).

### 2.1.6.7. Preparation of 1,10-phenanthroline-2,9-dicarbaldehyde, P<sup>3</sup> with DMSO and Iodine.

The method used in the formation of P<sup>3</sup> using DMSO and iodine was a method adapted from the previous method used for both P<sup>1</sup> and P<sup>2</sup>. This method was first carried out by Daran *et al.*,<sup>130</sup> and utilizes *t*-butyliodide as a reaction initiator.

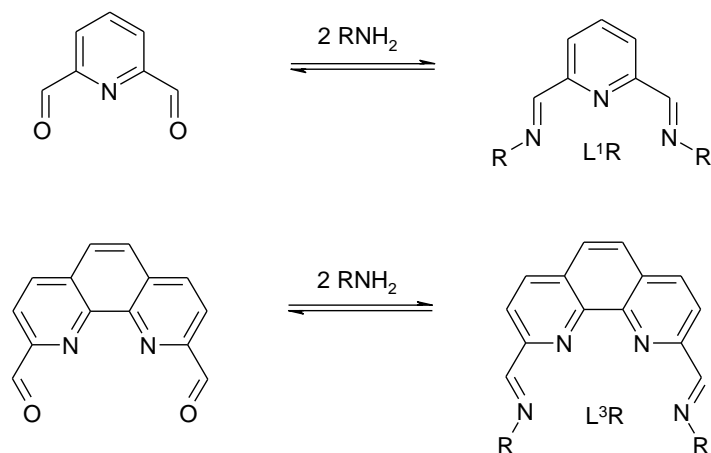


Iodine (7.02 g, 27.65 mmol, 2 equiv.), was added to a solution of neocuproine hemihydrate (2,9-dimethyl-1,10-phenanthroline, 3.0 g, 13.8 mmol, 1 equiv.), dissolved in DMSO (200 ml). The brown solution was stirred for 5 min at room temperature before 2-iodo-2-methylpropane (*t*-BuI, 3.42 ml, 28.7 mmol, 2.7 equiv.) was added. Finally TFA (3 ml, 38.94 mmol, 2.8 equiv.), was slowly added to the dark brown solution by syringe and the mixture was stirred under reflux for 2 h (148 °C). After this, the solution was allowed to cool to room temperature. The excess of iodine was neutralized by slow addition of a solution of Na<sub>2</sub>S<sub>2</sub>O<sub>3</sub> (16 g, 120 ml), and the dark precipitate formed was removed by filtration. The pH of the solution was then adjusted to pH = 4-5 by addition of aqueous NaHCO<sub>3</sub> (10%), extracted with dichloromethane (3 x 250 ml), and washed with water (1 x 250 ml). The organic phases were combined and dried over MgSO<sub>4</sub>, concentrated on the rotary evaporator and the resulting pale residue was washed with diethyl ether to remove traces of DMSO. The crude product was recrystallised from DMF / water, filtered at the pump and dried under vacuum to give

the pure compound (1.62 g, 50 %), mp decomposes  $>230$  °C, (lit., <sup>130</sup> 253 °C), m/z 236 (M)<sup>+</sup>; 208 (M-CO)<sup>+</sup>; 180 (M-2(CO))<sup>+</sup>,  $\nu_{\max}$  cm<sup>-1</sup> 3100, 3050, 3042 (aromatic C-H), 2852 (aldehyde C-H), 1702 (C=O),  $\delta_{\text{H}}$  (600 MHz, CDCl<sub>3</sub>) 10.55 (HC=O, 2H, s); 8.49 (H<sup>3/8</sup>, 2H, d, J = 8.1 Hz); 8.39 (H<sup>4/7</sup>, 2H, d, J = 8.1 Hz); 8.04 (H<sup>5/6</sup>, 2H, s).

## 2.1.7. Preparation of Ligands

### 2.1.7.1. General Procedure for the Preparation of Schiff base Ligands $L^1R$ and $L^3R$



The preparation of the free Schiff base ligands, was carried out by two methods depending on the primary amine used. All methods with volatile primary amines (i.e. alkyl amines) were carried out by refluxing the dicarbaldehyde  $P^1$  or  $P^3$  (1.85 mmol), with 2.2 equivalents of the appropriate primary amine (4.1 mmol), in anhydrous ethanol (Ca. 25 ml), over powdered 3Å molecular sieves (~1g). For aromatic amines (i.e. non volatile amines) LR was prepared by refluxing the dicarbaldehyde  $P^1$  or  $P^3$  (1.85 mmol), with 2 equivalents of the appropriate primary amine (3.7 mmol), in anhydrous ethanol (Ca. 25 ml), over powdered 3Å molecular sieves. These methods were taken from a procedure by Lions *et al.*<sup>131</sup> and modified to give better yields and cleaner products. The loss of  $P^1$  was monitored by TLC under 254nm UV light, ( $R_f$  0.45, DCM:MeOH, 95:5), every 15 minutes (spots for intermediate and product stuck to the baseline). When the spot for  $P^1$  was no longer observed the reaction time was noted, and the mass was allowed to reflux for the same time again to ensure full conversion for this consecutive

reaction. For P<sup>3</sup> compounds, P<sup>3</sup> did not elute on the TLC plate under various conditions, and so the reactions were allowed to proceed at reflux for 8 hours. Schiff base ligands with aryl tail groups tended to form crystalline solids, whereas ones with alkyl tail groups tended to form viscous, yellow to tan oils. The desired pure compounds were isolated by either:-

Where the Schiff base formed an oil, the product was isolated by filtering the warm suspension into a 50ml round bottomed flask, any residual product on the powdered sieves was washed into the flask with fresh dry ethanol (2 x 10ml). The solvent and any residual amine was removed by rotary evaporation at 40 °C to constant mass.

Where the Schiff base formed a crystalline solid, the product was isolated by filtering the hot suspension into a 50ml round bottomed flask, any residual product on the powdered sieves was washed into the flask with hot fresh dry ethanol (2 x 10ml). The mass was concentrated to saturation point by solvent removal on the rotary evaporator at 40 °C. After cooling, the crystalline product was isolated by filtration and dried *in vacuo* over P<sub>2</sub>O<sub>5</sub> for 24 hours.

The Schiff base compounds synthesized along with their analyses are given in Table 9 and Table 10 for L<sup>1</sup>R ligands and Table 11 for L<sup>3</sup>R ligands.

**Table 9.** Characterisation data for Schiff bases L<sup>1</sup>R.

Compound	Colour	Yield (solvent)	m.p.	Infra-red Spectrum (KBr) $\nu_{\max}$ cm <sup>-1</sup>	Mass Spectrum	<sup>1</sup> H NMR
(L <sup>1</sup> Et)	Tan	98%	Oil	3063w (aromatic C-H), 2968s, 2931s, 2925s (sp <sup>3</sup> C-H), 2870s (aldimine C-H), 1644s (aldimine C=N); 1591s, 1567s, 1458s (ring stretching)	ESI+ (MeOH); m/z 222 (M+ MeOH) <sup>+</sup>	$\delta_{\text{H}}$ (270 MHz, CDCl <sub>3</sub> ) 8.42 (2H, s, HC=N), 7.98 (H <sup>3/5</sup> , 2H, d, J = 8.1 Hz), 7.79 (H <sup>4</sup> , 1H, t, J = 8.1 Hz), 3.71 (H <sup>a</sup> , 4H, q, J = 7.2 Hz), 1.32 (H <sup>b</sup> , t, 6H, J = 7.2 Hz)
(L <sup>1</sup> Pr <sup>n</sup> )	Tan	97%	Oil	3059w (aromatic C-H), 2974s, 2931s, 2925s (sp <sup>3</sup> C-H), 2867s (aldimine C-H), 1644s (aldimine C=N) 1590s, 1570s, 1452s (ring stretching)	EI; m/z 217 (M) <sup>+</sup> , 188 (M-C <sub>2</sub> H <sub>5</sub> ) <sup>+</sup> , 174 (M-C <sub>3</sub> H <sub>7</sub> ) <sup>+</sup>	$\delta_{\text{H}}$ (270 MHz, CDCl <sub>3</sub> ) 8.40 (2H, s, HC=N), 7.99 (H <sup>3/5</sup> , 2H, d, J = 7.7 Hz), 7.78 (H <sup>4</sup> , 1H, t, J = 7.9 Hz), 3.64 (H <sup>a</sup> , 4H, t, J = 6.9 Hz), 1.76 (H <sup>b</sup> , m, 4H, J = 7.2 Hz), 0.95 (H <sup>c</sup> , t, 6H, J = 7.4 Hz)
(L <sup>1</sup> Pr <sup>i</sup> )	Tan	99%	Oil	3058m (aromatic C-H), 2968s, 2931s, 2925s (sp <sup>3</sup> C-H), 2868s (aldimine C-H), 1644s (aldimine C=N), 1590s, 1564s, 1458s (ring stretching)	ESI+ (MeOH); m/z 218 (M) <sup>+</sup>	$\delta_{\text{H}}$ (270 MHz, CDCl <sub>3</sub> ) 8.46 (2H, s, HC=N), 8.00 (H <sup>3/5</sup> , 2H, d, J = 7.7 Hz), 7.76 (H <sup>4</sup> , 1H, t, J = 8.0 Hz), 3.64 (H <sup>a</sup> , 2H, m, J = 6.3 Hz), 1.27 (H <sup>b</sup> , d, 12H, J = 6.3 Hz)
(L <sup>1</sup> Bu <sup>n</sup> )	Tan	96%	Oil	3061m (aromatic C-H), 2962s, 2925s (sp <sup>3</sup> C-H), 2870s (aldimine C-H), 1653s (aldimine C=N), 1586s, 1573s, 1462s (ring stretching)	EI; m/z 245 (M) <sup>+</sup> , 202 (M-C <sub>3</sub> H <sub>7</sub> ) <sup>+</sup>	$\delta_{\text{H}}$ (270 MHz, CDCl <sub>3</sub> ) 8.40 (2H, s, HC=N), 7.98 (H <sup>3/5</sup> , 2H, d, J = 7.8 Hz), 7.78 (H <sup>4</sup> , 1H, t, J = 7.8 Hz), 3.67 (H <sup>a</sup> , 4H, t, J = 7.2 Hz), 1.69 (H <sup>b</sup> , m, 4H, J = 7.2 Hz), 1.38 (H <sup>c</sup> , m, 4H, J = 7.2 Hz), 0.93 (H <sup>d</sup> , t, 6H, J = 7.2 Hz)
(L <sup>1</sup> Bu <sup>2</sup> )	Tan	99%	Oil	3061m (aromatic C-H), 2968s, 2931s (sp <sup>3</sup> C-H), 2870s (aldimine C-H), 1647s (aldimine C=N), 1586s, 1573s, 1462s (ring stretching)	ESI+ (MeOH); m/z 246 (M) <sup>+</sup>	$\delta_{\text{H}}$ (270 MHz, CDCl <sub>3</sub> ) 8.40 (2H, s, HC=N), 8.03 (H <sup>3/5</sup> , 2H, d, J = 7.7 Hz), 7.76 (H <sup>4</sup> , 1H, t, J = 8.0 Hz), 3.30 (H <sup>a</sup> , 2H, m, J = 6.4 Hz), 1.62 (H <sup>b</sup> , m, 4H, J = 7.1 Hz), 1.25 (H <sup>d</sup> , d, 6H, J = 6.3 Hz), 0.84 (H <sup>c</sup> , t, 6H, J = 7.4 Hz)
(L <sup>1</sup> Bu <sup>i</sup> )	Tan	98%	Oil	3055m (aromatic C-H), 2956s, 2925s, 2900s (sp <sup>3</sup> C-H), 2869 (aldimine C-H), 1654s (aldimine C=N), 1586s, 1567s, 1468s (ring stretching)	ESI+ (MeOH); m/z 246 (M) <sup>+</sup>	$\delta_{\text{H}}$ (270 MHz, CDCl <sub>3</sub> ) 8.36 (2H, s, HC=N), 8.00 (H <sup>3/5</sup> , 2H, d, J = 7.9 Hz), 7.78 (H <sup>4</sup> , 1H, t, J = 7.5 Hz), 3.48 (H <sup>a</sup> , 4H, d, J = 6.6 Hz), 2.03 (H <sup>b</sup> , m, 2H, J = 6.7 Hz), 0.95 (H <sup>c</sup> , d, 12H, J = 6.7 Hz)



**Table 10.** Characterisation data for Schiff bases L<sup>1</sup>R

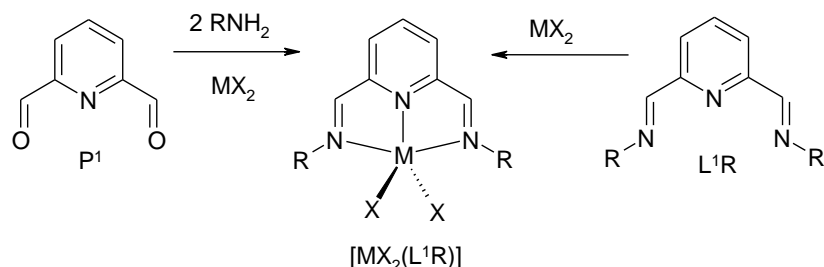
Compound	Colour	Yield (solvent)	m.p.	Infra-red Spectrum (KBr) $\nu_{\max}$ cm <sup>-1</sup>	Mass Spectrum	<sup>1</sup> H NMR
(L <sup>1</sup> Bu <sup>1</sup> )	Tan	97%	Oil	3060m (aromatic C-H), 2960s, 2925s (sp <sup>3</sup> C-H), 2866 (aldimine C-H), 1655s (aldimine C=N), 1587s, 1567s, 1466s (ring stretching)	ESI+ (MeOH); m/z 246 (M) <sup>+</sup>	$\delta_{\text{H}}$ (270 MHz, CDCl <sub>3</sub> ) 8.39 (2H, s, HC=N), 8.04 (H <sup>3/5</sup> , 2H, d, J = 7.67 Hz), 7.76 (H <sup>d</sup> , 1H, t, J = 7.36 Hz), 1.31 (H <sup>a</sup> , 18H, s)
(L <sup>1</sup> Cy)	Tan	98%	Oil	3051w (aromatic C-H), 2950s, 2925s (sp <sup>3</sup> C-H), 2864s (aldimine C-H), 1647s (aldimine C=N), 1590s, 1566s, 1455s (ring stretching)	ESI+ (MeOH); m/z 298 (M) <sup>+</sup>	$\delta_{\text{H}}$ (270 MHz, CDCl <sub>3</sub> ) 8.42 (2H, s, HC=N), 8.02 (H <sup>3/5</sup> , 2H, dd, J = 8.1 Hz), 7.75 (H <sup>d</sup> , 1H, t, J = 8.1 Hz), 3.29 (H <sup>a</sup> , 2H, m), 1.35-1.85 (H <sup>b</sup> , mm, 20H)
(L <sup>1</sup> CyMe)	Tan	97%	Oil	3049w (aromatic C-H), 2950s, 2926s (sp <sup>3</sup> C-H), 2861s (aldimine C-H), 1647s (aldimine C=N), 1591s, 1567s, 1456s (ring stretching)	ESI+ (MeOH); m/z 326 (M) <sup>+</sup>	$\delta_{\text{H}}$ (270 MHz, CDCl <sub>3</sub> ) 8.42 (2H, s, HC=N), 8.04 (H <sup>3/5</sup> , 1H, d, J = 7.8 Hz), 7.79 (H <sup>3/5 iso</sup> , 1H, d, J = 7.8 Hz), 7.75 (H <sup>d</sup> , 1H, t, J = 7.4 Hz), 3.46 (H <sup>a</sup> , 1H, m), 3.25 (H <sup>a iso</sup> , 1H, m), 1.85-1.50 (H <sup>b/c</sup> , mm, 16H), 1.15-1.00 (H <sup>d</sup> , 2H, m), 0.98 (H <sup>e</sup> , 3H, d, J = 6.6 Hz), 0.91 (H <sup>e iso</sup> , 3H, d, J = 6.6 Hz)
(L <sup>1</sup> Ph)	Yellow	80 % (EtOH)	108-110 °C	3070m, 3050m, 3030m, 2993m (aromatic C-H), 2870m (aldimine C-H), 1625m (aldimine C=N), 1597m, 1585m, 1480m (ring stretching)	EI; m/z 285 (M) <sup>+</sup> , 192 (M-C <sub>6</sub> H <sub>7</sub> N) <sup>+</sup>	$\delta_{\text{H}}$ (270 MHz, CDCl <sub>3</sub> ) 8.68 (HC=N, 2H, s), 8.29 (H <sup>3/5</sup> , 2H, d, J = 7.6 Hz), 7.93 (H <sup>d</sup> , 1H, t, J = 8.1 Hz), 7.42 (H <sup>b</sup> , 4H, tt, 7.6 Hz) 7.29 (H <sup>a/c</sup> , 6H, m)
(L <sup>1</sup> PhMe)	Pale Yellow	95 % (EtOH)	181-183 °C	3080m, 3050m, 3030m, 2999m (aromatic C-H) 2907m, 2882m (methyl C-H), 2863m (aldimine C-H), 1628m (aldimine C=N), 1575m, 1505s, 1468m (ring stretching)	EI; m/z 313 (M) <sup>+</sup> , 298 (M-CH <sub>3</sub> ) <sup>+</sup> , 222 (M-C <sub>7</sub> H <sub>7</sub> ) <sup>+</sup>	$\delta_{\text{H}}$ (600 MHz, CDCl <sub>3</sub> ) 8.69 (HC=N, 2H, s), 8.26 (H <sup>3/5</sup> , 2H, d, J = 7.2 Hz), 7.91 (H <sup>d</sup> , 1H, t, J = 7.8 Hz), 7.25 (H <sup>a</sup> , 4H, d, 7.8 Hz), 7.22 (H <sup>b</sup> , 4H, d, 8.4 Hz), 2.38 (H <sup>c</sup> , 6H, s)
(L <sup>1</sup> PhCl)	Pale Green	97 % (EtOH)	198-200 °C	3086m, 3050m, 3005m, 2969m, 2919m (aromatic C-H); 2869m (aldimine C-H); 1628m (aldimine C=N); 1586, 1567, 1486 (ring stretching)	EI; m/z 355 (M+2) <sup>+</sup> , 353 (M) <sup>+</sup> , 318 (M-Cl) <sup>+</sup> , 242 (M-C <sub>6</sub> H <sub>4</sub> Cl) <sup>+</sup>	$\delta_{\text{H}}$ (600 MHz, CDCl <sub>3</sub> ) 8.64 (HC=N, 2H, s), 8.27 (H <sup>3/5</sup> , 2H, d, J = 7.6 Hz), 7.95 (H <sup>d</sup> , 1H, t, J = 9.6 Hz), 7.39 (H <sup>b</sup> , 4H, d, 7.9 Hz), 7.25 (H <sup>a</sup> , 4H, d, 7.9 Hz)

**Table 11.** Characterisation data for Schiff bases L<sup>3</sup>R.

Compound	Colour	Yield (solvent)	m.p.	Infra-red Spectrum (KBr) $\nu_{\max}$ cm <sup>-1</sup>	Mass Spectrum	<sup>1</sup> H NMR
(L <sup>3</sup> Bu <sup>n</sup> )	Colourless	90%	Oil	3057w, 3010w (aromatic C-H), 2953s, 2925s (sp <sup>3</sup> C-H), 2865s (aldimine C-H), 1646s (aldimine C=N), 1622m, 1578m, 1567m, 1515m, 1405m (ring stretching)	EI; m/z 346 (M) <sup>+</sup> , 303 (M-C <sub>3</sub> H <sub>7</sub> ) <sup>+</sup>	$\delta_{\text{H}}$ (270 MHz, CDCl <sub>3</sub> ) 8.85 (2H, s, HC=N), 8.42 (H <sup>3/8</sup> , 2H, d, J = 8.4 Hz), 8.31 (H <sup>4/7</sup> , 2H, d, J = 8.4 Hz), 7.86 (H <sup>5/6</sup> , 2H, s), 3.77 (H <sup>a</sup> , 4H, t, J = 7.2 Hz), 1.75 (H <sup>b</sup> , 4H, m, J = 7.2 Hz), 1.44 (H <sup>c</sup> , 4H, m, 7.7 Hz), 0.96 (H <sup>d</sup> , 6H, t, J = 7.4 Hz)
(L <sup>3</sup> Bu <sup>2</sup> )	Colourless	90%	Oil	3055w, 3012w (aromatic C-H), 2961s, 2925s (sp <sup>3</sup> C-H), 2868s (aldimine C-H), 1647s (aldimine C=N), 1620m, 1580m, 1566m, 1514m, 1402m (ring stretching)	ESI+ (MeOH); m/z 447 (M) <sup>+</sup>	$\delta_{\text{H}}$ (600 MHz, CD <sub>3</sub> OD) 8.80 (2H, s, HC=N), 8.52 (H <sup>3/8</sup> , 2H, d, J = 8.2 Hz), 8.40 (H <sup>4/7</sup> , 2H, d, J = 8.2 Hz), 8.03 (H <sup>5/6</sup> , 2H, s), 3.45 (H <sup>a</sup> , 2H, m, J = 7.2 Hz), 1.68 (H <sup>b</sup> , 4H, m, J = 7.2 Hz), 1.31 (H <sup>d</sup> , 6H, d, J = 6.2 Hz), 0.89 (H <sup>c</sup> , 6H, t, J = 7.4 Hz)
(L <sup>3</sup> Bu <sup>i</sup> )	Colourless	95%	Oil	3050w, 3010w (aromatic C-H), 2959s, 2926s (sp <sup>3</sup> C-H), 2865s (aldimine C-H), 1647s (aldimine C=N), 1621m, 1580m, 1566m, 1514m, 1403m (ring stretching)	ESI+ (MeOH); m/z 447 (M) <sup>+</sup>	$\delta_{\text{H}}$ (600 MHz, CD <sub>3</sub> OD) 8.77 (2H, s, HC=N), 8.51 (H <sup>3/8</sup> , 2H, d, J = 8.4 Hz), 8.39 (H <sup>4/7</sup> , 2H, d, J = 8.4 Hz), 8.02 (H <sup>5/6</sup> , 2H, s), 3.61 (H <sup>a</sup> , 4H, d, J = 6.7 Hz), 2.08 (H <sup>b</sup> , 2H, m, J = 6.7 Hz), 1.01 (H <sup>c</sup> , 12H, d, J = 6.5 Hz)
(L <sup>3</sup> Bu <sup>f</sup> )	Colourless	94%	Oil	3058w, 3014w (aromatic C-H), 2970s, 2915s (sp <sup>3</sup> C-H), 2865s (aldimine C-H), 1647s (aldimine C=N), 1622m, 1579m, 1569m, 1515m, 1403m (ring stretching)	ESI+ (MeOH); m/z 447 (M) <sup>+</sup>	$\delta_{\text{H}}$ (270 MHz, CDCl <sub>3</sub> ) 8.84 (2H, s, HC=N), 8.46 (H <sup>3/8</sup> , 2H, d, J = 8.1 Hz), 8.29 (H <sup>4/7</sup> , 2H, d, J = 8.1 Hz), 7.85 (H <sup>5/6</sup> , 2H, s), 1.35 (H <sup>a</sup> , 18H, s)
(L <sup>3</sup> Cy)	Colourless	70%	Oil Solidifies on standing	3060w, 3010w (aromatic C-H), 2950s (sp <sup>3</sup> C-H), 2870s (aldimine C-H), 1647m (aldimine C=N), 1623m, 1580m, 1567m, 1510m, 1402m (ring stretching)	EI; m/z 398 (M) <sup>+</sup> , 314 (M-C <sub>6</sub> H <sub>12</sub> ) <sup>+</sup>	$\delta_{\text{H}}$ (270 MHz, CDCl <sub>3</sub> ) 8.88 (2H, s, HC=N), 8.42 (H <sup>3/8</sup> , 2H, d, J = 8.4 Hz), 8.27 (H <sup>4/7</sup> , 2H, d, J = 8.4 Hz), (H <sup>5/6</sup> , 2H, s), 3.42 (H <sup>a</sup> , 2H, tt, J <sup>ab</sup> = 3.5 Hz, J <sup>ab'</sup> = 10.5 Hz), 1.88-1.23 (H <sup>b/c/d</sup> , 20H, mm)
(L <sup>3</sup> Ph)	Yellow	75 % (Toluene)	>230 °C	3100w, 3050w, 3015w, 2931 w (aromatic C-H), 1604s (aldimine C=N); 1563w, 1550w, 1499s (ring stretching)	EI; m/z 386 (M) <sup>+</sup>	$\delta_{\text{H}}$ (270 MHz, CDCl <sub>3</sub> ) 9.15 (2H, s, HC=N), 8.67 (H <sup>3/8</sup> , 2H, d, J = 8.4 Hz), 8.38 (H <sup>4/7</sup> , 2H, d, J = 8.4 Hz), 7.91 (H <sup>5/6</sup> , 2H, s), 7.50-7.40 (H <sup>a/b</sup> , 8H, m), 7.31 (H <sup>c</sup> , 2H, m)
(L <sup>3</sup> PhMe)	Yellow	65% (MeOH)	210-214 °C	3086m, 3061m, 3018m, 2919m (aromatic C-H), 1623m (aldimine C=N), 1580m, 1554m, 1511s (ring stretching)	EI; m/z 414 (M) <sup>+</sup> , 399 (M-CH <sub>3</sub> ) <sup>+</sup> , 323 (M-C <sub>7</sub> H <sub>7</sub> ) <sup>+</sup>	$\delta_{\text{H}}$ (600 MHz, CDCl <sub>3</sub> ) 9.16 (2H, s, HC=N) 8.66 (H <sup>3/8</sup> , 2H, d, J = 8.3 Hz), 8.38 (H <sup>4/7</sup> , 2H, d, J = 8.3 Hz), 7.91 (H <sup>5/6</sup> , 2H, s), 7.35 (H <sup>a</sup> , 4H, d, J = 8.1 Hz), 7.25 (H <sup>b</sup> , 4H, d, 8.1 Hz), 2.39 (H <sup>c</sup> , 6H, s)
(L <sup>3</sup> PhCl)	Yellow	80% (MeOH)	>230 °C	3080m, 3059m, 3018m, 2920m (aromatic C-H), 1628m (aldimine C=N), 1580m, 1567w, 1499m (ring stretching)	EI; m/z 456 (M+2) <sup>+</sup> , 454 (M) <sup>+</sup> , 419 (M-Cl) <sup>+</sup> , 111 (C <sub>6</sub> H <sub>4</sub> Cl) <sup>+</sup>	$\delta_{\text{H}}$ (600 MHz, CDCl <sub>3</sub> ) 9.09 (2H, s, HC=N), 8.64 (H <sup>3/8</sup> , 2H, d, J = 8.3 Hz), 8.40 (H <sup>4/7</sup> , 2H, d, J = 8.3), 7.93 (H <sup>5/6</sup> , 2H, s), 7.41 (H <sup>b</sup> , 4H, d, J = 8.6 Hz), 7.34 (H <sup>a</sup> , 4H, d, J = 8.6 Hz)

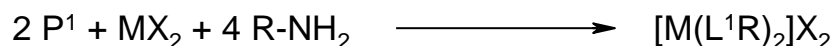
## 2.1.8. Preparation of Metal Complexes of $L^1R$ , $L^2R$ and $L^3R$

### 2.1.8.1. Preparation of $[MX_2L]$ complexes.



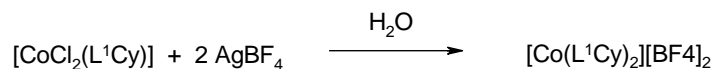
The preparation of the 1:1 ligand to metal complexes, were carried out by two methods which both involved stirring at room temperature for 0.5 hrs. The first was simply by stoichiometric mixing of 0.5 millimolar equivalents of the Schiff base ligand, with the appropriate metal salt, in an appropriate solvent (typically  $CH_3CN$  or MeOH (15 ml) depending on the salt solubilities). The second method which was the foremost method used was a template synthesis<sup>132, 133</sup> whereby the dicarbaldehyde  $P^1$ ,  $P^2$  or  $P^3$  (0.75 mmol) was mixed with 1 equivalent of the metal salt (0.75 mmol), in an appropriate solvent (typically solvents as above), and then two equivalents of primary amine (1.5 mmol), were added to form the 1:1 Schiff base metal complex. The complexes either spontaneously precipitated upon mixing or shortly thereafter to give microcrystalline powders. Complexes that did not precipitate, were crystallised or precipitated by reducing the volume of the reaction mixture to *ca.* 5 ml on the rotary evaporator and then vapour diffusion of diethyl ether. The products were isolated at the pump and washed with diethyl ether, typically (3 x 10 ml). The metal complexes synthesized along with their analyses are given in Table 12 to Table 21.

### 2.1.8.2. Preparation of $[ML_2]X_2$ Complexes of $L^1R$



The preparation of the 2:1 ligand to metal complexes, was carried out using the template effect only. The template synthesis was performed by stirring  $P^1$  (1.5 mmol) with 0.5 equivalent of the appropriate metal salt (0.75 mmol) in an appropriate solvent (typically  $CH_3CN$  [15 ml]), and then two equivalents of primary amine (3 mmol) were added to form the 2:1 Schiff base metal complex. The metal salts used to prepare the 2:1 complexes were  $Cu(BF_4)_2 \cdot 6H_2O$ ,  $Co(NCS)_2 \cdot xH_2O$  or  $Co(NO_3)_2 \cdot 6H_2O$ . The complexes either spontaneously precipitated upon mixing or shortly thereafter to give microcrystalline powders. Complexes that did not precipitate were crystallised or precipitated by reducing the volume of the reaction mixture to Ca. 5 ml on the rotary evaporator and then vapour diffusion of diethyl ether. The products were isolated at the pump and washed with diethyl ether, typically (3 x 10 ml). The metal complexes synthesized along with their analyses are given in tables 2.1.9.1a-g. **Note:** A few bis complexes were prepared by serendipity, when actually trying to obtain the 1:1 complex. For example  $[Co(L^1Cy)_2][NO_3]_2$ ,  $[Co(L^1Cy)_2][Co(NCS)_4]$  and  $[Co(L^1Cy)_2][BF_4]_2$ , the latter was prepared during an attempted ligand exchange reaction detailed below. Characterisation data is provided in Table 12 to Table 21.

### 2.1.8.3. Formation of $[\text{Co}(\text{H}_2\text{O})_2(\text{L}^1\text{Cy})][\text{BF}_4]_2$ .



$[\text{CoCl}_2(\text{L}^1\text{Cy})]$  (200 mg, 0.47 mmol) was dissolved in deionised water (10 ml) in a 25 ml round bottomed flask and was stirred. To the deep red solution was added two equivalents of  $\text{AgBF}_4$  (183 mg, 0.94 mmol) whereupon an off white precipitate started to form. The solution was left to stir for 1h, after which time the pinky precipitate was filtered through a Pasteur pipette plugged with a small ball of cotton wool. Water was then removed from the filtrate on the rotary evaporator to leave a dark red residue. The product was also extracted from the precipitate as well by washing with acetone (20 ml), to give a deep red solution. This was combined with the residue obtained from the filtrate and the solvent was reduced to *ca.* 5 ml on the rotary evaporator. The product was crystallized by slow vapour diffusion of diethyl ether into the acetone solution to give deep red block crystals (136 mg, 64 %). The product was identified through CHN microanalysis and later single crystal X-ray diffraction to be the 2:1 ligand to metal complex and was not the diaqua complex as anticipated. Characterisation data can be found in Table 17.

**Table 12.** Characterisation data for Cu<sup>II</sup> complexes of L<sup>1</sup>R; a) Peaks too broad to be observed.

Compound	Colour	Yield (solvent)	Microanalysis	Infra-red Spectrum (KBr) $\nu_{\max}$ cm <sup>-1</sup>	Mass Spectrum ESI+	<sup>1</sup> H NMR
[CuCl <sub>2</sub> (L <sup>1</sup> Et)]	Green	80% (EtOH)	Calc. C, 40.8%; H, 4.7%; N, 13.0%. Found. C, 41.1%; H, 4.7%; N, 12.7%.	3092m, 3061m, 3012m, (aromatic C-H); 2981m, 2937m, 2913m (sp <sup>3</sup> C-H); 2876m, (aldiminine C-H); 1637w, (aldimine C=N); 1591s, 1480m, (ring stretching)	m/z, 441 ( <sup>63</sup> Cu+2L-H) <sup>+</sup> , 287 ( <sup>63</sup> Cu+L+Cl-H) <sup>+</sup>	$\delta_{\text{H}}$ (600 MHz, D <sub>2</sub> O) 3.35 (H <sup>a</sup> , 4H, bt), 1.18 (H <sup>b</sup> , 6H, bd)
[CuCl <sub>2</sub> (L <sup>1</sup> Pr <sup>n</sup> )]	Green	76 % (CH <sub>3</sub> CN)	Calc. C, 44.4%; H, 5.4%; N, 12.0%. Found. C, 44.6%; H, 5.1%; N, 11.9%.	3092m, 3055m, 3025m, (aromatic C-H); 2968s, 2931s, (sp <sup>3</sup> C-H); 2870m, (aldiminine C-H); 1634w, (aldimine C=N); 1585s, 1474s, (ring stretching)	m/z 497, ( <sup>63</sup> Cu+2L-H) <sup>+</sup> , 315 ( <sup>63</sup> Cu+L+Cl-H) <sup>+</sup> , 249 ( <sup>63</sup> Cu+2L) <sup>2+</sup>	$\delta_{\text{H}}$ (600 MHz, D <sub>2</sub> O) 2.75 (H <sup>a</sup> , 4H, bt), 1.47 (H <sup>b</sup> , 4H, bm), 0.77 (H <sup>c</sup> , 6H, bt)
[Cu(NO <sub>3</sub> ) <sub>2</sub> (L <sup>1</sup> Pr <sup>n</sup> )]	Green	85% (CH <sub>3</sub> CN : Et <sub>2</sub> O)	Calc. C, 38.6%; H, 4.7%; N, 17.3%. Found. C, 38.6%; H, 4.6%; N, 17.5%.	3086w, 3025w, (aromatic C-H); 2974m, 2937m, (sp <sup>3</sup> C-H); 2876m, (aldiminine C-H); 1636w, (aldimine C=N); 1585s, 1486s, (ring stretching); 1412s, 1313s, 1011m (nitrate N-O)	m/z 341 ( <sup>63</sup> Cu+L+NO <sub>3</sub> -2H) <sup>+</sup> , 248.5 ( <sup>63</sup> Cu+2L) <sup>2+</sup>	$\delta_{\text{H}}$ (600 MHz, D <sub>2</sub> O) 2.77 (H <sup>a</sup> , 4H, bs), 1.65 (H <sup>b</sup> , 4H, bs), 0.78 (H <sup>c</sup> , 6H, bs)
[CuBr <sub>2</sub> (L <sup>1</sup> Pr <sup>n</sup> )]	Green	90% (EtOH)	Calc. C, 35.4%; H, 4.4%; N, 9.5%. Found. C, 35.5%; H, 4.5%; N, 9.6%.	3086w, 3055w, 3025w, (aromatic C-H); 2968s, 2931s, (sp <sup>3</sup> C-H); 2876m, (aldiminine C-H); 1634w, (aldimine C=N); 1585s, 1474s, (ring stretching)	m/z 359 ( <sup>63</sup> Cu+L+Br-H) <sup>+</sup>	$\delta_{\text{H}}$ (600 MHz, D <sub>2</sub> O) 2.80 (H <sup>a</sup> , 4H, bt), 1.52 (H <sup>b</sup> , 4H, bm), 0.81 (H <sup>c</sup> , 6H, bt)
[Cu(L <sup>1</sup> Pr <sup>n</sup> ) <sub>2</sub> ][BF <sub>4</sub> ] <sub>2</sub>	Green	50% (EtOH : CH <sub>3</sub> CN)	Calc. C, 46.5%; H, 5.7%; N, 12.5%. Found. C, 46.4%; H, 5.4%; N, 12.2%.	3093w, 3056w, 3040w, (aromatic C-H); 2954m, 2935m, (sp <sup>3</sup> C-H); 2873m, (aldiminine C-H); 1634wbr, (aldimine C=N); 1590m, 1470m, (ring stretching) 1057s, 1039s (BF <sub>4</sub> )	m/z 497 ( <sup>63</sup> Cu+2L-H) <sup>+</sup> , 248.5 ( <sup>63</sup> Cu+2L) <sup>2+</sup>	a
[CuCl <sub>2</sub> (L <sup>1</sup> Pr <sup>i</sup> )]	Green	88% (CH <sub>3</sub> CN)	Calc. C, 44.4%; H, 5.4%; N, 12.0%. Found. C, 44.2%; H, 5.4%; N, 12.0%.	3086m, 3055m, (aromatic C-H); 2980s, 2937m, (sp <sup>3</sup> C-H); 2869m, (aldiminine C-H); 1634w, (aldimine C=N); 1591s, 1477s, (ring stretching)	m/z 315 ( <sup>63</sup> Cu+L+Cl-H) <sup>+</sup>	$\delta_{\text{H}}$ (270 MHz, D <sub>2</sub> O) 3.33 (H <sup>a</sup> , 2H, bm), 1.15 (H <sup>b</sup> , 12H, bd)
[CuCl <sub>2</sub> (L <sup>1</sup> Bu <sup>n</sup> )]	Green	55 % (CH <sub>3</sub> CN : Et <sub>2</sub> O)	Calc. C, 47.4%; H, 6.1%; N, 11.1%. Found. C, 47.3%; H, 6.0%; N, 11.1%.	3065s, 3033s, 3005s, (aromatic C-H); 2955s, 2932s, (sp <sup>3</sup> C-H); 2871s, (aldiminine C-H); 1627w, (aldimine C=N); 1583s, 1472s, (ring stretching)	m/z 343 ( <sup>63</sup> Cu+L+Cl) <sup>+</sup>	$\delta_{\text{H}}$ (270 MHz, D <sub>2</sub> O) 2.85 (H <sup>a</sup> , 4H, bt), 1.48 (H <sup>b</sup> , 4H, bm), 1.23 (H <sup>c</sup> , 4H, bm), 0.75 (H <sup>d</sup> , 6H, bt)
[CuCl <sub>2</sub> (L <sup>1</sup> Bu <sup>2</sup> )]	Green	62 % (CH <sub>3</sub> CN : Et <sub>2</sub> O)	Calc. C, 47.4%; H, 6.1%; N, 11.1%. Found. C, 47.3%; H, 6.3%; N, 10.9%.	3063m, 3035m, 3003m (aromatic C-H); 2962s, 2931s, (sp <sup>3</sup> C-H); 2872m, (aldiminine C-H); 1628wbr, (aldimine C=N); 1585s, 1474s, (ring stretching)	m/z 553 ( <sup>63</sup> Cu+2L-H) <sup>+</sup> , 308 ( <sup>63</sup> Cu+L-H) <sup>+</sup> , 276.5 ( <sup>63</sup> Cu+2L) <sup>2+</sup>	$\delta_{\text{H}}$ (600 MHz, D <sub>2</sub> O) 3.11 (H <sup>b</sup> , 2H, bm), 1.49 (H <sup>c/c'</sup> , 2H, bm), 1.42 (H <sup>c/c'</sup> , 2H, bm), 1.10 (H <sup>a</sup> , 6H, bd), 0.79 (H <sup>d</sup> , 6H, bt)

**Table 13.** Characterisation data for Cu<sup>II</sup> complexes of L<sup>1</sup>R continued; a) Peaks too broad to be observed; b) Insoluble.

Compound	Colour	Yield (solvent)	Microanalysis	Infra-red Spectrum (KBr) $\nu_{\max}$ cm <sup>-1</sup>	Mass Spectrum ESI+	<sup>1</sup> H NMR
[CuCl <sub>2</sub> (L <sup>1</sup> Bu <sup>f</sup> )]	Green	86% (CH <sub>3</sub> CN : Et <sub>2</sub> O)	Calc. C, 47.4%; H, 6.1%; N, 11.1%. Found. C, 47.2%; H, 6.2%; N, 11.0%.	3056m, 3002m, (aromatic C-H); 2951s, 2940s, (sp <sup>3</sup> C-H); 2865s, (aldiminine C-H); 1628w, (aldimine C=N); 1585m, 1475m, (ring stretching)	m/z 343 ( <sup>63</sup> Cu+L+Cl) <sup>+</sup>	$\delta_{\text{H}}$ (270 MHz, D <sub>2</sub> O) 2.69 (H <sup>a</sup> , 4H, bd), 1.78 (H <sup>b</sup> , 2H, bm), 0.83 (H <sup>c</sup> , 12H, bd)
[CuCl <sub>2</sub> (L <sup>1</sup> Bu <sup>f</sup> )]	Green			No Solid Products Could be isolated.		
[CuCl <sub>2</sub> (L <sup>1</sup> Cy)]. (CH <sub>3</sub> CN)	Green	98% (CH <sub>3</sub> CN)	Calc. C, 53.3%; H, 6.4%; N, 11.9%. Found. C, 53.2%; H, 6.3%; N, 11.5%.	3072m, 3035m, 3005m, (aromatic C-H); 2925s, (sp <sup>3</sup> C-H); 2875s, (aldiminine C-H); 1638wbr, (aldimine C=N); 1585m, 1475m, (ring stretching)	m/z 395 ( <sup>63</sup> Cu+L+Cl+H) <sup>+</sup> , 359 ( <sup>63</sup> Cu+L) <sup>+</sup>	$\delta_{\text{H}}$ (600 MHz, D <sub>2</sub> O) 3.01 (H <sup>a</sup> , 2H, bm), 1.83 (H <sup>b/b'</sup> , 4H, bm), 1.67 (H <sup>c/c'</sup> , 4H, bm), 1.50 (H <sup>d/d'</sup> , 2H, bd), 1.19 (H <sup>b'/b''/c'/c''</sup> , 8H, bm), 1.02 (H <sup>d/d'</sup> , 2H, bm)
[Cu(L <sup>1</sup> Cy) <sub>2</sub> ][BF <sub>4</sub> ] <sub>2</sub> . 2.5(H <sub>2</sub> O)	Green	90% (CH <sub>3</sub> CN)	Calc. C, 52.0%; H, 6.5%; N, 10.0%. Found. C, 52.0%; H, 6.3% N, 9.4%.	3084w, (aromatic C-H); 2930s, (sp <sup>3</sup> C-H); 2855s, (aldiminine C-H); 1645wbr, (aldimine C=N); 1591m, 1467w, (ring stretching), 1080s, 1039s (BF <sub>4</sub> )	m/z 744 ( <sup>63</sup> Cu+2L+BF <sub>4</sub> ) <sup>+</sup> , 329 ( <sup>63</sup> Cu+2L) <sup>2+</sup>	a
<i>racemic</i> -[CuCl <sub>2</sub> (L <sup>1</sup> CyMe)]	Green	73 % (CH <sub>3</sub> CN)	Calc. C, 54.8%; H, 6.8%; N, 9.1%. Found. C, 54.8%; H, 6.6%; N, 9.1%.	3066m, 3030m, (aromatic C-H); 2925s, 2870m, (sp <sup>3</sup> C-H); 2850m, (aldiminine C-H); 1628wbr, (aldimine C=N); 1580m, 1474m, (ring stretching)	m/z 423 ( <sup>63</sup> Cu+L+Cl+H) <sup>+</sup> , 387 ( <sup>63</sup> Cu+L) <sup>+</sup>	$\delta_{\text{H}}$ (600 MHz, D <sub>2</sub> O) 3.20 (H <sup>a</sup> , 2H, bm), 2.95 (H <sup>a iso</sup> , 2H, bm), 1.84 (H <sup>b/b' iso</sup> , 4H, bm), 1.63 (H <sup>b''/b''' iso</sup> , 4H, bm), 1.60-1.52 (H <sup>b''/b'''</sup> , 8H, bmm), 1.49-1.43 (H <sup>c/c'</sup> , 4H, bm), 1.22 (H <sup>c''/c''' iso</sup> , 4H, bm), 1.22-1.15 (H <sup>c'/c''</sup> , H <sup>d/d' iso</sup> , 8H, bm), 0.88 (H <sup>c'/c'' iso</sup> , 4H, bm), 0.78 (H <sup>f</sup> , 6H, d), 0.73 (H <sup>f iso</sup> , 6H, d)
[CuCl <sub>2</sub> (L <sup>1</sup> Ph)]	Orange	100 % (CH <sub>3</sub> CN)	Calc. C, 54.4%; H, 3.6%; N, 10.0%. Found. C, 51.3%; H, 3.8%; N, 11.8%.	3053, 3016, (aromatic C-H); 2851 (aldimine C-H); 1550, 1495s, (ring stretching)	m/z 633 ( <sup>63</sup> Cu+2L) <sup>+</sup>	b
[CuCl <sub>2</sub> (L <sup>1</sup> PhMe)]	Orange	99 % (CH <sub>3</sub> CN)	Calc. C, 56.3%; H, 4.2%; N, 9.4%. Found. C, 56.0%; H, 4.0%; N, 9.2%.	3071m, 3040m, 3004m, (aromatic C-H); 2952m, 2930m, (sp <sup>3</sup> C-H); 2872 (aldiminine C-H); 1595m, 1549m, 1510m, 1470m, (ring stretching)	m/z 689 ( <sup>63</sup> Cu+2L+H) <sup>+</sup> , 411 ( <sup>63</sup> Cu+L+Cl+H) <sup>+</sup> , 376 ( <sup>63</sup> Cu+L+H) <sup>+</sup>	b
[CuCl <sub>2</sub> (L <sup>1</sup> PhCl)]	Orange	88 % (CH <sub>3</sub> CN)	Calc. C, 46.7%; H, 2.7%; N, 8.6%. Found. C, 46.6%; H, 2.6%; N, 8.5%.	3073m, 3036m, 3018m (aromatic C-H); 1620w (aldimine C=N) 1589m, 1560m, 1486s (ring stretching)	m/z 771 ( <sup>63</sup> Cu+2L) <sup>+</sup>	b
[CuCl <sub>2</sub> (L <sup>1</sup> PhNO <sub>2</sub> )]	Orange	96 % (CH <sub>3</sub> CN)	Calc. C, 44.8%; H, 2.6%; N, 13.7%. Found. C, 44.9%; H, 2.3%; N, 13.6%.	3100m, 3082m, 3054m, 3040m, (aromatic C-H); 2857m, (aldiminine C-H); 1605w, (aldimine C=N); 1580w, 1495m, (ring stretching); 1519s, 1345s, (N=O)	FAB-MS m/z ( <sup>63</sup> Cu+L+2Cl) <sup>+</sup>	b

**Table 14.** Characterisation data for Zn<sup>II</sup> complexes of L<sup>1</sup>R; a) Insoluble.

Compound	Colour	Yield (solvent)	Microanalysis	Infra-red Spectrum (KBr) $\nu_{\max}$ cm <sup>-1</sup>	Mass Spectrum ESI+	<sup>1</sup> H NMR
[ZnCl <sub>2</sub> (L <sup>1</sup> Et)]	Colourless	62 % (CH <sub>3</sub> CN)	Calc. C, 40.6%; H, 4.6%; N, 12.9%. Found. C, 40.7%; H, 4.7%; N, 12.8%.	3092m, 3061m, 3044m, (aromatic C-H); 2970m, 2950m, 2922m (sp <sup>3</sup> C-H); 2867m, (aldiminine C-H); 1650m, (aldimine C=N); 1591s, 1475m, (ring stretching)	m/z 288 ( <sup>65</sup> Zn+L+H <sub>2</sub> O+OH-H) <sup>+</sup> , 252 ( <sup>65</sup> Zn+L-2H) <sup>+</sup>	$\delta_{\text{H}}$ (600 MHz, (CD <sub>3</sub> ) <sub>2</sub> SO at 100 °C) 8.60 (2H, s, HC=N); 8.35 (H <sup>d</sup> , 1H, bt); 8.09 (H <sup>3/5</sup> , 2H, d, J = 7.4 Hz); 3.81 (H <sup>a</sup> , 4H, q, J = 6.4 Hz); 1.36 (H <sup>b</sup> , t, 6H, J = 6.5 Hz).
[ZnCl <sub>2</sub> (L <sup>1</sup> Pr <sup>o</sup> )]	Colourless	50 % (CH <sub>3</sub> CN)	Calc. C, 44.2%; H, 5.4%; N, 11.9%. Found. C, 44.3%; H, 5.5%; N, 11.8%.	3085m, 3063m, 3010m (aromatic C-H); 2968s, 2925s, 2877s, (sp <sup>3</sup> C-H); 2856s (aldiminine C-H); 1649m, (aldimine C=N); 1596, 1468s, (ring stretching)	m/z 249 (M+2L) <sup>2+</sup>	a
[ZnCl <sub>2</sub> (L <sup>1</sup> Pr <sup>i</sup> )]	Colourless	59 % (CH <sub>3</sub> CN)	Calc. C, 44.2%; H, 5.4%; N, 11.9%. Found. C, 44.1%; H, 5.5%; N, 11.8%.	3080m, 3048m, 3010m, (aromatic C-H); 2973s, 2908s, (sp <sup>3</sup> C-H); 2871s (aldiminine C-H); 1651m, (aldimine C=N); 1595, 1470s, (ring stretching)	m/z 316 ( <sup>65</sup> Zn+L+H <sub>2</sub> O+OH-H) <sup>+</sup>	$\delta_{\text{H}}$ (270 MHz, CD <sub>3</sub> CN) 8.51 (2H, s, HC=N); 8.36 (H <sup>d</sup> , 1H, t, J = 8.1 Hz); 7.96 (H <sup>3/5</sup> , 2H, t, J = 8.1 Hz); 4.13 (H <sup>a</sup> , 2H, m, J = 6.7 Hz); 1.46 (H <sup>b</sup> , d, 12H, J = 8.1 Hz)
[ZnCl <sub>2</sub> (L <sup>1</sup> Bu <sup>o</sup> )]	Colourless	63 % (CH <sub>3</sub> CN)	Calc. C, 47.2%; H, 6.1%; N, 11.0%. Found. C, 46.9%; H, 6.1%; N, 11.0%.	3075m, 3028m, (aromatic C-H); 2955s, 2927s, 2890s, (sp <sup>3</sup> C-H); 2857s, (aldiminine C-H); 1650m, (aldimine C=N); 1590s, 1465s, (ring stretching)	m/z 723 (2( <sup>65</sup> Zn)+2L+3Cl-H) <sup>+</sup> , 344 ( <sup>65</sup> Zn+L+H <sub>2</sub> O+OH-H) <sup>+</sup>	$\delta_{\text{H}}$ (270 MHz, (CD <sub>3</sub> ) <sub>2</sub> CO) 8.65 (2H, s, HC=N); 8.54 (H <sup>d</sup> , 1H, t, J = 7.6 Hz); 8.20 (H <sup>3/5</sup> , 2H, t, J = 7.7 Hz); 3.90 (H <sup>a</sup> , 4H, t, J = 6.7 Hz); 1.98 (H <sup>b</sup> , m, 4H, J = 7.7 Hz); 1.36 (H <sup>c</sup> , m, 4H, J = 7.6 Hz); 0.93 (H <sup>d</sup> , t, 6H, J = 7.3 Hz)
[ZnCl <sub>2</sub> (L <sup>1</sup> Bu <sup>2</sup> )]	Colourless	51 % (CH <sub>3</sub> CN)	Calc. C, 47.2%; H, 6.1%; N, 11.0%. Found. C, 47.5%; H, 6.0%; N, 10.9%.	3075m, 3030m, (aromatic C-H); 2970s, 2929s, (sp <sup>3</sup> C-H); 2869m, (aldiminine C-H); 1647m, (aldimine C=N); 1590s, 1460s, (ring stretching)	m/z 344 ( <sup>65</sup> Zn+L+H <sub>2</sub> O+OH-H) <sup>+</sup> , 277 ( <sup>65</sup> Zn+2L) <sup>2+</sup>	$\delta_{\text{H}}$ (600 MHz, (CD <sub>3</sub> ) <sub>2</sub> CO) 8.69 (2H, s, HC=N); 8.57 (H <sup>d</sup> , 1H, t, J = 7.8 Hz); 8.23 (H <sup>3/5</sup> , 2H, d, J = 7.8 Hz); 3.81 (H <sup>b</sup> , 2H, m, J = 7.2 Hz); 2.17 (H <sup>c/c'</sup> , 2H, m, J = 6.6 Hz); 1.79 (H <sup>c/c'</sup> , 2H, m, J = 5.5 Hz); 1.52 (H <sup>d</sup> , d, 6H, J = 5.4 Hz); 0.88 (Hd, 6H, t, J = 7.6 Hz)
[ZnCl <sub>2</sub> (L <sup>1</sup> Bu <sup>i</sup> )]	Colourless	70 % (CH <sub>3</sub> CN)	Calc. C, 47.2%; H, 6.1%; N, 11.0%. Found. C, 47.3%; H, 6.1%; N, 11.0%.	3092m, 3061m, 3044m, (aromatic C-H); 2970m, 2950m, 2922m (sp <sup>3</sup> C-H); 2867m, (aldiminine C-H); 1652m, (aldimine C=N); 1591s, 1475m, (ring stretching)	m/z 344 ( <sup>65</sup> Zn+L+H <sub>2</sub> O+OH-H) <sup>+</sup>	$\delta_{\text{H}}$ (270 MHz, (CD <sub>3</sub> ) <sub>2</sub> CO) 8.62 (2H, s, HC=N); 8.55 (H <sup>d</sup> , 1H, t, J = 7.7 Hz); 8.23 (H <sup>3/5</sup> , 2H, d, J = 7.7 Hz); 3.70 (H <sup>a</sup> , 4H, d, J = 6.6 Hz); 2.72 (H <sup>b</sup> , m, 2H, J = 7.0 Hz); 0.90 (H <sup>c</sup> , 12H, d, J = 6.8 Hz)
[ZnCl <sub>2</sub> (L <sup>1</sup> Bu <sup>i</sup> )]	Colourless	60 % (CH <sub>3</sub> CN)	Calc. C, 47.2%; H, 6.1%; N, 11.0%. Found. C, 47.5%; H, 6.3%; N, 11.4%.	3070m, 3030m, 3023m, (aromatic C-H); 2966s, 2929s, (sp <sup>3</sup> C-H); 2870m, (aldiminine C-H); 1644m, (aldimine C=N); 1595s, 1464s, (ring stretching)	m/z 344 ( <sup>65</sup> Zn+L+H <sub>2</sub> O+OH-H) <sup>+</sup>	$\delta_{\text{H}}$ (270 MHz, (CD <sub>3</sub> ) <sub>2</sub> CO) 8.77 (HC=N, 2H, s); 8.54 (H <sup>d</sup> , 1H, t, J = 8.1 Hz); 8.22 (H <sup>3/4</sup> , 2H, d, J = 8.1 Hz); 1.54 (H <sup>b</sup> , 18H, s)
[Zn(NO <sub>3</sub> ) <sub>2</sub> (L <sup>1</sup> Bu <sup>i</sup> )]	Colourless	70 % (CH <sub>3</sub> CN)	Calc. C, 41.4%; H, 5.3%; N, 16.1%. Found. C, 41.6%; H, 5.3%; N, 16.2%.	3080m, 3048m, 3030m, (aromatic C-H); 2970s, 2945s, (sp <sup>3</sup> C-H); 2875m, (aldiminine C-H); 1645m, (aldimine C=N); 1595s, 1473s, (ring stretching) 1490s, 1293s, 1018s nitrate N-O)	m/z 371 ( <sup>65</sup> Zn+L+NO <sub>3</sub> -H) <sup>+</sup> , 277 ( <sup>65</sup> Zn+2L) <sup>2+</sup>	$\delta_{\text{H}}$ (600 MHz, (CD <sub>3</sub> ) <sub>2</sub> SO) at 50 °C) 9.07 (HC=N, 2H, s); 8.88 (H <sup>d</sup> , 1H, t, J = 7.7 Hz); 8.55 (H <sup>3/4</sup> , 2H, d, J = 7.8 Hz); 0.90 (H <sup>b</sup> , 18H, s); 8.81 (HC=N, 1H, s); 8.58 (H <sup>d</sup> , 0.5H, t); 8.28 (H <sup>3/4</sup> , 1H, d, J = 7.4 Hz); 1.38 (H <sup>b</sup> , 9H, s)



**Table 15.** Characterisation data for Zn<sup>II</sup> complexes of L<sup>1</sup>R continued; a) Insoluble.

Compound	Colour	Yield (solvent)	Microanalysis	Infra-red Spectrum (KBr) $\nu_{\max}$ cm <sup>-1</sup>	Mass Spectrum ESI+	<sup>1</sup> H NMR
[Zn(AcO) <sub>2</sub> (L <sup>1</sup> Bu <sup>t</sup> )]	Colourless	44 % (CH <sub>3</sub> CN)	Calc. C, 53.2%; H, 6.8%; N, 9.8%. Found. C, 53.0%; H, 6.9%; N, 9.7%.	3073w, 3055w, 3025w, (aromatic C-H); 2974s, 2937m, (sp <sup>3</sup> C-H); 2876w, (aldiminine C-H); 1635s, (aldimine C=N); 1616s, (Coordinated OAc C=O); 1591s, 1468m, (ring stretching); 1326m, (OAc C-O)	m/z 427 ( <sup>65</sup> Zn+L+2AcO-H) <sup>+</sup> , 344 ( <sup>65</sup> Zn+L+H <sub>2</sub> O+OH-H) <sup>+</sup>	$\delta_{\text{H}}$ (270 MHz, CD <sub>3</sub> OD), $\delta$ ppm: 8.63 (HC=N, 2H, s); 8.39 (H <sup>d</sup> , 1H, t, J = 7.8 Hz); 8.06 (H <sup>3/4</sup> , 2H, d, J = 7.7 Hz); 1.80 (H <sup>OAc</sup> , 6H, s); 1.54 (H <sup>b</sup> , 18H, s)
[ZnCl <sub>2</sub> (L <sup>1</sup> Cy)]	Colourless	63 % (CH <sub>3</sub> CN)	Calc. C, 52.6%; H, 6.3%; N, 9.7%. Found. C, 52.8%; H, 6.6%; N, 9.6%.	3070m, 3042m, (aromatic C-H); 2930s, (sp <sup>3</sup> C-H); 2850m, (aldiminine C-H); 1648w, (aldimine C=N); 1592s, 1465m, (ring stretching)	m/z 396 ( <sup>65</sup> Zn+L+H <sub>2</sub> O+OH-H) <sup>+</sup> , 360 ( <sup>65</sup> Zn+L-2H) <sup>+</sup> , 329 ( <sup>65</sup> Zn+L-2H) <sup>2+</sup>	$\delta_{\text{H}}$ (600 MHz, ((CD <sub>3</sub> ) <sub>2</sub> SO)) 8.67 (2H, s, HC=N); 8.49 (H <sup>d</sup> , 1H, t, J = 7.6 Hz); 8.12 (H <sup>3/5</sup> , 2H, d, J = 7.9 Hz); 3.67 (H <sup>a</sup> , 2H, t, J = 11.0 Hz); 1.88 (H <sup>bb'</sup> , d, 4H, J = 11.0 Hz); 1.80 (H <sup>bb''</sup> , d, 4H, J = 12.0 Hz); 1.76 (H <sup>cc'</sup> , d, 4H, J = 15.5 Hz); 1.61 (H <sup>dd'</sup> , d, 2H, J = 12.7 Hz); 1.27 (H <sup>cc''</sup> , q, 4H, J = 12.7 Hz); 1.01 (H <sup>dd''</sup> , q, 2H, J = 13.1 Hz).
[ZnCl <sub>2</sub> (L <sup>1</sup> CyMe)]	Colourless	65 % (CH <sub>3</sub> CN)	Calc. C, 54.9%; H, 6.4%; N, 9.1%. Found. C, 54.2%; H, 6.4%; N, 9.1%.	3070m, 3035m, 3025m, (aromatic C-H); 2930s, (sp <sup>3</sup> C-H); 2851s, (aldiminine C-H); 1648m, (aldimine C=N); 1593s, 1469s, (ring stretching)	m/z 424 ( <sup>65</sup> Zn+L+H <sub>2</sub> O+OH-H) <sup>+</sup>	$\delta_{\text{H}}$ (600 MHz, CD <sub>3</sub> CN) 8.49 (2H, dd, HC=N, J = 2.76 Hz, J = 6.9 Hz); 8.33 (H <sup>d</sup> , 1H, tt, J = 3.12 Hz, J = 7.7 Hz); 7.94 (H <sup>3/5</sup> , 2H, dt, J = 7.02 Hz, J = 7.9 Hz); 3.76 (H <sup>a</sup> , 1H, m, J = 5.16 Hz); 3.69 (Ha, 1H, bm); 2.30-0.88 (remaining cyclohexyl and methyls, mm, 24H)
[ZnCl <sub>2</sub> (L <sup>1</sup> Ph)]	Yellow	70 % (CH <sub>3</sub> CN)	Calc. C, 54.1%; H, 3.6%; N, 10.0%. Found. C, 54.1%; H, 3.6%; N, 9.9%.	3064, 3044, 3005 (aromatic C-H); 1585, 1495s, (ring stretching)	m/z 348 ( <sup>65</sup> Zn+L-2H) <sup>+</sup>	$\delta_{\text{H}}$ (600 MHz, (CD <sub>3</sub> ) <sub>2</sub> SO at 100 °C) 8.75 (HC=N, 2H, s); 8.28 (H <sup>3/5</sup> , 3H, d, J = 6.9 Hz); 8.18 (H <sup>d</sup> , 2H, t, J = 7.2 Hz); 7.45 (H <sup>ab</sup> , 8H, m, J = 7.1 Hz); 7.33 (H <sup>c</sup> , 2H, t, J = 6.9 Hz)
[ZnCl <sub>2</sub> (L <sup>1</sup> PhMe)]	Yellow	92 % (DMF : Water)	Calc. C, 56.1%; H, 4.3%; N, 9.3%. Found. C, 55.9%; H, 4.3%; N, 9.3%.	3067m, 3049m, 3005m (aromatic C-H); 2956m, 2919m (sp <sup>3</sup> C-H); 2869 (aldiminine C-H); 1555s, 1480s, (ring stretching)	m/z 689 ( <sup>65</sup> Zn+2L-H) <sup>+</sup> , 376 ( <sup>65</sup> Zn+L-H) <sup>+</sup> , 345 ( <sup>65</sup> Zn+L-H) <sup>+</sup>	$\delta_{\text{H}}$ (270 MHz, (CD <sub>3</sub> ) <sub>2</sub> SO at 100 °C) 8.81 (HC=N, 2H, s); 8.27 (H <sup>d</sup> , 3H, t, J = 5.0 Hz); 8.26 (H <sup>3/4</sup> , 2H, brs); 7.43 (H <sup>ab</sup> , 4H, brd, J = 6.8 Hz); 7.29 (Ha/b, 4H, d, J = 8.4 Hz); 2.37 (H <sup>c</sup> , 6H, s)
[ZnCl <sub>2</sub> (L <sup>1</sup> PhCl)]	Yellow	100 % (CH <sub>3</sub> CN)	Calc. C, 46.5%; H, 2.7%; N, 8.6%. Found. C, 46.7%; H, 2.6%; N, 8.4%.	3073m, 3050m, 3025m (aromatic C-H); 1637w (aldimine C=N) 1589m, 1490s (ring stretching)	FAB-MS m/z 772 ( <sup>65</sup> Zn+2L)+, 454 ( <sup>65</sup> Zn+L-Cl) <sup>+</sup>	a
[ZnCl <sub>2</sub> (L <sup>1</sup> PhNO <sub>2</sub> )]	Yellow	90 % (CH <sub>3</sub> CN)	Calc. C, 44.6%; H, 2.6%; N, 13.7%. Found. C, 44.6%; H, 2.3%; N, 13.4%.	3101m, 3075m, 3032m, (aromatic C-H); 2932w, (sp <sup>3</sup> C-H); 2851w, (aldiminine C-H); 1604w, (aldimine C=N); 1586m, 1490m, (ring stretching); 1520s, 1349s, (N=O).	FAB-MS m/z 474 ( <sup>65</sup> Zn+L+Cl) <sup>+</sup>	a

**Table 16.** Characterisation data for Co<sup>II</sup> complexes of L<sup>1</sup>R.

Compound	Colour	Yield (solvent)	Microanalysis	Infra-red Spectrum (KBr) $\nu_{\max}$ cm <sup>-1</sup>	Mass Spectrum ESI+	$\mu_{\text{eff}}$	<sup>1</sup> H NMR
[CoCl <sub>2</sub> (L <sup>1</sup> Et)]				No solid products could be isolated.			
[CoCl <sub>2</sub> (L <sup>1</sup> Pr <sup>d</sup> )]	Dark Red	80 % (CH <sub>3</sub> CN : Et <sub>2</sub> O)	Calc. C, 45.0%; H, 5.5%; N, 12.1%. Found. C, 44.6%; H, 5.5%; N, 11.7%.	3065m, 3035m, (aromatic C-H); 2967s, 2931s, (sp3 C-H); 2875m, (aldimine C-H); 1630m, (aldimine C=N); 1585s, 1471s, (ring stretching)	m/z 311 ( <sup>59</sup> Co+L+Cl-H) <sup>+</sup>	4.13 BM	$\delta_{\text{H}}$ (270 MHz, CD <sub>3</sub> OD) 220.32 (HC=N, 2H, bs); 140.31 (H <sup>b</sup> , 2H, bs); 105.00 (H <sup>3/5</sup> , 1H, bs); 43.3 (H <sup>d</sup> , 4H, bs); -4.26 (H <sup>e</sup> , 6H, bs); -6.86 (H <sup>a</sup> , 4H, bs)
[CoCl <sub>2</sub> (L <sup>1</sup> Pr <sup>f</sup> )]	Dark Red	55 % (CH <sub>3</sub> CN : Et <sub>2</sub> O)	Calc. C, 45.0%; H, 5.5%; N, 12.1%. Found. C, 44.6%; H, 5.6%; N, 11.9%.	3061m, 3030m, (aromatic C-H); 2975s, 2930m, (sp3 C-H); 2880m, (aldimine C-H); 1630w, (aldimine C=N); 1591s, 1475s, (ring stretching)	m/z 311 ( <sup>59</sup> Co+L+Cl-H) <sup>+</sup>	4.92 BM	$\delta_{\text{H}}$ (270 MHz, CD <sub>3</sub> OD) 202.47 (HC=N, 2H, bs); 98.17 (H <sup>3/5</sup> , 2H, bs); 40.91 (H <sup>d</sup> , 1H, bs); -4.79 (H <sup>b</sup> , 12H, bs); -9.43 (H <sup>a</sup> , 2H, bs).
[CoCl <sub>2</sub> (L <sup>1</sup> Bu <sup>g</sup> )]	Dark Red	60 % (CH <sub>3</sub> CN)	Calc. C, 44.2%; H, 5.7%; N, 10.3%. Found. C, 44.1%; H, 5.8%; N, 10.2%.	3066m, 3025m, (aromatic C-H); 2954s, 2932s, (sp3 C-H); 2870s, (aldimine C-H); 1631w (aldimine C=N); 1590m, 1466m, (ring stretching)	m/z 339 ( <sup>59</sup> Co+L+Cl-H) <sup>+</sup>	4.49 BM	$\delta_{\text{H}}$ (270 MHz, CD <sub>3</sub> OD) 202.47 (HC=N, 2H, bs); 98.17 (H <sup>3/5</sup> , 2H, bs); 40.91 (H <sup>d</sup> , 1H, bs); -4.79 (H <sup>b</sup> , 12H, bs); -9.43 (H <sup>a</sup> , 2H, bs).
[CoCl <sub>2</sub> (L <sup>1</sup> Bu <sup>h</sup> )] · 2(H <sub>2</sub> O)	Dark Red	63 % (CH <sub>3</sub> CN)	Calc. C, 48.0%; H, 6.2%; N, 11.2%. Found. C, 48.3%; H, 6.2%; N, 11.5%.	3069m, 3030m, (aromatic C-H); 2973s, 2939s, (sp3 C-H); 2877m, (aldimine C-H); 1634m, (aldimine C=N); 1585s, 1467s, (ring stretching)	m/z 553 ( <sup>59</sup> Co+2L) <sup>+</sup> , 341 ( <sup>59</sup> Co+L+Cl) <sup>+</sup>	4.81 BM	$\delta_{\text{H}}$ (270 MHz, CD <sub>3</sub> OD) 198.08 (HC=N, 2H, bs); 93.20 (H <sup>3/5</sup> , 2H, bs); 38.28 (H <sup>d</sup> , 1H, bs); 3.04 (H <sup>e</sup> , 1H, bs); -0.21, -0.46 (H <sup>d</sup> , 6H, 2s); -3.89, -4.25 (H <sup>b</sup> , 4H, 2s); -8.57, -9.44 (H <sup>e</sup> , 6H, 2s)
[CoCl <sub>2</sub> (L <sup>1</sup> Bu <sup>i</sup> )] · 1.5(H <sub>2</sub> O)	Dark Red	68 % (CH <sub>3</sub> CN)	Calc. C, 44.8%; H, 6.5%; N, 10.5%. Found. C, 44.7%; H, 6.2%; N, 10.5%.	3063m, 3028m, (aromatic C-H); 2959s, 2931s, (sp3 C-H); 2857s, (aldimine C-H); 1634w, (aldimine C=N); 1587m, 1471s, (ring stretching)	m/z 372 ( <sup>59</sup> Co+L+2Cl-H) <sup>+</sup> , 303 ( <sup>59</sup> Co+L) <sup>+</sup>	4.22 BM	$\delta_{\text{H}}$ (270 MHz, CD <sub>3</sub> OD) 221.18 (HC=N, 2H, bs); 148.81 (H <sup>a</sup> , 4H, bs); 103.15 (H <sup>3/5</sup> , 2H, bs); 42.60 (H <sup>d</sup> , 1H, bs); 0.83 (H <sup>b</sup> , 2H, bs); -3.90 (H <sup>e</sup> , 12H, bs).
[CoCl <sub>2</sub> (L <sup>1</sup> Bu <sup>j</sup> )]	Green	50 % (CH <sub>3</sub> CN)	Calc. C, 48.0%; H, 6.2%; N, 11.2%. Found. C, 48.2%; H, 6.2%; N, 11.4%.	3060m, 3025m, (aromatic C-H); 2962s, 2931s, (sp3 C-H); 2864s, (aldimine C-H); 1636w (aldimine C=N); 1590m, 1472s, (ring stretching)	m/z 339 ( <sup>59</sup> Co+L+Cl-H) <sup>+</sup>	4.63 BM	$\delta_{\text{H}}$ (270 MHz, CD <sub>3</sub> OD) 222.00 (HC=N, 2H, bs); 103.15 (H <sup>3/5</sup> , 2H, bs); 42.60 (H <sup>d</sup> , 1H, bs); 8.88 (Ha, 18H, bs)
[CoCl <sub>2</sub> (L <sup>1</sup> Cy)]	Dark Red	97 % (CH <sub>3</sub> CN)	Calc. C, 53.4%; H, 3.4%; N, 9.8%. Found. C, 53.2%; H, 6.1%; N, 9.6%.	3060m, 3025m, (aromatic C-H); 2927s, (sp3 C-H); 2852s, (aldimine C-H); 1631wbr, (aldimine C=N); 1580m, 1468w, (ring stretching)	m/z 391 ( <sup>59</sup> Co+L+Cl-H) <sup>+</sup> , 326 ( <sup>59</sup> Co+2L) <sup>2+</sup>	4.53 BM	$\delta_{\text{H}}$ (600 MHz, D <sub>2</sub> O) 168.02 (HC=N, 2H, bs); 121.84 (H <sup>a</sup> , 2H, bs); 50.21 (H <sup>3/5</sup> , 2H, bs); 24.89 (H <sup>d</sup> , 1H, bs); 1.76 (H <sup>hb',c/c'</sup> , 4H, bs); 0.13 (H <sup>dd'</sup> , 2H, bs); -0.20 (H <sup>dd'</sup> , 2H, bs); -1.22 (H <sup>hb',c/c'</sup> , 4H, bs); -9.34 (H <sup>hb',c/c'</sup> , 4H, bs); -15.19 (H <sup>hb',c/c'</sup> , 4H, bs)
[CoBr <sub>2</sub> (L <sup>1</sup> Cy)]	Dark Red	38 % (CH <sub>3</sub> CN)	Calc. C, 44.2%; H, 5.3%; N, 8.1%. Found. C, 44.3%; H, 5.2%; N, 8.0%.	3057m, 3025m, (aromatic C-H); 2930s, (sp3 C-H); 2852s, (aldimine C-H); 1631wbr, (aldimine C=N); 1582m, 1466w, (ring stretching)	m/z 326 ( <sup>59</sup> Co+2L) <sup>2+</sup>	4.58 BM	$\delta_{\text{H}}$ (600 MHz, D <sub>2</sub> O) 167.89 (HC=N, 2H, bs); 121.89 (H <sup>a</sup> , 2H, bs); 50.28 (H <sup>3/5</sup> , 2H, bs); 24.79 (H <sup>d</sup> , 1H, bs); 1.79 (H <sup>hb',c/c'</sup> , 4H, bs); 0.15 (H <sup>dd'</sup> , 2H, bs); -0.18 (H <sup>dd'</sup> , 2H, bs); -1.18 (H <sup>hb',c/c'</sup> , 4H, bs); -9.31 (H <sup>hb',c/c'</sup> , 4H, bs); -15.12 (H <sup>hb',c/c'</sup> , 4H, bs).

**Table 17.** Characterisation data for Co<sup>II</sup> complexes of L<sup>1</sup>R continued; a) Uninterpretable, b) Insoluble.

Compound	Colour	Yield (solvent)	Microanalysis	Infra-red Spectrum (KBr) $\nu_{\max}$ cm <sup>-1</sup>	Mass Spectrum ESI+	$\mu_{\text{eff}}$	<sup>1</sup> H NMR
[Co(L <sup>1</sup> Cy) <sub>2</sub> ][NO <sub>3</sub> ] <sub>2</sub>	Dark Red	63 % (CH <sub>3</sub> CN : Et <sub>2</sub> O)	Calc. C, 54.4%; H, 6.5%; N, 15.0%. Found. C, 54.1%; H, 6.7%; N, 14.9%.	3082w, 3037w, (aromatic C-H); 2931m, (sp <sup>3</sup> C-H); 2851m, (aldimine C-H); 1630wbr, (aldimine C=N); 1587m, 1467w, (ring stretching); 1385s, (N-O)	m/z 326 ( <sup>59</sup> Co+2L) <sup>2+</sup>	4.52 BM	$\delta_{\text{H}}$ (600 MHz, D <sub>2</sub> O) 168.18 (HC=N, 2H, bs); 121.98 (H <sup>a</sup> , 2H, bs); 50.45 (H <sup>3/5</sup> , 2H, bs); 24.91 (H <sup>d</sup> , 1H, bs); 1.86 (H <sup>bb',c/c'</sup> , 4H, bs); 0.24 (H <sup>d/d'</sup> , 2H, bs); -0.10 (H <sup>d/d'</sup> , 2H, bs); -1.12 (H <sup>bb',c/c'</sup> , 4H, bs); -9.25 (H <sup>bb',c/c'</sup> , 4H, bs); -15.10 (H <sup>bb',c/c'</sup> , 4H, bs).
[Co(L <sup>1</sup> Cy) <sub>2</sub> ][BF <sub>4</sub> ] <sub>2</sub> · 2(H <sub>2</sub> O) · (CH <sub>3</sub> CN)	Dark Red	64 % (Ac <sub>2</sub> O : Et <sub>2</sub> O)	Calc. C, 53.1%; H, 6.8%; N, 10.8%. Found. C, 53.0%; H, 6.7%; N, 11.0%.	3080w, 3037w, (aromatic C-H); 2931m, (sp <sup>3</sup> C-H); 2857m, (aldimine C-H); 1630wbr, (aldimine C=N); 1587m, 1467w, (ring stretching); 1385s, (N-O)	m/z 326 ( <sup>59</sup> Co+2L) <sup>2+</sup>	4.59 BM	$\delta_{\text{H}}$ (600 MHz, D <sub>2</sub> O) 171.48 (HC=N, 2H, bs); 124.58 (H <sup>a</sup> , 2H, bs); 54.07 (H <sup>3/5</sup> , 2H, bs); 25.57 (H <sup>d</sup> , 1H, bs); 1.82 (H <sup>bb',c/c'</sup> , 4H, bs); 0.18 (H <sup>d/d'</sup> , 2H, bs); -0.10 (H <sup>d/d'</sup> , 2H, bs); -1.28 (H <sup>bb',c/c'</sup> , 4H, bs); -10.05 (H <sup>bb',c/c'</sup> , 4H, bs); -16.53 (H <sup>bb',c/c'</sup> , 4H, bs)
[Co(L <sup>1</sup> Cy) <sub>2</sub> ][Co(SCN) <sub>4</sub> ]	Dark Red	99% (CH <sub>3</sub> CN)	Calc. C, 53.4%; H, 5.8%; N, 14.8%. Found. C, 53.5%; H, 5.8%; N, 15.0%.	2930m, (sp <sup>3</sup> C-H); 2855m, (aldimine C-H); 2070s, (isothiocyanate C≡N); 1632wbr, (aldimine C=N); 1587w, 1470w, 1448w, (ring stretching)	m/z 326 ( <sup>59</sup> Co+2L) <sup>2+</sup>	4.88 BM	a
[Co(AcO) <sub>2</sub> (L <sup>1</sup> Cy)]	Red	68 % (CH <sub>3</sub> CN : Et <sub>2</sub> O)	Calc. C, 58.2%; H, 7.0%; N, 8.9%. Found. C, 58.1%; H, 7.1%; N, 8.5%.	3067w, 3020w, 3004w, (aromatic C-H); 2990w, 2931s, (sp <sup>3</sup> C-H); 2857m, (aldimine C-H); 1702m, (unidentate OAc C=O); 1624s, (aldimine C=N); 1591s (bidentate OAc C=O), 1580s, 1443s, (ring stretching); 1420s (OAc C-O)	m/z 415 ( <sup>59</sup> Co+L+AcO) <sup>+</sup> , 326 ( <sup>59</sup> Co+2L) <sup>2+</sup>	4.38 BM	$\delta_{\text{H}}$ (600 MHz, D <sub>2</sub> O) 168.02 (HC=N, 2H, bs); 121.84 (H <sup>a</sup> , 2H, bs); 50.21 (H <sup>3/5</sup> , 2H, bs); 24.89 (H <sup>d</sup> , 1H, bs); 1.76 (H <sup>bb',c/c'</sup> , 4H, bs); 0.13 (H <sup>d/d'</sup> , 2H, bs); -0.20 (H <sup>d/d'</sup> , 2H, bs); -1.22 (H <sup>bb',c/c'</sup> , 4H, bs); -9.34 (H <sup>bb',c/c'</sup> , 4H, bs); -15.19 (H <sup>bb',c/c'</sup> , 4H, bs).
[CoCl <sub>2</sub> (L <sup>1</sup> CyMe)]. 2.5(H <sub>2</sub> O)	Dark Red	26 % (CH <sub>3</sub> CN)	Calc. C, 50.6%; H, 6.9%; N, 8.4%. Found. C, 50.3%; H, 6.7%; N, 8.3%.	3062m, 3025m, (aromatic C-H); 2927s, (sp <sup>3</sup> C-H); 2870m, (aldimine C-H); 1640wbr, (aldimine C=N); 1585s, 1474s, (ring stretching)	m/z 419 ( <sup>59</sup> Co+L+Cl-H) <sup>+</sup> , 384 ( <sup>59</sup> Co+L-H) <sup>+</sup> , 355 ( <sup>59</sup> Co+2L) <sup>2+</sup>	4.77 BM	a
[CoCl <sub>2</sub> (L <sup>1</sup> Ph)]	Brown	95 % (CH <sub>3</sub> CN)	Calc. C, 55.0%; H, 3.6%; N, 10.1%. Found. C, 52.3%; H, 3.7%; N, 10.9%.	3055m, 3053m, 3024m, 3000m (aromatic C-H); 2931m (aldimine C-H); 1622w (aldimine C=N); 1567, 1486s, (ring stretching)	m/z 379 ( <sup>59</sup> Co+L+Cl-H) <sup>+</sup> , 344 ( <sup>59</sup> Co+L-H) <sup>+</sup> , 314 ( <sup>59</sup> Co+2L) <sup>2+</sup>	4.41 BM	$\delta_{\text{H}}$ (600 MHz, D <sub>2</sub> O) 165.63 (HC=N, 2H, bs); 47.70 (H <sup>3/5</sup> , 2H, bs); 26.28 (H <sup>d</sup> , 1H, bs); 12.33 (H <sup>d</sup> , 4H, bs); -0.13 (H <sup>e</sup> , 2H, bs); -15.30 (H <sup>e</sup> , 4H, bs).
[CoCl <sub>2</sub> (L <sup>1</sup> PhMe)]	Brown	84 % (CH <sub>3</sub> CN)	Calc. C, 56.9%; H, 4.3%; N, 9.5%. Found. C, 57.2%; H, 4.0%; N, 9.4%.	3065m, 3042m, 3006m, (aromatic C-H); 2950m, 2925m, 2920m, (sp <sup>3</sup> C-H); 2851m (aldimine C-H); 1595s, 1550s, 1495s, (ring stretching)	m/z 343 ( <sup>59</sup> Co+2L) <sup>2+</sup>	insol	b
[CoCl <sub>2</sub> (L <sup>1</sup> PhCl)]	Brown	95 % (DMSO : DCM)	Calc. C, 47.1%; H, 2.7%; N, 8.7%. Found. C, 47.2%; H, 2.6%; N, 8.7%.	3078m, 3050m, 3025m (aromatic C-H); 1620brw (aldimine C=N) 1586m, 1488s (ring stretching)	FAB MS m/z 765 ( <sup>59</sup> Co+L+(L-Cl)+Cl) <sup>+</sup>	insol	b
[CoCl <sub>2</sub> (L <sup>1</sup> PhNO <sub>2</sub> )]	Brown	94 % (CH <sub>3</sub> CN)	Calc. C, 45.2%; H, 2.6%; N, 13.9%. Found. C, 45.2%; H, 2.7%; N, 13.7%.	3101w, 3085w, 3052w, 3035w, (aromatic C-H); 2850w, (aldimine C-H); 1602m (aldimine C=N); 1587s, 1490w, (ring stretching); 1522m, 1339s, (N=O)	FAB MS m/z 809 (59Co+2L-H) <sup>+</sup>	insol	b

**Table 18.** Characterisation data for Ni<sup>II</sup> complexes of L<sup>1</sup>R.

Compound	Colour	Yield (solvent)	Microanalysis	Infra-red Spectrum (KBr) $\nu_{\max}$ cm <sup>-1</sup>	Mass Spectrum ESI+	$\mu_{\text{eff}}$
[NiCl(H <sub>2</sub> O) <sub>2</sub> (L <sup>1</sup> Et)]Cl	Green	69 % (CH <sub>3</sub> CN)	Calc. C, 37.2%; H, 5.4%; N, 11.8%. Found. C, 37.6%; H, 5.0%; N, 11.5%.	3353s, 3158s, (coordinated H <sub>2</sub> O); 2981m, 2934m, (sp <sup>3</sup> C-H); 2869w, (aldimine C-H); 1639brw, (aldimine C=N); 1592m, 1471m, (ring stretching)	m/z 264 ( <sup>58</sup> Ni+L+OH) <sup>+</sup>	3.41 BM
$\mu_2$ -Cl-[NiCl(L <sup>1</sup> Pr <sup>n</sup> )] 2.H <sub>2</sub> O	Green	55 % (CH <sub>3</sub> CN)	Calc. C, 42.8%; H, 5.8%; N, 11.5%. Found. C, 42.8%; H, 5.6%; N, 11.9%.	3425 (lattice H <sub>2</sub> O); 3053w, 3005w, (aromatic C-H); 2968s, 2925s, (sp <sup>3</sup> C-H); 2876m (aldimine C-H); 1634w, (aldimine C=N); 1585s, 1474m, (ring stretching)	m/z 310 ( <sup>58</sup> Ni+L+Cl-H) <sup>+</sup>	3.27 BM
[NiCl <sub>2</sub> (L <sup>1</sup> Bu <sup>n</sup> )]	Green	73 % (CH <sub>3</sub> CN)	Calc. C, 48.1%; H, 6.2%; N, 11.2%. Found. C, 48.0%; H, 6.5%; N, 11.5%.	3060m, 3025m, (aromatic C-H); 2965s, 2925 (sp <sup>3</sup> C-H); 2867m (aldimine C-H); 1634w, (aldimine C=N); 1585m, 1472m, (ring stretching)	m/z 274 ( <sup>58</sup> Ni+2L-H) <sup>2+</sup>	3.15 BM
[NiCl <sub>2</sub> (L <sup>1</sup> Cy)]	Green	75 % (CH <sub>3</sub> CN)	Calc. C, 53.4%; H, 6.4%; N, 9.8%. Found. C, 53.0%; H, 6.3%; N, 9.8%.	3070m, 3031m, (aromatic C-H); 2928s, (sp <sup>3</sup> C-H); 2855m (aldiminine C-H); 1632w, (aldimine C=N); 1585m, 1470m, (ring stretching)	m/z 326 ( <sup>58</sup> Ni+2L-H) <sup>2+</sup>	3.25 BM
[Ni(AcO) <sub>2</sub> (L <sup>1</sup> Cy)]. CH <sub>3</sub> CN	Green	71 % (CH <sub>3</sub> CN)	Calc. C, 58.3%; H, 7.0%; N, 10.9%. Found. C, 58.4%; H, 7.1%; N, 10.9%.	3074m, 3020m, (aromatic C-H); 2934s, (sp <sup>3</sup> C-H); 2860s (aldiminine C-H); 1652, (AcO C=O); 1620w, (aldimine C=N); 1587m, 1455m, (ring stretching)	m/z 414 ( <sup>58</sup> Ni+L+AcO) <sup>+</sup> , 326 ( <sup>58</sup> Ni+2L) <sup>2+</sup>	3.27 BM
[NiCl <sub>2</sub> (L <sup>1</sup> Ph)]	Orange	50 % (CH <sub>3</sub> CN)	Calc. C, 55.0%; H, 3.6%; N, 10.1%. Found. C, 55.0%; H, 3.7%; N, 10.6%.	3067w, 3005w, (aromatic C-H); 1640m, (aldimine C=N); 1585m, 1495m, (ring stretching)	m/z 315 ( <sup>58</sup> Ni+2L) <sup>2+</sup>	3.43 BM
[NiCl <sub>2</sub> (L <sup>1</sup> PhMe)]	Orange	52 % (CH <sub>3</sub> CN)	Calc. C, 56.9%; H, 4.3%; N, 9.5%. Found. C, 56.7%; H, 4.3%; N, 9.5%.	3070m, 3008m, (aromatic C-H); 2928m, 2924m, (sp <sup>3</sup> C-H); 2860m (aldiminine C-H); 1632wbr, (aldimine C=N); 1592m, 1578w, 1508m, 1470m, (ring stretching)	m/z 406 ( <sup>58</sup> Ni+L+Cl-H) <sup>+</sup> , 343 ( <sup>58</sup> Ni+2L) <sup>2+</sup>	3.34 BM

**Table 19.** Characterisation data for Cu<sup>II</sup> complexes of L<sup>3</sup>R.

Compound	Colour	Yield (solvent)	Microanalysis	Infra-red Spectrum (KBr) $\nu_{\max}$ cm <sup>-1</sup>	Mass Spectrum FAB
[CuCl <sub>2</sub> (L <sup>3</sup> Bu <sup>n</sup> )]	Yellow	(CH <sub>3</sub> CN) 53%	Calc. C, 54.9%; H, 5.5%; N, 11.7%. Found. C, 54.6%; H, 5.7%; N, 11.3%.	3038m, 3012m, (aromatic C-H); 2956s, 2935s, (sp <sup>3</sup> C-H); 2864s, (aldimine C-H); 1637s, (uncoordinated aldimine C=N); 1615s, (coordinated aldimine C=N); 1604s, 1570s 1492s, (C=C)	m/z 445 [ <sup>63</sup> Cu+L+Cl] <sup>+</sup> , 410 [ <sup>63</sup> Cu+L] <sup>+</sup>
[CuCl <sub>2</sub> (L <sup>3</sup> Bu <sup>2</sup> )]	Yellow	(CH <sub>3</sub> CN) 51%	Calc. C, 54.9%; H, 5.5%; N, 11.7%. Found. C, 55.0%; H, 5.3%; N, 11.5%.	3049m, 3015m, 3012w, (aromatic C-H); 2962s, 2925s, (sp <sup>3</sup> C-H); 2870m, (aldimine C-H); 1644w, (uncoordinated aldimine C=N); 1610m, (coordinated aldimine C=N); 1585w, 1567m, 1492s, (C=C)	m/z 445 [ <sup>63</sup> Cu+L+Cl] <sup>+</sup> , 410 [ <sup>63</sup> Cu+L] <sup>+</sup>
[CuCl <sub>2</sub> (L <sup>3</sup> Bu <sup>1</sup> )]	Yellow	(CH <sub>3</sub> CN) 56%	Calc. C, 54.9%; H, 5.5%; N, 11.7%. Found. C, 55.0%; H, 5.5%; N, 12.0%.	3067m, 3042m, 3015w, (aromatic C-H); 2956s, 2925s, (sp <sup>3</sup> C-H); 2863s, 2833m (aldimine C-H); 1647m, (uncoordinated aldimine C=N); 1604m, (coordinated aldimine C=N); 1585m, 1567m, 1492s, (C=C)	m/z 445 [ <sup>63</sup> Cu+L+Cl] <sup>+</sup> , 410 [ <sup>63</sup> Cu+L] <sup>+</sup>
[CuCl <sub>2</sub> (L <sup>3</sup> Bu <sup>1</sup> )]	Yellow	(CH <sub>3</sub> CN) 48%	Calc. C, 54.9%; H, 5.5%; N, 11.7%. Found. C, 55.3%; H, 5.6%; N, 11.8%.	3066m, 3040m, 3012w, (aromatic C-H); 2957s, 2928s, (sp <sup>3</sup> C-H); 2863s (aldimine C-H); 1640m, (uncoordinated aldimine C=N); 1610m, (coordinated aldimine C=N); 1585m, 1566m, 1492s, (C=C)	m/z 445 [ <sup>63</sup> Cu+L+Cl] <sup>+</sup> , 410 [ <sup>63</sup> Cu+L] <sup>+</sup>
[CuCl <sub>2</sub> (L <sup>3</sup> Cy)]	Yellow	(DMF) 44%	Calc. C, 58.6%; H, 5.7%; N, 10.5%. Found. C, 58.6%; H, 5.7%; N, 10.4%.	3066m, 3020w (aromatic C-H); 2968, 2925s (sp <sup>3</sup> C-H); 2870s (aldimine C-H); 1641m, (uncoordinated aldimine C=N); 1610m, (coordinated aldimine C=N); 1585m, 1560m, 1499s (C=C)	m/z 497 [ <sup>63</sup> Cu+L+Cl] <sup>+</sup> , 462 [ <sup>63</sup> Cu+L] <sup>+</sup>
[CuCl <sub>2</sub> (L <sup>3</sup> Ph)]	Brown	(DMF) 65%	Calc. C, 60.0%; H, 3.5%; N, 10.8%. Found. C, 59.6%; H, 3.4%; N, 10.9%.	3049m, 3012m (aromatic C-H); 2925m (aldimine C-H); 1653s (uncoordinated aldimine C=N); 1615w, (coordinated aldimine C=N); 1605w, 1570m, 1498s, (C=C)	m/z 485 [ <sup>63</sup> Cu+L+Cl] <sup>+</sup> , 450 [ <sup>63</sup> Cu+L] <sup>+</sup> 418, [ <sup>63</sup> Cu+2L-H] <sup>2+</sup>
[CuCl <sub>2</sub> (L <sup>3</sup> PhMe)]	Brown	(DMF) 76%	Calc. C, 61.3%; H, 4.0%; N, 10.2%. Found. C, 58.9%; H, 3.9%; N, 9.8%.	3055m, 3045m, 3030m, 3005m (aromatic C-H); 2925m (sp <sup>3</sup> C-H); 2864w (aldimine C-H); 1660s (uncoordinated aldimine C=N); 1616w, (coordinated aldimine C=N); 1605w, 1574m, 1497s, (C=C)	m/z 513 [ <sup>63</sup> Cu+L+Cl] <sup>+</sup> , 477 [ <sup>63</sup> Cu+L] <sup>+</sup>
[CuCl <sub>2</sub> (L <sup>3</sup> PhCl)]	Brown	(DMF) 71%	Calc. C, 53.0%; H, 2.7%; N, 9.5%. Found. C, 53.0%; H, 2.5%; N, 10.0%.	3086m, 3049m, 3030m, 3000m, (aromatic C-H); 2937m, (aldimine C-H); 1670s, (uncoordinated aldimine C=N); 1615w, (coordinated aldimine C=N); 1600w, 1573m, 1495s, (C=C)	m/z 553 [ <sup>63</sup> Cu+L+Cl] <sup>+</sup> , 518 [ <sup>63</sup> Cu+L] <sup>+</sup>

**Table 20.** Characterisation data for Zn<sup>II</sup> complexes of L<sup>3</sup>R; a) Insoluble.

Compound	Colour	Yield (solvent)	Microanalysis	Infra-red Spectrum (KBr) $\nu_{\max}$ cm <sup>-1</sup>	Mass Spectrum FAB	<sup>1</sup> H NMR
[ZnCl <sub>2</sub> (L <sup>3</sup> Bu <sup>n</sup> )]	Colourless	(CH <sub>3</sub> CN) 68%	Calc. C, 54.7%; H, 5.4%; N, 11.6%. Found. C, 54.7%; H, 5.3%; N, 11.7%.	3066w, 3025w, (aromatic C-H); 2956m, 2928m, (sp <sup>3</sup> C-H); 2864, (aldimine C-H); 1641s, (uncoordinated aldimine C=N); 1618m, (coordinated aldimine C=N); 1604m, 1563m, 1490w, (ring breathing).	m/z 445 [ <sup>65</sup> Zn+L+Cl] <sup>+</sup>	$\delta_{\text{H}}$ (600 MHz, (CD <sub>3</sub> ) <sub>2</sub> SO) 9.25 (2H, s, HC=N), 8.73 (H <sup>3/8</sup> , 2H, d, J = 8.4 Hz), 8.45 (H <sup>4/7</sup> , 2H, d, J = 8.4 Hz), 8.30 (H <sup>5/6</sup> , 2H, s), 4.03 (H <sup>a</sup> , 4H, t, J = 7.0 Hz), 2.03 (H <sup>b</sup> , 4H, m, J = 7.0 Hz), 1.62 (H <sup>c</sup> , 4H, m, 7.6 Hz), 1.05 (H <sup>d</sup> , 6H, t, J = 7.5 Hz)
[ZnCl <sub>2</sub> (L <sup>3</sup> Bu <sup>t</sup> )]	Colourless	(CH <sub>3</sub> CN) 65%	Calc. C, 54.7%; H, 5.4%; N, 11.6%. Found. C, 54.9%; H, 5.4%; N, 11.9%.	3075m, 3020m, (aromatic C-H); 2956m, 2928m, (sp <sup>3</sup> C-H); 2873m, (aldimine C-H); 1646s, (uncoordinated aldimine C=N); 1618m, (coordinated aldimine C=N); 1609m, 1563m, 1490w, (ring breathing)	m/z 445 [ <sup>65</sup> Zn+L+Cl] <sup>+</sup>	$\delta_{\text{H}}$ (600 MHz, (CD <sub>3</sub> ) <sub>2</sub> SO) 9.21 (2H, s, HC=N), 8.76 (H <sup>3/8</sup> , 2H, d, J = 8.4 Hz), 8.44 (H <sup>4/7</sup> , 2H, d, J = 8.4 Hz), 8.29 (H <sup>5/6</sup> , 2H, s), 3.98 (H <sup>a</sup> , 4H, d, J = 6.6 Hz), 2.20 (H <sup>b</sup> , 2H, m, J = 6.6 Hz), 1.13 (H <sup>c</sup> , 12H, d, J = 6.3 Hz)
[ZnCl <sub>2</sub> (L <sup>3</sup> Bu <sup>2</sup> )]	Colourless	(CH <sub>3</sub> CN) 56%	Calc. C, 54.7%; H, 5.4%; N, 11.6%. Found. C, 54.5%; H, 5.1%; N, 11.7%.	3066m, (aromatic C-H); 2964m, 2928m, (sp <sup>3</sup> C-H); 2870m, (aldimine C-H); 1638m, (uncoordinated aldimine C=N); 1618m, (coordinated aldimine C=N); 1609m, 1563m, 1490w, (ring breathing)	m/z 445 [ <sup>65</sup> Zn+L+Cl] <sup>+</sup>	$\delta_{\text{H}}$ (600 MHz, CD <sub>3</sub> CN:(CD <sub>3</sub> ) <sub>2</sub> CO:CD <sub>3</sub> OD) 9.23 (2H, s, HC=N), 8.86 (H <sup>3/8</sup> , 2H, d, J = 8.4 Hz), 8.50 (H <sup>4/7</sup> , 2H, d, J = 8.4 Hz), 8.22 (H <sup>5/6</sup> , 2H, s), 3.86 (H <sup>a</sup> , 2H, m, J = 6.5 Hz), 2.03 (H <sup>bb</sup> , 1H, m, J = 7.5 Hz), 1.90 (H <sup>bb'</sup> , 1H, m, J = 7.5 Hz) 1.56 (H <sup>d</sup> , 6H, d, J = 6.5 Hz), 1.04 (H <sup>e</sup> , 6H, t, J = 7.3 Hz)
[ZnCl <sub>2</sub> (L <sup>3</sup> Bu <sup>f</sup> )]	Colourless	(CH <sub>3</sub> CN) 57%	Calc. C, 54.7%; H, 5.4%; N, 11.6%. Found. C, 54.5%; H, 5.3%; N, 11.6%.	3066m, 3012m (aromatic C-H); 2964, 2928s (sp <sup>3</sup> C-H); 2863s (aldimine C-H); 1636m, (uncoordinated aldimine C=N); 1618m, (coordinated aldimine C=N); 1585m, 1563m, 1490m, (ring breathing)	m/z 445 [ <sup>65</sup> Zn+L+Cl] <sup>+</sup>	$\delta_{\text{H}}$ (270 MHz, (CD <sub>3</sub> ) <sub>2</sub> SO) 9.23 (2H, s, HC=N), 8.99 (H <sup>3/8</sup> , 2H, d, J = 8.1 Hz), 8.53 (H <sup>4/7</sup> , 2H, d, J = 8.1 Hz), 8.33 (H <sup>5/6</sup> , 2H, s), 1.47 (Ha, 18H, s)
[ZnCl <sub>2</sub> (L <sup>3</sup> Cy)]	Colourless	(CH <sub>3</sub> CN) 59%	Calc. C, 58.4%; H, 5.7%; N, 10.5%. Found. C, 58.7%; H, 5.8%; N, 10.4%.	3061m, 3025m (aromatic C-H); 2969s, 2937s, (sp <sup>3</sup> C-H); 2882s, (aldimine C-H); 1641s, (uncoordinated aldimine C=N); 1618m, (coordinated aldimine C=N); 1610m, 1511m, 1567m, 1468w, (ring breathing)	m/z 497 [ <sup>65</sup> Zn+L+Cl] <sup>+</sup>	$\delta_{\text{H}}$ (600 MHz, (CD <sub>3</sub> ) <sub>2</sub> SO, 100°C) 9.14 (2H, s, HC=N), 8.90 (H <sup>3/8</sup> , 2H, d, J = 7 Hz), 8.43 (H <sup>4/7</sup> , 2H, d, J = 7 Hz), 8.24 (H <sup>5/6</sup> , 2H, s), 3.66 (H <sup>a</sup> , 2H, br), 2.00-1.0 (H <sup>b/c/d</sup> , 20H, br mm)
[ZnCl <sub>2</sub> (L <sup>3</sup> Ph)]	Yellow	(DMF) 70%	Calc. C, 59.7%; H, 3.5%; N, 10.7%. Found. C, 59.6%; H, 3.3%; N, 11.0%.	3092w, 3069w, 3050w, (aromatic C-H); 2870w, 2860w, (aldimine C-H); 1620m, (uncoordinated aldimine C=N); 1610w, (coordinated aldimine C=N); 1590w, 1581w, 1501w, (ring breathing)	m/z 485 [ <sup>65</sup> Zn+L+Cl] <sup>+</sup>	$\delta_{\text{H}}$ (270 MHz, (CD <sub>3</sub> ) <sub>2</sub> SO, 30°C) 9.58 (2H, s, HC=N), 9.11 (H <sup>3/8</sup> , 2H, d, J = 8.4 Hz), 8.73 (H <sup>4/7</sup> , 2H, d, J = 8.4 Hz), 8.42 (H <sup>5/6</sup> , 2H, s), 7.79 (H <sup>a</sup> , 4H, d, J = 7.3 Hz), 7.59 (H <sup>b</sup> , 4H, t, J = 7.3 Hz), 7.46 (H <sup>c</sup> , 2H, t, J = 7.3 Hz)
[ZnCl <sub>2</sub> (L <sup>3</sup> PhMe)]	Yellow	(DMF) 77%	Calc. C, 61.1%; H, 4.0%; N, 10.2%. Found. C, 61.0%; H, 4.0%; N, 10.2%.	3089w, 3060w, 3024w, (aromatic C-H) 2963w, 2919w, (sp <sup>3</sup> C-H); 2857w, (aldimine C-H); 1624m, (uncoordinated aldimine C=N); 1610w, (coordinated aldimine C=N); 1590w, 1581w, 1501w, (ring breathing)	m/z 478 [ <sup>65</sup> Zn+L+Cl] <sup>+</sup>	$\delta_{\text{H}}$ (270 MHz, (CD <sub>3</sub> ) <sub>2</sub> SO, 60°C) 9.58 (2H, s, HC=N) 9.08 (H <sup>3/8</sup> , 2H, d, J = 8.3 Hz), 8.68 (H <sup>4/7</sup> , 2H, d, J = 8.3 Hz), 8.39 (H <sup>5/6</sup> , 2H, s), 7.70 (H <sup>a</sup> , 4H, d, J = 8.1 Hz), 7.38 (H <sup>b</sup> , 4H, d, 8.1 Hz), 2.41 (H <sup>c</sup> , 6H, s)
[Zn(NO <sub>3</sub> ) <sub>2</sub> (L <sup>3</sup> PhMe)]	Yellow	(CH <sub>3</sub> CN) 74%	Calc. C, 55.7%; H, 3.7%; N, 13.9%. Found. C, 55.9%; H, 3.9%; N, 13.8%.	3089w, 3060w, 3024w, (aromatic C-H) 2963w, 2919w, (sp <sup>3</sup> C-H); 2857w, (aldimine C-H); 1624m, (uncoordinated aldimine C=N); 1610w, (coordinated aldimine C=N); 1590w, 1581w, 1501w, (ring breathing)	m/z 540 [ <sup>65</sup> Zn+L+NO <sub>3</sub> ] <sup>+</sup>	a
[ZnCl <sub>2</sub> (L <sup>3</sup> PhCl)]	Yellow	(DMF) 45%	Calc. C, 52.8%; H, 2.7%; N, 9.5%. Found. C, 52.6%; H, 2.7%; N, 9.6%.	3089w, 3060w, 3024w, (aromatic C-H) 2963w, 2919w, (sp <sup>3</sup> C-H); 2857w, (aldimine C-H); 1624m, (uncoordinated aldimine C=N); 1610w, (coordinated aldimine C=N); 1590w, 1581w, 1501w, (ring breathing)	m/z 553 [ <sup>65</sup> Zn+L+Cl] <sup>+</sup>	$\delta_{\text{H}}$ (270 MHz, (CD <sub>3</sub> ) <sub>2</sub> SO, 100°C) 9.44 (2H, s, HC=N), 8.96 (H <sup>3/8</sup> , 2H, d, J = 8.3 Hz), 8.66 (H <sup>4/7</sup> , 2H, d, J = 8.3), 8.30 (H <sup>5/6</sup> , 2H, s), 7.71 (H <sup>b</sup> , 4H, d, J = 8.6 Hz), 7.54 (H <sup>a</sup> , 4H, d, J = 8.5 Hz)

**Table 21.** Characterisation data for Zn<sup>II</sup> complexes of L<sup>2</sup>R.

Compound	Colour	Yield (solvent)	Microanalysis	Infra-red Spectrum (KBr) $\nu_{\max}$ cm <sup>-1</sup>	Mass Spectrum ESI+	<sup>1</sup> H NMR
[ZnCl <sub>2</sub> (L <sup>2</sup> Cy)]	Colourless	(CH <sub>3</sub> CN) 42%	Calc. C, 51.1%; H, 5.4%; N, 14.9%. Found. C, 51.0%; H, 5.2%; N, 14.9%.	not obtained	m/z 563 [ <sup>65</sup> Zn+L+2NO <sub>3</sub> ] <sup>+</sup> , 501 [ <sup>65</sup> Zn+L+NO <sub>3</sub> ] <sup>+</sup>	$\delta_{\text{H}}$ (270 MHz, (CD <sub>3</sub> ) <sub>2</sub> SO, 140°C) 8.88 (2H, br s, HC=N), 8.60 (H <sup>3,8</sup> , 2H, d, J = 8.0 Hz), 8.28 (H <sup>d,7</sup> , 2H, br t), 8.13 (H <sup>5,6</sup> , 2H, d J = 8.0 Hz), 3.61 (H <sup>f</sup> , 2H, br m), 2.00-1.00 (H <sup>b,c,d</sup> , 20H, br mm)
[Zn(NO <sub>3</sub> )(H <sub>2</sub> O)(L <sup>2</sup> PhMe)][NO <sub>3</sub> ]	Yellow	(CH <sub>3</sub> CN) 63%	Calc. C, 53.9%; H, 3.8%; N, 14.5%. Found. C, 53.8%; H, 3.6%; N, 14.6%.	not obtained	m/z 579 [ <sup>65</sup> Zn+L+2NO <sub>3</sub> ] <sup>+</sup> , 517 [ <sup>65</sup> Zn+L+NO <sub>3</sub> ] <sup>+</sup>	$\delta_{\text{H}}$ (600 MHz, CDCl <sub>3</sub> :CD <sub>3</sub> OD:CD <sub>3</sub> CN) 9.06 (2H, br s, HC=N), 8.72 (H <sup>3,8</sup> , 2H, d, J = 9.0 Hz), 8.54 (H <sup>d,7</sup> , 2H, t, J = 8.9 Hz), 8.27 (H <sup>5,6</sup> , 2H, d, J = 9.0 Hz), 7.53 (H <sup>a</sup> , 4H, d, J = 8.3 Hz), 7.35 (H <sup>b</sup> , 4H, d, J = 8.1 Hz), 2.46 (Hc, 6H, s)

**Table 22.** Characterisation data for Ru<sup>III</sup> complex of L<sup>1</sup>R.

Compound	Colour	Yield (solvent)	Microanalysis	Infra-red Spectrum (KBr) $\nu_{\max}$ cm <sup>-1</sup>	Mass Spectrum ESI+	<sup>1</sup> H NMR
[RuCl <sub>3</sub> (L <sup>1</sup> PhMe)]	Deep Red	90% (EtOH)	Calc. C, 48.4%; H, 3.7%; N, 8.1%. Found. C, 48.1%; H, 3.4%; N, 8.1%.	not obtained	m/z 526 (Ru+L+2Cl+CH <sub>3</sub> CN-H) <sup>+</sup>	-

## **2.2. Biological Methods**

### **2.2.1. *In vitro* Cell Culture and Chemosensitivity**

All media and supplements were obtained from Gibco BRL (Paisley, UK) unless otherwise stated. All other chemicals were obtained from Sigma-Aldrich (Dorset, UK) unless otherwise stated. Three tumour cell lines were used for cytotoxicity assays, these were the human cell lines H460 (human Non Small Cell Lung Carcinoma), HT-29 (human colon adenocarcinoma) and DLD-1 (human colon adenocarcinoma), obtained from the ECACC. All cells were routinely maintained as monolayer cultures at 37 °C in a humidified, CO<sub>2</sub>-enriched (5%) environment and cultured in RPMI 1640 supplemented with 10% foetal calf serum, sodium pyruvate (2 mM), L-glutamine (2 mM) and buffered with HEPES (25 mM). *In vitro* chemosensitivity was determined using the MTT assay in 96-well cell-culture clusters. All experiments were carried out in an aseptic environment, in a class II laminar air flow cabinet (Hepaire Manufacturing Ltd, UK).

#### **2.2.1.1. Routine Subculture of Cells**

Cells were allowed to reach confluence before subculture was undertaken. All cell lines adhered to the bottom of the flask. The old culture medium was discarded and the cell monolayer washed twice with Hanks Balanced Salt Solution (HBSS, 2x10 ml). Trypsin-EDTA (0.25% trypsin, 0.02% EDTA), was added (0.5 ml in 25 cm<sup>2</sup> flask), and the flask incubated for 5 min. The flask was then gently agitated to remove cells adhered to the base of the flask. Once the cells had detached, culture medium (10 ml) was added and the cells were detached by gentle shaking. The number of cells in suspension was determined using an improved Neubauer haemocytometer, as described in section

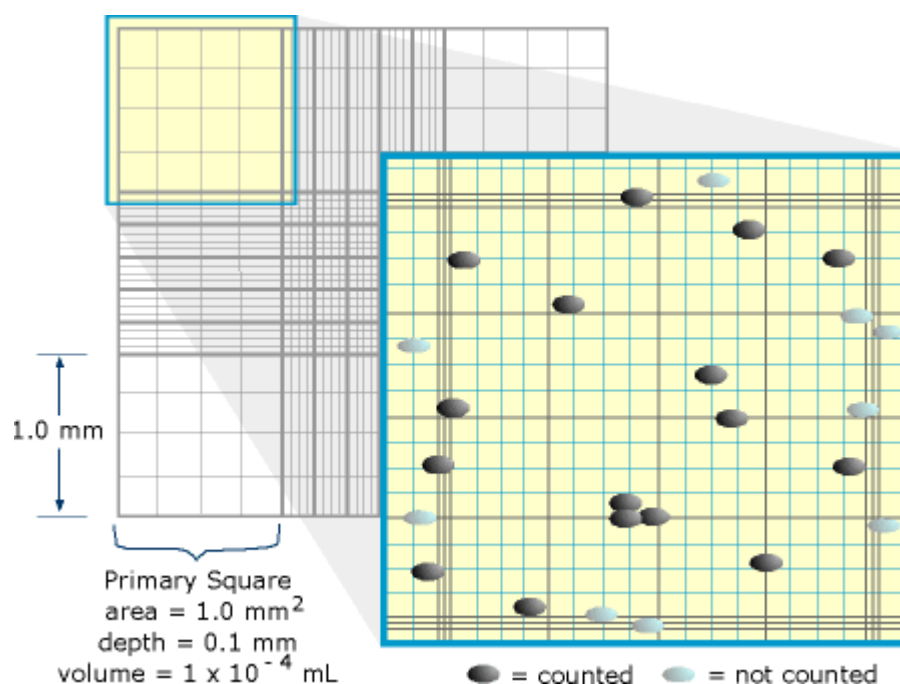


2.2.1.2. Cell suspensions of  $1 \times 10^4$  cells  $\text{ml}^{-1}$  of fresh culture medium were made and aliquots (10 ml) were incubated in  $25 \text{ cm}^2$  flasks. This procedure was routinely followed in order to maintain all cell lines.

### **2.2.1.2. Counting Cells in Suspension**

An improved Neubauer haemocytometer was used to count the number of cells in suspension. The haemocytometer is a modified microscope slide, which has two polished surfaces, each of which has a ruled grid. The grid has 9 primary squares, with sides of 1 mm, which are limited by 3 lines  $2.5 \mu\text{m}$  apart. These lines are used to decide which cells should and indeed should not, be included when counting cells in the grid. Each primary square is further divided into smaller squares to help with counting. This is shown in Figure 14. The plane of the grid lies 0.1 mm below ridges and these support a cover slip. There is a bevelled edge at the outer edge of each surface, where cell suspension is added and drawn across the grid by capillary action. The number of cells in the top left, top right, bottom left, bottom right and centre primary squares are counted. If the haemocytometer is correctly loaded, then the volume of cell suspension occupying each primary square is  $1 \times 10^{-4}$  ml.

**Figure 14.** The improved Neubauer haemocytometer.<sup>134</sup>



The average number of cells per primary square is then determined from the sum of the cells in the 5 counted primary squares. The total cell concentration is then given by:-

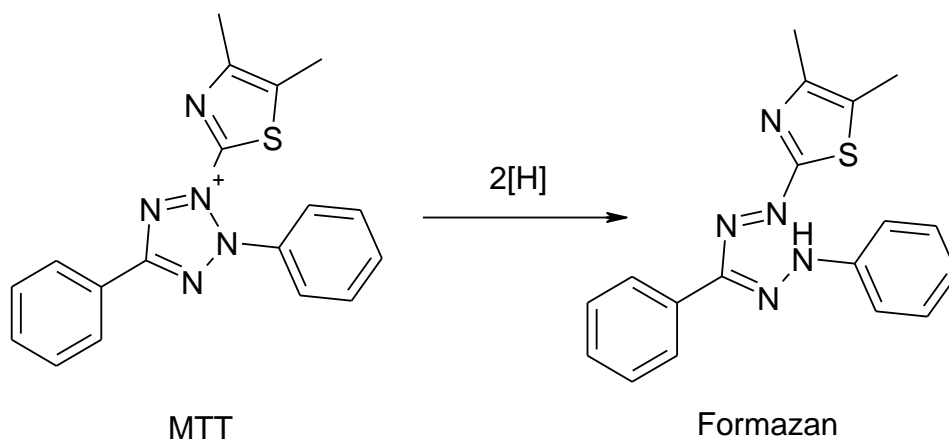
$$\text{No. Cells per ml} = \text{average number of cells per primary square} \times 10^4$$

### 2.2.1.3. MTT Colorimetric Assay

The MTT (3-[4,5-dimethylthiazol-2-yl]-2,5-diphenyl-tetrazoliumbromide) colorimetric assay is a quantitative method, developed to enable visualisation of growth inhibition in *in vitro* chemosensitivity experiments. MTT is converted to coloured formazan crystals (Figure 15) by mitochondrial dehydrogenase activity in living cells. Although the amount of dehydrogenase content varies between cell lines, it is fairly consistent amongst cells of the same origin. The amount of coloured formazan produced is

proportional to viable cell number and can therefore be used to provide a visual indication of the quantity of viable cells.<sup>135</sup>

**Figure 15.** Reduction of MTT to formazan due to mitochondrial dehydrogenase activity.

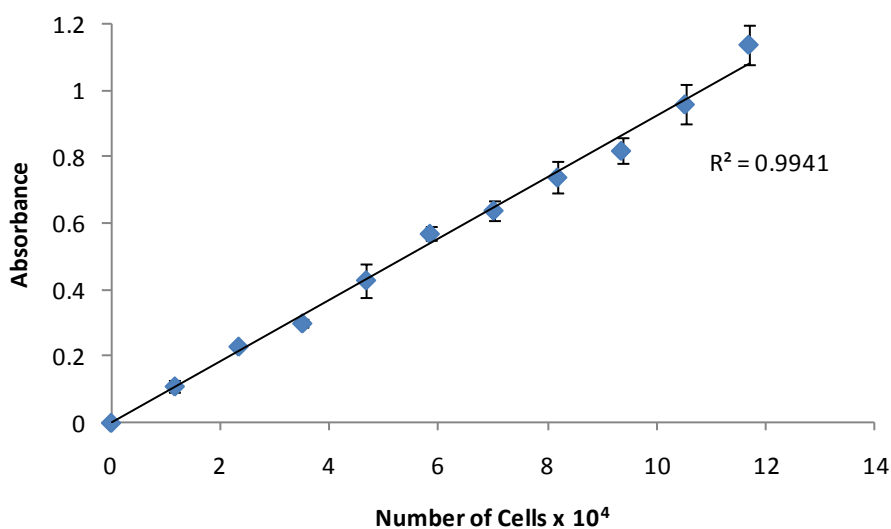


MTT was stored as a  $5 \text{ mg ml}^{-1}$  solution in distilled water at  $4^\circ\text{C}$ . MTT solution ( $20 \text{ }\mu\text{l}$ ) was added to each well of a 96-well cell culture cluster, which was requiring analysis post drug-exposure, or during validation experiments. The cell culture cluster was then incubated for 4 h. All of the MTT solution and old culture medium was removed by suction and replaced with DMSO ( $150 \text{ }\mu\text{l}$  per well). The DMSO and formazan crystals were carefully mixed by repeat pipetting. The absorbance of the resulting solution was read at  $550 \text{ nm}$ , using a multiskan plus V2.03 plate reader and the data collected by the Genesis V1.6 software package (Labsystems).

### **2.2.1.3.1. Validation of the MTT Assay**

In order to confirm the assumption made in the previous section that the amount of formazan produced in the MTT assay is proportional to cell number, a simple validation assay was carried out. In short, a plot of cell number against absorbance should be linear. A 25 cm<sup>2</sup> flask of confluent H460 cells was used. A suspension of cells in cell culture medium was obtained as described in section 2.2.1.1. The number of viable cells in suspension was determined using the improved Neubauer haemocytometer as outlined in section 2.2.1.2. Cells were transferred to 96 well plates (range of cell numbers used was typically 0-2x10<sup>5</sup> cells per well, with 8 wells used per cell density) and MTT (17 µl per well) added. Following a 4h incubation, the MTT assay as described in section 2.2.1.3, was employed to provide a measure of the absorbance in each well. The mean absorbance of each lane was calculated. Graphs of mean absorbance against cell number were constructed. The relationship between cell number and formazan production, is shown in Figure 16.

**Figure 16.** Plot of absorbance against number of cells for the MTT validation assay, showing that number of cells is proportional to absorbance in the cell densities of this study. Each value represents the mean +/- standard deviations of (n=8) for a single experiment. Two independent experiments were conducted (only the results of one experiment are shown here).



#### 2.2.1.3.2. MTT assay

All drugs were dissolved in DMSO or distilled water at a concentration of 100mM and stored at -20°C. Cells in exponential growth were exposed to a range of drug concentrations for 120 h and a select few compounds for 1 h (at 37 °C) under aerobic conditions. Trypsinised cells from cultures in exponential growth were washed twice with Hanks Balanced Salt Solution, re-suspended in RPMI 1640 growth medium and 1 x 10<sup>4</sup> cells plated into lanes 2-12 of a 96-well plate. Lane 1 was left empty for the addition of a blank at a later stage. The cell culture cluster was then incubated overnight. A 1 in 2 serial dilution in cell culture medium of the drug under test was then carried out to give 10 samples of decreasing drug concentration. The highest dose was 100µM and the lowest was 0.39µM. Culture medium was then removed from the cell

culture cluster. Fresh culture medium (150µl) was added to each well of lane 1. Cell culture medium (150µl per well) either alone or containing 0.1% DMSO was added to lane 2 as a control (DMSO concentration during drug exposure was no more than 0.1% for the highest concentrations in all cases). A sample of the lowest drug concentration (150µl per well) was added to lane 3 and repeated in lanes 4-12 inclusively, adding the next most concentrated drug solution each time. Following incubation at 37 °C for 6 days, medium was removed and replaced with fresh RPMI 1640 (150µl) prior to addition of MTT (20 µl, 5 mg ml<sup>-1</sup>) per well. After a 4 h incubation at 37 °C media plus MTT solution was removed and formazan crystals were dissolved in 150 µl of DMSO. The absorbance of the resulting solution was read at 550 nm using an ELISA spectrophotometer and percent cell survival determined as the corrected absorbance of treated wells divided by the corrected absorbance of the control (corrected absorbance = absorbance of test well – absorbance of blank well). Each experiment was repeated in triplicate. Plots of percentage survival for the concentration range were constructed and IC<sub>50</sub> values (drug concentration required to inhibit 50% of the cell population) were determined. Reported IC<sub>50</sub> values given in the biological evaluation section therefore represent the mean +/- standard deviation (n=3) for three independent experiments.

### **2.2.2. DNA Damaging Assay**

The ability of a range of complexes to cause single-strand breaks in DNA, was assessed by following *in vitro* the conversion of supercoiled plasmid-DNA to the relaxed circular configuration.<sup>136</sup> The DNA-damaging abilities of the remaining library of compounds was not investigated due to insufficient laboratory time. All complexes were synthesised as outlined in section 2.1. EO9 was obtained from the New Drug

Development Office, Amsterdam. All drugs were stored as 100 mM solutions in either DMSO or water at -20°C.

### **2.2.2.1. Harvesting and Lysis of Bacteria**

#### **2.2.2.1.1. Harvesting**

*E.Coli* cells transfected with pRSET B plasmid were obtained from Dr RM Philips (Institute of cancer therapeutics, University of Bradford). A single bacterial colony was transferred into LB medium (2 ml) containing ampicillin (1µg/ml) in a loosely capped 15 ml tube. The culture was incubated overnight at 37 °C with vigorous shaking. The culture (1.5 ml) was poured into a microfuge tube and centrifuged at 12,000 g for 30 seconds at 4 °C in a microfuge. The medium was then removed by aspiration with a micropipette leaving the bacterial pellet as dry as possible.

#### **2.2.2.1.2. Lysis by Alkali**

1. The bacterial pellet (obtained in the harvesting stage) was resuspended in 100 µl of ice cold Solution I by vigorous vortexing.

Solution I

50 mM glucose

25 mM Tris.Cl (pH 8.0)

10 mM EDTA (pH 8.0)

Solution I was prepared in batches of approximately 100 ml, autoclaved for 15 minutes at 10 lb / sq. in. on liquid cycle and stored at 4 °C.

2. Then 200 µl of freshly prepared Solution II was added.

### Solution II

0.2 N NaOH (freshly diluted from 10 N stock)

1% SDS

The tube was closed tightly and the contents were mixed by inverting the tube rapidly five times. It was essential that the entire surface of the tube came into contact with Solution II. The tube was then stored on ice.

3. 150  $\mu$ l of ice-cold Solution III was then added.

### Solution III

5M potassium acetate 60 ml

Glacial acetic acid 11.5 ml

H<sub>2</sub>O 28.5 ml

The resulting solution is 3M with respect to potassium and 5M with respect to acetate.

The tube was then closed and gently vortexed in an inverted position for 10 seconds to disperse Solution III through the viscous bacterial lysate. The tube was then stored on ice for 5 mins.

4. The tube was then centrifuged at 12,000g for 5 minutes at 4 °C in a microfuge. The supernatant was then transferred to a fresh tube.



5. The double stranded DNA was then precipitated with 2 volumes of ethanol at room temperature. The contents were mixed by vortexing. The mixture was then allowed to stand for 2 mins at room temperature.
6. The tube was centrifuged at 12,000g for 5 minutes at 4 °C in a microfuge.
7. The supernatant was removed by gentle aspiration. The tube was allowed to stand in an inverted position on a paper towel to allow all of the fluid to drain away. Any drops of fluid adhering to the walls of the tube were also removed.
8. The pellet of double stranded DNA was rinsed with 1 ml of 70 % ethanol at 4 °C. The supernatant was then removed as in step 7 and the pellet of nucleic acid was allowed to dry in air for 10 mins.
9. The nucleic acid was then dissolved in 50 µl of TE (pH 8.0) containing DNAase free pancreatic RNAase (20 µg/ml), vortexed briefly and stored at -20 °C until needed.

#### **2.2.2.2. Treatments of Plasmid DNA for Assay**

The assay was carried out according to Walton *et al.*<sup>136</sup> 12 reactions were made of the following mixtures to give 100µl total volume each containing plasmid DNA (10µl) isolated by method 2.2.2.1.2, sodium phosphate buffer (0.1 M, pH 7.4 + 0.14% BSA [volume as quoted below]):-

Lane 1 (Blank control): Phosphate buffer (90 µl)

Lane 2 (H<sub>2</sub>O<sub>2</sub> control): H<sub>2</sub>O<sub>2</sub> (10µl, 5mM); Phosphate buffer (90 µl)

Lane 3 (Positive control): NQO1 (2µl, [77.8ng µl<sup>-1</sup>]); EO9 (1µl, [10mM]); NADH (10µl, [10mM])

Lane 4 (Cisplatin): Cisplatin (10µl, [10mM]); Phosphate buffer (80 µl)

Lane 5: [CuCl<sub>2</sub>(L<sup>1</sup>Pr<sup>n</sup>)] (10μl, [1mM]); Phosphate buffer (80 μl)

Lane 6: [CuCl<sub>2</sub>(L<sup>1</sup>Pr<sup>n</sup>)] (10μl, [1mM]); H<sub>2</sub>O<sub>2</sub> (10μl, [5mM]) Phosphate buffer (70 μl)

Lane 7: [CoCl<sub>2</sub>(L<sup>1</sup>Cy)] (10μl, [1mM]); Phosphate buffer (80 μl)

Lane 8: [CoCl<sub>2</sub>(L<sup>1</sup>Cy)] (10μl, [1mM]); H<sub>2</sub>O<sub>2</sub> (10μl, [5mM]) Phosphate buffer (70 μl)

Lane 9: [ZnCl<sub>2</sub>(L<sup>1</sup>Bu<sup>i</sup>)] (10μl, [1mM]); Phosphate buffer (80 μl)

Lane 10:[ZnCl<sub>2</sub>(L<sup>1</sup>Bu<sup>n</sup>)] (10μl, [1mM]); H<sub>2</sub>O<sub>2</sub> (10μl, [5mM]) Phosphate buffer (70 μl)

Lane 11: [CuCl<sub>2</sub>(L<sup>3</sup>Bu<sup>i</sup>)] (10μl, [1mM]); Phosphate buffer (80 μl)

Lane 12:[CuCl<sub>2</sub>(L<sup>3</sup>Bu<sup>i</sup>)] (10μl, [1mM]); H<sub>2</sub>O<sub>2</sub> (10μl, [5mM]) Phosphate buffer (70 μl)

All final drug and H<sub>2</sub>O<sub>2</sub> concentrations were 100μM and 500μM respectively. All reaction tubes were incubated for 1h at 37°C. After this period, stop buffer (25 μl of a solution in distilled water of 5 mM EDTA, 0.5% SDS, 60% (v/v) glycerol and 0.01% bromophenol blue), was added to each tube. Samples (40 μl), were separated on an ethidium bromide stained 1% agarose gel containing 0.5 x TBE buffer. Running conditions were 100 V for 3h, using 0.5 x TBE buffer. The gel was visualized under ultraviolet light and scanned to preserve the result.

### 3. Synthesis of Precursors and Ligands

In order to improve reactions, an understanding of the reaction mechanism is often a good starting point. From this understanding, certain parameters can be manipulated in order to promote the desired course of a reaction. Clearly the building block approach adopted in this study requires efficient synthesis of precursor compounds, not only is it advantageous to optimise yield, but also less toxic and more environmentally friendly routes are generally desired. In the following sections the reaction mechanisms, route selections, subsequent reaction optimisations and product characterisations from the syntheses carried out in section 2.1 are described and compared to established methods.

#### 3.1. Oxidation to Dialdehydes

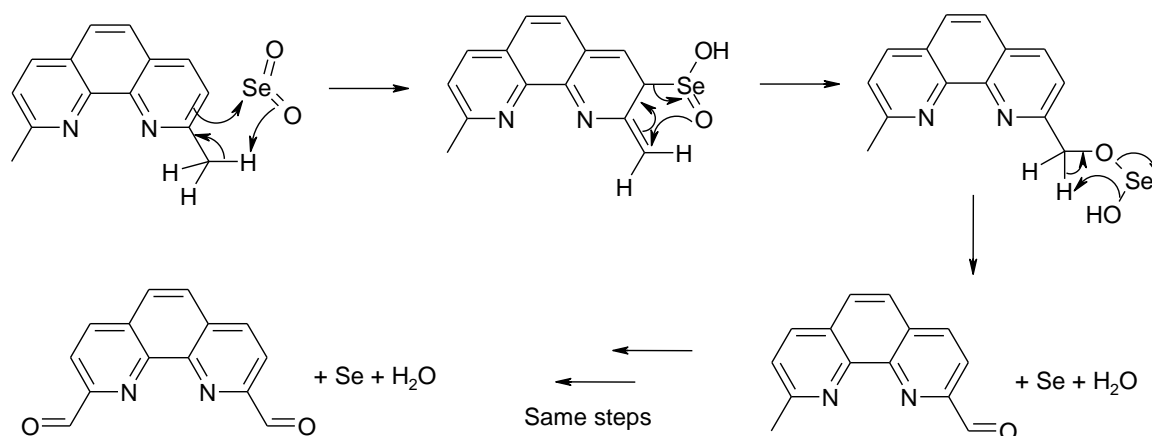
Oxidations of the three precursor head groups to their corresponding dialdehydes, P<sup>1</sup>, P<sup>2</sup> and P<sup>3</sup>, were carried out by two methods. At least one of these methods was successful in producing the pure dialdehyde for each of the compounds P<sup>1</sup>, P<sup>2</sup> and P<sup>3</sup>.

The first method used was by controllably oxidizing the corresponding dimethyl precursors to their corresponding dialdehydes using selenium dioxide (with the exception of P<sup>1</sup>, which was prepared from the dimethanol). The controlled oxidation of a methyl substituted aromatic using selenium dioxide is a reliable and well established method<sup>137</sup> and preferred to other common controllable oxidizing agents such as pyridinium chlorochromate and manganese dioxide.<sup>138</sup> In particular selenium dioxide has been widely applied to the selective oxidation of methyl pyridines including the oxidation of pyridine-2,6-dimethanol, 6,6'-dimethyl-2,2'-bipyridine and 2,9-dimethyl-1,10-phenanthroline.<sup>124, 127, 129</sup>

This work had variable success and some problems were encountered with selenium contamination of products (isolated products often turned pink on prolonged standing). After completion of the reaction, the selenium separates as a dark red/black form which is difficult to filter, and some of it is retained in solution as a solute or colloid, which is evident when a black selenium precipitate is obtained over time from retained filtrate mother liquors. (Also the oxidation of 6,6'-dimethyl-2,2'-bipyridine to P<sup>2</sup> was not totally successful when attempted with SeO<sub>2</sub>, with impure product being isolated). In addition, from an environmental viewpoint the replacement of SeO<sub>2</sub> by another oxidant is desirable, hence iodine and DMSO was used later in the program.

The mechanism of selenium dioxide oxidation of methyl precursors is generally accepted to involve two steps. Firstly an ene reaction to yield the arylsellenic acid, which rearranges to the aryl selenoxate, which is cleaved thermally or hydrolytically (Figure 17).<sup>139</sup> This mechanism consumes two moles of selenium dioxide per mole of substrate, hence explaining the larger relative quantities used in comparison with oxidation of the methanol analogue. This mechanism has limited support by the observed series of colour changes of the reaction mass corresponding to the +4 and +2 oxidation states of selenium and finally precipitating solid selenium at the end.

**Figure 17.** Plausible mechanism of selenium dioxide oxidation of methyl precursors.

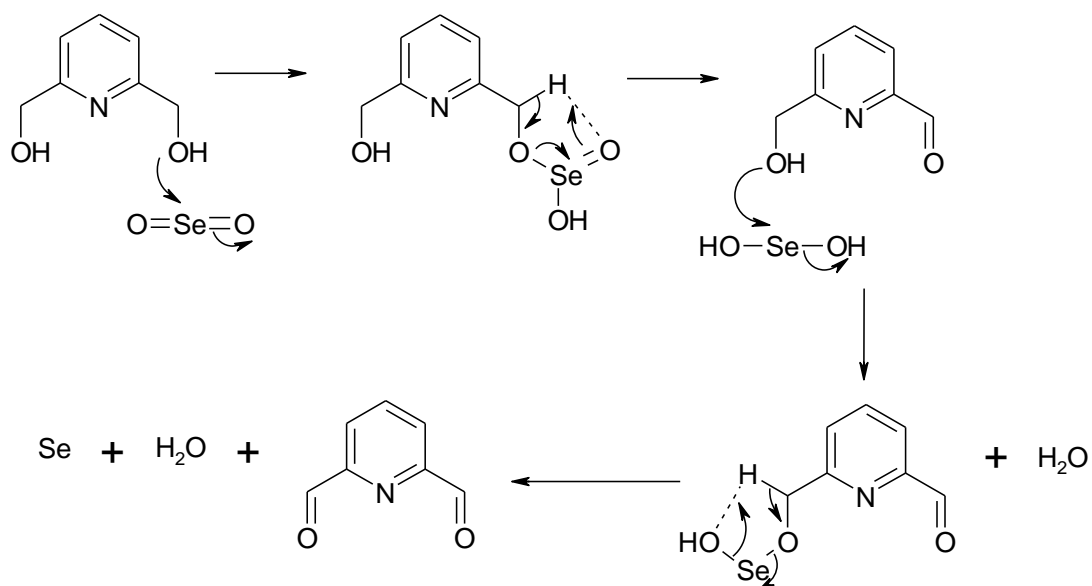


Hence the relative success of application of this reaction in preparation of  $\text{P}^1$ ,  $\text{P}^2$  and  $\text{P}^3$  correlates with the acidity of the precursors methyl protons. As the structures go from pyridine to phenanthroline the relative acidity of their methyl protons increases. This can be nicely demonstrated by the proton NMR signals 2.50, 2.61 and 2.80 ppm of pyridine, bipyridine and phenanthroline respectively. This is related to the stabilisation of the anion with the extended aromatic structure of phenanthroline. This gives some support to the proposed mechanism in Figure 17, where the first step of the reaction involves deprotonation of the methyl group.

The Mechanism of selenium dioxide oxidation of 2,6-pyridine dimethanol however is not fully understood and an extensive search of the literature did not provide the answer. From the reaction stoichiometry of the literature preparation and by comparing the isolated yield obtained in this study to the equivalents of selenium dioxide used in the lab preparation does suggest that the mechanism is almost certainly not the same as for the methyl precursors. The mechanism is likely to consume one mole of selenium dioxide for every two alcohol units (i.e. for every mole of pyridine dimethanol). In the first preparation of  $\text{P}^1$  using the literature procedure, ~ 80% conversion of the mono-

aldehyde intermediate was observed. This was likely a consequence of not using freshly distilled and dried 1,4-dioxan. Residual water in the solvent is likely to hydrolyse any selenous intermediates preventing further oxidation (may stop at alcohol). Later modifications using a larger quantity (quantity was still less than 2 equivalents), of selenium dioxide and dry dioxane soon overcame this problem. A plausible mechanism has been proposed for this particular transformation and can be seen in Figure 18.

**Figure 18.** Proposed mechanism for the transformation of pyridine dimethanol to pyridine dialdehyde, P<sup>1</sup> with selenium dioxide.

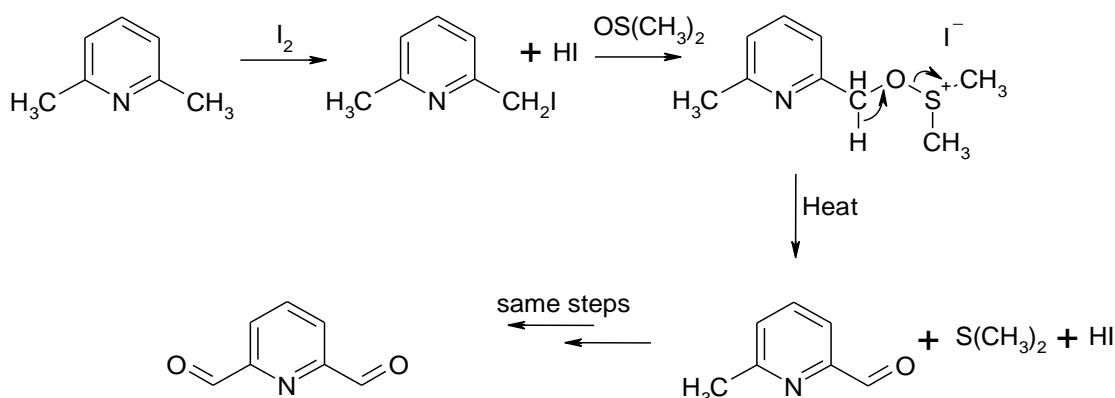


In order to overcome some of the disadvantages of  $\text{SeO}_2$  based oxidations, a second method was used to form dialdehydes. This proved to be a much cleaner procedure but also had varying success. Iodine in refluxing DMSO method has been used to controllably oxidise methyl to formyl groups in heteroaromatic derivatives.<sup>128</sup> The method was later improved by using *t*-butyl iodide.<sup>130</sup> The role of the *t*-butyl iodide is to presumably act as a free radical initiator to aid in the halogenation of the methyl group in the first step of the reaction. But although this has been reported as an improved

method, this method was utilized to prepare P<sup>3</sup> only. The method has been previously applied to the oxidation of 2,6-dimethylpyridine<sup>128</sup> and 2,9-dimethyl-1,10-phenanthroline,<sup>130</sup> but had not been used for 6,6'-dimethyl-2,2'-bipyridine and therefore herein is reported an improved synthesis of P<sup>2</sup>.

The oxidation of methyl heteroaromatics to formyl heteroaromatics involves treatment of the dimethyl precursor with 2 equivalents of iodine in DMSO. The solution is heated to 140-160°C, where upon a vigorous exothermic reaction occurs and dimethyl sulfide is evolved. The mechanism in the conversion of methylpyridines into pyridinealdehydes potentially proceeds through the following sequence (Figure 19), with 2,6-dimethylpyridine as an example.

**Figure 19.** Mechanism of controllable oxidation of methyl heteroaromatics utilising DMSO and I<sub>2</sub>.



The initial 2,6-dimethylpyridine-iodine complex, on heating, forms the transient 2,6-diiodomethylpyridine, which reacts with DMSO to form 2,6-pyridyloxydimethyl sulfonium iodide. The latter decomposes on heating (or by treatment with base), to form pyridine-2,6-dicarboxaldehyde and dimethyl sulphide.<sup>128</sup>

### 3.1.1. Pyridine-2,6-dicarbaldehyde, P<sup>1</sup>

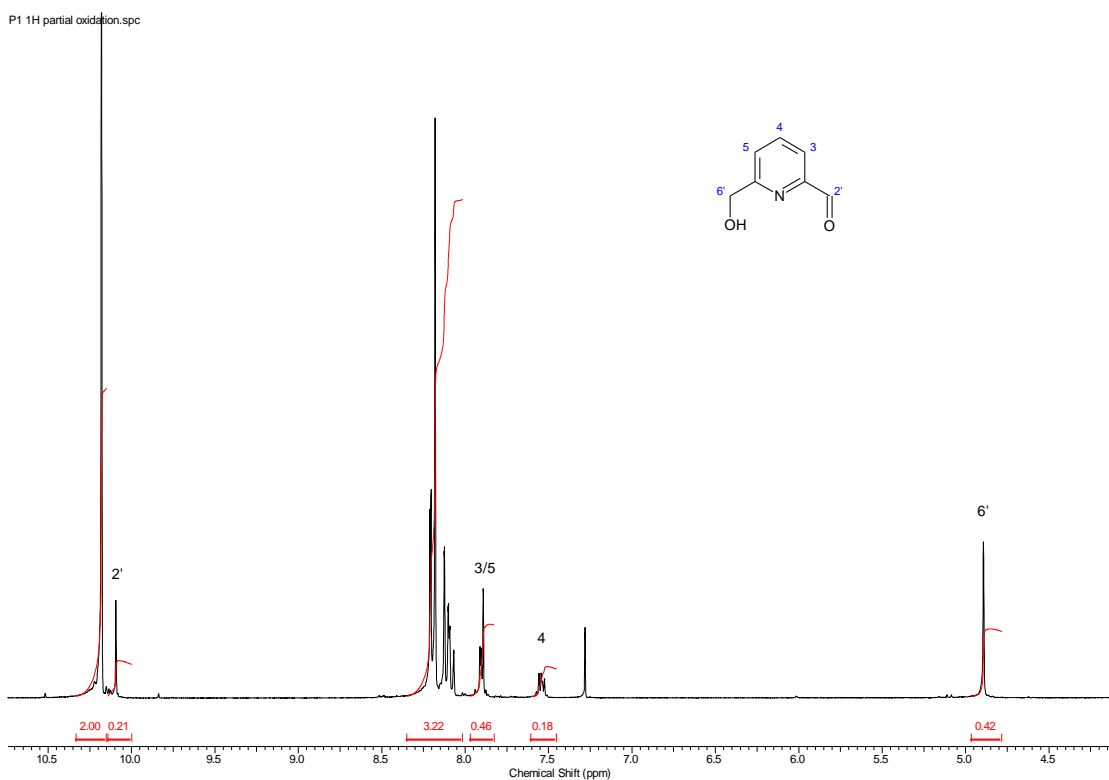
As mentioned in the previous section the precursor compound P<sup>1</sup> was prepared by two methods. The first method was the most common method found in the literature for this compound, and involved the selective oxidation of pyridine-2,6-dimethanol by selenium dioxide in refluxing 1,4-dioxane.<sup>124, 137</sup> By this method, the product was isolated in very good yields (70-80%), and of fairly high purity, although trace contamination with selenium was often a problem and this was indicative when the cream compound turned slightly pink over time. This method was also the main method of choice for this work mainly due to the high yields, good purity and practicality of the synthesis. With DMSO and iodine the potential of obtaining the desired product without any selenium contamination was desirable, although not essential. This method was also potentially much more desirable since it utilised the much cheaper 2,6-lutidine. The synthetic method was carried out as described in the literature,<sup>128</sup> only to obtain a very small amount of a dark liquid substance after extraction. NMR of the oil revealed that two main compounds were present; one was the starting material and the other the desired product in a ratio of 1:2 respectively. With some modification this method could have potential but time did not permit and so this method was abandoned for P<sup>1</sup>.

Initial attempts to prepare P<sup>1</sup> via the SeO<sub>2</sub> method yielded a mixture of the desired P<sup>1</sup> and the monocarbaldehyde (*Ca.* 4:1 respectively by NMR of isolate). Enough residual intermediate was present at the end of reaction to impair the resulting literature crystallization procedure. Every time the product P<sup>1</sup> came out of solution it was joined by the intermediate as an amorphous precipitate or microcrystalline material.



Characterisation of the mixture provided firm evidence for the monoaldehyde. From the MS it was possible to differentiate between monoaldehyde and dialdehyde by isotopic distributions. The MS revealed a peak at  $m/z$  136 significantly greater than the expected  $^{13}\text{C}$  satellite peak for that of the dicarbaldehyde at  $m/z$  135, which indicated the mono carbaldehyde. The IR spectrum revealed a sharp medium peak at  $3400\text{ cm}^{-1}$ , indicating the presence of a OH group. The NMR spectrum showed peaks consistent with the dicarbaldehyde and extra peaks at 10.0 ppm, peaks overlapping with the pyridyl peaks of the dicarbaldehyde, and a peak at 4.83 ppm, which corresponded with the monocarbaldehyde in approximately 20% (Figure 20).

**Figure 20.**  $^1\text{H}$  NMR Spectrum (270MHz in  $\text{CDCl}_3$ ) of attempted oxidation of pyridine-2,6-dimethanol to pyridine-2,6-dicarbaldehyde. The annotated peaks correspond to proton signals of the intermediate mono-oxidised species.



As a result of this initial problem, the quantity of selenium dioxide was increased and the isolated product was identified as pure desired P<sup>1</sup> in good yield (typically 72 %), and its melting point (132-134 °C), consistent with that of the literature.<sup>124</sup>

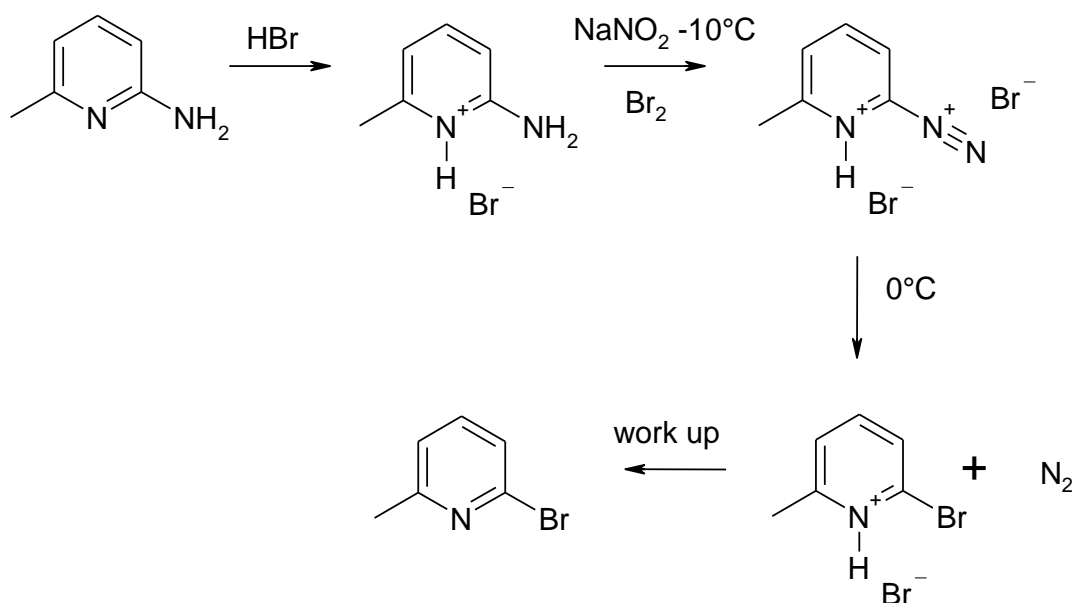
### **3.1.2. 2,2'-bipyridine-6,6'-dicarbaldehyde, P<sup>2</sup>**

Synthesis of P<sup>2</sup> involved three steps: Synthesis of 2-bromo-6-methyl pyridine followed by coupling the 2-bromopyridine to form the 6,6'-dimethylprecursor. At each step products were isolated and characterised by MS, NMR and IR. Two methods were investigated for oxidation of 6,6'-dimethyl-2,2'-bipyridine in the preparation of the target compound P<sup>2</sup>. The use of DMSO and iodine proved to be more efficient than other methods, requiring only one step and was a much more practical synthesis and P<sup>2</sup> was obtained in good yield (71%), with high purity. This is the first time this compound has been prepared by this method

#### **3.1.2.1. Step 1 – 2-bromo-6-methylpyridine, P<sup>2a</sup>**

This nucleophilic substitution of an aromatic ring is typically carried out by a Sandmeyer reaction<sup>140</sup> which goes via *in situ* generation of the aryl diazonium salt at low temperature, followed by raising the temperature in the presence of a nucleophile (in our case bromide) to give the bromo substituted aromatic as shown in Figure 21.

**Figure 21.** Steps in the nucleophilic aromatic substitution analogous to the Sandmeyer reaction.



2-bromo-6-methylpyridine was isolated in moderate to good yield (68 %), as a clear, liquid after vacuum distillation (b.p. at 1.6 – 1.7 mmHg, 54 – 56 °C), consistent with the literature.<sup>141</sup> MS revealed the  $[M]^+$ ; at  $m/z$  171, along with the <sup>81</sup>Br satellite with equal intensity.<sup>142</sup> The characteristic fragment corresponding to  $[M-Br]^+$ ; was also observed at  $m/z$  92. IR revealed the symmetric and asymmetric C-H stretching vibrations of the methyl group around 2900 cm<sup>-1</sup>, along with the C=N/C=C ring skeletal stretch at 1590 cm<sup>-1</sup>, and a strong band at ca. 580 cm<sup>-1</sup>, which can be attributed to the C-Br stretch. NMR gave rise to 3 aromatic peaks with the expected splitting pattern of two doublets and a triplet each integrating to 1H and a singlet in the aliphatic region integrating to 3H which corresponds to the lone methyl group.

### 3.1.2.2. Step 2 – 6,6'-dimethyl-2,2'-bipyridine, P<sup>2b</sup>

Nickel is a common reagent in biaryl synthesis.<sup>143</sup> Rayney nickel has been used to couple the two aryl groups in this clean but low yielding reaction. P<sup>2b</sup> was isolated by

recrystallisation from pet spirit (b.p. 40-60) as cream crystals in low yield (19 %) with a m.p. of 92-94 °C. This all agreed with that of the literature. The low yield can probably be attributed to the fact that the rayney nickel slurry would contain significant water impurity which would lead to the hydrolysis or aquation of the nickel(II)bromide complex and loss of P<sup>2b</sup>. The MS afforded peaks at  $m/z$  184, 183 and 169, which correlated to  $[M]^+$ ;  $[M-H]^+$ ; and  $[M-CH_3]^+$ ; respectively. The IR spectrum revealed peaks at similar positions to 2-bromo-6-methyl pyridine. The methyl stretches along with the skeletal aromatic C=N / C=C stretches at 2900  $cm^{-1}$  and 1400-1500 $cm^{-1}$ , respectively and also no intense band at ca. 580 $cm^{-1}$  was observed, indicating that C-Br had been replaced.

### 3.1.2.3. Step 3 – 2,2'-bipyridine-6,6'-dicarbaldehyde, P<sup>2</sup>

Synthesis of P<sup>2</sup> was initially attempted by controlled oxidation with selenium dioxide under conditions used successfully for P<sup>1</sup> and P<sup>3</sup>. A literature report<sup>127</sup> that P<sup>2</sup> has been prepared previously using selenium dioxide as oxidant but experimental details were incomplete and no quantities of reagents were given for the procedure. The same equivalents of selenium dioxide to P<sup>2a</sup>, as for the preparation of P<sup>3</sup> were used and the mixture was refluxed in glacial acetic acid for 24 h. Upon cooling, a white precipitate formed and was isolated by filtration. However the precipitate showed properties inconsistent with dialdehyde.<sup>127</sup> Soxhlet extraction of the solid with xylene was employed and upon cooling the extract in the fridge, cream crystals formed. The IR spectrum of the crystals showed features characteristic of the dicarbaldehyde product with a very strong absorption at 1703  $cm^{-1}$  for the carbonyl group. The EI-MS gave the  $[M]^+$ ; at  $m/z$  212, and the characteristic fragmentation peaks for  $[M-CO]^+$ ; and  $[M-(CO)(CHO)]^+$ ; at  $m/z$  184 and 155 respectively. The NMR spectrum was recorded in

DMSO but while the desired product was clearly present, significant quantity of mono-oxidised impurity was present.

Due to inadequate characterization and purification of P<sup>2</sup> a second method was attempted, using the DMSO / iodine method.<sup>128</sup> This time the highly pure product was isolated in good yield (71%). The <sup>1</sup>H NMR revealed only the fully oxidized 2-fold symmetric product P<sup>2</sup> was present, as identified by loss of the single methyl peak at 2.61 ppm and three aromatic peaks integrating equally, with the correct fine structure of two doublets and a triplet. The 2-fold symmetry also indicates P<sup>2</sup> has a low barrier to rotation at the pyridyl bridge, and indicates the *anti* and *syn* conformations are in fast equilibrium at ambient temperature. Once again the MS revealed the same [M]<sup>+</sup>; at *m/z* 212, and the characteristic fragmentation peaks for [M-CO]<sup>+</sup>; and [M-(CO)(CHO)]<sup>+</sup>; at *m/z* 184 and 155 respectively.

The crystal structure of the isolated P<sup>2</sup> (Figure 13) was also obtained after recrystallisation by slow evaporation of a chloroform solution. Interestingly the structure identified the *syn*-conformation of the bipy nitrogens, a coplanar ring system and both aldehyde groups in *trans* geometries.

### 3.1.3. 1,10-phenanthroline-2,9- dicarbaldehyde, P<sup>3</sup>

P<sup>3</sup> was prepared in moderate to good yield (65-75%), as very fine cream needle crystals, (m.p. > 235 °C), consistent with literature values.<sup>129</sup> EI-MS gave rise to peaks at *m/z* 235, 208 and 180. The highest peak was attributed to that of [M]<sup>+</sup>; and the peaks at *m/z* 208 and 180 were assigned to the characteristic fragmentations of [M-CO]<sup>+</sup>; and [M-2(CO)]<sup>+</sup>; respectively. The IR spectrum produced very strong absorption at 1702 cm<sup>-1</sup>,

characteristic of the carbonyl stretching frequency and loss of the methyl stretching bands around  $2900\text{-}3000\text{ cm}^{-1}$ , indicating the product was fully oxidized.  $^1\text{H}$  NMR spectroscopy identified that the pure compound was isolated, showing four sets of peaks required for the four distinct hydrogen environments of  $\text{P}^3$ , with 2-fold symmetry, three sets of the peaks appearing in the aromatic region of the spectrum and a singlet appearing slightly downfield as expected, for the aldehyde proton. All peaks integrated to equal area, and the three sets of aromatic peaks demonstrated the correct splitting pattern of two doublets and a singlet expected for  $\text{P}^3$ .

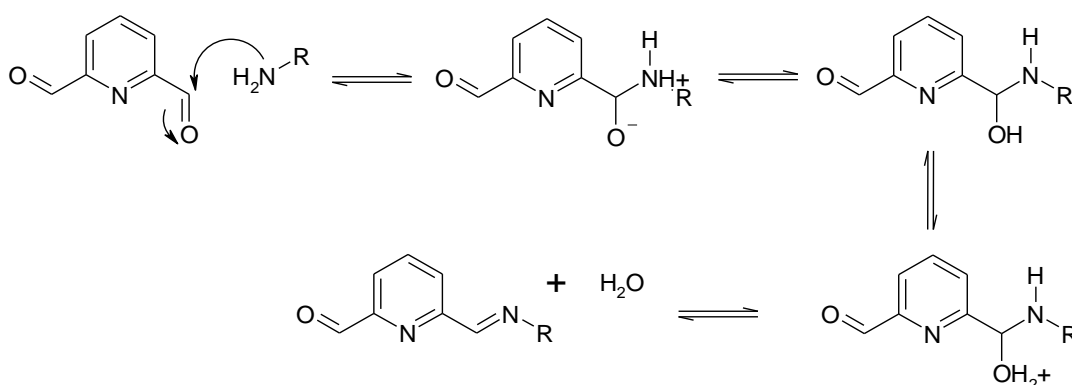
### 3.2. Schiff Base Ligands

The formation of the Schiff base ligands was possible by reacting the diformyl precursors with two equivalents of the appropriate primary amine, in a Schiff base condensation. The mixture could be refluxed or stirred at room temperature.

The reaction mechanism involved in the formation of a Schiff base compound is very well known and involves nucleophilic addition of the primary amine to the electron deficient aldehydic carbon, followed by elimination of a water molecule (Figure 22).<sup>144</sup>

145

**Figure 22.** The mechanism of addition elimination in a Schiff base condensation.



This reaction is reversible and so to ensure the reaction proceeds to completion there are several principles that could be utilised to drive the equilibrium to the products. By Le Chateliers principle, a system in equilibrium will react to oppose any changes imposed upon it,<sup>146</sup> therefore by introducing excess amine and keeping the initial mixture and also reaction mixture as dry as possible (using dry solvents, molecular sieves and carrying out the reaction under nitrogen), will force the equilibrium to the products. The reaction can also be catalysed by the presence of catalytic quantities of acid, which would protonate the carbonyl oxygen making the carbonyl carbon more electrophilic and the reaction more facile. This however depends upon the pKa and reactivity of the subsequent amine. If the pH of the mass is lowered two units below the pKa of the reacting amine, 99.9% of the amine will be in the non reactive salt form.<sup>147</sup> Base can also be used as a reagent to deprotonate less basic amines.

Schiff base ligands of aliphatic amines were found to form orange to tan coloured viscous oils after reflux and evaporation of solvent. The reactions were generally complete within 60 mins and good yields were isolated after optimisation of conditions (as discussed later in this section).

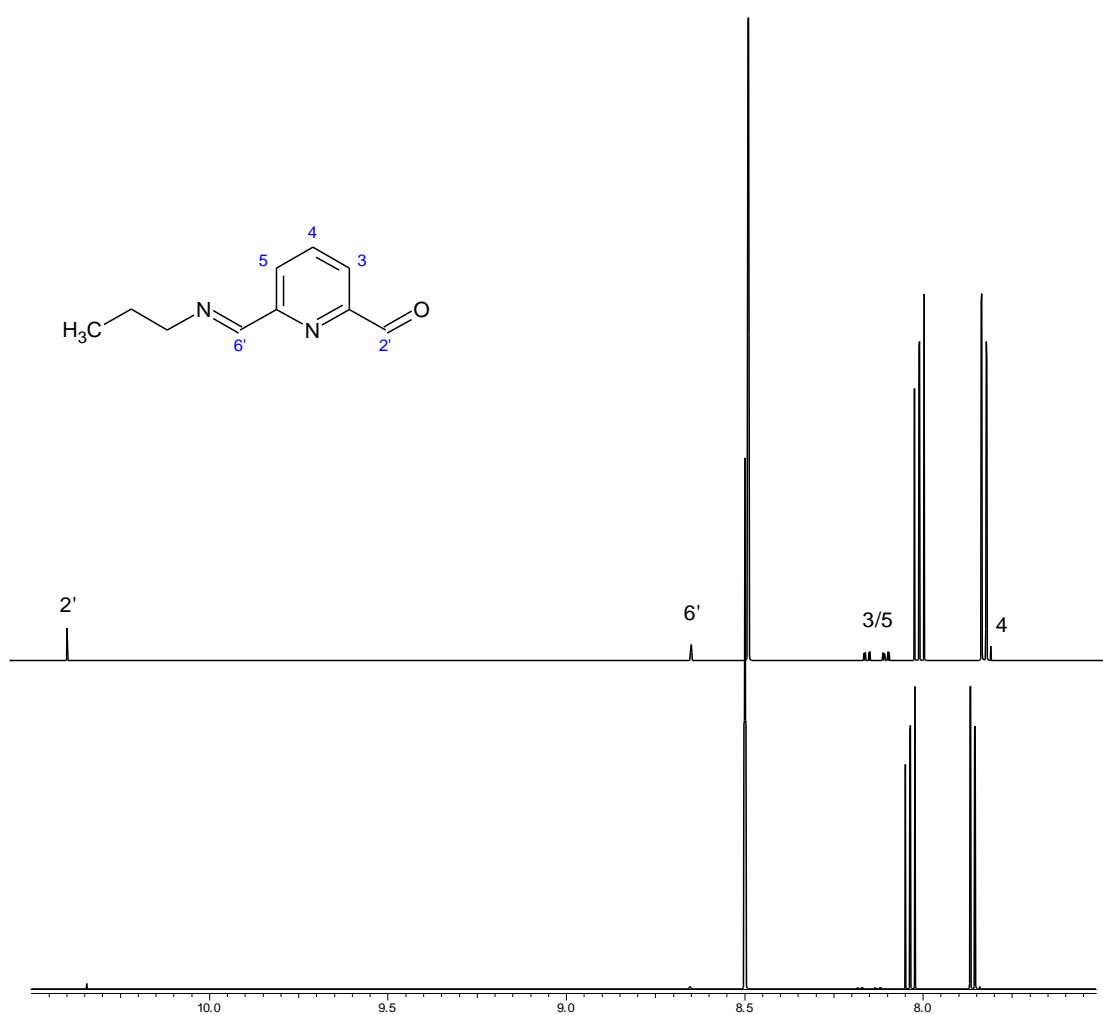
When forming the Schiff base ligands with aromatic tail groups, they were generally isolated as yellow to green crystalline solids. The reaction mixtures were refluxed and were typically complete within 90 mins). The aromatic ligands were isolated in good yield, and were analytically pure due to their crystalline nature.

A preliminary reaction of P<sup>1</sup> with Pr<sup>n</sup>Amine to generate the L<sup>1</sup>Pr<sup>n</sup> alkyl ligand carried out with GPR grade solvents and also without any molecular sieves, showed the

reaction did not fully go to completion. The approximate amount of monoimine present on isolation was determined by NMR, and was in the order of ~5%. Conditions were further improved (slight excess amine, dried solvents, molecular sieves), and the reaction went to completion with minimal residual starting material and monoimine (just at the limit of detection by NMR <1%, see Figure 23).



**Figure 23.**  $^1\text{H}$  NMR Spectra (600 MHz in  $\text{CD}_3\text{OD}$ ) of isolated material from synthesis of  $\text{L}^1\text{Pr}^n$ . The top overlay spectrum identifies desired product along with approximately 5% monoimine under initial conditions. The bottom spectrum identifies desired product along with a significant reduction in undesired monoimine intermediate after optimization of conditions.



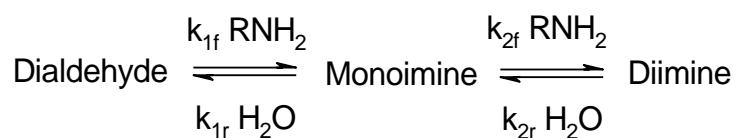
It was possible to follow the disappearance of P<sup>1</sup> to approximate the reactivity of the various amines with dialdehyde. The conversion times roughly follow the trend of amine basicities (Table 23) as would be expected.

**Table 23.** Crude conversion times and isolated yields for Schiff bases of L<sup>1</sup>

Ligand	Time to convert P <sup>1</sup> / mins (By TLC analysis)	Isolated Yield / %	Calculated pKa of Protonated amine.
L <sup>1</sup> Et	30	98	10.6
L <sup>1</sup> Pr <sup>n</sup>	30	97	10.7
L <sup>1</sup> Pr <sup>i</sup>	15	99	10.9
L <sup>1</sup> Bu <sup>n</sup>	15	96	10.7
L <sup>1</sup> Bu <sup>i</sup>	15	98	10.5
L <sup>1</sup> Bu <sup>2</sup>	15	99	10.6
L <sup>1</sup> Bu <sup>t</sup>	30	97	10.9
L <sup>1</sup> Cy	15	98	10.6
L <sup>1</sup> CyMe	15	97	10.5
L <sup>1</sup> Ph	45	80	4.2
L <sup>1</sup> PhMe	45	95	5.7
L <sup>1</sup> PhCl	45	97	4.0

The formation of diimine from dialdehyde is a consecutive reaction which is second order in both forward steps and in reverse (Figure 24).<sup>148</sup>

**Figure 24.** Kinetic parameters of diimine formation



The effect of altering the conditions to obtain the maximum amount of product can be demonstrated using mathematical modelling software.<sup>149</sup> Using the equilibria in Figure

24 the basic stoichiometric reaction can be shown to reach equilibrium as in Figure 25 below.

**Figure 25.** Predicted profile of the stoichiometric reaction of primary amine to dialdehyde.

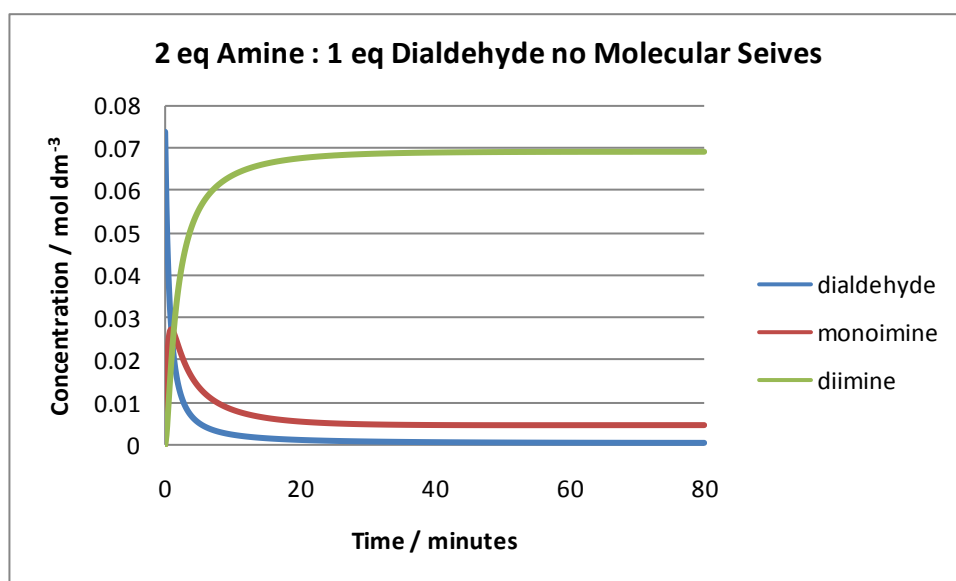
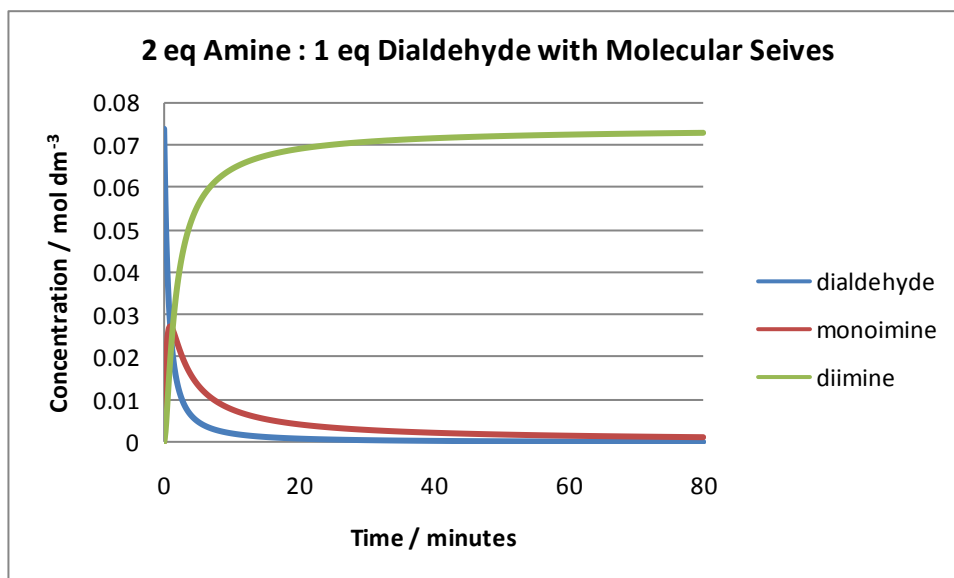


Figure 25 depicts the standard reaction from the method taken from Lions procedure<sup>131</sup> and the original procedure used for the first aliphatic ligand L<sup>1</sup>Pr<sup>n</sup> generated in this thesis (i.e. 2 equivalents of primary amine to 1 equivalent of dialdehyde under reflux). The forward and reverse rate constants have been manipulated to give ~5% residual monoimine at equilibrium and to give almost full conversion of dialdehyde after ~30 minutes (subsequent 2<sup>nd</sup> order rate constants used for both forward steps was 7.5 M<sup>-1</sup> min<sup>-1</sup> and both reverse steps was 0.05 M<sup>-1</sup> min<sup>-1</sup>, see appendix 1.1). It is clear since monoimine conversion is not complete there is ~5% loss in yield and the isolation method of aliphatic tail groups uses no purification step (TLC analysis was hampered by problems with products sticking to silica and alumina columns). Figure 26 however

predicts the profile of the same reaction with simulated molecular sieves added i.e. a pathway is added to simulate water removal (see Appendix 11.1).

**Figure 26.** Predicted profile of the stoichiometric reaction of primary amine and dialdehyde with molecular sieves added (water removal).



It is clear from the profile that there has been a further yield improvement at equilibrium. The intermediate monoimine has been reduced to ~2% (Figure 26). The conditions of this reaction have been used to generate ligands with aromatic amine precursors in this study, since when tried with an excess of amine crystallisation gave poor yields (<60%) and often it was difficult to remove the residual amine, even after several washes, presumably the residual amine forms a fraction of co-crystals which is isolated. Whereas since the aliphatic amines were volatile and the excess could be easily removed at the end of reaction, an excess of amine was possible.

**Figure 27.** Predicted profile with a slight excess of amine added to the reaction with dialdehyde.

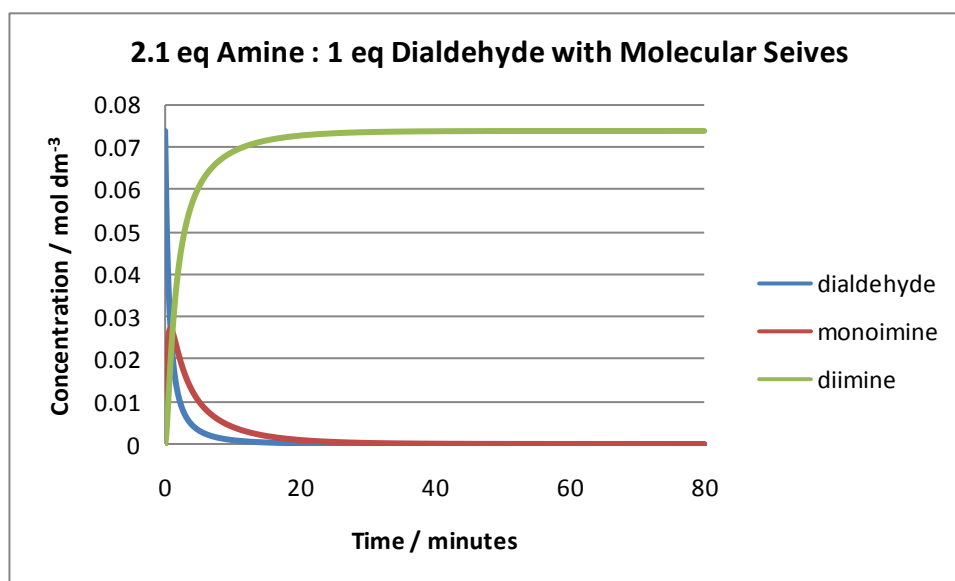
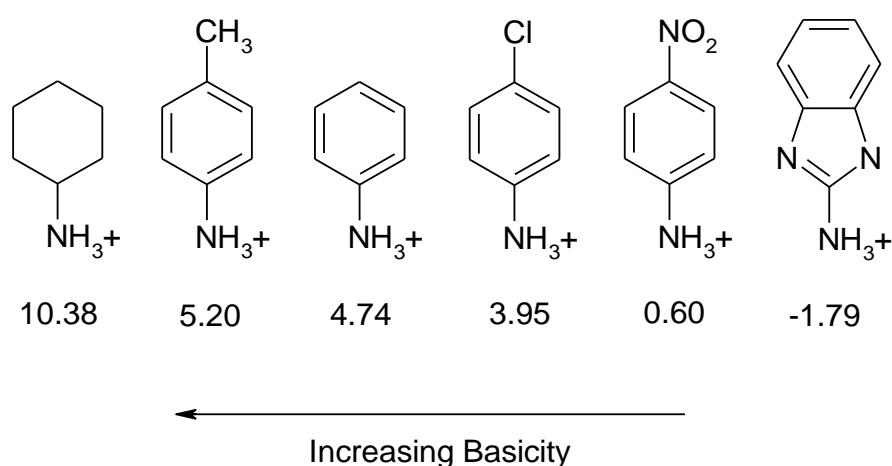


Figure 27 shows the effect of adding an excess of amine and clearly demonstrates firstly how the reaction rate increases, the time at which equilibrium is achieved is quicker and also 100% conversion of dialdehyde and monoimine is observed. These small modifications to the original reaction show how yield, time and purity benefits can be achieved. Also although the formation of aromatic ligands was slower than aliphatic ligands, the fact that aromatic ligands are fully conjugated would likely mean the equilibrium constant is more in favour of the diimine.

Although the Schiff base reactions of the *p*-anilines to form L<sup>1</sup>Ph, L<sup>1</sup>PhMe, L<sup>1</sup>PhCl, worked well, the Schiff base reactions of *p*-nitroaniline and 2-aminobenzimidazole did not proceed to completion. Particularly the reaction of *p*-nitroaniline which did not proceed at all, this was verified by TLC and NMR. This could be explained due to the poor basicity of the amines. Because *p*-nitroaniline contains the electron withdrawing nitro group, the lone pair of the amine are likely to be strongly involved in resonance

and are therefore unavailable for donation, as with 2-aminobenzimidazole the lone pair is also involved in resonance with the imidazole ring, which also makes the amine a poor base. The ease of formation of the Schiff bases of these aromatic amines can be rationalized by looking at their  $pK_a$ . (Figure 28).

**Figure 28.** Calculated  $pK_a$  of cyclic amines used in this study ( $pK_a$  calculations using chem office).



### 3.2.1. Characterisation of Ligands

#### 3.2.1.1. IR Spectroscopy

The formation of the free Schiff base ligands was initially analysed by IR spectroscopy to identify loss of C=O stretching bands for P<sup>1</sup> and P<sup>3</sup> precursors around 1720 and 1702  $\text{cm}^{-1}$ , respectively and the appearance of the imine C=N stretching bands between 1680-1600  $\text{cm}^{-1}$ . Then the mass and NMR spectra were obtained to further characterize the compounds made and to identify the purities.

The IR spectra of all aliphatic ligands have very much the same pattern. Due to all of the aliphatic ligands being oils the spectra were obtained as thin films between KBr windows and all bands were particularly intense. All contained a lone weak aromatic C-

H stretch between 3063-3045  $\text{cm}^{-1}$ , followed by strong absorptions between 3000-2840  $\text{cm}^{-1}$  corresponding to the stretching vibrations of the aliphatic C-H's of the tail groups. Schiff bases of aromatic tail groups were obtained as solid KBr discs and showed C-H stretching in the region of 3086-3000  $\text{cm}^{-1}$ , as would be expected, but unusually several C-H stretching bands were also observed below 3000  $\text{cm}^{-1}$ , which must be aromatic C-H stretching since several of such bands were observed. The bands closer to 3000  $\text{cm}^{-1}$  have been tentatively assigned to aromatic  $\nu\text{C-H}$  and below 2900  $\text{cm}^{-1}$  assigned to the aldimine C-H stretching. In all Schiff base compounds of the form  $\text{L}^1\text{R}$ , substitution of the ring could also be confirmed by the appearance of four weak overtones between 2000-1750  $\text{cm}^{-1}$ , characteristic of *meta* substitution.<sup>150</sup> Confirmation of imine bond formation was evident by the appearance of a single band between 1653-1604  $\text{cm}^{-1}$ . For the Schiff bases of aliphatic tail groups the C=N stretch appeared between 1653-1644  $\text{cm}^{-1}$  and was very strong in intensity, on the other hand the Schiff bases with aromatic tail groups were much lower in intensity and wavenumber (1628-1604  $\text{cm}^{-1}$ ). The effect in intensity is likely due to a change in the dipole moment of the fully conjugated system and the lowering in wavenumber is as expected since conjugation either side of the imine bond is now introduced, which gives rise to a greater amount of canonical structures and hence more single bond character for C=N. Further to the above mentioned observations, aromatic ring breathing vibrations were also present in all cases between 1597-1452  $\text{cm}^{-1}$ .

### 3.2.1.2. $^1\text{H}$ NMR Spectroscopy

The NMR spectra of all the Schiff base ligands of  $\text{L}^1\text{R}$  and  $\text{L}^3\text{R}$  both showed 2-fold symmetric compounds which indicates the *E,E*; *Z,Z*; *E,Z* conformations are in rapid equilibrium. As examples the proton spectra of  $\text{L}^1\text{Bu}^n$  and  $\text{L}^1\text{Ph}$  are shown in Figure 29

and Figure 30 respectively and indicate the typical splitting pattern of the pyridyl and aldimine moieties and evidence of 2-fold symmetry.

**Figure 29**  $^1\text{H}$  NMR (270 MHz) spectrum of  $\text{L}^{\text{tBu}}$  obtained in  $\text{CDCl}_3$ .

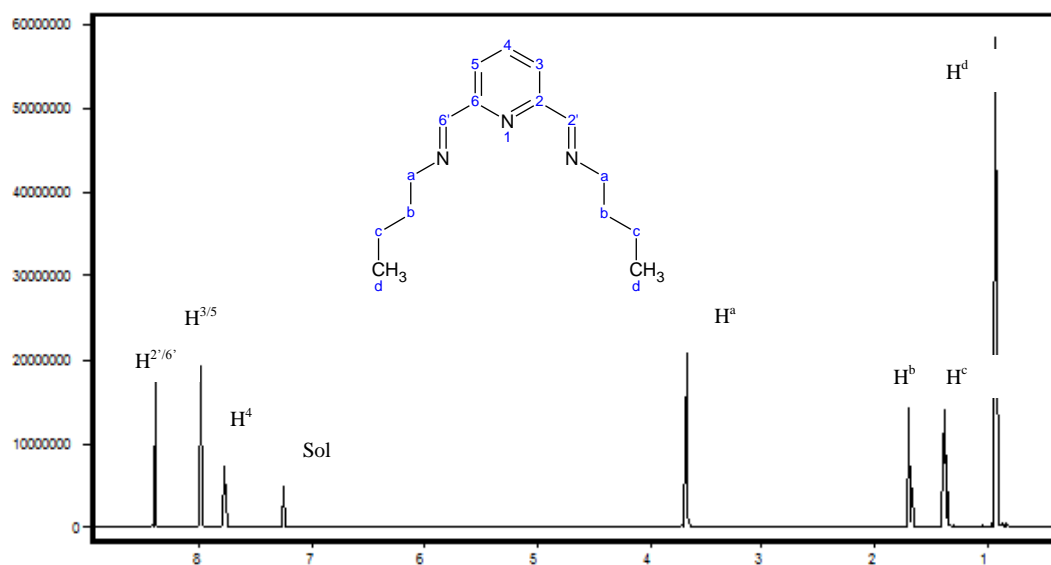
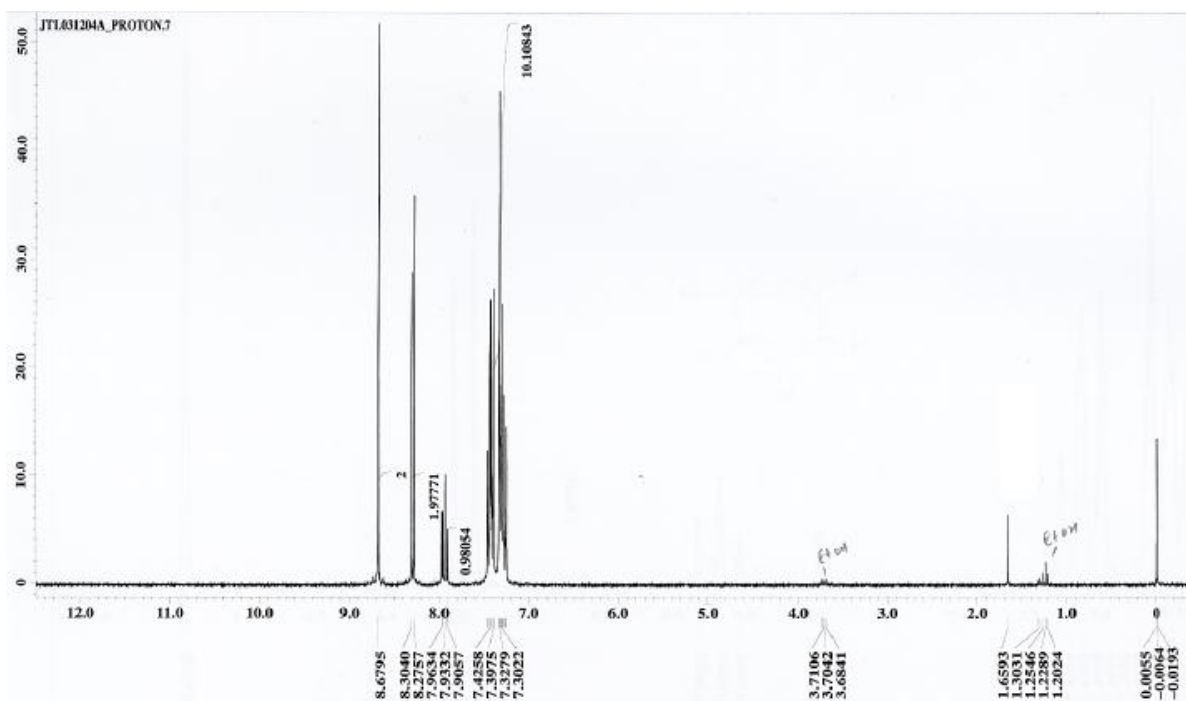


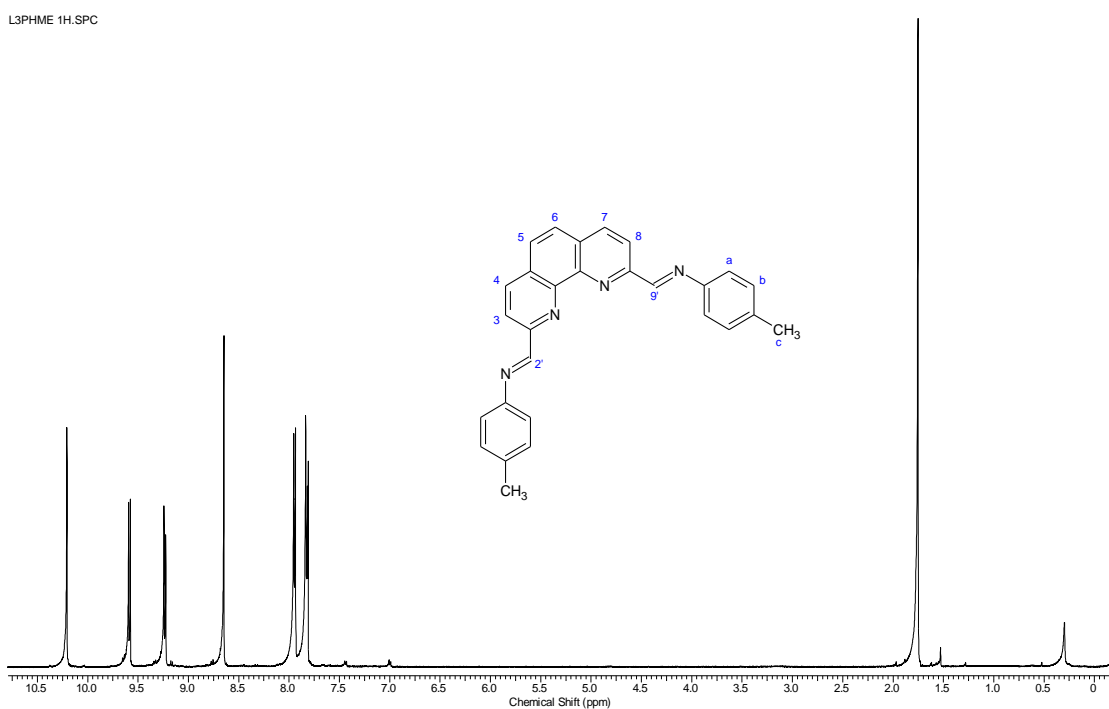
**Figure 30**  $^1\text{H}$  NMR (270 MHz) spectrum of  $\text{L}^{\text{Ph}}$  obtained in  $\text{CDCl}_3$ .





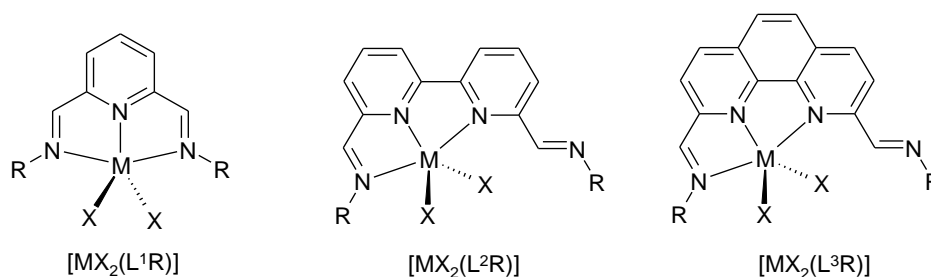
All spectra of L<sup>1</sup>R showed peaks in the aromatic region corresponding to the *m*- and *p*-pyridyl protons, showing a doublet and a triplet, integrating to 2:1 respectively and a singlet downfield of the aromatic region integrating to two protons, which was assigned to the aldimine protons of the head group.

**Figure 31.** <sup>1</sup>H NMR (600 MHz) spectrum of L<sup>3</sup>PhMe obtained in CDCl<sub>3</sub>.



All of the <sup>1</sup>H NMR spectra of L<sup>3</sup>R ligands showed three peaks in the aromatic region consisting of two doublets and a singlet of the 1,10-phenanthroline head protons integrating to two protons each, followed by a singlet downfield of the aromatic region integrating to two protons assigned to the aldimine moiety.

#### 4. Synthesis of Metal Complexes



To understand the role of the prepared complexes in section 2.1 to their biological activities given in section 7, a good knowledge of the structural chemistry of these compounds is required to aid this understanding. Since characterization of inorganic/co-ordination compound geometries are not as straight forward as organic molecules, and in particular paramagnetic complexes, a variety of techniques have been utilised to determine their precise co-ordination chemistry in the solid state and in solution as reported herein.

The formation of all complexes was achieved at room temperature. In nearly all cases the reaction products were isolated as analytically pure species on spontaneous precipitation usually as microcrystalline powders, when not they either crystallised by vapour diffusion or by crystallization from a suitable solvent. In both templated and non-templated reactions, yields recorded varied between 23-100 %, the Co<sup>II</sup> and Cu<sup>II</sup> yields being no less than 73 %. As initial observations identified that templated yields were comparably greater than those of the free ligand and reactions were effectively complete at time of mixing, it was decided that it was advantageous to preferentially prepare the complexes via the template method. Also this way a greater overall yield would be achieved in a one pot one step synthesis. The template synthesis of this class of open (acyclic), Schiff base ligands has not been observed in any of the literature, and

the non-templated preparation has been the only method seen previously for this class of compound.

#### **4.1. The Template Reaction**

Coordination complexes are traditionally prepared by mixing the preformed organic ligand with an appropriate metal source.<sup>151</sup> It is a pre requisite of this approach that the organic ligand must be stable and isolable. Many problems arise when the ligand sizes become large, particularly for macrocyclic compounds, and the conformation control in bringing the two ends of a chain together in the final cyclization step can be troublesome.<sup>151</sup> The template effect is a widely used strategy which circumvents these problems.<sup>152, 153</sup> In essence the method involves the incorporation of additional donor atoms into the chain and performing the cyclization reaction in the presence of a metal ion that can coordinate to these. The idea is that the metal ion will coordinate to the donor atoms and pre-organize the various intermediates in the conformation required to give the desired cyclic products. This is shown schematically (Figure 32) along with an example in Figure 33.

**Figure 32.** Schematic view of the cyclisation step involved in a template macrocycle synthesis. The filled and red circles represent mutually reactive functional groups and the squares are additional donor atoms. The binding of the metal to the donor atoms pre-organises the ligand into the conformation required for cyclisation.

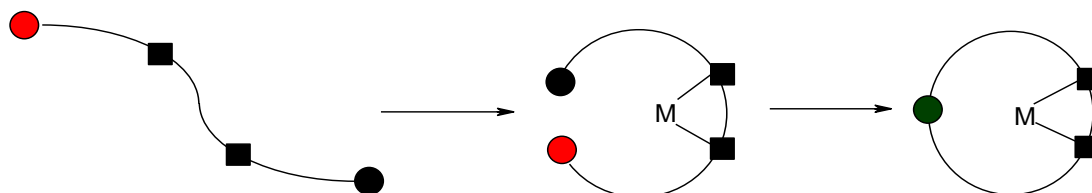
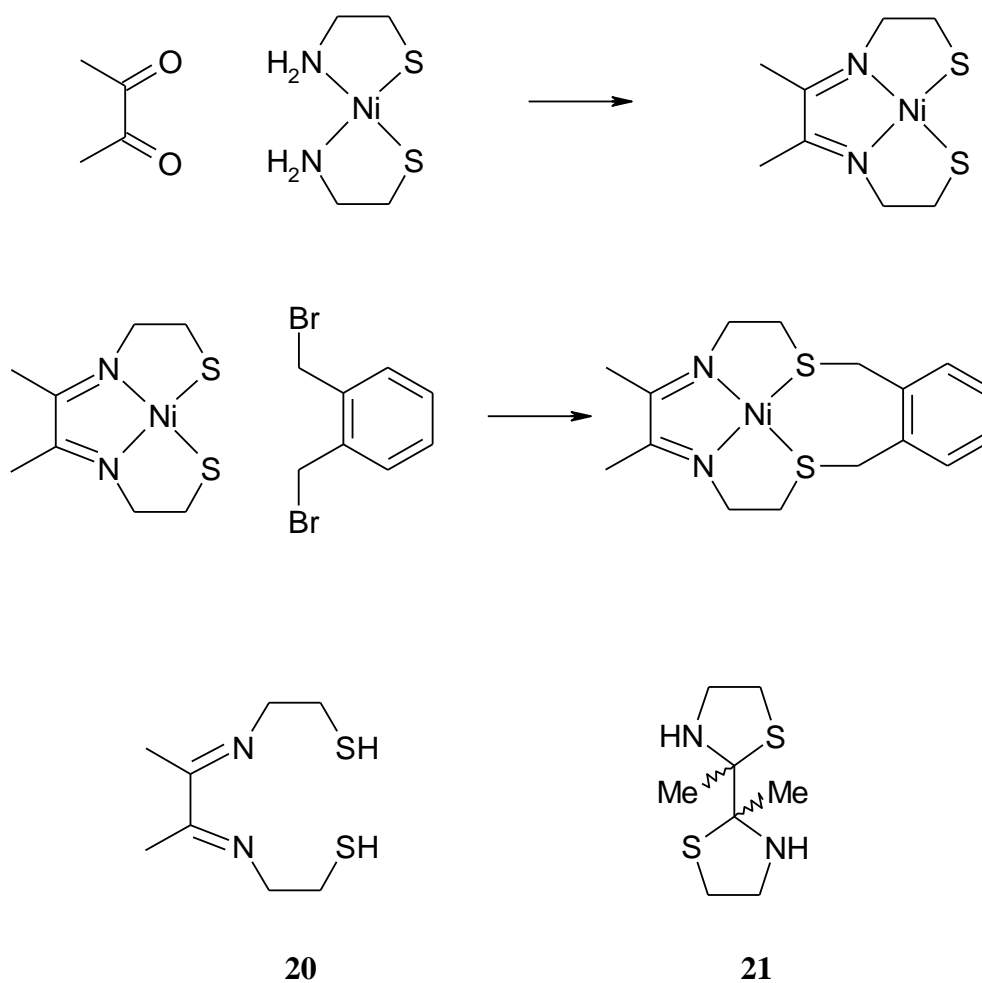


**Figure 33.** The template synthesis of a Nickel<sup>II</sup> macrocyclic complex.<sup>154</sup>



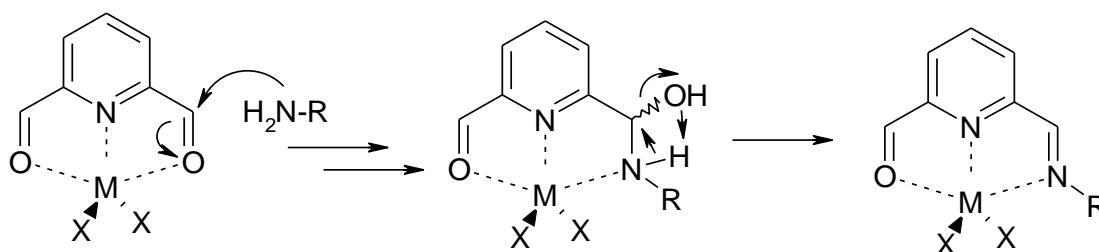
The metal atom plays a number of roles in the above reaction. The stabilization of the acyclic intermediate is achieved in a number of ways. As a free ligand, **20** possesses nucleophilic thiol and electrophilic imine groups and cyclisation arises by attack of the thiol upon the carbon of the imine to give **21**. When **20** is coordinated to Ni<sup>II</sup>, the nucleophilicity of the thiolate is reduced because it is bonded to an electropositive centre, the thiolate is constrained so that it cannot approach the imine and the imine is made less electrophilic by the back donation of the *d*-electron density into the  $\pi^*$  orbitals. The metal also pre-organises the two thiolate groups so that they are correctly orientated for reaction with the electrophilic 1,2-bis(bromomethyl)benzene to give the macrocyclic ligand.<sup>155</sup>

But for the complexes prepared via the template reaction in this study, no macrocycles were formed. These complexes can be best described as coordination macroacyles and this class of complex is not generally prepared via the template synthesis. Previous groups preparing similar compounds used the non-template method only.<sup>25, 156-158</sup> The reason for this is because these ligands cannot form cyclic compounds, since condensation is with mono amine precursors, and no bridging can therefore occur. This in addition makes synthesis of the free ligand simpler due to there being no possibility of polymerization or any higher order cyclic compounds being made.<sup>159-162</sup>

In contrast to the traditional metal template approach, the role of the metal ion in the template reaction of these complexes is proposed to work in a slightly different mechanism to that of the example in Figure 33. It is plausible that the metal does work by stabilising and organizing a conformation of the dialdehyde, but because the metal is a lewis acid it has empty *d* orbitals to accept a lone pair of electrons from the two

carbonyl oxygens. Therefore the metal acts analogously to a Bronsted acid by increasing the electrophilicity of the carbonyl carbon by withdrawing electron density through the oxygen, and therefore increasing the rate of condensation compared to reactions without a metal source. Also the conformation of the dialdehyde is maintained in a planar configuration and nucleophilic attack can occur freely from above or below the plane of the molecule at the Bürgi-Dunitz angle,<sup>163</sup> which is favourable for nucleophilic addition to a carbonyl carbon (Figure 34).<sup>164</sup>

**Figure 34.** Proposed mechanism of the acyclic Schiff base template reaction.



This mechanism is given some support from observations during the preparation. When the copper(II)chloride salt is added to a solution of P<sup>1</sup> in acetonitrile, a colour change is observed from colourless to orange, suggesting a complex is formed between the dialdehyde and metal (copper(II)chloride in acetonitrile is green).

The main differences between our proposed mechanism and the one described in Figure 33 is the opposite co-ordination of the metal. In our example the metal initially coordinates to dialdehyde which would be facilitated by the pyridine nitrogen. This can be best described as carbonyl activation and quite readily speeds up the condensation reaction compared to the non-templated approach (as evident in observed reaction times). The template reaction described in Figure 33 shows that the diamine reactant

firstly co-ordinates to the metal and pre-organises itself. This in itself would sequester a lot of the negative charge of the amine and render it less reactive.

The added bonus of the template reaction is that the final Schiff base is stabilized by coordination to a metal centre. Schiff bases are  $\pi$ -acceptors and therefore hydrolysis is less likely, so there is very little or no Schiff base equilibrium. The reactions are visually observed as being complete at time of mixing or shortly thereafter, by colour change or precipitation of product. However one disadvantage to this approach is when the free ligand is required and to remove the metal reductive demetallation is a common procedure, although the amine is thus produced. Addition of cyanide to sequester the metal as the cyano complex is also possible to generate the free ligand,<sup>155</sup> experiments of this type were not necessary in this project.

#### 4.2. Characterisation of Metal Complexes

On the basis of elemental analyses, all complexes (whatever was the method of preparation), exhibited an unequivocal metal-to-ligand stoichiometry of 1:1, with the exception of complexes of  $\text{Cu}(\text{BF}_4)_2$ ,  $\text{Co}(\text{BF}_4)_2$ ,  $\text{Co}(\text{NCS})_4$ ,  $\text{Co}(\text{NO}_3)_2$  salts, where no matter what the method of preparation (even when 1:1 equivalents of metal to ligand were used), the complexes exhibited metal-to-ligand stoichiometry of 1:2 (bis complex). In some cases half, one or two molecule of solvent was present ( $\text{CH}_3\text{CN}$ ,  $\text{H}_2\text{O}$ ,  $\text{DMF}$ ), and often a mixture of two. Moreover the CHN data showed that all complexes present existed as monomers with the exception of  $[\mu\text{Cl}_2\text{-}\{\text{NiCl}(\text{L}^1\text{Pr}^n)\}_2]$ .

Data obtained by ESI-MS indicated that monocationic species were observed. They predominantly correspond to the complex ligand/metal having lost one proton  $[L + M - H]^+$  or having retained one of the two anionic labile ligands  $[L + M + X^-]^+$ . The presence of one or two solvent molecules ( $CH_3CN$ ,  $MeOH$ ,  $H_2O$ ), are usually observed. In addition, minor peaks were observed, probably generated in the MS machine, corresponding to bis species of the type 2:1 (cases of  $M + 2L - H$ ,  $M + 2L$ ,  $M + 2L - H$ , plus  $M + 2L + Cl$ ). But in several cases dicationic species having relative intensities of 100%, corresponding to the bis species of the type 2:1 were also observed.

### 4.3. Complexes of the Ligand $L^1PhNO_2$

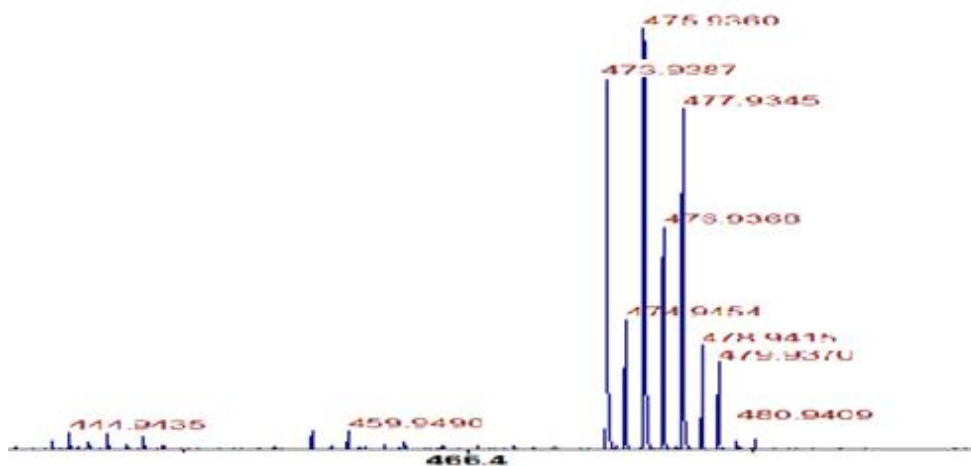
Although attempts to produce the free ligand of  $L^1PhNO_2$  were unsuccessful, attempts to produce its transition metal complex  $[MCl_2(L^1PhNO_2)]$  via the template method were not and all compounds were isolated as analytically pure powders after spontaneous precipitation from acetonitrile solvent. Analysis of these complexes in the solid state indeed show they had been prepared and in excellent yield. Microanalysis results showed a ligand to metal stoichiometry of 1:1, and colours agreed with the colours seen for other aromatic complexes of the particular metals used, (cobalt(II) - brown, copper(II) - orange, zinc(II) - yellow). Infrared spectra identified characteristic bands for  $C=N$  at  $1602-1605\text{ cm}^{-1}$  and the absence of any primary amine stretches around  $3200-3400\text{ cm}^{-1}$  neither any aldehyde  $C=O$  stretch at  $1700\text{ cm}^{-1}$ , were consistent with formation of the complex. Attempts to crystallize the complexes proved unsuccessful due to their very poor solubilities in nearly all organic and polar solvents. The complexes showed solubility in hot DMSO, but crystallization attempts with temperature or anti-solvent approaches were unsuccessful. Therefore further characterization by single crystal x-ray diffraction was not possible.



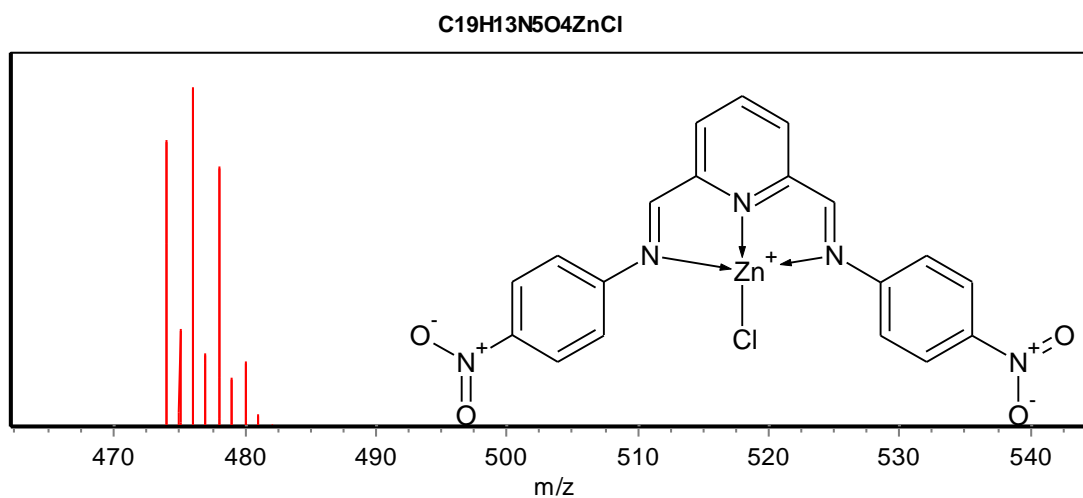
FAB mass spectrometry ultimately provided the concluding evidence that the desired complexes had been formed and in all cases fragments for the molecule having lost one  $\text{Cl}^-$  were observed with the correct isotope patterns. The complex  $[\text{ZnCl}_2(\text{L}^1\text{PhNO}_2)]$  is given as an example in Figure 35 and identified that the complex cation  $[\text{ZnCl}(\text{L}^1\text{PhNO}_2)]^+$  had been generated having lost one H and a Cl giving  $m/z$  474. The isotope pattern subsequently matched the predicted pattern almost identically which concluded that the desired complexes had indeed been generated.

**Figure 35.** FAB mass spectrum of  $[\text{ZnCl}_2(\text{L}^1\text{PhNO}_2)]$  (a) and the calculated isotope pattern for the observed fragment  $[\text{ZnCl}(\text{L}^1\text{PhNO}_2)]^+$  (b).

a)



b)



<sup>1</sup>H NMR of the zinc and cobalt complexes in DMSO-*d*<sub>6</sub> solution at elevated temperature were consistent with hydrolysis of the ligand. The zinc spectrum was somewhat complex with a mass of peaks abundant in the aromatic region, there was also the appearance of two singlets in the region of an aldehydic proton and also in the region for an aldiminic proton. There were also several doublets in the region of the free *p*-nitroaniline area, along with broad peaks which could be assigned to exchangeable protons of an amine. The spectrum therefore identified that in DMSO solution and with heating the intact complex is not observed and a mixture of free ligand to starting materials are most likely observed. The presence of water in DMSO could be the reason why the ligand hydrolyses back to the aldehyde and amine along with heating. This hydrolysis can then explain the poor solubility of the compound in cold DMSO yet after dissolution in hot DMSO the compound does not come back out of solution after cooling, the solubility of the starting materials are different to the actual intact complex.

For the Cobalt complex the expected isotropically shifted and singlet broadened peaks would be expected due to the paramagnetic nature of the cobalt centre, instead peaks

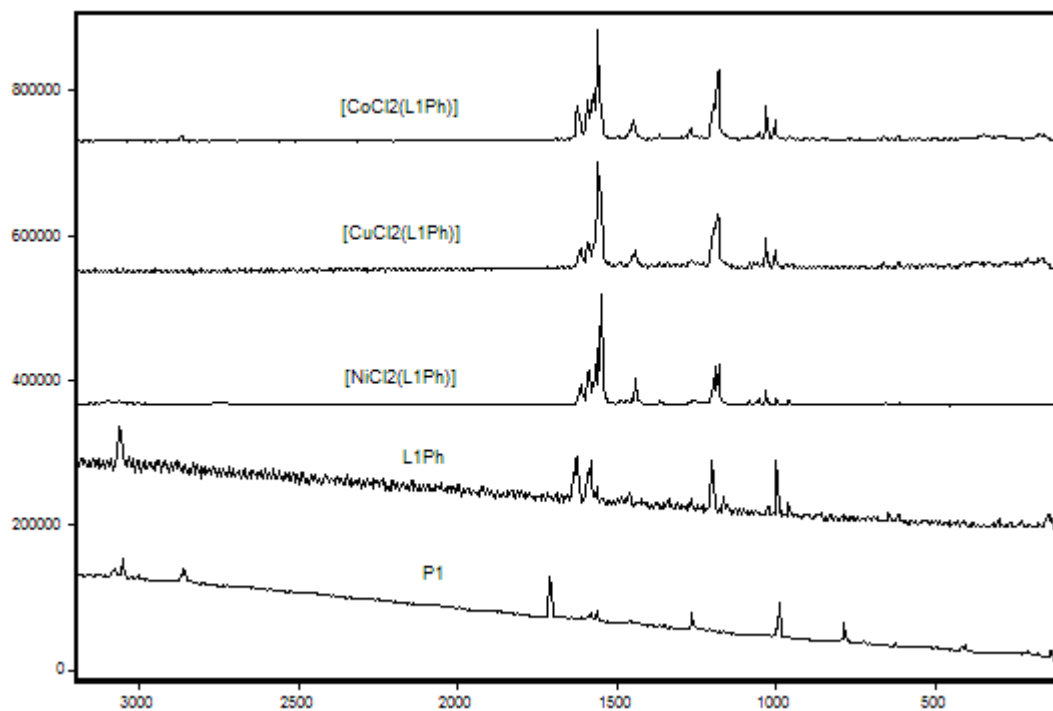
more distinguishable as diamagnetic resonances are observed and again a somewhat complex spectrum is observed. This is indicative of hydrolysis of the metal and ligand.

#### 4.4. Vibrational Spectroscopy of Complexes

Although IR spectroscopy is a difficult technique to unequivocally assign stretching modes of all functional groups, it is still a good tool to tentatively deduce certain features of a complex and has been used in combination with Raman spectroscopy to help interrogate the coordination characteristics of this class of complex.

The IR and Raman spectra of the complexes nearly all show aromatic C-H and C=C / C=N, stretches in their anticipated regions (3200-3000  $\text{cm}^{-1}$  and 1600-1400  $\text{cm}^{-1}$  respectively), and they all show weak to medium aldimine C=N stretches. Figure 36 shows the typical pattern of peaks for  $L^1R$  ligands and its complexes. Also included in the figure is the spectrum of the dialdehyde precursor  $P^1$ . Clearly the aldehyde C=O stretch disappears, from  $P^1$  to the ligand and in all complexes. The slight shift to lower frequency and decrease in the imine C=N stretch around 1625  $\text{cm}^{-1}$  is also evident going from  $L^1Ph$  to the complexed ligand.

**Figure 36.** Stack plot of Raman spectra of precursor P<sup>1</sup> to the Ligand L<sup>1</sup>Ph through its complexed form.



The infra-red spectra of the complexes gave interesting trends for the imine stretching frequencies for different metal centres. The Co<sup>II</sup> complexes demonstrated that aldimine stretches are observed between 1640-1622 cm<sup>-1</sup>, for the Cu<sup>II</sup> complexes the stretches are also observed in the same region. However for the Zn<sup>II</sup> complexes the window is shifted to higher frequency, between 1650-1622 cm<sup>-1</sup> (Table 24).

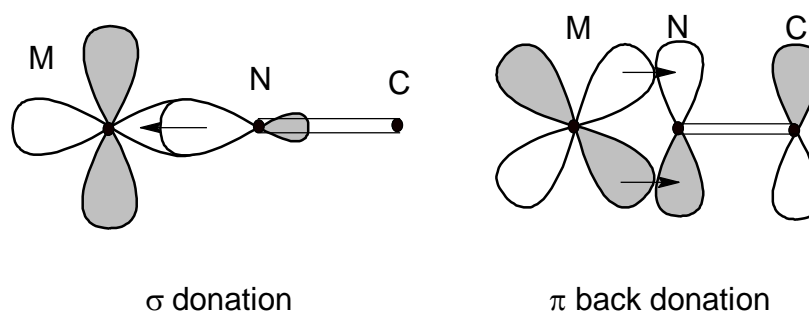
**Table 24.** FT-IR Imine stretching frequencies for various ligands and their Co<sup>II</sup>, Ni<sup>II</sup> Cu<sup>II</sup> and Zn<sup>II</sup> dichloride complexes.

	Free Ligand	Co <sup>II</sup>	Ni <sup>II</sup>	Cu <sup>II</sup>	Zn <sup>II</sup>	
	L <sup>1</sup> Et	1644 s	-	1639 w	1637 w	1650 m
	L <sup>1</sup> Pr <sup>n</sup>	1644 s	1630 w	1634 w	1634 w	1649 m
	L <sup>1</sup> Pr <sup>i</sup>	1644 s	1630 w	-	1634 w	1651 m
	L <sup>1</sup> Bu <sup>n</sup>	1653 s	1631 w	1634 w	1627 w	1650 m
Aliphatic	L <sup>1</sup> Bu <sup>2</sup>	1647 s	1634 w	-	1628 w	1647 m
	L <sup>1</sup> Bu <sup>i</sup>	1653 s	1634 w	-	1628 w	1652 m
	L <sup>1</sup> Bu <sup>t</sup>	1655 s	1636 w	-	-	1644 m
	L <sup>1</sup> Cy	1647 s	1631 w	1632 w	1638 w	1648 w
	L <sup>1</sup> CyMe	1647 s	1640 w	-	1628 w	1648 w
	L <sup>1</sup> Ph	1625 m	1622 w	1640 w	No band	No band
Aromatic	L <sup>1</sup> PhMe	1628 m	No band	1632 w	No band	No band
	L <sup>1</sup> PhCl	1628 m	1620 w	-	1620 w	1637 w
	L <sup>1</sup> PhNO <sub>2</sub>	-	1602 w	-	1605 w	1604 w

As for trends across the ligand variation it is fairly difficult to see any other than for aromatic tail groups. Clearly the C=N stretch of complexes of L<sup>1</sup>PhNO<sub>2</sub> shifts quite dramatically to lower frequency, (compared to L<sup>1</sup>PhCl), this is not surprising since the electron withdrawing power of the *p*-nitro group would reduce the imine bond strength. By the same token, it is strangely observed that the C=N stretches of the *p*-Cl variants seem to actually increase from the L<sup>1</sup>Ph complexes which is rather counterintuitive based on the same reasoning as the nitro group.

When we compare the free ligands to the complexed ligands a clear difference is observed in C=N stretching frequency. For ligands of alkyl tail groups, the stretching frequency is lowered on coordination to transition metals  $\text{Co}^{\text{II}}$ ,  $\text{Ni}^{\text{II}}$ ,  $\text{Cu}^{\text{II}}$  and raised on coordination to  $\text{Zn}^{\text{II}}$ . It was not possible to make this distinction for aromatic ligands, and in fact the opposite is observed. An explanation for the reason that transition metals shift the peaks to lower frequency is because of  $\pi$ -back donation from  $d$ -electrons of transition metals to the  $\pi^*$  antibonding orbitals of the C=N bond (Figure 37).

**Figure 37.** Orbitals and bonding of Schiff base ligands with transition metals.



When C=N acts as a ligand where the  $\sigma$ -orbital acts as a donor to a metal atom and forms a  $\sigma$  bond with the central metal atom (Figure 37). The LUMO's of the imine are the  $\pi^*$  orbitals. These two orbitals play a crucial role because they can overlap with metal  $d$  orbitals that have local  $\pi$  symmetry (such as the  $d_{xy}$ ,  $d_{xz}$ ,  $d_{yz}$  orbitals for square based pyramidal and octahedral complexes). The  $\pi$  interaction leads to the delocalization of electrons from the filled  $d$  orbitals on the metal atom into the empty  $\pi^*$  orbitals on imine ligands, so the ligand acts as a  $\pi$  acceptor. Population of the  $\pi^*$  orbitals weakens C=N by withdrawing electron density from C=N making it more single bond in character, therefore lowering the vibrational frequency.

As for the  $Zn^{II}$  complexes, since they contain no empty  $d$ -orbitals ( $Zn d^{10}$ ) to accept the  $\sigma$  electrons of the ligand, it is not possible for  $\pi$  back donation from the  $Zn^{II}$  centre into the  $\pi^*$  orbitals of  $C=N$  and therefore does not effect the imine frequency in the same sense. However Zinc is the most electropositive metal of this series and so electron density may be pushed toward the imine bond from  $Zn^{II}$  generating a stronger  $C=N$  bond and hence an increase in the vibrational frequency.

#### 4.4.1. Binding Modes of Parent Ligands

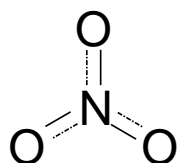
All infra-red and raman spectra of the  $L^1$  complexes showed ligand bands overlaying those of the bands in the complexes, with slight shifts in peaks and intensity and additional peaks likely of metal-ligand vibrations and metal-anion vibrations. The biggest noticeable shifts were as expected for the  $C=N$  stretch, which in all cases was a single stretch in the  $1600-1650\text{ cm}^{-1}$  region of the spectrum. This indicated that there was no loss in ligand symmetry and it was likely the ligands were acting as tridentate ligands with approximate  $C_2$  symmetry.

However when the infra red spectra of the  $L^3$  complexes was inspected, two distinct bands for the imine were observed along with a more complex mass of peaks, indicating a loss in the  $C^2$  symmetry of the free ligand. Also one imine stretch was generally unchanged from the free ligand band in both frequency and intensity, whereas the other band was lower in frequency and in intensity. This indicated the  $L^3$  ligand was acting in a tridentate mode with one bound and one free imine group.

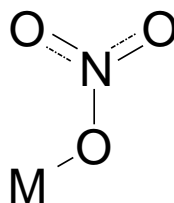
## 4.4.2. Binding Modes of Anionic Ligands

### 4.4.2.1. Nitrate complexes

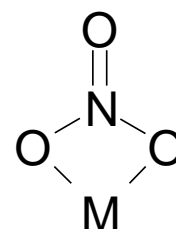
The nitrate anion can coordinate to the metal in one of two ways:



Free ion ( $D_{3h}$ )



Unidentate ( $C_s$ )



Bidentate ( $C_{2v}$ )

The bidentate mode can also be bridging. The free ion which is a planar 4 atom molecule ( $XY_3$ ) of  $D_{3h}$  symmetry is lowered to  $C_s$  and  $C_{2v}$  upon coordination. It is pretty difficult to differentiate between these structures by vibrational spectroscopy since the symmetry of the nitrate ion differs very little among them. Even so, vibrational spectroscopy is still useful in distinguishing unidentate and bidentate ligands. It is commonly perceived that the unidentate  $NO_3$  group exhibits three NO stretching bands, as expected for its  $C_{2v}$  symmetry.<sup>165</sup> For example  $[Ni(en)_2(NO_3)]$  (unidentate) shows three bands as follows:

$\nu_5$ ( $B_2$ )	$1420\text{ cm}^{-1}$	$\nu_a$ ( $NO_2$ )
$\nu_1$ ( $A_1$ )	$1305\text{ cm}^{-1}$	$\nu_s$ ( $NO_2$ )
$\nu_2$ ( $A_1$ )	$(1008)\text{ cm}^{-1}$	$\nu$ ( $NO_2$ )



whereas  $[\text{Ni}(\text{en})_2(\text{NO}_3)]\text{ClO}_4$  (chelating bidentate) exhibits three bands at the following:

$\nu_1 (\text{A}_1)$	$1476 \text{ cm}^{-1}$	$\nu (\text{N}=\text{O})$
$\nu_5 (\text{B}_2)$	$1290 \text{ cm}^{-1}$	$\nu_a (\text{NO}_2)$
$\nu_2 (\text{A}_1)$	$(1025) \text{ cm}^{-1}$	$\nu_s (\text{NO}_2)$

The separation of the two highest frequency bands is  $115 \text{ cm}^{-1}$  for the unidentate complex, whereas it is  $186 \text{ cm}^{-1}$  for the bidentate complex.

In this study, five nitrate complexes were prepared overall, three complexes of the  $\text{L}^1$  series were prepared  $[\text{Cu}(\text{NO}_3)_2(\text{L}^1\text{Pr}^n)]$ ,  $[\text{Zn}(\text{NO}_3)_2(\text{L}^1\text{Bu}^t)]$ ,  $[\text{Co}(\text{L}^1\text{Cy})_2][\text{NO}_3]_2$  along with one of the  $\text{L}^2$  and  $\text{L}^3$  ligands  $[\text{Zn}(\text{NO}_3)(\text{H}_2\text{O})(\text{L}^2\text{PhMe})][\text{NO}_3]$ , and  $[\text{Zn}(\text{NO}_3)_2(\text{L}^3\text{PhMe})]$  respectively. Unfortunately an interpretable infra-red and raman spectrum of the phenanthroline complex could not be collected for some reason and only the raman spectrum of the bipyridine complex was possible. Below are listed the observed bands and predicted coordination mode for the nitrate complexes.

**Table 25.** ( $\text{NO}_3^-$ ) infrared and Raman stretching modes observed for complexes of Ligand  $\text{L}^1\text{R}$  and  $\text{L}^2\text{R}$ .

Complex	Mode of coordination	$\nu_5$	$\nu_1$	$\nu_2$
$[\text{Cu}(\text{NO}_3)_2(\text{L}^1\text{Pr}^n)]$	Unidentate	1412 (IR)	1313 (IR)	1011 (IR)
	Bidentate	1486 (IR)	1289 (IR)	980 (IR)
$[\text{Co}(\text{L}^1\text{Pr}^n)_2][\text{NO}_3]_2$	Non-coordinated	-	1381 (IR)	1029 (IR)
$[\text{Zn}(\text{NO}_3)_2(\text{L}^1\text{Bu}^t)]$	Unassigned	1473 (IR)	1314 (IR)	-
$[\text{Zn}(\text{NO}_3)(\text{H}_2\text{O})(\text{L}^2\text{PhMe})][\text{NO}_3]$	Unidentate	1424 (R)	1324 (R)	1028 (R)

Both complexes in Table 25 show differences in their infrared spectra. The  $\text{Cu}^{\text{II}}$  complex showed several bands for  $\text{NO}_3^-$ . It can be best interpreted that since there are more bands than anticipated there must be a mixture of chelating modes or a distinct difference in symmetry between the two  $\text{NO}_3^-$  ions in the complex. Bands were observed at 1412 and  $1313\text{cm}^{-1}$  and correspond to  $\nu_5$  and  $\nu_1$  of a unidentate chelate respectively and bands 1486 and 1289 correspond to  $\nu_5$  and  $\nu_1$  of a bidentate chelate respectively. The differences in the bands agrees with the numbers in the example above proposed for the two chelation types.

The Zinc complex on the other hand appeared much more straight forward and only two bands of a chelated  $\text{NO}_3^-$  ion were observed. The difference between the two bands ( $159\text{cm}^{-1}$ ) being somewhere between the numbers for unidentate and bidentate chelates. This made the assignment of the coordination difficult and so none could be directly inferred from this data alone. But when considering that only one particular type of nitrate

ligand is observed, it is highly unlikely that a bidentate mode of coordination is possible since it would mean a unidentate or spectator nitrate would be present. These very different species would likely give rise to two sets of stretching vibrations in the IR spectrum. However it was very interesting to observe by  $^1\text{H}$  NMR spectroscopy, that in  $\text{DMSO-}d_6$  solution at  $50^\circ\text{C}$ , this particular complex gave rise to two particular species, which could possibly be a mixture of the unidentate-unidentate nitrate complex and the unidentate-bidentate nitrate complex. Otherwise aquation of the metal centre may have occurred giving rise to the second spectrum.

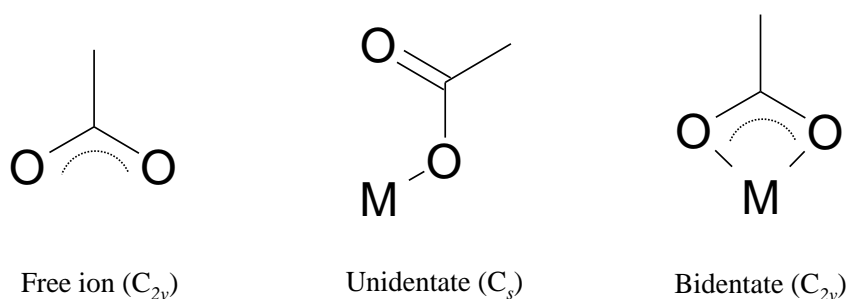
The structure of  $[\text{Co}(\text{L}^1\text{Cy})_2][\text{NO}_3]_2$  was inferred first of all from its CHN analysis which identified that a ratio of 2:1:2 for ligand:metal:anion. This strongly suggested a bis ligated complex with both  $\text{NO}_3^-$  ions as spectators which would require the  $\text{NO}_3^-$  as a free ion. This was difficult to interpret in the infra-red spectrum since the only bands that could be drawn out were ones at  $1381\text{ cm}^{-1}$  and  $1029\text{ cm}^{-1}$  which do have a similar correlation to observed bands for salt like  $\text{NH}_4\text{NO}_3$  of  $1350\text{ cm}^{-1}$  and  $1050\text{ cm}^{-1}$  corresponding to the  $\nu_3$  and  $\nu_1$  N-O of the  $\text{NO}_3^-$  ion with  $\text{C}_{2v}$  symmetry.

For the bipyridine complex  $[\text{Zn}(\text{NO}_3)(\text{H}_2\text{O})(\text{L}^2\text{PhMe})][\text{NO}_3]$ , only the Raman spectrum was obtained and sharp bands were observed for the N-O vibrations. In total three bands were observed as shown in Table 25 and these are very consistent with bands of a unidentate coordination mode of the nitrate ion, strangely no other bands for nitrate were observed and so it was not possible to assign with confidence in this case.

#### 4.4.2.2. Acetato complexes

In this study three acetato complexes were prepared, namely  $[\text{Zn}(\text{AcO})_2(\text{L}^1\text{Bu}^t)]$ ,  $[\text{Co}(\text{AcO})_2(\text{L}^1\text{Cy})]$  and  $[\text{Ni}(\text{AcO})_2(\text{L}^1\text{Cy})]$ . The infrared spectra of such complexes was consulted to help elucidate the coordination modes of the acetate ion.

The acetate ion may coordinate to a metal in the same fashion as the nitrate ion:



Unlike the nitrate ion free acetate and its bidentate chelate have the same symmetry, but similarly to the nitrate ion acetate can also form a bridging bidentate chelate. Previous research making careful examinations of many acetates having known X-ray crystal structures arrived at the following conclusions about the acetate stretching frequencies and chelating modes:<sup>165</sup>

1. Unidentate complexes exhibit  $\Delta$  values  $[\nu_a(\text{CO}_2^-) - \nu_s(\text{CO}_2^-)]$  which are much greater than the ionic complexes.
2. Chelating (bidentate) complexes exhibit  $\Delta$  values which are significantly less than the ionic values.

3. The  $\Delta$  values for bridging complexes are greater than those of chelating (bidentate) complexes and close to ionic values.

Table 26 lists some examples of infrared frequencies with chelating mode and their corresponding  $\Delta$  values.

**Table 26.** Infra-red stretching frequencies of various acetate complexes.<sup>165</sup>

Compound	$\nu_a(\text{CO}_2^-)$	$\nu_s(\text{CO}_2^-)$	$\Delta$	Structure
$\text{CH}_3\text{COO}^- (\text{AcO}^-)$	1578	1414	164	ionic
$\text{Ru}(\text{AcO})(\text{CO})_2(\text{PPh}_3)$	1613	1315	298	Unidentate
$\text{RuCl}(\text{AcO})(\text{CO})(\text{PPh}_3)_2$	1507	1465	42	Bidentate
$\text{Ph}_2\text{Sn}(\text{AcO})_2$	1610	1335	265	Asym. bidentate
$\text{Rh}_2(\text{AcO})_2(\text{CO})_3(\text{PPh}_3)$	1580	1440	140	Bridging
$\text{CrO}_2(\text{AcO})_2$	1710	1240	470	Unidentate
	1610	1420	190	Bidentate

**Table 27.** Observed vibrational frequencies of the acetate anion and the assigned mode of coordination for three acetate complexes generated in this study.

Complex	$\nu_a(\text{CO}_2^-)$	$\nu_s(\text{CO}_2^-)$	$\Delta$	Structure
$[\text{Co}(\text{AcO})_2(\text{L}^1\text{Cy})]$	1703 (IR)			Unidentate
	1591 (IR)	1420 (IR)	171	Bidentate
$[\text{Ni}(\text{AcO})_2(\text{L}^1\text{Cy})]$	1652 (IR)	1345 (IR)	307	Unidentate
	1568 (IR)	1410 (IR)	158	Bidentate
$[\text{Zn}(\text{AcO})_2(\text{L}^1\text{Bu}^f)]$	1616 (IR)	1326 (IR)	290	Unidentate

Taking into consideration the criteria for assigning the stretching frequencies of the acetate anion, it was possible to tentatively deduce the various binding modes present in the three complexes of this study.  $[\text{Co}(\text{AcO})_2(\text{L}^1\text{Cy})]$  provided three distinguishable bands for the acetate ligand. One single carbonyl stretch at  $1703\text{ cm}^{-1}$  was assigned to that of the unidentate chelate based on similar observation for  $\text{CrO}_2(\text{AcO})_2$  as given in Table 26. A further two bands at  $1591\text{ cm}^{-1}$  and  $1420\text{ cm}^{-1}$  assigned to the asymmetric and symmetric stretches of a bidentate acetate chelate was consistent with those observations in Table 26 based on  $\Delta$ . Since no crystal structure of this complex was obtained, the structural characterisation of  $[\text{Co}(\text{AcO})_2(\text{L}^1\text{Cy})]$  is based upon the vibrational spectroscopic assignments, NMR, MS, and CHN. Since CHN results suggest an analytically pure M:L 1:1 complex as suggested, and since it is highly unlikely that methathesis to cobalt tetraacetate would occur to give the bis complex, it can be reasonably assumed that a distorted octahedral structure is likely containing in the coordination sphere three N-donors of the  $\text{L}^1\text{Cy}$  ligand, two O-donors of a bidentate acetate and one O-donor of a unidentate acetate.

The Nickel (II) acetate complex obtained in this study gave infra-red bands consistent with that demonstrated by the crystal structure. Clearly two types of acetate were distinguishable from the IR spectrum and gave rise to 4 bands (Table 27) distinguishable as a bidentate and unidentate acetate complex. This agrees with the symmetric and asymmetric acetates identified from the crystal structure (Section 6.3.2) and M-O distances were consistent with unidentate and bidentate acetates.

The complex  $[\text{Zn}(\text{AcO})_2(\text{L}^1\text{Bu}^f)]$ , gave rise to two distinguishable bands associated with asymmetric and symmetric stretches of a single acetate moiety with a  $\Delta$  value of 290.

This observation indicates only one type of acetate coordination in this complex, and from  $\Delta$  it is most probable that this complex contains two coordinated unidentate acetates at the  $Zn^{II}$  centre.

#### 4.4.2.3. Isothiocyanato Complexes

The  $[SCN]^-$  ions are called pseudohalide ions, since they resemble halide ions in their chemical properties. The SCN group may coordinate to a metal through the nitrogen or the sulphur or both as shown below:

M-SCN thiocyanato complex

M-NCS isothiocyanato complex

M-NCS-M'

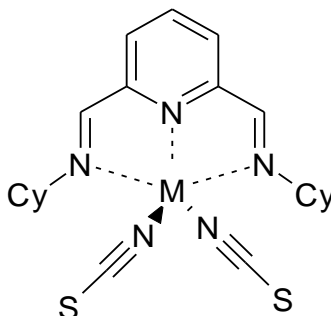
In general, harder metals (first transition series, such as  $Cr^{II}$ ,  $Mn^{II}$ ,  $Fe^{II}$ ,  $Co^{II}$ ,  $Ni^{II}$ ,  $Cu^{II}$  and  $Zn^{II}$ ) form M-N bonds, whereas softer metals (second half of the second and third series, such as  $Rh^{II}$ ,  $Pd^{II}$ ,  $Ag^I$ ,  $Cd^{II}$ ,  $Ir^{II}$ ,  $Pt^{II}$ ,  $Au^I$  and  $Hg^I$ ) form M-S bonds.<sup>165</sup> However, other factors such as the oxidation state of the metal, the nature of other ligands in a complex and steric consideration, also influence the mode of coordination.

Several empirical criteria have been developed to determine the bonding type of the NCS group in metal complexes.<sup>165</sup>

1. The CN stretching frequencies  $<2050cm^{-1}$  in N-bonded complexes, near  $2100cm^{-1}$  in S bonded complexes and bridging (M-NCS-M') exhibit  $\nu(CN)$  well above  $2100cm^{-1}$ .

2.  $\nu(\text{CS})$  can be used for structural diagnosis: 860-780 for N-bonded and 720-690  $\text{cm}^{-1}$  for S-bonded complexes.

The single isothiocyanato complex of this project was finally determined by single crystal X-ray diffraction (section 6.3.4), but it was initially anticipated that the monoligated complex with two isothiocyanato anions coordinated would have been the structure obtained as shown below.



After analysis of the isolated product by CHN gave a formula  $\text{ML}(\text{NCS})_2$  and ESI-MS in positive mode identified the above molecular ion, it was anticipated that the structure was indeed that of the desired molecule. However the raman and infra-red spectra (Figure 38 and Figure 39 respectively), of the complex confused things slightly when a single  $\nu(\text{CN})$  band at  $2064 \text{ cm}^{-1}$  in the infra red spectrum was observed but two bands at  $2094$  and  $2067 \text{ cm}^{-1}$  were observed in the raman spectrum. The indication from the two bands was that two modes of coordination were present for the  $[\text{NCS}]^-$  ion, one being silent in the infra-red spectrum.



**Figure 38.** IR Spectrum of  $[\text{Co}(\text{L}^1\text{Cy})_2][\text{Co}(\text{NCS})_4]$

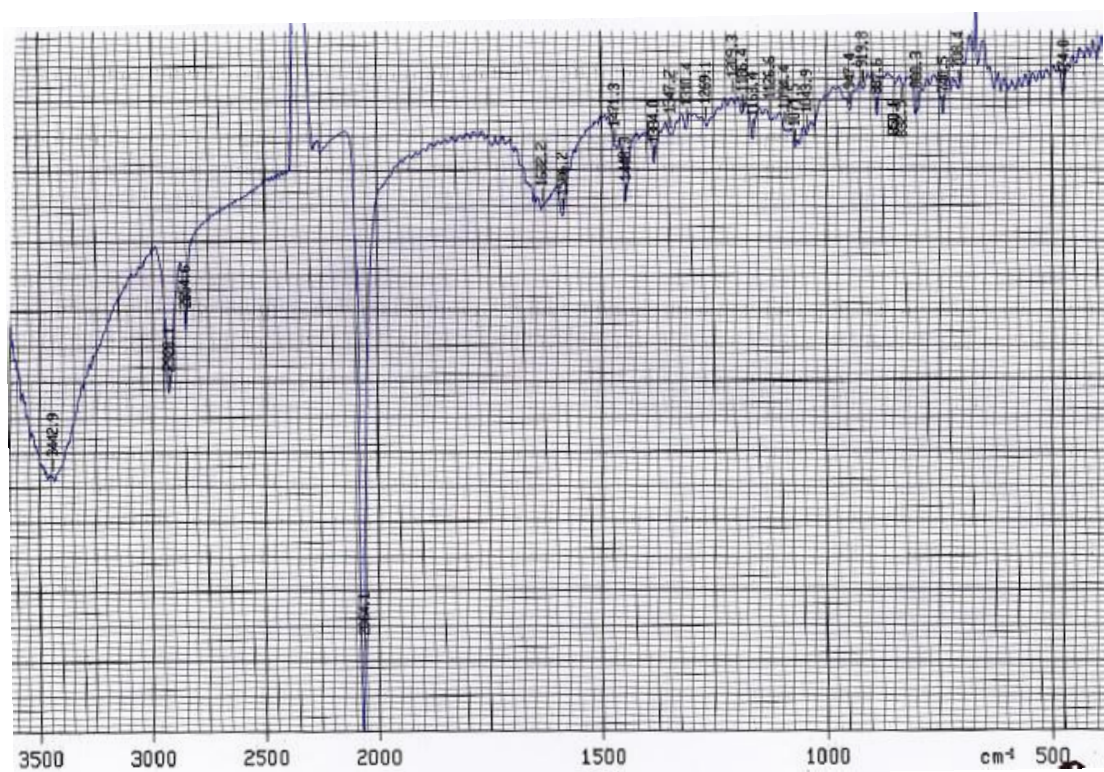
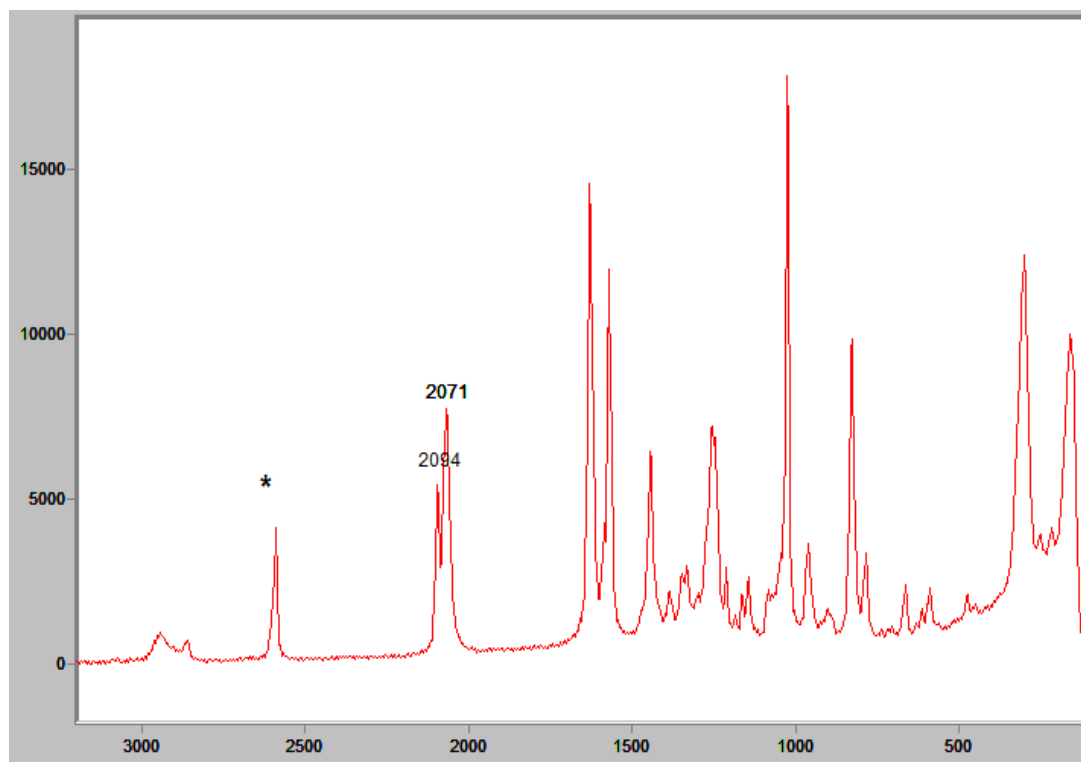
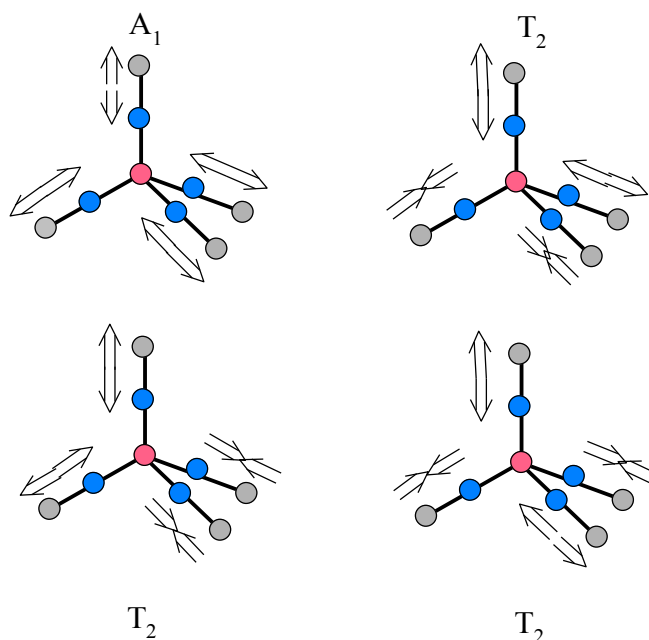


**Figure 39.** Raman Spectrum of  $[\text{Co}(\text{L}^1\text{Cy})_2][\text{Co}(\text{NCS})_4]$ , \* denotes an artifact of the instrument laser line.



When comparing the raman stretching frequencies to the criteria outlined above it could be inferred that the stretch at  $2094\text{ cm}^{-1}$  could be that of an S bound ligand and the stretch at  $2067\text{ cm}^{-1}$  that of an N bound ligand. On the other hand infra-red spectra alone could have given rise to the assignment that only the N coordinated  $\text{NCS}^-$  ion is present. This observation was a difficult one to interpret and even when the crystal structure of the complex was obtained it was still difficult to understand what was really happening in the raman spectrum. The crystal structure actually identified that the desired complex had not been prepared and instead a bis-ligated complex with a  $[\text{Co}(\text{NCS})_4]^{2-}$  counterion was obtained. The IR spectrum did indeed identify correctly that only N coordination was present at the coordination sphere, which also goes with a prediction based on the hardness of the Co and N atoms. The  $[\text{Co}(\text{NCS})_4]^{2-}$  complex was identified as tetrahedral with very slight distortion in the crystal structure. However the vibrational modes of the molecule that arise from stretching motions of the CN groups are the four combinations of the four CN displacement vectors. Reference to SALC's of the  $T_d$  point group identified that four atomic *s* orbitals give one  $A_1$  SALC and three  $T_2$  SALC's. The analogous linear combinations of the CN displacements are depicted in Figure 40.

**Figure 40.** The CN stretching modes of  $[\text{Co}(\text{NCS})_4]^{2-}$ . The  $A_1$  mode is non-degenerate; the  $T_2$  modes are triply degenerate.



After consulting the character table for the  $T_d$  point group it became apparent that the combination labelled  $A_1$  transforms like  $x^2 + y^2 + z^2$  indicating that it will be Raman active but not IR active. In contrast,  $x$ ,  $y$  and  $z$  and the products  $xy$ ,  $yx$  and  $zx$  transform as  $T_2$ , so the  $T_2$  modes are both Raman and infrared active. Consequently the tetrahedral  $[\text{Co}(\text{NCS})_4]^{2-}$ , fits nicely to the Raman and IR spectra and shows how by combining both techniques molecular symmetry can be inferred. One thing that does not quite fit from this explanation is why the asymmetric vibration observed in both the Raman and IR spectra comes at lower frequency to the symmetric vibration.

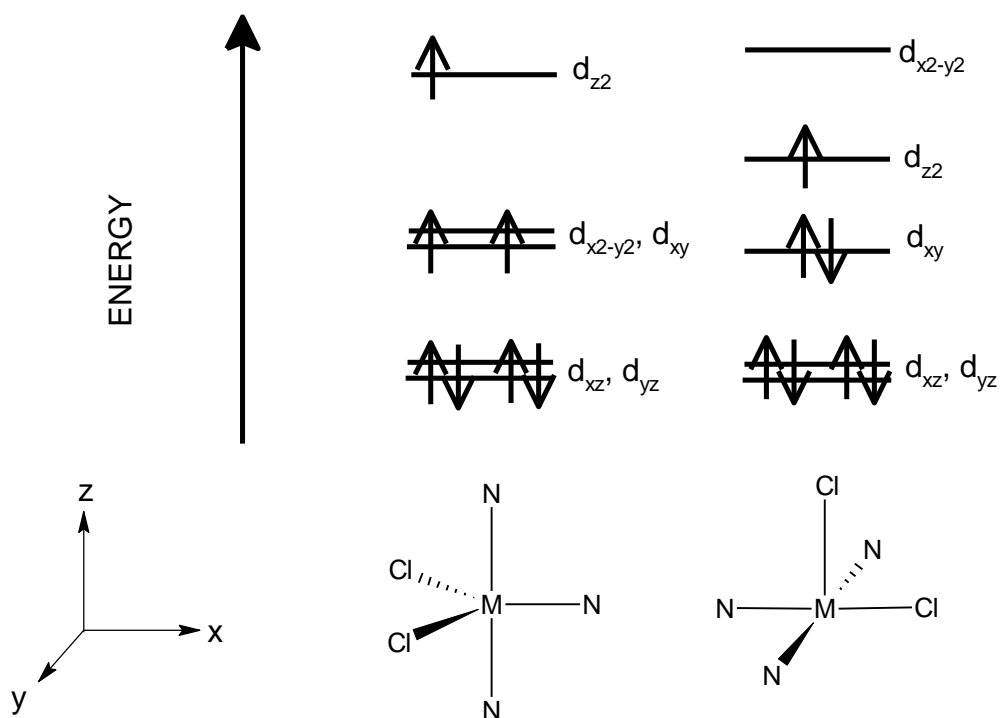
## 5. Solution Studies of Metal Complexes

### 5.1. Magnetic Susceptibility in Solution by NMR

All complexes prepared in this study are paramagnetic, with the exception of the zinc complexes which do not have partially filled *d*-orbitals and are essentially therefore non transition metals. The magnetic moments of cobalt, copper and nickel complexes were determined by the Evans NMR method.<sup>123</sup> The Co<sup>II</sup> complexes afford magnetic moments between 4.2 and 5  $\mu_B$ , which suggests a high spin configuration of three unpaired electrons, the values are somewhat larger than the spin only value of 3.87  $\mu_B$ , but within the observed values for the Co<sup>II</sup> centre, (4.3 – 5.2  $\mu_{obs}$ ).<sup>156, 166</sup> It has been generalized that departure from the spin-only magnetic moments is large for high spin *d*<sup>7</sup> complexes.<sup>166</sup> For Co<sup>II</sup>, altering the Schiff base ligand tail groups does not affect the high spin configuration of the metal centre, but the change in the total magnetic moment is evident due to orbital contributions, though no correlation can be drawn out.

Assuming the Co<sup>II</sup> complexes in solution form distorted trigonal bipyramidal or distorted square based pyramidal geometry, the frontier orbital energies have been proposed to be as shown in Figure 41.

**Figure 41.** The energy level diagrams of trigonal bipyramidal and square based pyramidal structures along with the high and low spin configurations of  $\text{Co}^{\text{II}}$ .<sup>167</sup>



From the energy level diagrams predicted in Figure 41 it seems likely that  $\text{Co}^{\text{II}}$  complexes are more likely to take on a trigonal bipyramidal geometry based on the observed magnetic moment, however it is not known what effects the ligands have on the splitting of the orbital energies, it is likely there could be some splitting between  $d_{xz}$  and  $d_{yz}$  orbitals and the higher orbitals could actually be relatively close in energy. Since the magnetic susceptibilities were determined in solution, it is very likely that the geometry at the metal centre is dynamic, and the geometry could be constantly changing from square-pyramidal to trigonal-bipyramidal. In that case based on the model in Figure 41, a mixed magnetic moment between 1 and 3 unpaired electrons would likely arise, due to this dynamic process. Since this is not observed it does suggest that the energy levels  $d_{xy}$ ,  $d_z^2$ ,  $d_x^2-d_y^2$  are of similar energy and three lone electrons are free to

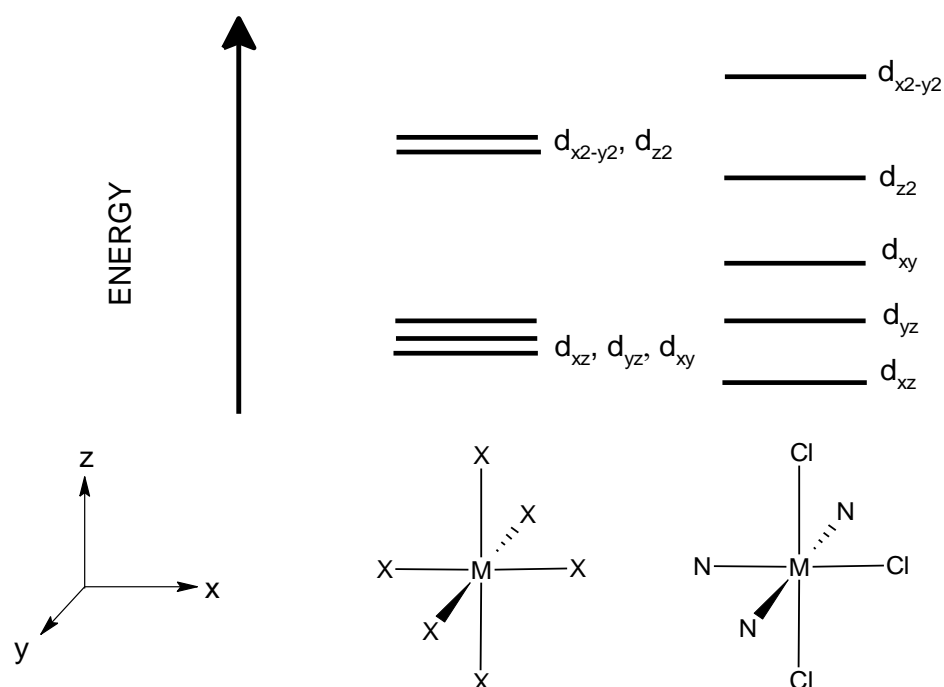
occupy the three orbitals. It is later observed in the crystal structure of  $[\text{CoCl}_2(\text{L}^1\text{Ph})]$  that distorted trigonal bipyramidal geometry is evident in monoligated  $\text{Co}^{\text{II}}$  complexes.

The copper complexes examined exhibited the expected magnetic moment for the +2 oxidation state of  $1.73 \mu_{\text{B}}$ . Because  $\text{Cu}^{\text{II}}$  a  $d^9$  transition metal ion contains one unpaired electron and no high spin or low spin configurations are possible in any crystal field since its lone electron cannot be paired under any circumstance. Nevertheless the observation of a magnetic moment is further proof of a  $\text{Cu}^{\text{II}}$  oxidation state since  $\text{Cu}^{\text{I}}$  is diamagnetic.

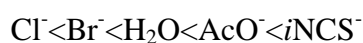
The  $\text{Ni}^{\text{II}}$  complexes typically exhibited magnetic moments between  $3.15\text{-}3.43 \mu_{\text{B}}$  which is consistent with that of the high spin  $\text{Ni}^{\text{II}}$  centre. The magnetic moment is slightly larger than that of the spin only value ( $2.83 \mu_{\text{B}}$ ) so orbital contributions must play a part in the total magnetic moment observed. It is clear that no low spin complexes form since in all cases there is a magnetic moment observed. In low spin  $\text{Ni}^{\text{II}}$  all 8 electrons are paired and hence no magnetic moment is possible. In a pure octahedral field (i.e. all ligands identical) it would only be possible for  $\text{Ni}^{\text{II}}$  to be high spin since the lower  $t_{2g}$  energy levels would be forced to fill and the higher energy, doubly degenerate  $e_g$  orbitals would each receive an unpaired electron. For the  $\text{Ni}^{\text{II}}$  complexes of this series however is it not possible that a pure octahedral splitting of the energy levels would occur and since each orbital would receive a different combination of ligands it's likely there would be no degeneracy (Figure 42). In this model it is possible for  $\text{Ni}^{\text{II}}$  to be either high or low spin and so in the case of the ligands of this study, it is clear they lower the energy of the highest orbital or the two highest energy orbitals are approximately of similar energy, making it possible for two electrons to occupy their

own orbitals. The latter case is more likely true since imine ligands are  $\pi$  acceptors and would come high up in the spectrochemical series. The higher a ligand is in the spectrochemical series the the greater stabilization effect it will have on the ligand field splitting, so it is likely that it does not separate  $d_z^2$  from  $d_{x^2-y^2}$  by too much.

**Figure 42.** Proposed orbital splitting from pure octahedral to non-degeneracy in a non-pure octahedral system. Relative orbital energies would vary depending on which combinations of ligand occupy or lie between them.



Evidently from the observed magnetic moments for  $\text{Co}^{\text{II}}$  and  $\text{Ni}^{\text{II}}$  complexes of the  $\text{L}^1\text{R}$  ligand class, and by subsequently changing the anionic ligand in the monoligated complexes through the series placed roughly in the order of the spectrochemical series:<sup>168</sup>



It is pretty clear that none of the ligands have any observed impact on the ligand field stabilization energy within the complex.

## 5.2. NMR Studies

NMR data was obtained for almost all complexes and ligands. Not all complexes could be studied due to lack of solubility or in the case of copper complexes with aromatic tail groups, no resonances could be detected by the NMR instrument, attributed to the rapid relaxation of the proton spin as a consequence of the paramagnetic copper centre, giving Heisenberg broadening of the isotropically shifted resonances.<sup>169</sup> It was observed however after evaluating some copper<sup>II</sup> complexes that if the tail groups were alkyl, then the resonances for those protons were observed and in some cases fine structure could be observed for those peaks. Also they didn't appear to be isotropically shifted peaks since they were observed in the correct regions of the spectrum as for equivalent free ligand protons. Possibly due to the lack of aromaticity and conjugation in alkyl tail groups the electron spin of the copper couples weakly if not at all with the spin of the proton and normal resonances are observed as expected for diamagnetic compounds. All proton spectra were obtained in D<sub>2</sub>O for the copper complexes, most complexes were readily soluble and the spectra revealed in all cases the intact ligand was still present and its symmetry was retained. The fact that the pyridyl and aldimine shifts were barely observable due to Heisenberg broadening is a good indicator that the ligand remains coordinated to the copper in solution. D<sub>2</sub>O solubility indicates the complexes are ionic in nature. The bis-ligated complex gives rise to significantly broadened tail group resonances and all mono ligated complexes give rise to normal diamagnetic proton resonances indicating the monoligated complexes do not metathesise to the bis-complex during the experiments.

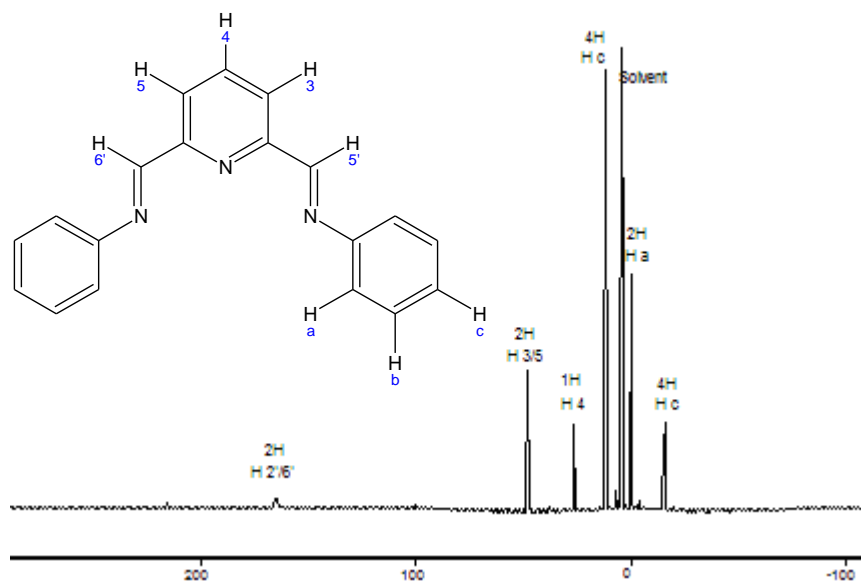


For cobalt complexes which are also paramagnetic, isotropically shifted resonances are observed which appear as broad singlets. These signals can be assigned on the basis of peak areas, proximity to the metal centre and comparison with spectra of similar paramagnetic structures; although not in all cases and 2D correlation techniques therefore need to be employed if obtainable.

The following complexes  $[\text{CoCl}_2(\text{L}^1\text{Ph})]$ ,  $[\text{CoCl}_2(\text{L}^1\text{Bu}^i)]$  and  $[\text{CoCl}_2(\text{L}^1\text{Cy})]$  are given here as examples of how the solution structures of paramagnetic complexes could be inferred from NMR spectroscopy.

### 5.2.1. $^1\text{H}$ NMR Assignment of Complex $[\text{CoCl}_2(\text{L}^1\text{Ph})]$

**Figure 43** Proton NMR Spectrum of  $[\text{CoCl}_2(\text{L}^1\text{Ph})]$  obtained in  $\text{D}_2\text{O}$ .



The spectrum of  $[\text{CoCl}_2(\text{L}^1\text{Ph})]$  shown here in Figure 43 afforded six peaks, two of which integrated to four protons, three to two protons and one peak to one proton, as expected for the compound with 2-fold symmetry. Initially the first peak was assigned on the basis of integration, which was the peak at 26.28 ppm and integrates to 1H, therefore must be that of the *p*-pyridyl proton ( $\text{H}^4$ ). The downfield peaks at 165.63 and 47.70 ppm which both integrate to 2H, are assigned to the aldimine protons ( $\text{H}^{2/6'}$ ) and the *m*-pyridyl protons ( $\text{H}^{3/5}$ ), respectively, on the basis of their close proximity to the metal centre and comparison to similar lanthanide bis-(imino)pyridine complexes.<sup>170</sup> The next peak to be assigned, on the basis of integration was at -0.13 ppm which integrates to 2H and must be that of the *p*-phenyl proton. The remaining two peaks at 12.33 and -15.30 could then be assigned to *meta*, ( $\text{H}^c$ ) and *ortho*, ( $\text{H}^b$ ), phenyl protons respectively, on the basis of comparison to similar iron bis(imino)pyridine complexes.<sup>171</sup>

### 5.2.2. $^1\text{H}$ NMR Assignment of Complex $[\text{CoCl}_2(\text{L}^1\text{Bu}^i)]$

$[\text{CoCl}_2(\text{L}^1\text{Bu}^i)]$  reveals an NMR spectrum consisting of six peaks, one peak integrating to twelve protons, one peak integrating to four protons, three peaks integrating to two protons and one peak integrating to one proton as expected for the complex with 2-fold symmetry. Initially it is obvious that the peaks at 42.60 ppm, integrating to 1H, 148.81 ppm integrating to 4H and -3.90 ppm integrating to 12H can be assigned to protons  $\text{H}^d$ ,  $\text{H}^a$  and  $\text{H}^c$ , respectively on the basis of integration. The peak at 221.18 ppm integrating to 2H can be assigned to the aldimine protons ( $\text{H}^{2'/6'}$ ), on the basis of proximity to the metal centre. The remaining *m*-pyridyl protons ( $\text{H}^{3/4}$ ) can be assigned to the peak at 103.15 ppm integrating to 2H on the basis of comparison to other similar lanthanide bis(imino)pyridine complexes.<sup>172</sup> Therefore the last remaining peak at 0.68 ppm integrating to 2H is assigned to  $\text{H}^b$ .

### 5.2.3. $^1\text{H}$ NMR Assignment of Complex $[\text{CoCl}_2(\text{L}^1\text{Cy})]$

The complex  $[\text{CoCl}_2(\text{L}^1\text{Cy})]$ , gave rise to 10 isotropically shifted broad singlets in the  $^1\text{H}$  NMR spectrum, four of which integrated to four protons, five to two protons and one to one proton, as expected for the 2-fold symmetric compound. Again the obvious starting point was to assign the lone *p*-pyridyl proton to the lone peak integrating to 1H at 24.89 ppm. The broader downfield peaks at 168.01 and 121.84 ppm, both arising from 2H can be assigned, to the aldimine ( $\text{H}^{2'/6'}$ ) and cyclohexyl ( $\text{H}^a$ ), respectively. Noticeably these two protons appear downfield due to connections to the N atom through two bonds and the broadness of the peaks is a result of a greater coupling to the unpaired electron spins of cobalt consequently increasing the speed of relaxation of the proton nuclear spin. The remaining *m*-pyridyl proton, ( $\text{H}^{3/5}$ ), was next assigned to the

peak at 50.21 ppm, integrating to 2H, on the basis of comparison to similar lanthanide bis(imino)pyridine paramagnetic complexes,<sup>172</sup> again it is noticeable from this and the previous spectrum of [CoCl<sub>2</sub>(L<sup>1</sup>Ph)], that the pyridyl resonances appear further downfield than for the tail group resonances, whether aromatic or not. This is possibly a consequence of the metal centre having greater electronic influence through the  $\pi$ -electrons of the C=N. The remaining six peaks are therefore those of the remaining cyclohexyl, protons. The reason six peaks are observed and not three, is due to the fact that the protons on the same carbon atom are magnetically inequivalent. The first two of these remaining six peaks at 0.13 and -0.20 ppm, integrating to 2H each, can be assigned to both the d and d' protons. It is not possible to assign the remaining four peaks from the <sup>1</sup>H spectrum by either 1D or 2D techniques.

#### 5.2.4. Co<sup>II</sup> Solution Chemistry

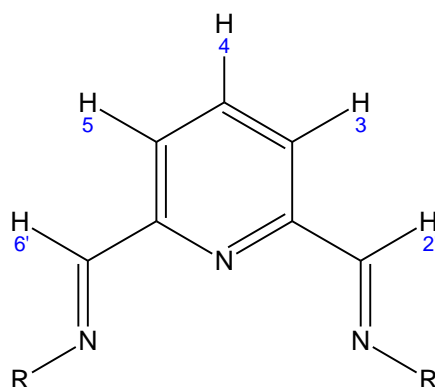
As it can be seen from Table 28, the pyridyl and aldimine proton shifts are very much similar for ligands (L<sup>1</sup>Cy) and (L<sup>1</sup>Ph), varying by 1-2 ppm for each proton, indicating the aromaticity of the tail group in (L<sup>1</sup>Ph) has little or no electronic effects on the head group. Table 28 lists the pyridyl and aldimine proton shifts of all Co<sup>II</sup> complexes obtained. There is a clear difference in shift for complexes obtained in D<sub>2</sub>O as opposed to CD<sub>3</sub>OD. Spectra obtained in CD<sub>3</sub>OD have shifts over 50 ppm downfield than those obtained in D<sub>2</sub>O for the aldimine and *m*-pyridyl protons. This solvent effect is more than likely due to solvolysis at the metal centre, or at least hydrolysis is certainly likely to be occurring in D<sub>2</sub>O. In CD<sub>3</sub>OD there is the possibility that the original anionic ligands are retained and the spectrum observed is that of the original complex. The fact that the complexes are soluble in D<sub>2</sub>O is a good indicator that the chloride ligand dissociates. Conductivity measurements would have been ideal in this instance to identify whether

the solvolysis gives the 1:1 or 1:2 electrolytes  $[\text{CoX}(\text{Sol})(\text{L}^1\text{Cy})]^+ \text{X}^-$  and  $[\text{Co}(\text{Sol})_2(\text{L}^1\text{Cy})]^{2+} 2\text{X}^-$  respectively, in either case 2-fold symmetry is retained.

After obtaining the proton spectrum from *Ca.* 5 mins after sample preparation and monitoring after leaving the sample at ambient lab temperature for several minutes, hours and days no significant change occurred indicating the solvolysis process is fast and complete at time of mixing, the same was also observed in  $\text{CD}_3\text{OD}$ .

A further possibility is that the complexes could have undergone metathesis to the 2:1 complexes forming  $[\text{Co}(\text{L}^1\text{R})_2][\text{CoX}_4]^{2-}$  species and hence why almost identical shifts are observed for the ligands. But after inspection of the  $\text{D}_2\text{O}$  solvated ligand shifts, it is apparent that the only significant shift difference between complexes was between the bis complex  $[\text{Co}(\text{L}^1\text{Cy})_2][\text{BF}_4]_2$  when all its analogues  $[\text{CoX}_2(\text{L}^1\text{Cy})]$  (all obtained in  $\text{D}_2\text{O}$ ), had identical shifts. This indeed indicates that the mono ligated complex is still present for those complexes of ligands with greater co-ordinating power.

**Table 28.** Pyridyl and aldimine proton shifts (in ppm) for various Co<sup>II</sup> complexes of ligand L<sup>1</sup>. Proton NMR obtained in, a CD<sub>3</sub>OD, b D<sub>2</sub>O.

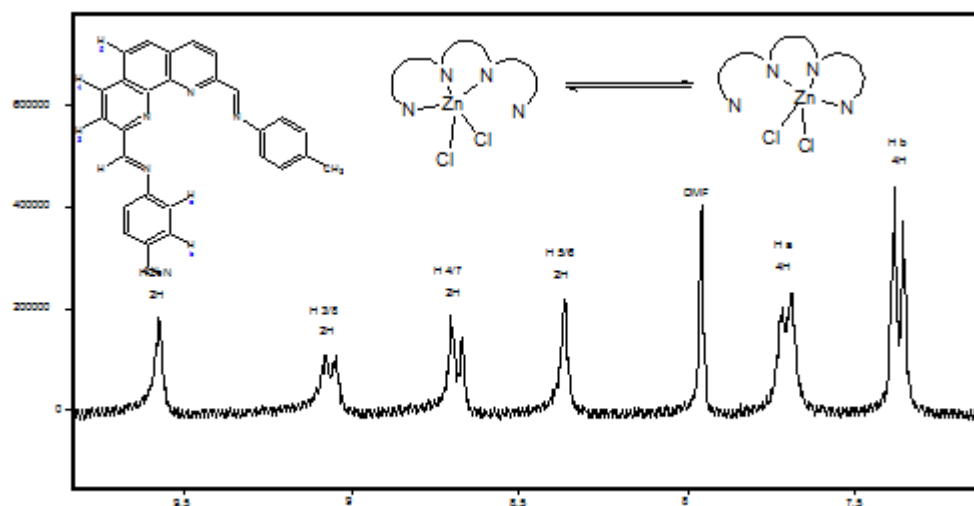


Complex	H <sup>2'/6'</sup>	H <sup>3/5</sup>	H <sup>4</sup>
[CoCl <sub>2</sub> (L <sup>1</sup> Pr <sup>n</sup> )] <sup>a</sup>	220	105	43
[CoCl <sub>2</sub> (L <sup>1</sup> Pr <sup>t</sup> )] <sup>a</sup>	203	98	41
[CoCl <sub>2</sub> (L <sup>1</sup> Bu <sup>n</sup> )] <sup>a</sup>	198	93	41
[CoCl <sub>2</sub> (L <sup>1</sup> Bu <sup>2</sup> )] <sup>a</sup>	221	103	43
[CoCl <sub>2</sub> (L <sup>1</sup> Bu <sup>i</sup> )] <sup>a</sup>	222	103	43
[CoCl <sub>2</sub> (L <sup>1</sup> Bu <sup>t</sup> )] <sup>a</sup>	221	103	42
[CoCl <sub>2</sub> (L <sup>1</sup> Cy)] <sup>b</sup>	168	50	25
[CoBr <sub>2</sub> (L <sup>1</sup> Cy)] <sup>b</sup>	168	50	25
[Co(AcO) <sub>2</sub> (L <sup>1</sup> Cy)]	168	50	26
[Co(L <sup>1</sup> Cy) <sub>2</sub> ][BF <sub>4</sub> ] <sub>2</sub> <sup>b</sup>	172	54	26
[CoCl <sub>2</sub> (L <sup>1</sup> Ph)] <sup>b</sup>	166	48	26

### 5.2.5. NMR Spectra of Zinc Complexes of Bipyridine L<sup>2</sup> and Phenanthroline L<sup>3</sup>

NMR spectra of both Bipyridine and Phenanthroline ligands show 2-fold symmetry of the ligand and this is also carried forward into the complexed ligand, which suggests that the ligand is acting in a tetradentate fashion (Typical spectrum of ligand given in Figure 44).

**Figure 44.** Proton NMR spectrum of  $[\text{ZnCl}_2(\text{L}^3\text{PhMe})]$  obtained in  $(\text{CD}_3)_2\text{SO}$  at  $60^\circ\text{C}$ .

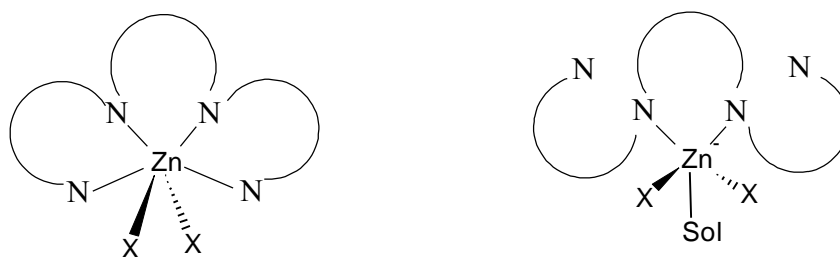


This however is contradicted by the single crystal data, where these complexes exhibit tridentate co-ordination in the solid state (exception of  $[\text{Zn}(\text{NO}_3)(\text{H}_2\text{O})(\text{L}^2\text{PhMe})][\text{NO}_3]$  where tetradentate is observed). It is suggested however that in solution these complexes are actually tridentate and a fluxional process between the two Schiff base co-ordinating sites is actually occurring, whereby the co-ordinating sites are exchanging and the rate of this exchange is too fast to be observed on the NMR timescale. More exactly, for separate resonances to be observed corresponding to the two sites in

equilibrium, the rate of exchange between sites must be less than  $2\pi\Delta\nu$ , where  $\Delta\nu$  is the difference between resonances of exchanging sites.

Variable temperature experiments were carried out to identify if this was indeed the case and to determine the Gibbs free energy of activation for the exchange. Proton NMR spectra of the complex  $[\text{ZnCl}_2(\text{L}^3\text{PhMe})]$  made to dissolve to  $\sim 1\text{ mg ml}^{-1}$  in a mixed deuterated solvent system of  $\text{CD}_3\text{CN}:\text{CD}_3\text{OD}:(\text{CD}_3)_2\text{CO}$  of 3:2:1 were thus collected. Spectra were obtained from  $25^\circ\text{C}$  where 2-fold symmetry and fine structure was observed and spectra were collected every  $10^\circ\text{C}$  increment to  $-65^\circ$ . Strangely no coalescence was observed and slight peak broadening at lower temperatures was attributed to increasing viscosity of the solution. It is difficult to understand what is exactly happening in the system for no coalescence to occur at  $-65^\circ\text{C}$ , the possibility that the energy barrier to interconversion is so low is difficult to believe when similar fluxional processes where slow exchange can be resolved at temperatures as high as  $-10^\circ\text{C}$  have been demonstrated for terpyridine complexes of  $\text{Pt}^{\text{II}}$  and  $\text{Ru}^{\text{II}}$ .<sup>173</sup> Whether in the particular solution under study a symmetrical coordination mode was at play is a possibility since the crystals for the tridentate crystal structure were obtained by recrystallisation from DMF. It is possible therefore that acetonitrile may compete with the imine N-donors of the ligand as shown in Figure 45 below.

**Figure 45.** Competition between solvent and imine donors for coordination sites.





## 6. X-Ray Structural Studies of Metal Complexes

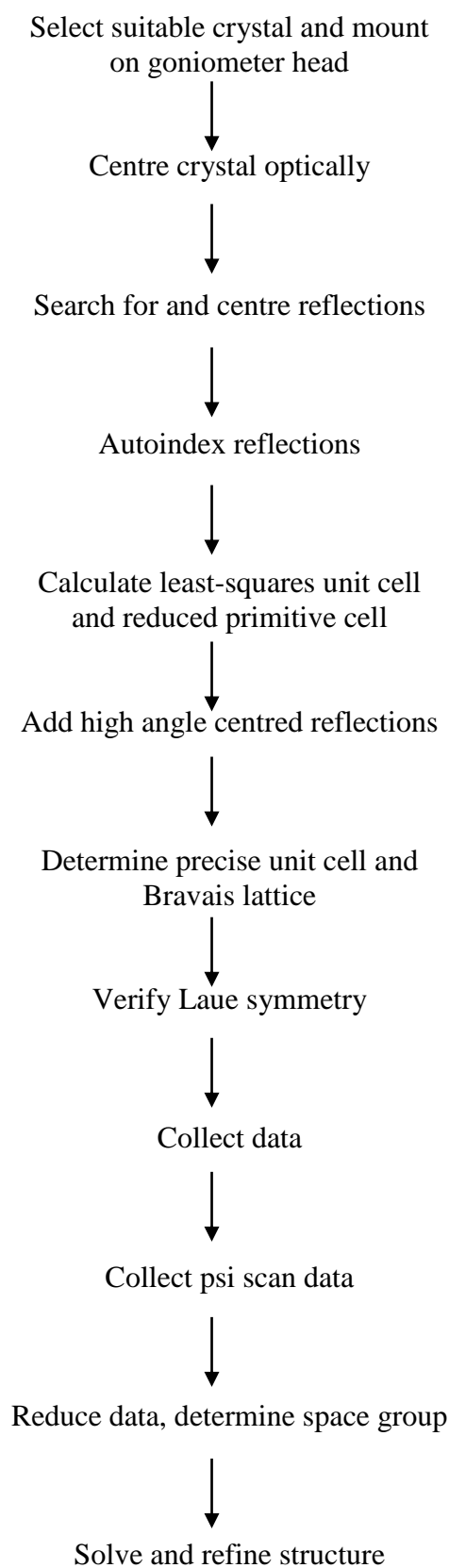
This section details the experimental description of the X-ray structure determination carried out for this study. Overall 35 crystal structures from this study were obtained, however it is beyond the scope of this thesis to list and report on every structure determined, instead an example of how the crystal structure of  $[\text{Cu}(\text{NO}_3)_2(\text{L}^1\text{Pr}^n)]$  was solved and refined is given followed by structure reports on a selection of the most interesting compounds. Details of data collection and refinement parameters for structures reported are given in following tables. Structure solution and refinement were performed using the SHELX-97<sup>174</sup> suite of programmes operating with WinGX.<sup>175</sup> All diagrams were generated using Mercury viewer.<sup>176</sup>

### 6.1. Data Collection

X-ray data collection was carried out by standard methods for all compounds reported. Intensity measurements were collected on either a Stoe STADI-4 four circle diffractometer with single point detector or a Bruker Apex X8 with area detection using the Bruker smart software package.<sup>177</sup> A crystal with maximum dimensions of 0.5 mm was selected and attached to a quartz fibre with epoxy resin or for air sensitive compounds the crystals were mounted under oil and frozen solid under a stream of nitrogen at -170°C. The crystal was then mounted in the goniometer head of the diffractometer and centred. After the crystal had been centred the four circles were incrementally driven by the computer until 15 reflections [ $I > 3\sigma(I)$ ] were detected. From the position of these reflections, unit cell geometry and orientation with respect to the diffractometer geometry was determined by computer software. The resulting UB-matrix gives four angles required to orient the crystal in the position necessary to

measure reflections from a particular set of planes ( $hkl$ ) in the crystal. For each  $hkl$  the  $\omega$  and  $2\theta$  circles synchronously scanned the diffracted beam with a suitable scan width (typically  $1^\circ$ ) and the total counts,  $I_t$ , for the scan were recorded together with background counts at the beginning and end of the scan. To refine the matrix (and cell parameters) a set of reflections were selected that were well separated in reciprocal space (typically with high indices in  $h, k, l, h+k, h+l$  or  $k+l$ ) and their Laue symmetry equivalents added. The resulting set of reflections was centred to determine the precise orientation matrix (and unit cell). Prior to data collection, reference reflections in the  $\theta$ -range  $3-5^\circ$  were chosen, typically 3 with high indices in  $h, k$  or  $l$  and then data collection was started. After data collection a precise determination of the unit cell was obtained from recording the set of high angle reflections at  $\pm\theta$  and where appropriate a set of reflections for  $\chi$ -scan were collected (generally  $\chi$  close to  $90^\circ$ ).

**Figure 46.** Flow diagram showing a typical experiment in determining a crystal structure.



## 6.2. Structure Solution and Refinement for [Cu(NO<sub>3</sub>)<sub>2</sub>(L<sup>1</sup>Pr<sup>n</sup>)]

Single turquoise/green crystals of [Cu(NO<sub>3</sub>)<sub>2</sub>(L<sup>1</sup>Pr<sup>n</sup>)] were grown by slow vapour diffusion of diethyl ether into a saturated acetonitrile solution of the named compound. The crystals were mounted on a glass fibre and X-ray intensity data was collected on a Bruker apex X8 diffractometer using graphite monochromated Mo-K $\alpha$  radiation at 273K. Preliminary inspection of the data set established no intensity relationship other than,  $I_{hkl} \equiv I_{-h-k-l}$ , indicating a triclinic crystal system and the assignment is consistent with the unit cell dimension  $a \neq b \neq c$  and  $\alpha \neq \beta \neq \gamma$ .

The density calculation indicated a density of 1.50 g cm<sup>-3</sup> for four molecules in the unit cell using the proposed formula and hence the space group was assigned *P-1* in the subsequent analysis. Data was corrected for absorption using a semi-empirical method based on  $\chi^2$ .

The structure was solved using Patterson syntheses and the resulting fourier map gave rise to two copper atoms in the asu, along with 6 O atoms automatically labelled by the software.

**Figure 47.** Initial fourier map from Patterson syntheses of diffraction data with two independent Cu complexes apparent and N atoms modelled in the asu.



Since it was plausible that the software had incorrectly assigned the O atoms, these were remodelled as nitrogen atoms since it looked like they could have been the N donor set of the terdentate ligands. This new model (Figure 47) was used to generate the difference fourier synthesis of the data (Figure 48), giving rise to a calculation of a difference fourier map  $R_1$  of 0.3583. Clearly from the resulting fourrier map the appearance of new Q peaks identified that some of the N atoms labelled in the previous model were indeed wrong and one in each independent molecule were relabelled as O atoms of co-ordinated nitrate ligands (Figure 49).

**Figure 48.** Fourier map after 1<sup>st</sup> refinement of diffraction data identifying incorrect assignment of two N atoms and revealing further atoms.

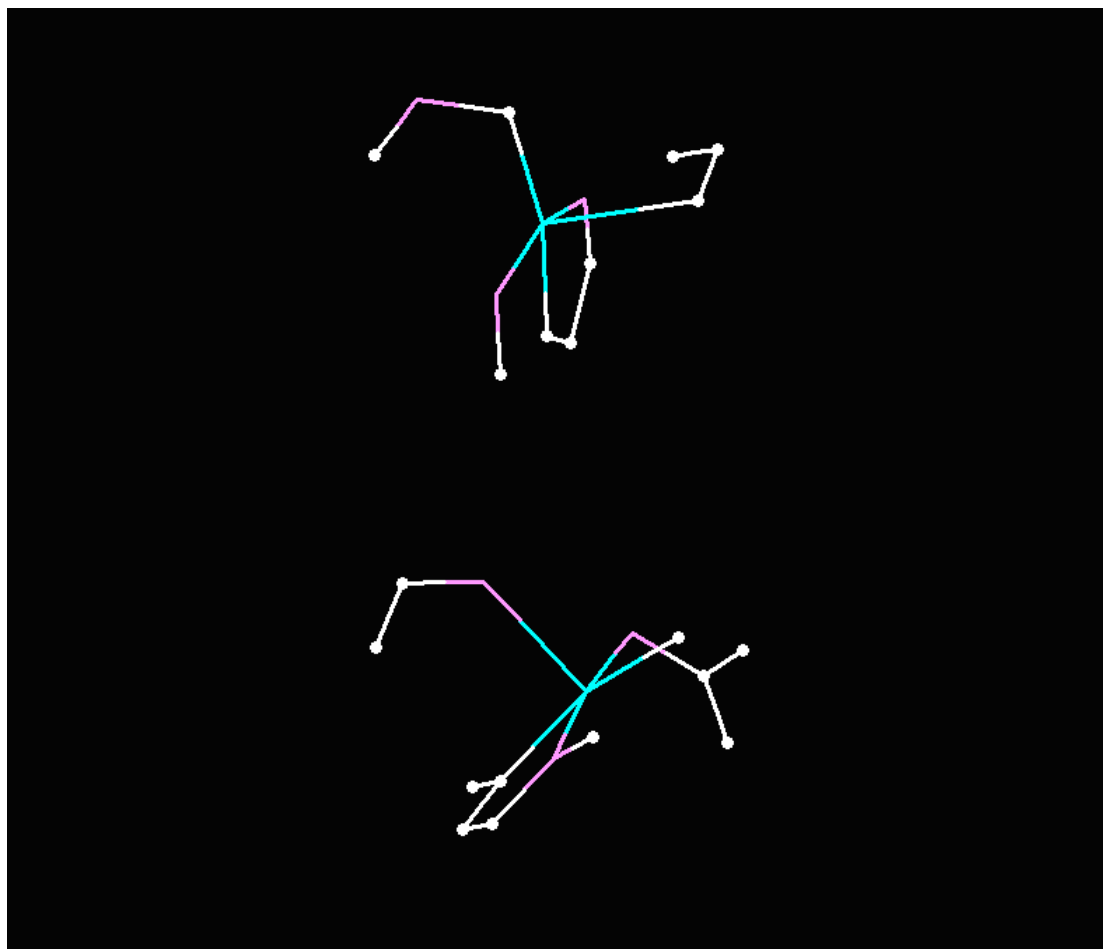
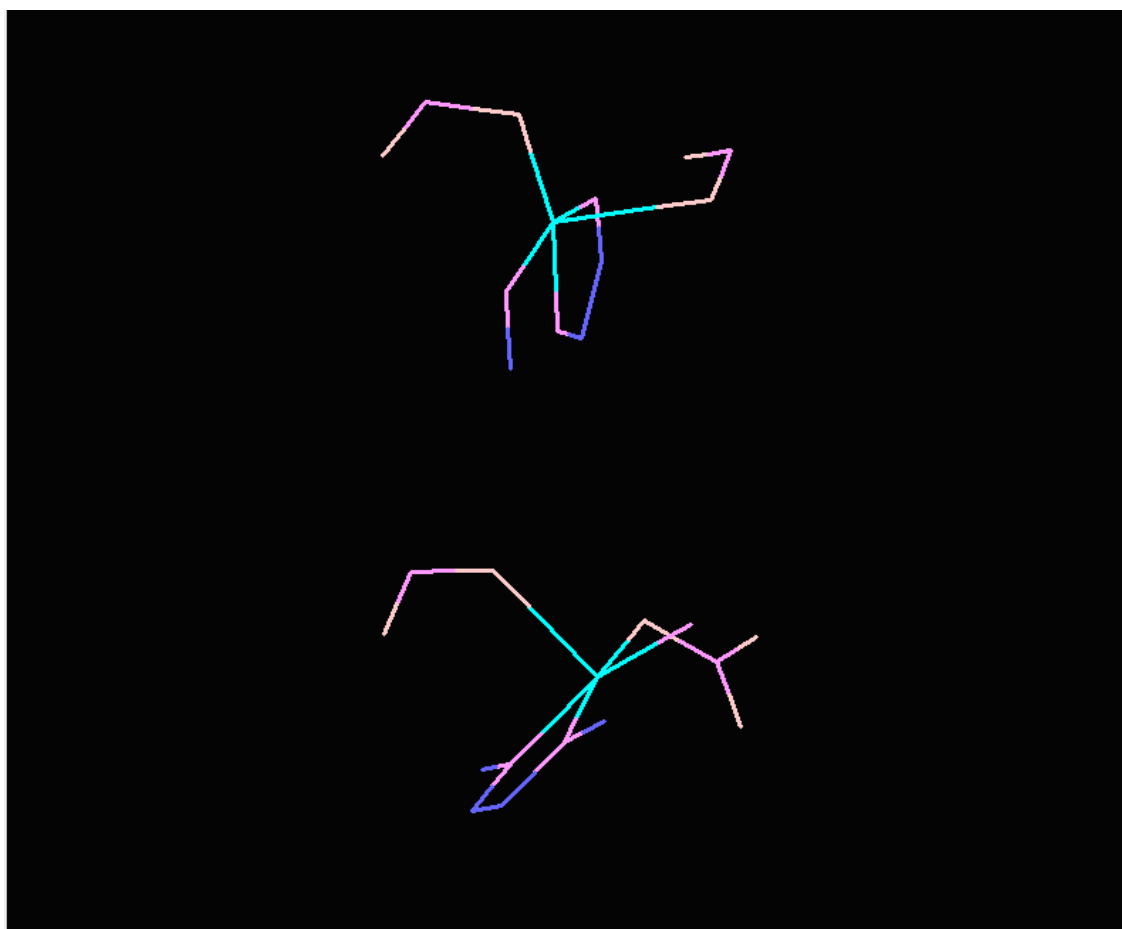
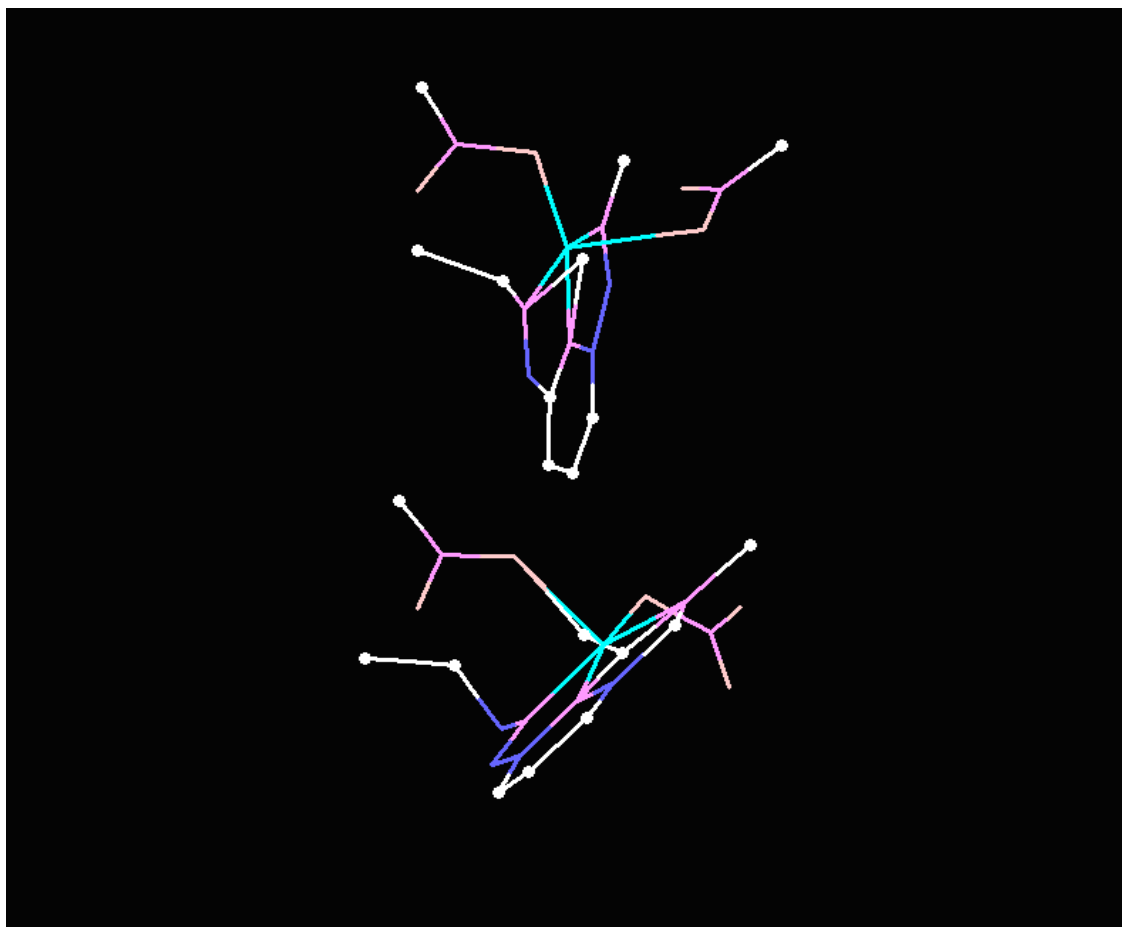


**Figure 49.** Model generated after 1<sup>st</sup> refinement cycle with partial assignment of nitrate and pyridyl head groups.



Other non hydrogen atoms identifiable as parts of the nitrate moiety and L<sup>1</sup>Pr<sup>n</sup> ligand were added to the new model and again a difference fourier synthesis was generated (Figure 50) and  $R_1$  reduced to 0.2406. In the resulting map the remainder of the non-hydrogen atoms of the pyridyl ligand head group were identified along with the remainder of the nitrate ligand atoms. Some carbon atoms of the tail groups could also be observed and were subsequently modelled.

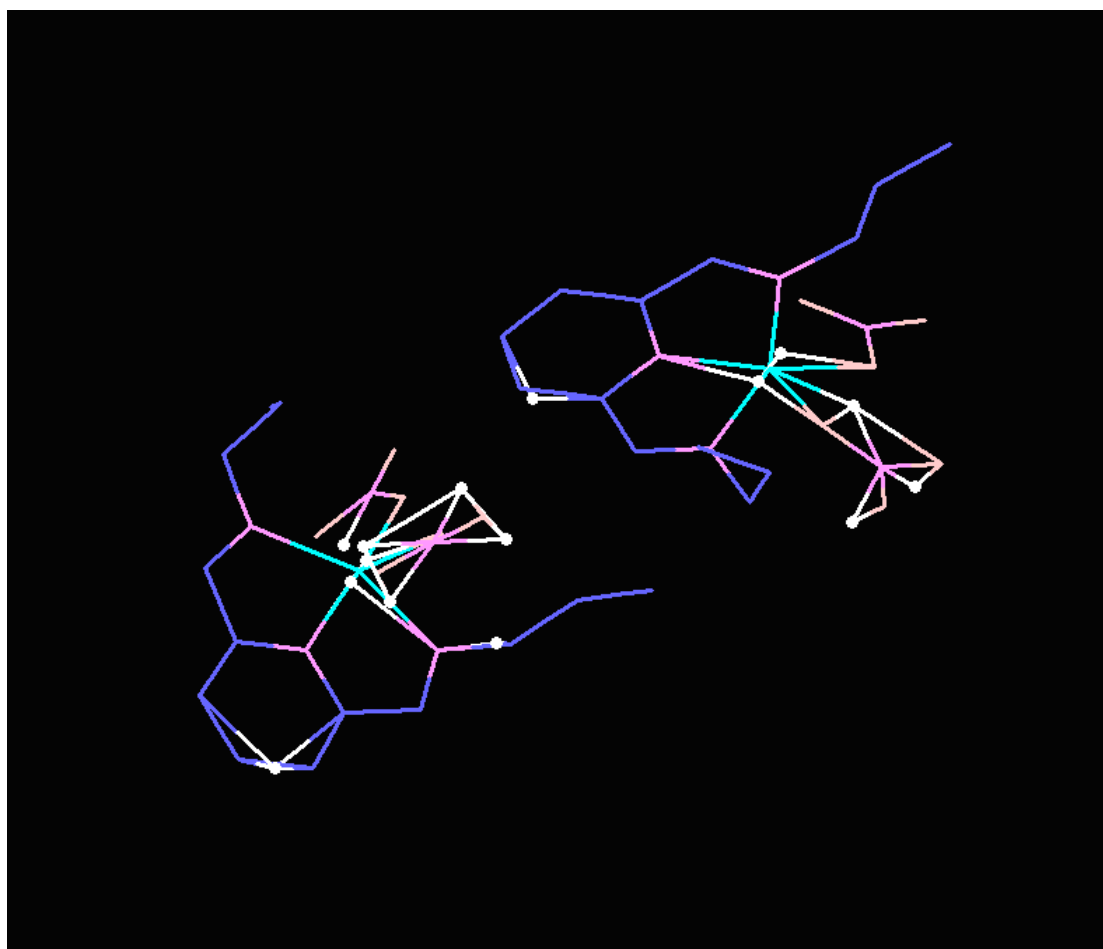
**Figure 50.** Fourier map after 2<sup>nd</sup> refinement of diffraction data identifying remainder of nitrate ligands and pyridyl head groups.



In the difference fourier synthesis of the model,  $R_1$  reduced further to 0.1339 and the remainder of non-hydrogen atoms of the ligand tail groups were identifiable and subsequently modelled. The largest peaks that remained ( $>1 \text{ e}\text{\AA}^{-3}$ ) were centred very close to the Cu atoms, these were subsequently identified as diffraction ripples and ignored (Figure 51).



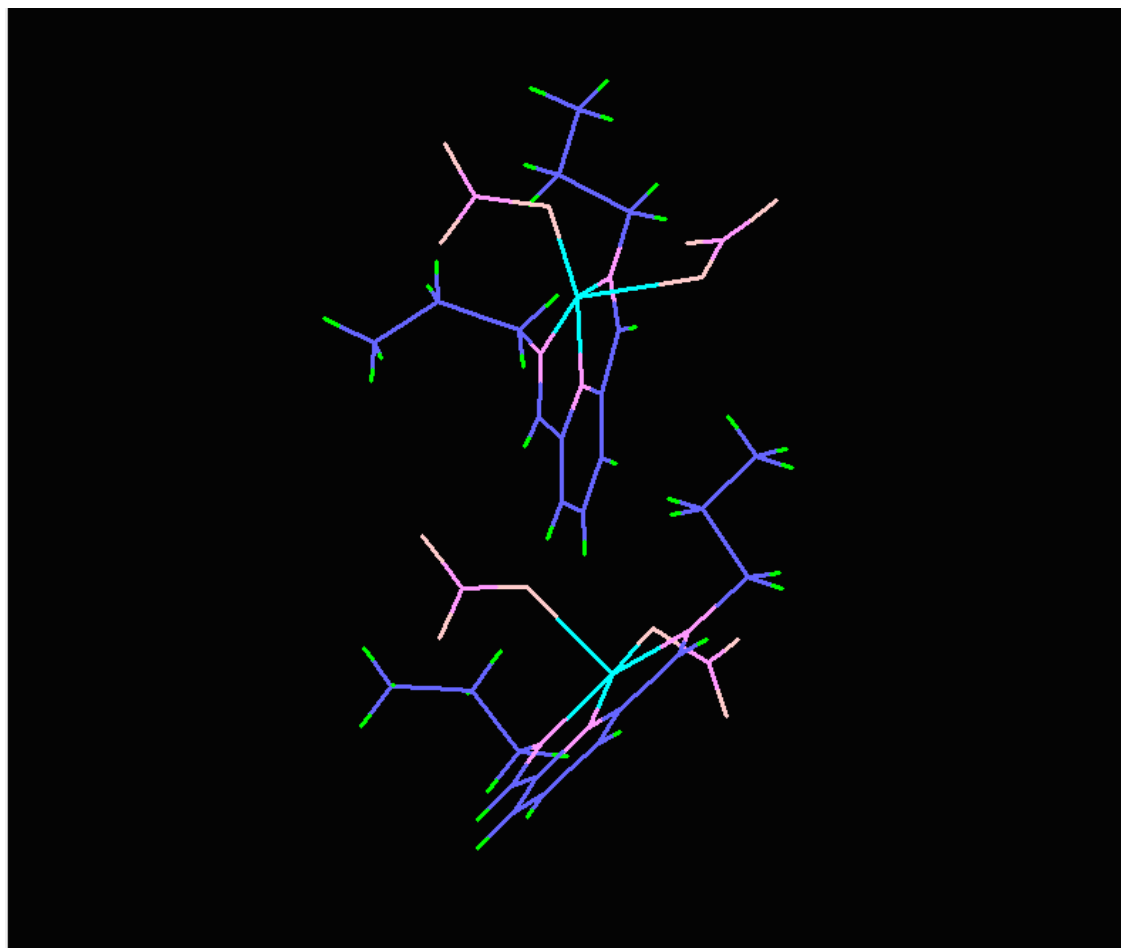
**Figure 51.** Fourier map after 3<sup>rd</sup> refinement of diffraction data identifying remainder of tail groups and Q peaks located next to the metal centre due to diffraction ripples .



The resulting e-map gave  $R_1$  to be 0.0966. All non-hydrogen atoms were further refined by setting anisotropic displacement parameters and a weighting scheme  $w^{-1} = \sigma^2 F_o^2 + (0.0488 P)^2 + 0.000 P$  where  $P = [(\max F_o^2, 0) + 2F_c^2]/3$  was applied. A further least squares cycle gave  $R_1$  to be 0.0467. In the subsequent e-map all hydrogen atoms of the ligand were fixed in idealised positions, riding on the position of the parent carbon. Isotropic displacement parameters for all but methyl hydrogens were fixed as  $1.2 U_{eq}$  of the parent carbon atom,  $U_{iso}$  for methyl hydrogens was  $1.5 U_{eq}$  after a final least squares cycle refinement converged at  $R_1$  0.0361 [ $I \geq 3\sigma(I)$ ] and  $wR^2 = 0.1007$  (all data), mean

$\Delta/\sigma = 0.0000$ ,  $\max \Delta/\sigma = 0.0000$ . The final map contained no features above  $1 \text{ e}\text{\AA}^{-3}$ . The final model is given in Figure 52.

**Figure 52.** Final fourier map after final least squares cycle with Q peaks omitted.



### 6.3. Structural Descriptions and Comparisons

#### 6.3.1. $\text{Cu}^{\text{II}}$ Complexes of $\text{L}^1\text{R}$

In all 10 crystal structures of copper(II)diacido complexes were solved in this study of them 5 of the structures are reported. Details of data collection and refinement parameters for structures reported are given in Table 29. On initial inspection of complexes of  $[\text{MX}_2(\text{L}^1\text{Pr}^n)]$  it is clear that both halide complexes are isomorphous both

crystallising in the monoclinic crystal system with similar unit cell dimensions and the same space group  $C2/c$ . The nitrate complex crystallised in a triclinic- $P$  lattice. The complexes  $[\text{CuCl}_2(\text{L}^1\text{PhMe})]$  and  $[\text{CuCl}_2(\text{L}^1\text{PhCl})]$  are essentially isomorphous, both crystallise orthorhombic  $Fdd2$  space group with very similar unit cell dimensions.

All five copper complexes show a 5-coordinate geometry about the metal centre with all of the nitrogen donors of the the  $\text{L}^1\text{R}$  ligands binding in a terdentate mode. The overall molecular symmetry of the complexes appears to depend on the nature of the ‘tail’ groups: all complexes with alkyl tail groups show molecular  $C_s$  symmetry whereas those with aromatic tails show two-fold symmetry around an axis incorporating metal, pyridyl nitrogen and the  $\gamma$ -CH unit of the pyridyl ring and hence are assigned to the  $C_2$  point group (Figure 53).

**Figure 53.** The molecular symmetry of  $[\text{CuX}_2(\text{L}^1\text{R})]$  complexes: (a) the  $C_s$  symmetry of the alkyl-substituted ligands illustrated with  $[\text{CuCl}_2(\text{L}^1\text{Pr}^n)]$ ; (b) the  $C_2$  symmetry of the aryl-substituted ligands illustrated with  $[\text{CuCl}_2(\text{L}^1\text{PhCl})]$ .

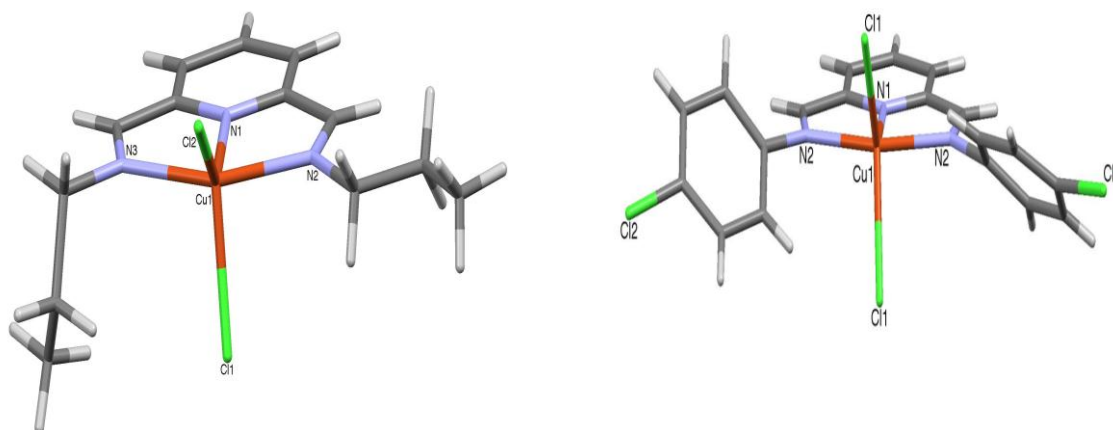
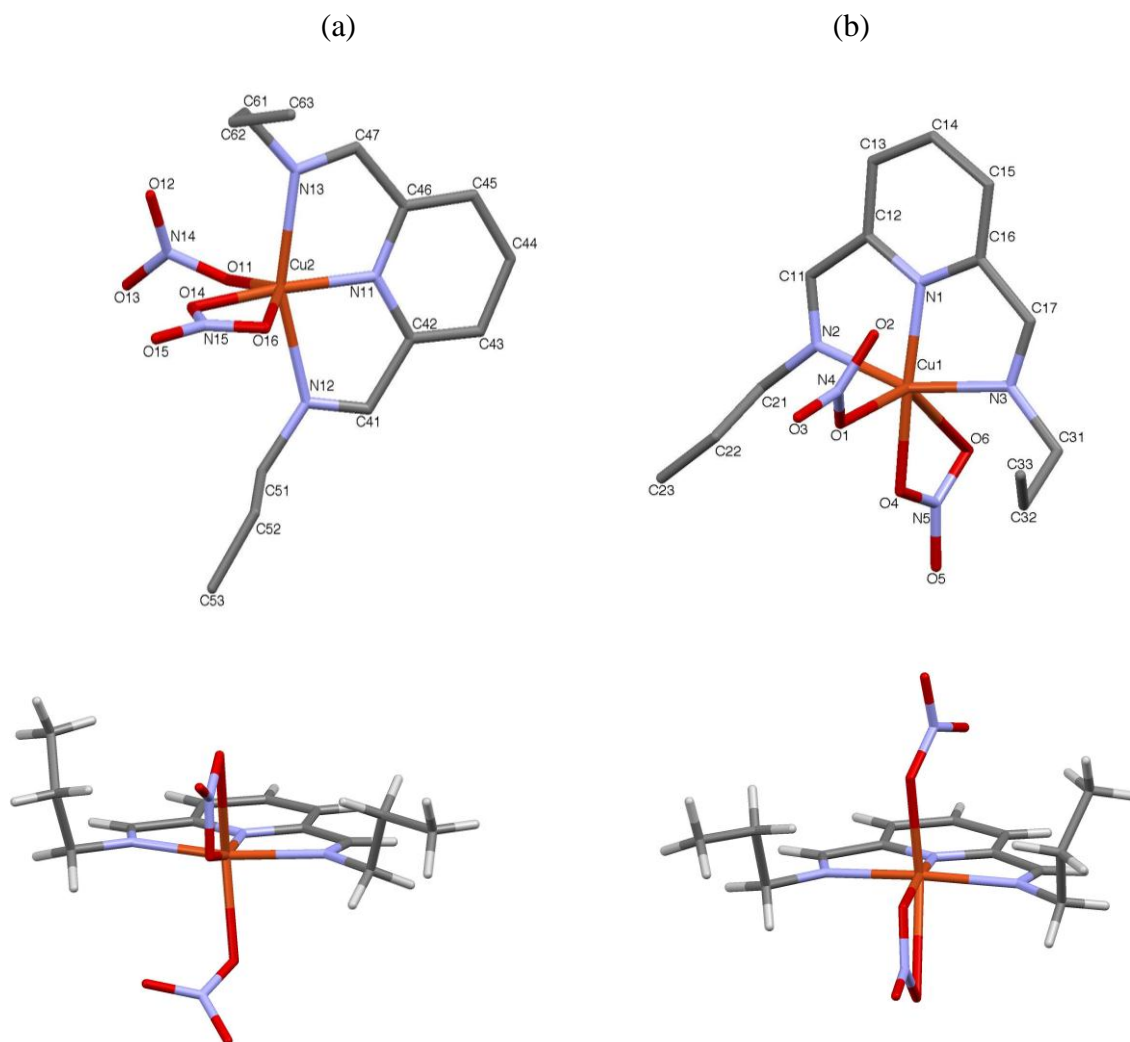


**Table 29.** X-ray structure and refinement parameters for complexes of [CuX<sub>2</sub>(L<sup>1</sup>R)]

Compound	[CuCl <sub>2</sub> (L <sup>1</sup> Pr <sup>n</sup> )]	[CuBr <sub>2</sub> (L <sup>1</sup> Pr <sup>n</sup> )]	[Cu(NO <sub>3</sub> ) <sub>2</sub> (L <sup>1</sup> Pr <sup>n</sup> )]	[CuCl <sub>2</sub> (L <sup>1</sup> PhMe)]	[CuCl <sub>2</sub> (L <sup>1</sup> PhCl)]
Chemical Formula	C <sub>13</sub> H <sub>19</sub> Cl <sub>2</sub> CuN <sub>3</sub>	C <sub>13</sub> H <sub>19</sub> Br <sub>2</sub> CuN <sub>3</sub>	C <sub>13</sub> H <sub>19</sub> CuN <sub>5</sub> O <sub>6</sub>	C <sub>21</sub> H <sub>19</sub> Cl <sub>2</sub> CuN <sub>3</sub>	C <sub>19</sub> H <sub>13</sub> Cl <sub>4</sub> CuN <sub>3</sub>
Formula Weight	351.75	440.67	404.87	447.83	488.66
Crystal System	Monoclinic	Monoclinic	Triclinic	Orthorhombic	Orthorhombic
Space Group	<i>C2/c</i>	<i>C2/c</i>	<i>P-1</i>	<i>Fdd2</i>	<i>Fdd2</i>
<i>a</i> / Å	17.405 (4)	17.8714 (3)	9.1643 (7)	11.6251 (17)	11.811 (2)
<i>b</i> / Å	12.839 (3)	12.9305 (2)	14.3273 (10)	35.662 (5)	35.080 (6)
<i>c</i> / Å	14.900 (3)	15.0986 (2)	14.6679 (11)	9.3523 (12)	9.3386 (15)
<i>α</i> / °	90	90	109.090 (4)	90	90
<i>β</i> / °	110.11 (3)	110.3380 (10)	92.799 (4)	90	90
<i>γ</i> / °	90	90	98.544 (4)	90	90
<i>V</i> / Å <sup>3</sup>	3126.6 (11)	3271.56 (9)	1790.0 (2)	3877.2 (9)	3869.4 (12)
<i>T</i> / K	293 (2)	273 (2)	273 (2)	273 (2)	273 (2)
<i>Z</i>	8	8	4	8	8
<i>S</i>	0.98	0.94	0.83	1.08	0.91
No. unique data ( <i>R</i> <sub>int</sub> )	2744	7217	12259	5717	5010
No. measured reflections	3381	31117	63213	32142	39665
<i>R</i> <sub>obs</sub> / <i>wR</i> ( <i>F</i> <sup>2</sup> ) <sub>obs</sub>	0.031/0.073	0.055/0.130	0.035/0.087	0.049/0.110	0.054/0.136

For the nitrate complex, two crystallographically independent molecules (shown as *a* and *b* in Table 29 and diagrammatically in Figure 54 form the asymmetric unit. Each copper centre is coordinated to the Schiff-base ligand in an endodentate N<sub>3</sub> mode with the coordination sphere completed by monodentate and pseudo-bidentate nitrate ligands. The two complexes differ by the relative arrangements of the nitrate ligands with respect to the ligand 'tails'. The tails are aligned on one side of the N<sub>3</sub> plane of the ligand and the coordinated nitrates on this side of the complex occupy a 'cleft' formed by the alky chains. In one complex this cleft is occupied by a pseudo-bidentate nitrate (labelled molecule, *a*), in the second, by a monodentate nitrate (*b*).

**Figure 54.** (a) Asymmetric unit of  $[\text{Cu}(\text{NO}_3)_2(\text{L}^{\text{IPr}''})]$  showing the structure of two independent molecules (hydrogen atoms omitted for clarity). (b) Comparison of the structures of the two molecules in the asymmetric unit (*a* left; *b* right).



As might be expected, these two arrangements influence the dimensions of the metal coordination spheres. Metal-oxygen interactions in the pseudo-bidentate nitrates are highly asymmetric and the longer M-O distances are in excess of 2.5 Å. Therefore geometry about the  $\text{Cu}^{\text{II}}$  centre for both independent molecules can be best described as distorted square pyramidal with oxygens of the monodentate nitrates [ $\text{X}(1) \equiv \text{O}(1)$  and  $\text{O}(11)$ ] occupying the apical positions. The distortion to the square-pyramidal geometry

is illustrated by angles N(1)-Cu-X(1) of 103.84(6) and 102.62(7) compared to 90° for ideal square based pyramid. The interplay between the regular 5-coordinate geometries can be evaluated with the  $\tau$ -parameter introduced by Reedijk and co-workers.<sup>178</sup> In this context, the parameter is given by  $\tau = (\beta - \alpha)/60$  [ $\alpha$  = smallest angle between N(2)-Cu-N(3) and N(1)-Cu-X(2) and  $\beta$  = largest angle between N(2)-Cu-N(3) and N(1)-Cu-X(2)]. This gives the values 0.24 and 0.16 for the independent molecules, *a* and *b* respectively. Since  $\tau$  is a parameter used as an index of the degree of trigonality,<sup>178</sup> these values support a square pyramidal geometry ( $\tau$  close to zero) and are in agreement with a structure closer to the perfect square pyramidal ( $\tau = 0$ ) than trigonal bipyramidal ( $\tau = 1$ ). Clearly there is a large difference in  $\tau$  between the two independent molecules in the asymmetric unit, which can also be further demonstrated by comparing the X(1)-Cu-X(2) bond angles. These show a relatively large difference: 85.00(6) vs. 90.14(6)° for *a* and *b* respectively. The equatorial positions of the complex are occupied by the three nitrogen donors of the ligand and X(2)  $\equiv$  O(4) and O(14) with N(1)-Cu-X(2) angles of 171.00 (6) and 167.05 (6)° for *a* and *b* respectively (180° for an ideal square pyramidal basal plane). The Cu-X bonds are noticeably asymmetric with that to the apical bond being significantly longer [av 2.2266 (15) Å] than that to its basal counterpart [av 1.9496 (14) Å].

It could be argued also that the complex is in fact distorted octahedral with the equatorially bound nitrate group offering a bidentate geometry and a second donor in an axial position with an average distance [av Cu-X(3) = 2.630 Å], (X(3)  $\equiv$  O(6) and O(16)). In this context, this asymmetry may be influenced by Jahn-Teller effects at the  $d^9$  Cu<sup>II</sup> centre.<sup>167</sup> Similar observations with regard to distorted octahedral M(NO<sub>3</sub>)<sub>2</sub> complexes have been reported where highly asymmetrical nitrate co-ordination for the

Cu<sup>II</sup> species have been made in the series of related trispyridine and 2,6-bis[1-(phenylimino)ethyl]pyridine, L, complexes [(py)<sub>3</sub>M(NO<sub>3</sub>)<sub>2</sub>] and [M(NO<sub>3</sub>)<sub>2</sub>L] where (M = Co<sup>II</sup>, Cu<sup>II</sup> and Zn<sup>II</sup>, <sup>179</sup>Ni<sup>II</sup> and Cd<sup>II</sup>, <sup>180</sup>) given in Table 30.

**Table 30.** Metal(II)–nitrate bidentate co-ordination in [M(NO<sub>3</sub>)<sub>2</sub>L] and [(py)<sub>3</sub>M(NO<sub>3</sub>)<sub>2</sub>] complexes and [Cu(NO<sub>3</sub>)<sub>2</sub>(L<sup>1</sup>Pr<sup>n</sup>)] for comparison. Δ = difference in M-O distance.

Metal Complex	M-O <sub>(eq)</sub> (Å)	M-O <sub>(ax)</sub> (Å)	Δ (Å)
[(Py) <sub>3</sub> Cd(NO <sub>3</sub> ) <sub>2</sub> ]	2.444 (9)	2.491 (10)	0.047
[Ni(NO <sub>3</sub> ) <sub>2</sub> L]	2.070 (4)	2.138 (5)	0.068
[(Py) <sub>3</sub> Co(NO <sub>3</sub> ) <sub>2</sub> ]	2.207 (9)	2.311 (9)	0.104
[(Py) <sub>3</sub> Zn(NO <sub>3</sub> ) <sub>2</sub> ]	2.232 (13)	2.418 (12)	0.186
[Cu(NO <sub>3</sub> ) <sub>2</sub> L]	1.968 (3)	2.533 (5)	0.565
[(Py) <sub>3</sub> Cu(NO <sub>3</sub> ) <sub>2</sub> ]	2.154 (7)	2.732 (9)	0.578
[Cu(NO <sub>3</sub> ) <sub>2</sub> (L <sup>1</sup> Pr <sup>n</sup> )]	1.9496 (14)	2.630	0.680

The structural identification of multiple bonding modes for the nitrate-ligands is consistent with the bulk sample analysis with infra-red spectroscopy which was also consistent with unidentate and bidentate co-ordination. Further support for the assignment of the apical nitrate anion as unidentate comes from close inspection of N-O bond lengths (Table 31). In ‘pure’ unidentate coordination a local C<sub>2</sub> rotational axis exists through the nitrate N(4)-O(1) bond (Figure 55). In the complex, the N-O(1) bond length is substantially longer than either N(4)-O(2) and N(4)-O(3). Importantly, the distances N(4)-O(2) and N(4)-O(3) are nearly identical (within error), consistent with delocalisation of the double bond about these two bonds. Clearly more single bond

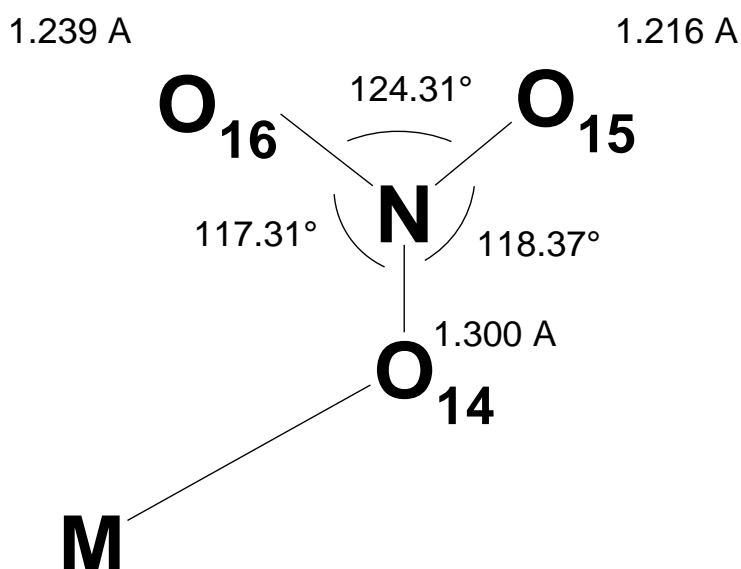


character is inferred at the bond N(4)-O(1) . These observations are mirrored in the second complex in the asymmetric unit.

**Table 31.** Nitrogen-oxygen bond lengths in the nitrato ligands of [Cu(NO<sub>3</sub>)<sub>2</sub>(L<sup>1</sup>Pr<sup>n</sup>)]

N4-O1	1.262(2)	N5-O4	1.294(2)
N4-O2	1.214(2)	N5-O5	1.219(2)
N4-O3	1.229(2)	N5-O6	1.234(2)
N14-O11	1.260(2)	N15-O14	1.300(2)
N14-O12	1.207(2)	N15-O15	1.216(2)
N14-O13	1.215(3)	N15-O16	1.239(2)

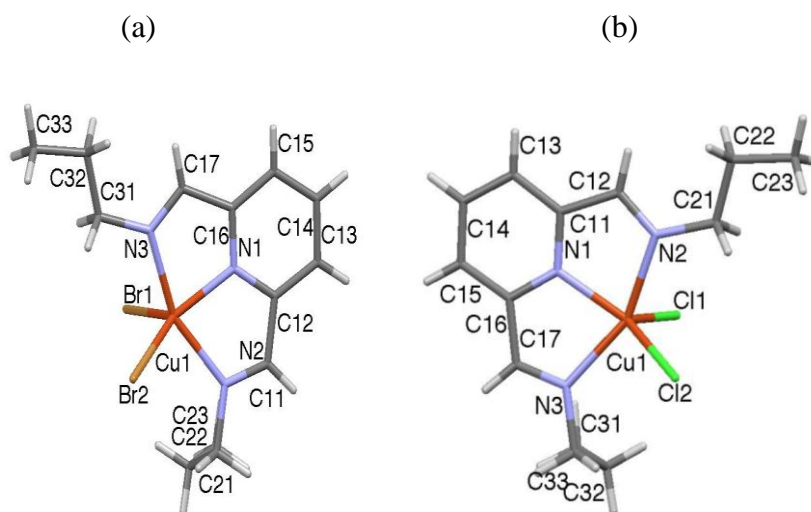
**Figure 55.** Geometrical parameters about the equatorial ligated nitrato ligand.



The complexes [CuCl<sub>2</sub>(L<sup>1</sup>Pr<sup>n</sup>)] and [CuBr<sub>2</sub>(L<sup>1</sup>Pr<sup>n</sup>)] are essentially isostructural apart from subtle differences in metal co-ordination geometries. The bond lengths and angles for the co-ordination sphere and other bonds are listed in Table 44 and Table 45 (see Appendix 11.2). The only significant differences lie in the M-X bonds and angles

involving the halogen atoms. The difference in radius of the two halogens results in significantly different metal halogen bonds. In each structure (Figure 56), the metal geometry can be best described as intermediate between distorted square based pyramidal and trigonal bipyramidal. This is confirmed by  $\tau$ -values<sup>178</sup> of 0.33 and 0.41 for the chloro and bromo complex respectively. If considering the structure to be distorted trigonal bipyramidal then the axial positions are occupied by two nitrogen atoms N(2) and N(3) [N(2)-M-N(3) = 155.45 (11)° and 155.77 (10)° for chloro and bromo complexes respectively]. The equatorial plane is made by the two halogen atoms and the atom N(1) of the pyridine fragment. The most noticeable difference between the coordination spheres of the two complexes is in the difference of the M-X bond lengths in the complex: for the bromo complex the difference is 0.0282 Å [M-X: 2.4333(4) Å and 2.4615 (5) Å], whereas the difference, at 0.0575 Å, is much larger in the chloro complex [M-X: 2.2839(9) and 2.3414 (10) Å]. This difference may originate in the relative donor strength of the ligands. This is exemplified in the spectrochemical series where Br<sup>-</sup> comes lower than Cl<sup>-</sup> in terms of its effect on increasing the energy of the LFSE.<sup>167</sup> Halogens contribute to a small ligand-field splitting parameter since they come low down in the spectrochemical series, but since Cl<sup>-</sup> is higher in the series than Br<sup>-</sup> it would contribute to an increase in the LFSE and result in a greater axial distortion.

**Figure 56.** X-ray crystal structures of isostructural complexes (a)  $[\text{CuBr}_2(\text{L}^1\text{Pr}^n)]$  and (b)  $[\text{CuCl}_2(\text{L}^1\text{Pr}^n)]$ .

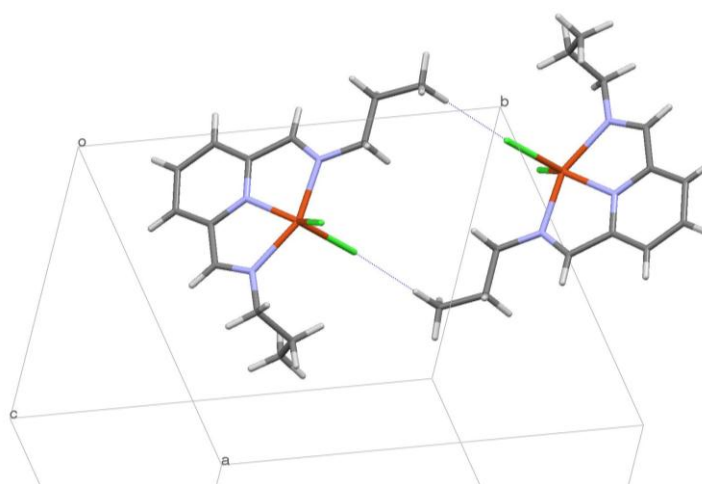


The packing in the crystal features offset face-to-face  $\pi$ - $\pi$  interactions between pyridyl head groups of adjacent complexes (Figure 57). The isomorphous nature of the structures results from similar crystal packing requirements – importantly the nature of the halide appears to exert little differential influence. However, there is evidence of close contact between the coordinated halides and adjacent C-H systems in the structures. The C-H...halogen interaction has been studied in some detail,<sup>181-184</sup> with chloride and bromide this is generally consistent with the halogen acting as a hydrogen bond acceptor with the strength of the interaction depending on the charge density of the halide. Two distinct CH...halide interactions are apparent: (i) halide...CH interactions to the aliphatic methyls of the n-propyl ‘tail’ unit and (ii) halide...CH interactions to the imine hydrogens. The aliphatic CH...X interactions lead to a centrosymmetric dimer motif based on short CH...X contacts (2.92 and 3.00 Å for  $\text{Cl}^-$  and  $\text{Br}^-$  respectively) and nearly linear C-H...X orientation (166.4 and 161.0° for  $\text{Cl}^-$  and  $\text{Br}^-$  respectively) (Figure 57 (b)). The imine CH...X interactions appear to support the face-to-face  $\pi$ - $\pi$  interactions between pyridyl head groups. In these, the halides interact with two imine

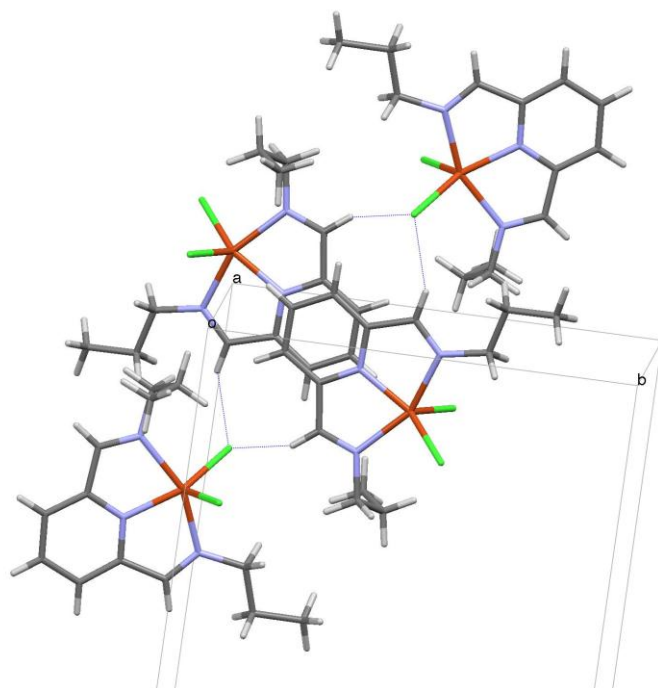
CH units and may be regarded as a bifurcated acceptor in the formation of a tetrameric assembly (Figure 57 (b)). Again, the assembly is based on relatively short CH...X distances (2.92 and 2.79 Å for Cl<sup>-</sup>; 2.98 and 2.86 Å for Br<sup>-</sup>) but the essentially parallel arrangement of opposing pyridyl units moves the C-H...X angles away from a linear arrangement (117.0 and 142.3° for Cl<sup>-</sup>; 129.5 and 142.6° for Br<sup>-</sup> respectively) consistent with the bifurcated nature of the interaction. Interestingly, the angles at the bifurcated halides are similar – 119.8° for Cl<sup>-</sup>, 120.1° for Br<sup>-</sup>.

**Figure 57.** The crystal packing in isostructural complexes [CuBr<sub>2</sub>(L<sup>1</sup>Pr<sup>n</sup>)] and [CuCl<sub>2</sub>(L<sup>1</sup>Pr<sup>n</sup>)] features three distinct motifs: (a) a centrosymmetric dimer from methyl CH...halide interactions; (b) a centrosymmetric tetramer from bifurcated halide... HC imine in conjunction with offset face-to-face  $\pi$ - $\pi$  interactions between pyridyl head groups of adjacent complexes; (c) the crystal packing of the complexes viewed down the *a*-axis of the unit cell.

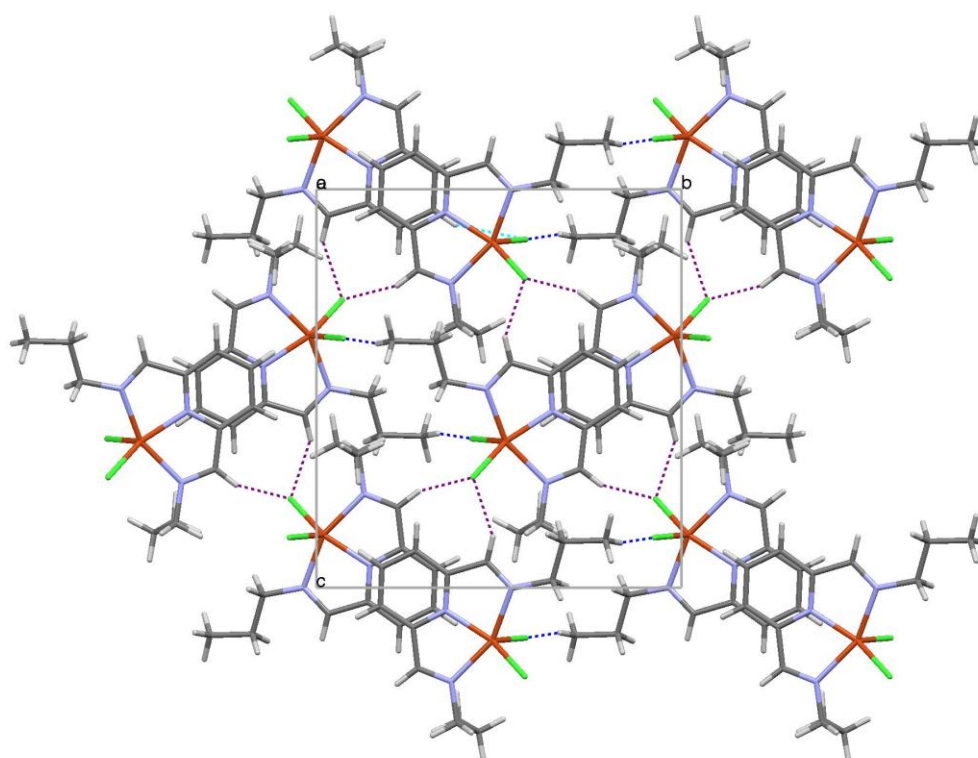
(a)



(b)



(c)

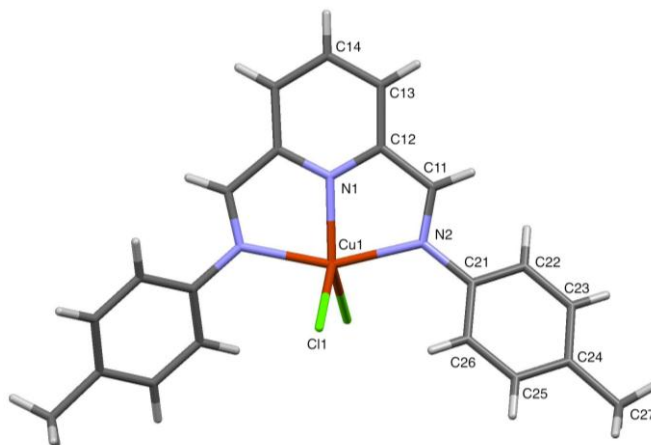


Copper complexes of  $L^1R$  where the substituent is an aromatic ‘tail’ group show contrasting structural chemistry to the alkyl analogues. Structures were obtained from

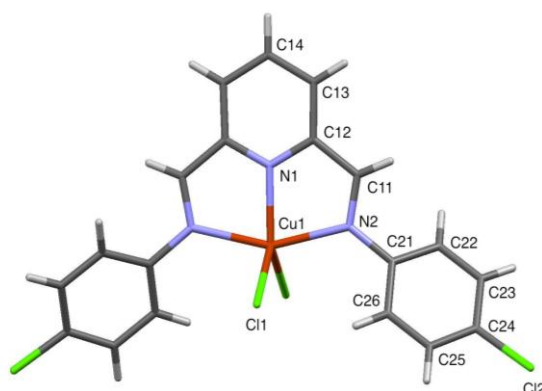
the complexes  $[\text{CuCl}_2(\text{L}^1\text{PhMe})]$  and  $[\text{CuCl}_2(\text{L}^1\text{PhCl})]$ . The complexes give rise to 2-fold symmetric chiral molecular structures that are essentially isostructural and isomorphous. Each crystallises in an orthorhombic unit cell containing 8 molecules and structures were successfully determined in the  $Fdd2$  space group (16 equivalent positions in the unit cell). The molecules have crystallographic 2-fold symmetry about an axis defined by the  $\gamma$ -CH and nitrogen atoms of the pyridyl ring, and the metal atom. In the setting for the asymmetric unit chosen, the remainder of the complex molecule is related by the symmetry operation  $-x+1, -y, z$ , consistent with the 2-fold axis parallel to the  $c$ -axis of the unit cell. In the complexes  $[\text{CuCl}_2(\text{L}^1\text{PhMe})]$  and  $[\text{CuCl}_2(\text{L}^1\text{PhCl})]$ , bond lengths and angles are very similar, apparently indicating negligible influence of the aromatic substituent on the complex. However, the respective roles of  $p$ -chloro and  $p$ -methyl groups in crystal packing interactions is worthy of detailed consideration as it might be expected that these may play a more significant role in determining the solid state structure.

**Figure 58.** X-ray crystal structures of isostructural complexes  $[\text{CuCl}_2(\text{L}^1\text{PhMe})]$  (a) and  $[\text{CuCl}_2(\text{L}^1\text{PhCl})]$  (b).

(a)



(b)



The geometry at the  $\text{Cu}^{\text{II}}$  centre of the two aromatic complexes tends more toward distorted trigonal bipyramidal which is given by  $\tau$  to be 0.51 and 0.50 for  $\text{L}^1\text{PhMe}$  and  $\text{L}^1\text{PhCl}$  complexes respectively. The two-fold rotational axis about M-N(1) imposes a trigonal equatorial plane, with bond angles [ $\text{av N}(1)\text{-M-X}(1) = 124.81^\circ$  and  $\text{av X}(1)\text{-M-X}(2) = 110.26^\circ$ ], these angles are much closer to the ideal trigonal angles of  $120^\circ$  than their related alkyl ‘tail’ group analogues. The fact that there is less distortion toward

square pyramidal in these two complexes indicates the ligand plays a big role in influencing the co-ordination geometry in this complex.

When comparing bond lengths and angles for all the Cu<sup>II</sup> complexes reported, there are a lot of similarities between structures but at the same time subtle differences are apparent. The main similarities between the complexes are the N-M-N angles and bond lengths which mainly arise due to constraints of the tridentate chelating ligand L<sup>1</sup>R. The metal salt and co-ordination has little influence on the bite angles [av N(1)-M-N(2)/N(3) = 77.77° for the halide complexes and 78.99° for the nitrate complex] however as insignificant as this 1° increase in the angle may seem, in reality it can be clearly explained when comparing the N-M bond lengths for the complexes. The slight increase in bite angle can be attributed to a contraction in bond length about the N(1)-M bond (average = 1.9252 Å for [Cu(NO<sub>3</sub>)<sub>2</sub>(L<sup>1</sup>Pr<sup>n</sup>)] compared to average 1.959 (2), 1.957 (2) for the chloro and bromo analogue of the same ligand), this is clearly a consequence of the anionic ligands attached. This ligand field effect is also likely at play in the complexes [CuCl<sub>2</sub>(L<sup>1</sup>PhMe)] and [CuCl<sub>2</sub>(L<sup>1</sup>PhCl)] where an elongation about the N(1)-M bond [av N(1)-M = 1.986 Å] is brought about likely as a consequence of the electron rich ligands, this in turn gives rise to an axial elongation [av M-N(2) = 2.123 Å]. In all cases of this study (and in all crystal structures of other metal salts of L<sup>1</sup>R), the N-M bond distances where N is from the pyridyl moiety are shorter than the N-M bond distance where N is a Schiff base donor.

For complexes containing alkyl 'tail' groups the imine C-N bond retains its double bond character with imine bond lengths in the range 1.255-1.275 Å comparable to standard imine bond lengths, (1,8-bis(imino)carbazolide, 1.273(3) Å)<sup>185</sup> however a longer bond



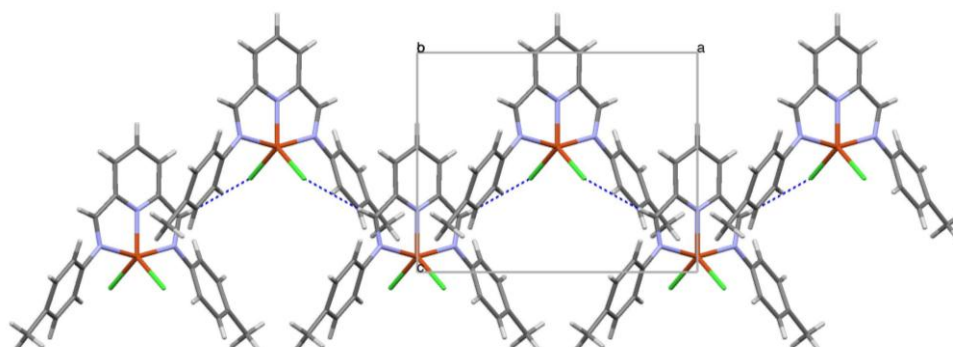
length of 1.300(3) Å is observed in the complex [CuCl<sub>2</sub>(L<sup>1</sup>PhCl)] indicating either delocalisation of the imine electrons into the ring of the tail group or purely via the inductive effect of the *p*-chloro aryl ‘tail’ group or a larger degree of Cu-π\* back bonding in this complex.

The crystal packing in the isomorphous crystals of [CuCl<sub>2</sub>(L<sup>1</sup>PhCl)] and [CuCl<sub>2</sub>(L<sup>1</sup>PhMe)] is significantly different to the alkyl analogues. The higher C<sub>2</sub> symmetry of the complex allied to the steric demands of the aryl substituents imposes a significant difference in the crystal packing. The most noticeable interaction is between the coordinated chlorides and the acidic imine hydrogens which give rise to chains running parallel to the *a*-axis of the unit cell (Figure 59 (b)). The imine CH...Cl distance is 2.7492(9) for L<sup>1</sup>PhMe but considerably longer at 2.801(1) Å in L<sup>1</sup>PhCl complexes. Both distances are considerably less than the sum of the respective Van der Waals radii.<sup>186</sup> Additionally, the juxtaposition of complexes, introduces close contacts within a sandwich of phenyl rings and the pyridyl head unit of adjacent molecules. This ‘stack’ may further stabilise the chain through π-π interactions. Further imine CH...Cl interactions produce a sheet of complexes parallel to the *B*-face of the cell. It is noticeable that the propagation of the sheet parallel to the *c*-axis involves complexes stacked above one-another (aligned along the 2-fold axis) and, in this arrangement, the cleft produced by the CuCl<sub>2</sub> unit accommodates the pyridyl head unit of the adjacent complex. While the γ-pyridyl hydrogen to chloride distances are 3.062(1) Å, and therefore represent, at best, a weak halogen interaction, it is likely that this arrangement represents a ‘best fit’ for the complexes, optimising steric and Van der Waals interactions within the sheet. The symmetry of the space group repeats the sheets through glide planes parallel to the *b*-axis (Figure 59 (c)). There is some evidence of

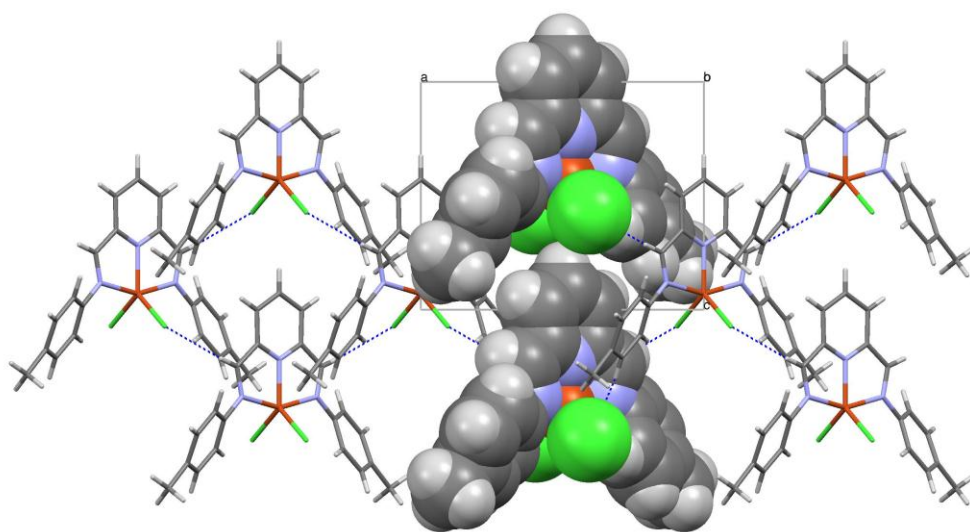
weak interactions between the sheets due to the proximity of para-aryl substituent to the imine methine proton. In the  $L^1PhCl$  complex (Figure 59 (d)), this results in a  $CH...ClPh$  distance of 2.848(1) Å with a  $C-H...Cl$  angle of  $133.7(2)^\circ$ . The interaction at the methine proton in this arrangement therefore may be considered as bifurcated with the  $Cl...H...Cl$  angle of  $84.37(3)^\circ$  and this may explain the elongation of chloride...HC distance in comparison to the 4-methyl analogue. In this  $L^1PhMe$  complex, corresponding inter-sheet interactions are likely from similarly weak  $CH_3...Cl$  hydrogen bonds. Hence it is reasonable to conclude that the correspondence of interactions in the systems gives rise to very similar solid state structures.

**Figure 59.** Packing motifs in the isomorphous crystal structures of  $[CuCl_2(L^1PhCl)]$  and  $[CuCl_2(L^1PhMe)]$  {illustrated with  $[CuCl_2(L^1PhMe)]$ }: (a) chains of complex molecules propagating parallel to the  $a$ -axis of the unit cell linked through imine  $CH...Cl$  interactions; (b) propagation of chains parallel to the  $B$ -face of the cell produces sheets described by further imine  $CH...Cl$  interactions and the steric demands of the complex; (c) crystal packing of  $[CuCl_2(L^1PhMe)]$  viewed parallel to the  $c$ -axis of the unit cell; (d) inter-sheet interactions in  $[CuCl_2(L^1PhCl)]$  arising from the bifurcated  $Cl...H...Cl$  interaction at the imine methine proton due to the  $p$ -chloro substituent of the ligand.

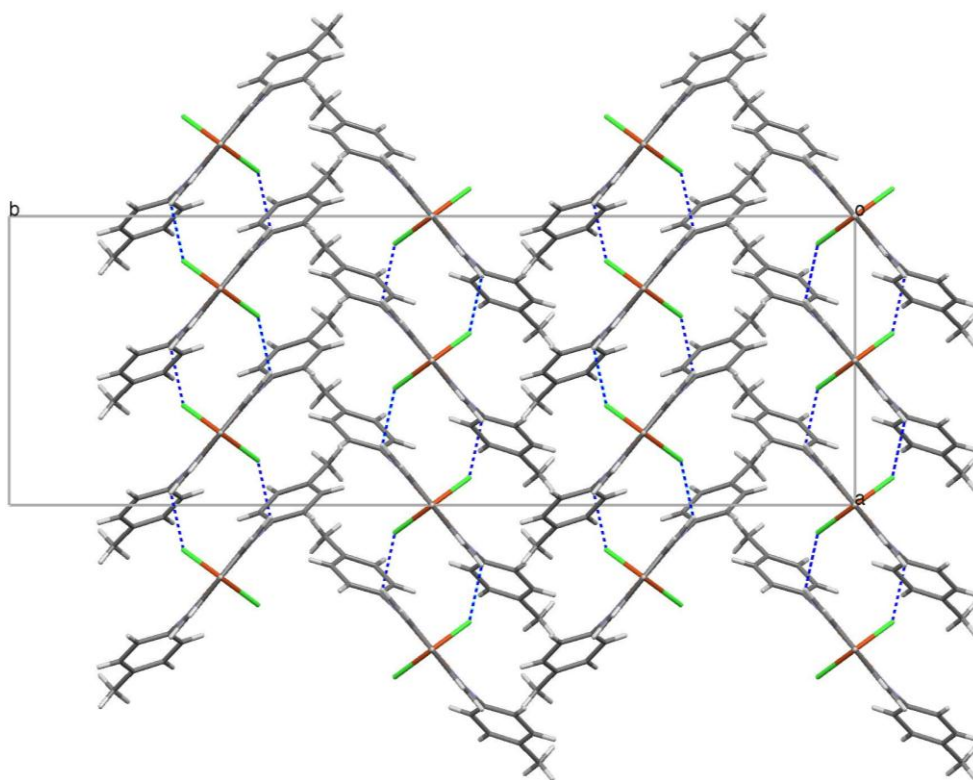
(a)



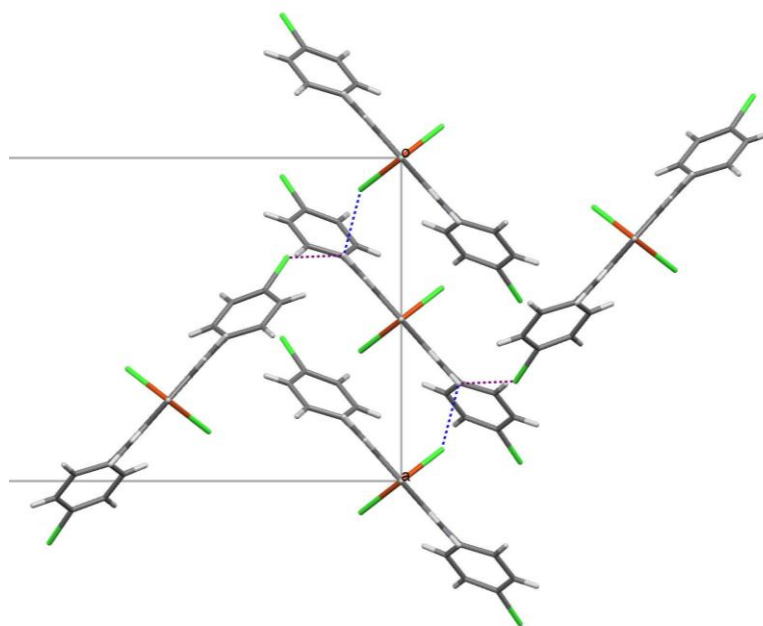
(b)



(c)



(d)



### 6.3.2. Ni<sup>II</sup> Complexes of L<sup>1</sup>R

Crystal structures were obtained for three nickel(II) complexes of L<sup>1</sup>R with ethyl, *n*-propyl and cyclohexyl substituents. In contrast to the five-coordinate copper(II) species, the nickel(II) complexes exhibited 6-coordinate structures based on distorted octahedral coordination spheres. The primary distortion to the octahedron originates with the rigidity of ligand structure at the pyridyldimethimine unit that imposes a reduced bite angle for the 5-coordinate chelate rings of the NNN donor set of L<sup>1</sup>R. In all cases, the metal centres coordinate to one L<sup>1</sup>R ligand, with the metal coordination sphere being completed by coordinated anions {[Ni(AcO)<sub>2</sub>(L<sup>1</sup>Cy)] and [μ-Cl<sub>2</sub>{NiCl(L<sup>1</sup>Pr<sup>n</sup>)}<sub>2</sub>]} or aqua ligands {[NiCl(H<sub>2</sub>O)<sub>2</sub>(L<sup>1</sup>Et)]Cl}.

In the complex, [Ni(AcO)<sub>2</sub>(L<sup>1</sup>Cy)], the six-coordinate sphere is completed by three oxygen donors from unidentate and bidentate acetates. The bidentate acetate introduces

a further distortion to the octahedral geometry (Table 46 to Table 48 and Figure 60). The coordination of the bidentate acetate is highly symmetrical with essentially metal-oxygen distances  $\{d[\text{Ni-O}(41)] = 2.111 (3) \text{ \AA}, d[\text{Ni-O}(42)] = 2.110 (3) \text{ \AA}\}$ . The symmetrical character is reflected in the equivalent carbon-oxygen bond lengths  $\{d[\text{C}(41)\text{-O}(41)] = 1.249, \text{ and } d[\text{C}(41)\text{-O}(42)] = 1.257 \text{ \AA}\}$  and angles at each oxygen donor atom  $\{\angle[\text{Ni-O}(41)\text{-C}(41)] = 89.18^\circ \text{ and } \angle[\text{Ni-O}(42)\text{-C}(41)] = 88.96^\circ\}$ . Clearly, in this mode, the electron density is delocalised between the two C-O bonds of the acetate.

The six-co-ordination about the  $\text{Ni}^{\text{II}}$  centre of the acetate complex is completed by the unidentate acetate. The metal-oxygen bond is unremarkable  $\{d[\text{Ni-O}(51)] = 1.961 \text{ \AA}\}$  and the asymmetry of the carbon-oxygen bond lengths  $\{d[\text{O}(51)\text{-C}(51)] = 1.260 \text{ \AA}; d[\text{O}(52)\text{-C}(51)] = 1.215 \text{ \AA}\}$  are consistent with localised single and one double bonds within the acetate group. The slight elongation of O(51)-C(51) coupled with a relatively short intermolecular contact to the water of crystallisation  $\{d[\text{O}(51)\dots\text{O}(61)] = 2.869 \text{ \AA}\}$  is consistent with a C=O...HOH hydrogen bond.

The cyclohexyl 'tail' groups adopt the favourable chair conformation within this structure and are aligned approximately perpendicular to the plane of the NNN donor set, presumably to minimise steric interactions as the acetates complete the metal coordination sphere.

**Figure 60.** X-ray crystal structure of the complex  $[\text{Ni}(\text{AcO})_2(\text{L1Cy})]$ , hydrogen atoms and solvate molecules omitted for clarity.

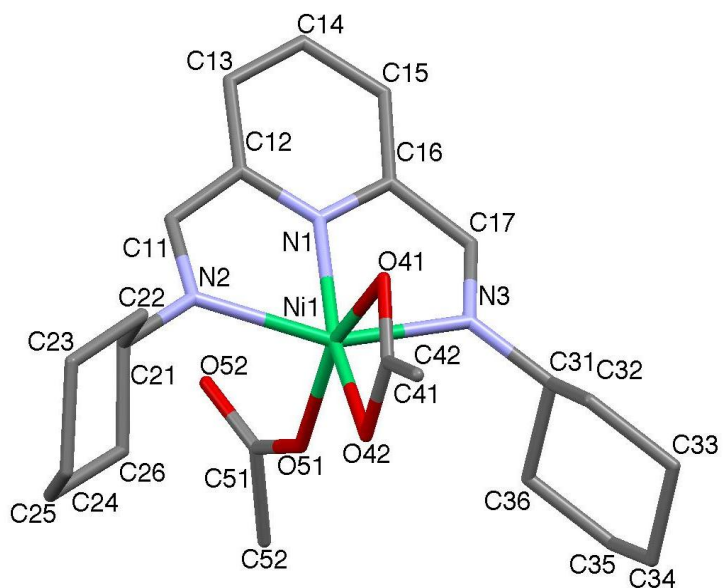
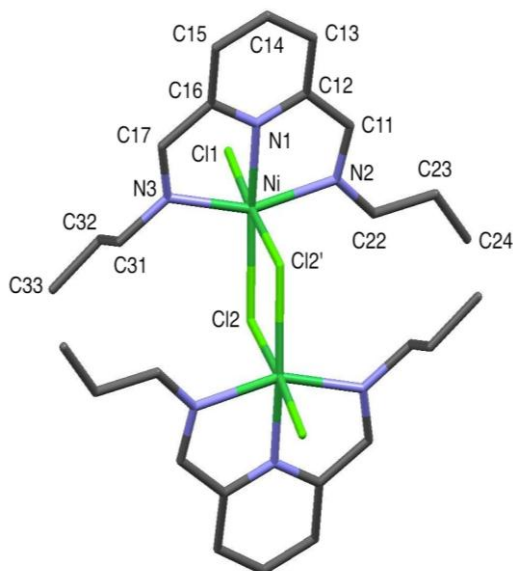


**Table 32.** X-ray structure and refinement parameters for Ni<sup>(II)</sup> complexes of L<sup>1</sup>R.

Compound	[Ni(AcO) <sub>2</sub> (L <sup>1</sup> Cy)]. CH <sub>3</sub> CN.H <sub>2</sub> O	[μ-Cl <sub>2</sub> {NiCl(L <sup>1</sup> Pr <sup>n</sup> )} <sub>2</sub> ]
Chemical Formula	C <sub>25</sub> H <sub>33</sub> N <sub>4</sub> NiO <sub>5</sub>	C <sub>26</sub> H <sub>38</sub> Cl <sub>4</sub> N <sub>6</sub> Ni <sub>2</sub>
Formula Weight	528.26	693.84
Crystal System	Monoclinic	Monoclinic
Space Group	<i>P</i> 2 <sub>1</sub> / <i>c</i>	<i>P</i> 2 <sub>1</sub> / <i>c</i>
<i>a</i> / Å	9.2608 (12)	10.127 (2)
<i>b</i> / Å	15.6053 (19)	11.982 (2)
<i>c</i> / Å	18.191 (2)	13.116 (3)
<i>α</i> / °	90	90
<i>β</i> / °	91.220 (7)	103.75 (3)
<i>γ</i> / °	90	90
<i>V</i> / Å <sup>3</sup>	2628.4 (6)	1545.9 (5)
<i>T</i> / K	293 (2)	293 (2)
<i>Z</i>	4	4
<i>S</i>	1.036	1.023
No. unique data ( <i>R</i> <sub>int</sub> )	13402	2712
No. measured reflections	122357	3410
<i>R</i> <sub>obs</sub> / <i>wR</i> ( <i>F</i> <sup>2</sup> ) <sub>obs</sub>	0.088/0.272	0.025/0.069

The complex  $[\mu\text{-Cl}_2\{\text{NiCl}(\text{L}^1\text{Pr}^n)\}_2]$  arises from a centrosymmetric  $\mu$ -chloro dimer formed from two asymmetric units related through an inversion centre of symmetry. The complex features six coordinate nickel atoms, from coordination of three N atoms of the ligand  $\text{L}^1\text{Pr}^n$   $\{d[\text{Ni}(1)\text{-N}(1)] = 1.9819 (18) \text{ \AA}$ ,  $d[\text{Ni}(1)\text{-N}(2)] = 2.1211 (19) \text{ \AA}$ ,  $d[\text{Ni}(1)\text{-N}(3)] = 2.1222 (19) \text{ \AA}\}$ , with the three remaining sites being occupied by two symmetry-related bridging chlorides and a single terminal chloride. Metal-chlorine distances cover a wide range, the bridging atoms show very different metal-chlorine distances  $\{d[\text{Ni}(1)\text{-Cl}(2)] = 2.3313 (10) \text{ \AA}$ ;  $d[\text{Ni}(1)\text{-Cl}(2')] = 2.5981 (7) \text{ \AA}\}$ , while the final co-ordination site is finished with a terminal Cl ion  $\{d[\text{Ni}(1)\text{-Cl}(1)] = 2.4159 (7) \text{ \AA}\}$ .

**Figure 61.** Crystal structure of the dimeric  $[\mu\text{-Cl}_2\{\text{NiCl}(\text{L}^1\text{Pr}^n)\}_2]$  with hydrogen atoms omitted for clarity showing the numbering of the asymmetric unit.



In the 4-membered dimer, the Ni-Ni distance is  $3.682 \text{ \AA}$ , while the Ni- $\mu$ -Cl-Ni angle is  $96.61^\circ$ . The distances and angles are comparable to those known for such  $\text{Ni}^{\text{II}}$

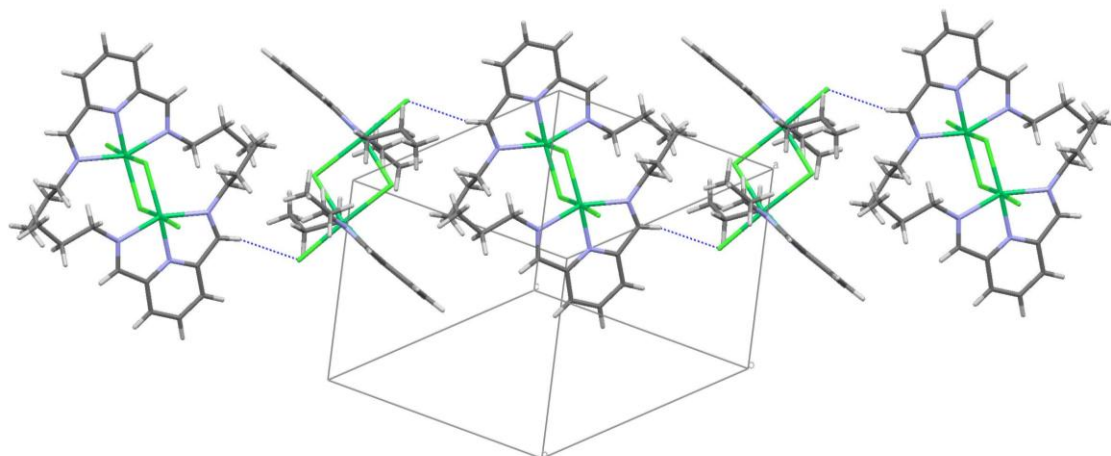


species,<sup>187-190</sup> while the distances and angles of the ligand are comparable with those of the related Ni<sup>II</sup> complexes of this series.

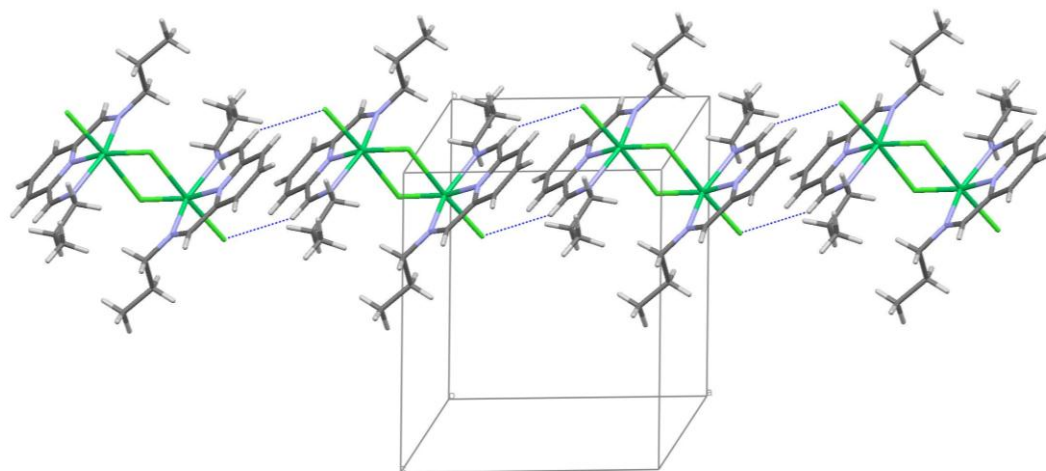
The dimeric Ni<sup>II</sup> complex crystallises in the primitive monoclinic unit. The crystal packing within the unit cell is dominated by CH...Cl contact, consistent with halogen bonds (see section 6.3.1). Again, the acidic imine CH groups of the ligand give rise to chain and ring structures in the crystal (Figure 62).

**Figure 62.** The crystal packing of  $[\mu\text{-Cl}_2\{\text{NiCl}(\text{L}^{\text{1Pr}^n})\}_2]$  showing molecular packing dominated by imine  $\text{CH}\dots\text{Cl}$  intermolecular interactions. (a) Linear chains of dimers and (b)  $\mu\text{-chloro}$  dimers forming a ring structure through  $\text{CH}\dots\text{Cl}$  interactions

(a)



(b)



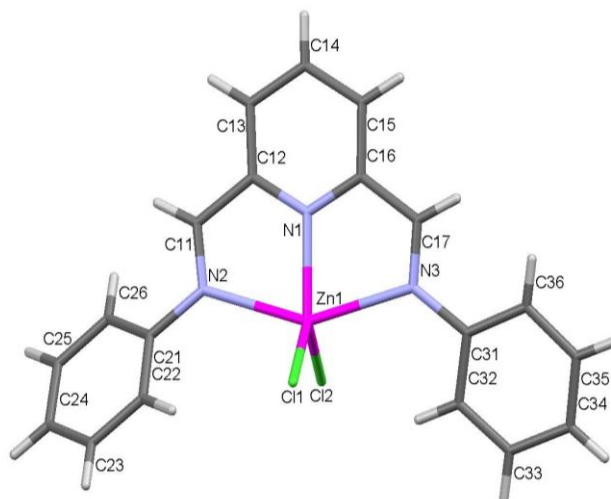
### 6.3.3. Zn<sup>II</sup> Complexes of L<sup>1</sup>R

Several crystal structures of Zn<sup>II</sup> complexes were obtained and provide an interesting comparison with the structures of the analogous Cu(II) and Ni(II) complexes. In particular, the structures demonstrate that the  $d^{10}$  configuration of Zn(II) imposes fewer geometric requirements on the metal coordination sphere than the transition metal analogues. Principal bond lengths and angles in the metal coordination spheres are given in Table 49 and Table 50. Structures were obtained from two species with aliphatic tail groups { [Zn(NO<sub>3</sub>)<sub>2</sub>(L<sup>1</sup>Bu<sup>t</sup>)] and [ZnCl<sub>2</sub>(L<sup>1</sup>Bu<sup>t</sup>)].CH<sub>3</sub>CN }, and three with aromatic tail groups { [ZnCl<sub>2</sub>(L<sup>1</sup>Ph)].CH<sub>3</sub>CN, [ZnCl<sub>2</sub>(L<sup>1</sup>PhMe)] and [ZnCl<sub>2</sub>(L<sup>1</sup>PhCl)] }.

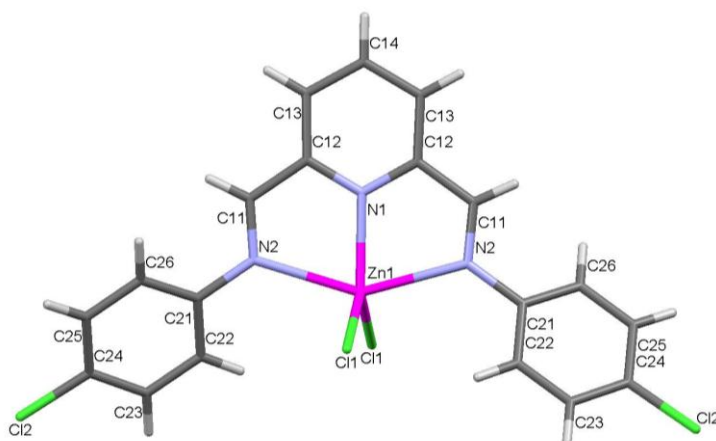
Structures of three complexes with aromatic tail groups L<sup>1</sup>Ph, L<sup>1</sup>PhMe and L<sup>1</sup>PhCl are based on similar metal coordination geometries (Figure 63).

**Figure 63.** The metal complexes in the crystal structures of (a)  $[\text{ZnCl}_2(\text{L}^1\text{Ph})]\cdot\text{CH}_3\text{CN}$ , (b)  $[\text{ZnCl}_2(\text{L}^1\text{PhCl})]$  and (c)  $[\text{ZnCl}_2(\text{L}^1\text{PhMe})]$  showing the numbering scheme adopted.

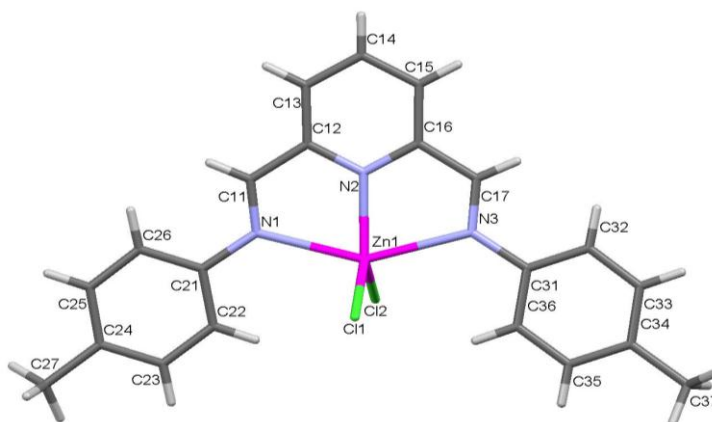
(a)



(b)



(c)

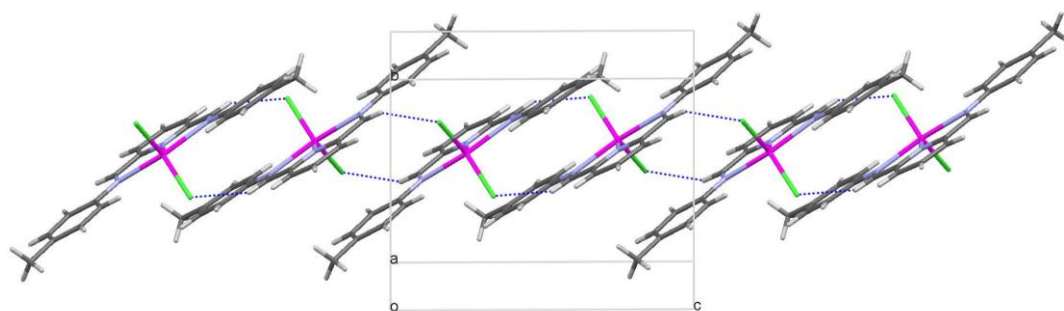


However even though the structures adopted in complexes are based on similar distorted trigonal bipyramidal structures with the coordinated chlorides lying approximately equidistant above and below the  $N_3M$  plane: X(1)-Zn-X(2) bond angles are in the range  $118.340(18) - 119.53(6)^\circ$  and the axial bond angle N(2)-Zn-N(3) in the range  $147.97(16) - 149.01(15)^\circ$ . In common with all the complexes of the pyridyl-diylimine, the N(2)-Zn-N(3) angle parameter is imposed by the bite of the tridentate ligand. Thus the complexes adopt distorted trigonal bipyramidal coordination spheres. However, there are subtle differences in bond lengths and geometries around the respective coordination spheres. The complex  $[ZnCl_2(L^1PhCl)]$  exhibits the crystallographic 2-fold symmetry around an axis defined by  $\gamma$ -pyridyl carbon, the pyridyl nitrogen and the metal which imposes equal Zn-N(imine) bond lengths. In contrast, the complex  $[ZnCl_2(L^1Ph)]$  exhibits significantly different Zn-N(imine) bond distances  $\{d[M-N(2)] = 2.304(4) \text{ \AA}; d[M-N(3)] = 2.336(4) \text{ \AA}\}$ . Within this series of complexes, the relatively small differences in metal coordination sphere dimensions are difficult to ascribe to functional group changes with any confidence and while the ligand basicity may be influenced by differing inductive effects from para-substituents, such effects are likely to be outweighed by crystal packing forces.

The orientation of the aromatic substituents within the complexes is interesting. While the 4-chlorophenyl and phenyl complexes show the same chiral propeller arrangement as observed in the copper analogues, the p-tolyl species is distinctly different. This shows a configuration of the phenyl rings that is considerably closer to coplanar with the pyridine ring. In this configuration, increased steric interaction between the imine hydrogen and the hydrogen in the ortho position of the aromatic ring might be anticipated. Close inspection of the crystal packing shows that this apparently

unfavourable arrangement facilitates extended face-to-face  $\pi$ - $\pi$  stacking between complexes (Figure 64). Notably, this stacked arrangement compliments short contacts between imine hydrogens and chlorides from adjacent complexes  $\{d[\text{CH}\dots\text{Cl}] = 2.842 \text{ \AA}\}$  that result in the formation of centrosymmetric structural units propagating parallel to the  $c$ -axis of the unit cell.

**Figure 64.**  $\pi$ - $\pi$  Stacking interactions propagating parallel to the  $c$ -axis in the crystal structure of  $[\text{ZnCl}_2(\text{L}^1\text{PhMe})]$  complimented by imine-CH...Cl interactions.

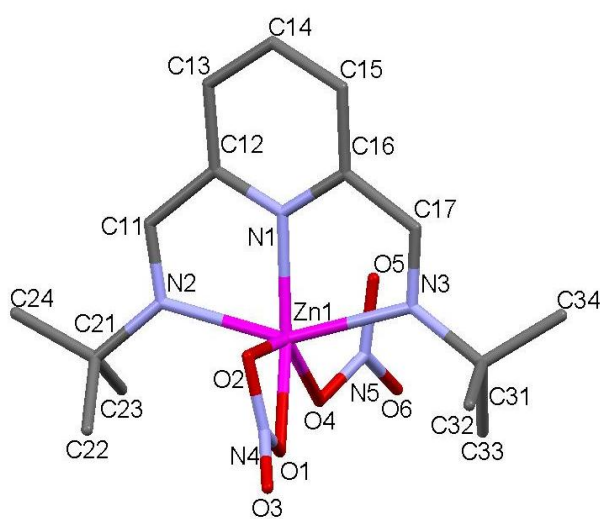


The  $[\text{ZnCl}_2(\text{L}^1\text{Bu}^t)]$  and  $[\text{Zn}(\text{NO}_3)_2(\text{L}^1\text{Bu}^t)]$  complexes of the  $t$ -butyl functionalised ligand show largely similar influences on metal coordination to the aromatic analogues. As might be expected, the dominant influence on the structure arises from nature of the coordinated counterions (Figure 65). The most noticeable feature is the differing conformation of the  $t$ -butyl group with respect to the pyridyldiimine unit of the ligand. Torsion angles at the N-C(quaternary) bond show two distinct conformers: in the dichloro complex  $[\text{ZnCl}_2(\text{L}^1\text{Bu}^t)]$ , the methyl groups closest to the pyridyldiimine plane in each ‘tail’ (C24 and C32) are antiperiplanar  $\{\tau[\text{C}11\text{-N}2\text{-C}21\text{-C}24] = 179.4(4)^\circ$ ;  $\tau[\text{C}17\text{-N}3\text{-C}31\text{-C}32] = 158.7(2)^\circ\}$  with respect to the imine bond while in  $[\text{Zn}(\text{NO}_3)_2(\text{L}^1\text{Bu}^t)]$ , the corresponding methyl groups are synperiplanar  $\{\tau[\text{C}11\text{-N}2\text{-C}21\text{-C}24] = 4.0(1)^\circ$ ;  $\tau[\text{C}17\text{-N}3\text{-C}31\text{-C}34] = 27.2(1)^\circ\}$ . Inspection of spacefilling models of

the complexes indicate that these arrangements might arise to accommodate the steric demands of the coordinated anions (Figure 66).

**Figure 65.** The metal complexes in the crystal structures of (a)  $[\text{Zn}(\text{NO}_3)_2(\text{L}^1\text{Bu}^f)]$  and (b)  $[\text{ZnCl}_2(\text{L}^1\text{Bu}^f)].\text{CH}_3\text{CN}$  showing the numbering scheme adopted (hydrogens are omitted for clarity).

(a)



(b)

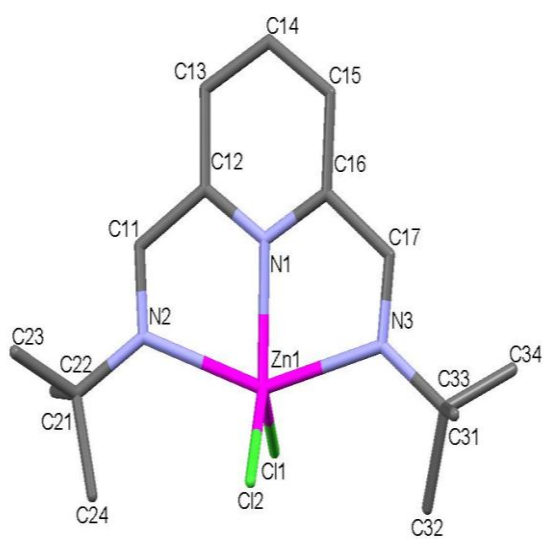
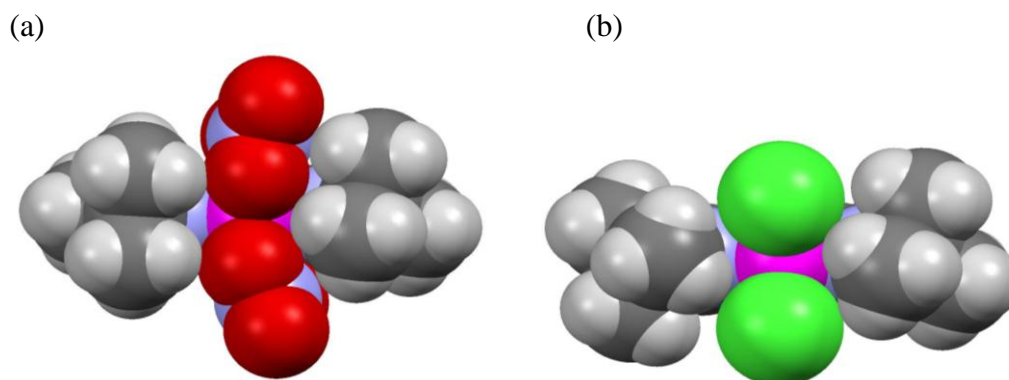


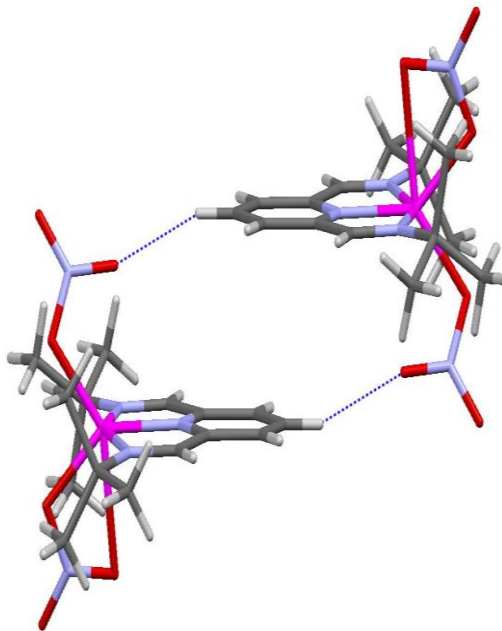
**Figure 66.** Space filling models of the crystal structures of (a)  $[\text{Zn}(\text{NO}_3)_2(\text{L}^1\text{Bu}^t)]$  and (b)  $[\text{ZnCl}_2(\text{L}^1\text{Bu}^t)]$  viewed parallel to M-N(py) vector showing the different conformations of the *tert*-butyl group that apparently arise from the steric demands of the coordinated anions. The  $\text{N}_3$  coordinating plane of the ligand lies approximately horizontal in each view.



Some consideration of crystal packing influences is worthwhile to indicate the potential origin of the monodentate and pseudo-bidentate binding modes for the nitrates of  $[\text{Zn}(\text{NO}_3)_2(\text{L}^1\text{Bu}^t)]$ . While the pseudo-bidentate nitrate interacts solely with the metal atom, the monodentate nitrate shows a close contact with the  $\gamma$ -pyridyl hydrogen of an adjacent complex molecule related by inversion symmetry  $\{d[\text{C}14\text{-H}14\dots\text{O}5] = 2.3826(9) \text{ \AA}, \angle[\text{C}14\text{-H}14\dots\text{O}5] = 158.43(7)\}$ . While relatively long, such contact parameters could be considered consistent with CH...nitrate hydrogen bonding. The resulting centrosymmetric dimer is likely to be stabilised through additional face-to-face  $\pi$ - $\pi$  interactions between the pyridine units of adjacent complexes Figure 67.



**Figure 67.** The centrosymmetric dimer motif in the crystal packing of  $[\text{Zn}(\text{NO}_3)_2(\text{L}^1\text{Bu}^t)]$  featuring  $\pi$ - $\pi$  stacking and potential pyH...nitrate hydrogen bonds.



Compound	[Zn(NO <sub>3</sub> ) <sub>2</sub> (L <sup>1</sup> Bu <sup>t</sup> )]	[ZnCl <sub>2</sub> (L <sup>1</sup> Bu <sup>t</sup> )].CH <sub>3</sub> CN	[ZnCl <sub>2</sub> (L <sup>1</sup> Ph)].CH <sub>3</sub> CN	[ZnCl <sub>2</sub> (L <sup>1</sup> PhMe)]	[ZnCl <sub>2</sub> (L <sup>1</sup> PhCl)]
Chemical Formula	C <sub>15</sub> H <sub>23</sub> N <sub>5</sub> O <sub>6</sub> Zn	C <sub>15</sub> H <sub>23</sub> Cl <sub>2</sub> N <sub>3</sub> Zn	C <sub>21</sub> H <sub>18</sub> Cl <sub>2</sub> N <sub>4</sub> Zn	C <sub>21</sub> H <sub>19</sub> Cl <sub>2</sub> N <sub>3</sub> Zn	C <sub>19</sub> H <sub>13</sub> Cl <sub>4</sub> N <sub>3</sub> Zn
Formula Weight	434.75	381.63	462.66	449.66	490.49
Crystal System	Monoclinic	Trigonal	Monoclinic	Triclinic	Orthorhombic
Space Group	<i>P2<sub>1</sub>/c</i>	<i>R3c</i>	<i>P2<sub>1</sub>/n</i>	<i>P-1</i>	<i>Fddd</i>
<i>a</i> / Å	11.2793 (2)	26.048 (4)	7.5643 (8)	9.5167 (5)	12.0528 (4)
<i>b</i> / Å	11.6999 (2)	26.048 (4)	14.7970 (17)	9.9677 (5)	35.4317 (14)
<i>c</i> / Å	15.9061 (3)	15.046 (3)	19.292 (2)	12.5624 (5)	9.2326 (3)
<i>α</i> / °	90	90	90	89.7810 (10)	90
<i>β</i> / °	108.2450 (10)	90	96.085 (4)	90.0130 (10)	90
<i>γ</i> / °	90	120	90	61.4650 (10)	90
<i>V</i> / Å <sup>3</sup>	1993.55 (6)	8840 (3)	2147.1 (4)	1046.90 (9)	3942.8 (2)
<i>T</i> / K	273 (2)	293 (2)	273 (2)	273 (2)	273 (2)
<i>Z</i>	4	16	4	2	8
<i>S</i>	0.811	1.037	0.780	0.932	0.761
No. unique data ( <i>R</i> <sub>int</sub> )	12683	6947	6518	6989	1790
No. measured reflections	207723	34268	92348	16387	10254
<i>R</i> <sub>obs</sub> / <i>wR</i> ( <i>F</i> <sup>2</sup> ) <sub>obs</sub>	0.028/0.064	0.035/0.095	0.086/0.211	0.030/0.074	0.030/0.046

**Table 33.** X-ray structure and refinement parameters for complexes of [ZnX<sub>2</sub>(L<sup>1</sup>R)].

#### 6.3.4. Co<sup>II</sup> Complexes of L<sup>1</sup>R

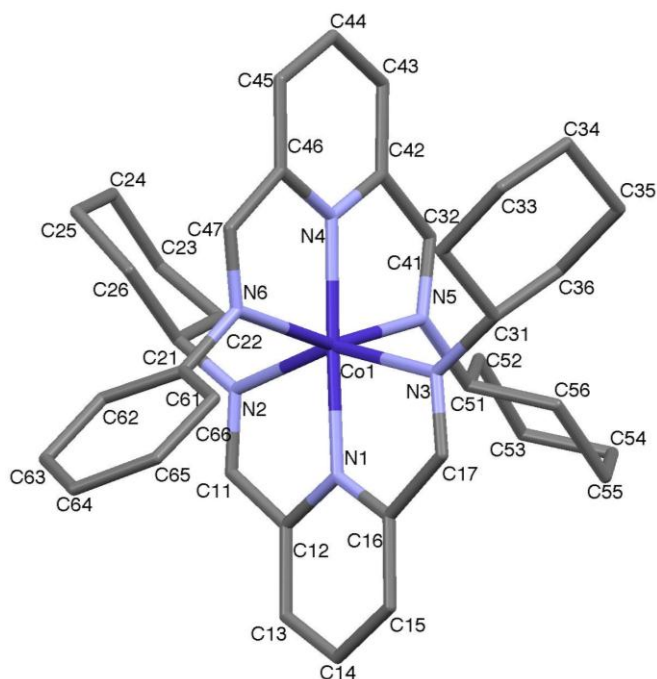
Cobalt complexes of L<sup>1</sup>R cobalt complexes of L<sup>1</sup>R yielded few crystals suitable for structural study and of these, only one monoligated structure was obtained, the complex [CoCl<sub>2</sub>(L<sup>1</sup>PhCl)]. This complex is essentially isomorphous and isostructural to the copper complexes of the L<sup>1</sup>PhCl ligands (Figure 58) where they crystallise in the same space group (orthorhombic, *Fdd2*), with similar unit cell dimensions.

The remaining crystal structures obtained for cobalt were bis-complexes of the ligand L<sup>1</sup>Cy. Three structures were obtained for the complex cation [Co(L<sup>1</sup>Cy)<sub>2</sub>]<sup>2+</sup> with the nitrate, tetrafluoroborate and tetrakisothiocyanatocobaltate(II) {[Co(NCS)<sub>4</sub>]<sup>2-</sup>} counterions. The complex cations of all three complexes are very similar with a distorted octahedral cobalt metal centre arising from coordination of two L<sup>1</sup>Cy ligands binding in a tridentate fashion (Figure 68).

The distortion to octahedral co-ordination sphere originates in the bite imposed by the rigid nature of the terdentate pyridyl-diylidimine donor unit. The deviation of N2-M-N3 and N5-M-N6 bond angles from 180° arises because the approach of metal to the pyridyl nitrogens is limited, thereby promoting the observed geometry.

**Figure 68.** X-ray structure of the complex cation  $[\text{Co}(\text{L}^1\text{Cy})_2]^{2+}$  in the complexes (a)  $[\text{Co}(\text{L}^1\text{Cy})_2][\text{NO}_3]_2 \cdot 2\text{H}_2\text{O} \cdot \text{CH}_3\text{CN}$  and (b)  $[\text{Co}(\text{L}^1\text{Cy})_2][\text{BF}_4]_2 \cdot 2\text{H}_2\text{O} \cdot \text{CH}_3\text{CN}$  showing the numbering schemes adopted.

(a)



(b)

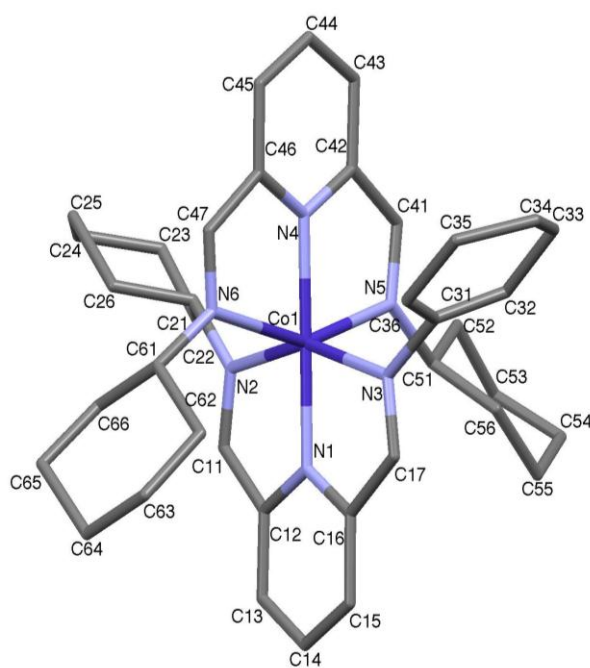
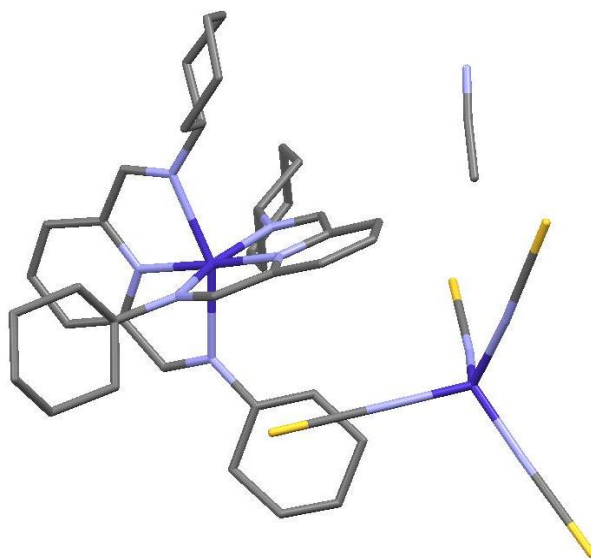
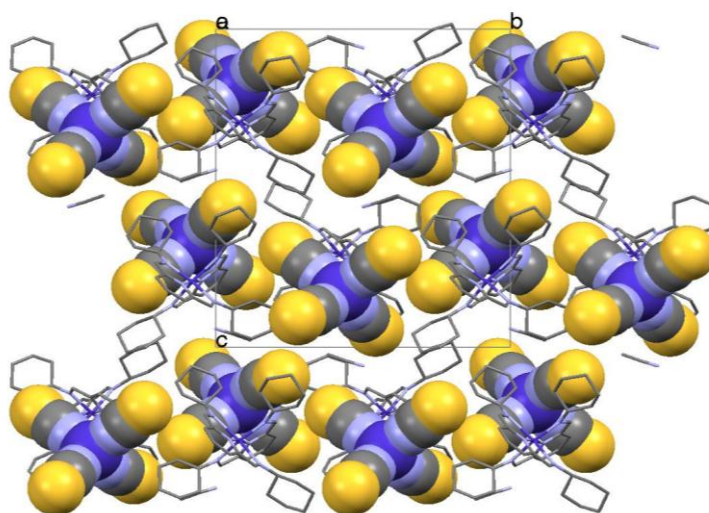


**Figure 69.** Crystal structure of  $[\text{Co}(\text{L}^1\text{Cy})_2][\text{Co}(\text{SCN})_4]\cdot\text{CH}_3\text{CN}$ : (a) the asymmetric unit and (b) the crystal packing viewed down the  $a$ -axis showing the tetraisothiocyanatocobaltate(II) counterions in space fill.

(a)



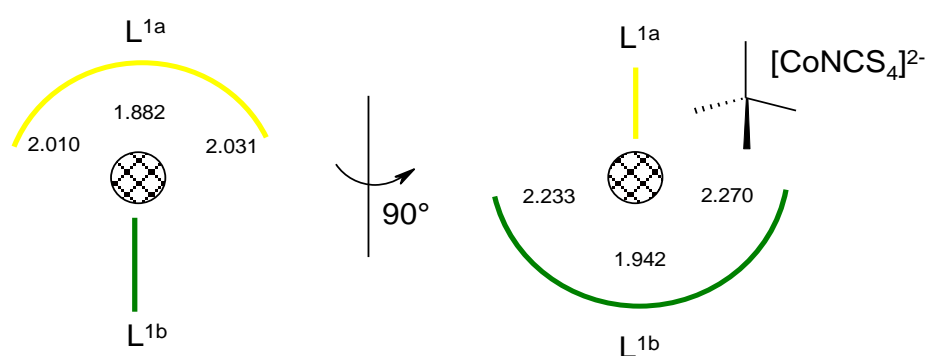
(b)



The coordination of the metal within the terdentate chelates is also asymmetric with each ligand showing significantly different metal-ligand bond lengths. In the complex, the two independent ligands (labelled  $\text{L}^{1a}$  and  $\text{L}^{1b}$ ) show similar but distinctly different

metal coordination. This asymmetry may be viewed as different (asymmetric) occupation of the chelate ‘pockets’ presented by the two ligands (Table 34) This situation is presented schematically in Figure 70. It is not totally understood why this asymmetry arises, but the role of the counterion in exerting different electrostatic crystal packing forces on the ligands may be important. Noticeably, counterion lies adjacent to  $L^{1a}$  intersecting the perpendicular ligand  $L^{1a}$  with the Co-N3 bond of  $L^{1b}$ . It may be that the attraction of the counterion to the metal causes a steric repulsion of the counterion with ligand  $L^{1b}$  and hence pushing the ligand away from the metal.

**Figure 70.** Pictorial depiction of the hole size of the two independent ligands  $L^{1a}$  and  $L^{1b}$  in the complex  $[\text{Co}(\text{L}^1\text{Cy})_2][\text{CoNCS}_4]$ .



The converse effect of the interaction of the cation with the counter dianion, is a slight distortion in the tetrahedral geometry which can be seen when looking at the N-Co-N bond angles of the complex (Table 52). The ideal bond angle of a symmetrical tetrahedron is roughly  $109^\circ$ , clearly large deviations above and below this are observed for the dianion. [N(9)-Co-N(8) and N(10)-Co-N(8), bond angles of  $115.8^\circ$  and  $105.2^\circ$  respectively].

Compound	[CoCl <sub>2</sub> (L <sup>1</sup> PhCl)]	[Co(L <sup>1</sup> Cy) <sub>2</sub> ][BF <sub>4</sub> ] <sub>2</sub> . CH <sub>3</sub> CN. 2H <sub>2</sub> O	[Co(L <sup>1</sup> Cy) <sub>2</sub> ][NO <sub>3</sub> ] <sub>2</sub> . CH <sub>3</sub> CN. 2H <sub>2</sub> O	[Co(L <sup>1</sup> Cy) <sub>2</sub> ] [CoNCS <sub>4</sub> ].CH <sub>3</sub> CN
Chemical Formula	C <sub>19</sub> H <sub>13</sub> Cl <sub>4</sub> CoN <sub>3</sub>	C <sub>19</sub> H <sub>31</sub> B <sub>2</sub> CoF <sub>8</sub> N <sub>3</sub> O <sub>2</sub>	C <sub>20</sub> H <sub>27</sub> Co <sub>0.50</sub> N <sub>4.50</sub> O <sub>4</sub>	C <sub>22</sub> H <sub>27</sub> CoN <sub>5.50</sub> S <sub>2</sub>
Formula Weight	484.05	566.02	423.93	491.54
Crystal System	Orthorhombic	Monoclinic	Monoclinic	Orthorhombic
Space Group	<i>Fdd2</i>	<i>P2<sub>1</sub>/n</i>	<i>P2<sub>1</sub>/n</i>	<i>P2<sub>1</sub>2<sub>1</sub>2<sub>1</sub></i>
<i>a</i> / Å	11.9376 (19)	17.8919 (9)	17.3547 (6)	12.8967 (6)
<i>b</i> / Å	35.056 (6)	13.8446 (6)	13.9813 (5)	18.3596 (9)
<i>c</i> / Å	9.2382 (13)	18.9099 (10)	18.4021 (6)	20.7305 (10)
<i>α</i> / °	90	90	90	90
<i>β</i> / °	90	98.948 (3)	96.394 (2)	90
<i>γ</i> / °	90	90	90	90
<i>V</i> / Å <sup>3</sup>	3866.1 (11)	4627.1 (4)	4437.3 (3)	4908.5 (4)
<i>T</i> / K	273 (2)	273 (2)	273 (2)	293 (2)
<i>Z</i>	8	8	8	8
<i>S</i>	1.036	1.030	1.093	0.829
No. unique data ( <i>R</i> <sub>int</sub> )	1588	14610	9990	4480
No. measured reflections	11245	179646	181288	67529
<i>R</i> <sub>obs</sub> / <i>wR</i> ( <i>F</i> <sup>2</sup> ) <sub>obs</sub>	0.049/0.103	0.073/0.239	0.067/0.204	0.047/0.098

**Table 34.** X-ray structure and refinement parameters for Co<sup>(II)</sup> complexes of L<sup>1</sup>R.

### 6.3.5. Complexes of L<sup>2</sup>R and L<sup>3</sup>R.

The crystal structures of the complexes of L<sup>2</sup> and L<sup>3</sup> ligands were more difficult to obtain than for L<sup>1</sup> complexes owing to several reasons. Firstly due to the smaller library of complexes prepared in this study, secondly due to the inherent insolubility of complexes of this particular ligand and thirdly the quality of the crystal obtained was not always satisfactory. However 4 crystal structures of this class of ligand were obtained and identified the denticity of such complexes appears to be very different to what was expected based on NMR data. The 4 complexes along with their refinement parameters are listed in Table 35, and their crystal structure diagrams are shown in Figure 71 a-d.

Based on structural, particularly NMR, studies in solution data, it was anticipated that the metal coordination of all ligands was through the potentially quadridentate ligand utilising all of its donors to produce a pseudo-two-fold symmetric complex. It was anticipated that the counterions might be involved in completing distorted six-coordinate metal spheres.

In the solid state, the ligands are observed to coordinate in a terdentate fashion giving an asymmetric ligand. Only the zinc complex [Zn(NO<sub>3</sub>)(H<sub>2</sub>O)(L<sup>2</sup>PhMe)][NO<sub>3</sub>], showed the ligand binding in a tetradentate fashion. However the similar complex [ZnCl<sub>2</sub>(L<sup>3</sup>PhMe)] is clearly terdentate in the crystal structure. The explanation could be purely down to the difference in ligand from bipyridine to phenanthroline, or it could be due to solvation effects, where a tight DMF solvate in [ZnCl<sub>2</sub>(L<sup>3</sup>PhMe)] could force a terdentate chelate.



Compound	[ZnCl <sub>2</sub> (L <sup>2</sup> Cy)]	[Zn(NO <sub>3</sub> )(H <sub>2</sub> O)(L <sup>2</sup> PhMe)] [NO <sub>3</sub> ]	[ZnCl <sub>2</sub> (L <sup>3</sup> PhMe)]. 2DMF	[CuCl <sub>2</sub> (L <sup>3</sup> Bu <sup>i</sup> )].CH <sub>3</sub> CN.H <sub>2</sub> O
Chemical Formula	C <sub>26</sub> H <sub>32</sub> Cl <sub>2</sub> N <sub>5</sub> Zn	C <sub>26</sub> H <sub>24</sub> N <sub>6</sub> O <sub>7</sub> Zn	C <sub>32</sub> H <sub>29</sub> Cl <sub>2</sub> N <sub>6</sub> O <sub>2</sub> Zn	C <sub>23</sub> H <sub>26</sub> Cl <sub>2</sub> CuN <sub>5</sub> O
Formula Weight	551.34	597.88	656.88	519.43
Crystal System	Triclinic	Monoclinic	Monoclinic	Monoclinic
Space Group	<i>P</i> -1	<i>P</i> 2 <sub>1</sub> / <i>n</i>	<i>C</i> 2/ <i>c</i>	<i>P</i> 2 <sub>1</sub> / <i>n</i>
<i>a</i> / Å	11.9728 (16)	14.2027 (4)	24.1825 (12)	13.3340 (6)
<i>b</i> / Å	14.6569 (19)	11.4274 (4)	15.1249 (8)	11.8161 (5)
<i>c</i> / Å	16.3402 (16)	16.4237 (4)	16.9676 (8)	16.5059 (7)
<i>α</i> / °	87.116 (4)	90	90	90
<i>β</i> / °	76.631 (3)	105.531 (2)	91.652 (3)	105.477 (2)
<i>γ</i> / °	86.222 (4)	90	90	90
<i>V</i> / Å <sup>3</sup>	2781.9 (6)	2568.23 (13)	6203.5 (5)	2506.30 (19)
<i>T</i> / K	273 (2)	293 (2)	293 (2)	273 (2)
<i>Z</i>	4	4	8	4
<i>S</i>	1.118	0.711	0.756	0.905
No. unique data ( <i>R</i> <sub>int</sub> )	5282	7105	10520	11572
No. measured reflections	42335	51099	112784	118425
<i>R</i> <sub>obs</sub> / <i>wR</i> ( <i>F</i> <sup>2</sup> ) <sub>obs</sub>	0.080/0.243	0.037/0.059	0.070/0.166	0.038/0.108

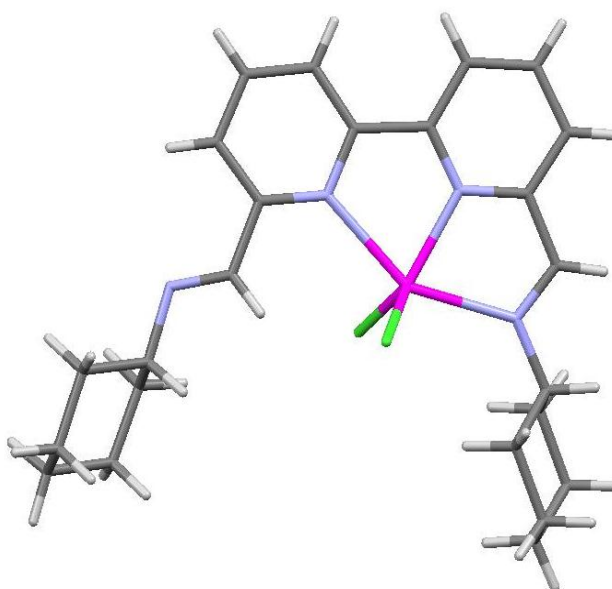
**Table 35.** X-ray structure and refinement parameters for complexes of L<sup>2</sup>R and L<sup>3</sup>R.

However it is highly likely that the reason the dichloro complexes do not give a tetradentate complex is solely due to the steric effect of these bulky anions.

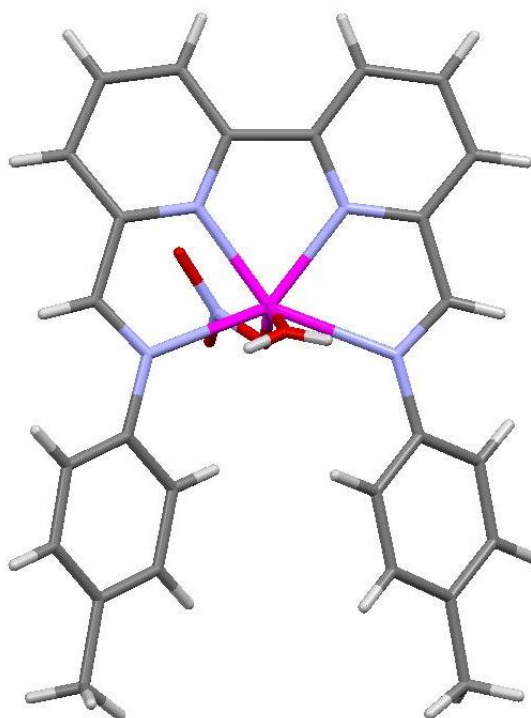
The tetradentate complex contains a co-ordinated water ligand, which is much less sterically demanding than  $\text{NO}_3^-$  or  $\text{Cl}^-$ , and would mean the metal can more easily accommodate a tetradentate chelate. This can partly be backed up by another crystal structure that was solved but could not be satisfactorily refined for the complex  $[\text{Zn}(\text{NO}_3)_2(\text{L}^3\text{PhMe})]$ . This analogous structure was clearly observed to be terdentate with both nitrate anions co-ordinated to zinc in a unidentate fashion.

**Figure 71.** Crystal structures of a)  $[\text{ZnCl}_2(\text{L}^2\text{Cy})]$ , b)  $[\text{Zn}(\text{NO}_3)(\text{H}_2\text{O})(\text{L}^2\text{PhMe})]$ ,  $[\text{NO}_3]$  anion omitted for clarity, c)  $[\text{CuCl}_2(\text{L}^3\text{Bu}^i)]$ , d)  $[\text{ZnCl}_2(\text{L}^3\text{PhMe})]$ . 2DMF solvate omitted for clarity.

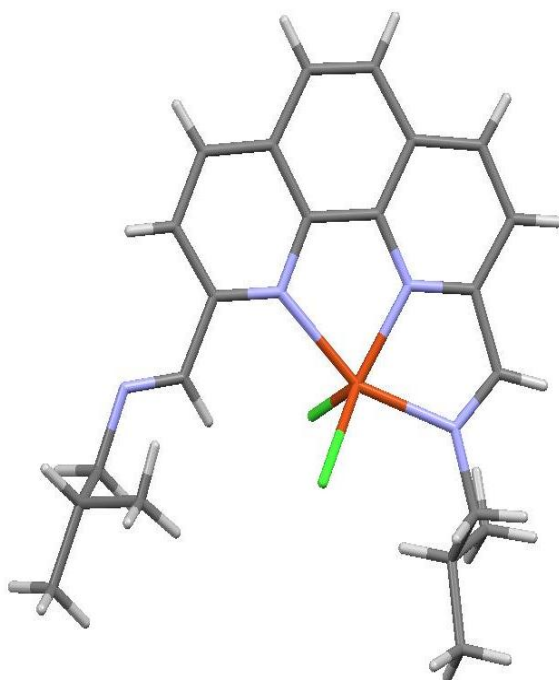
(a)



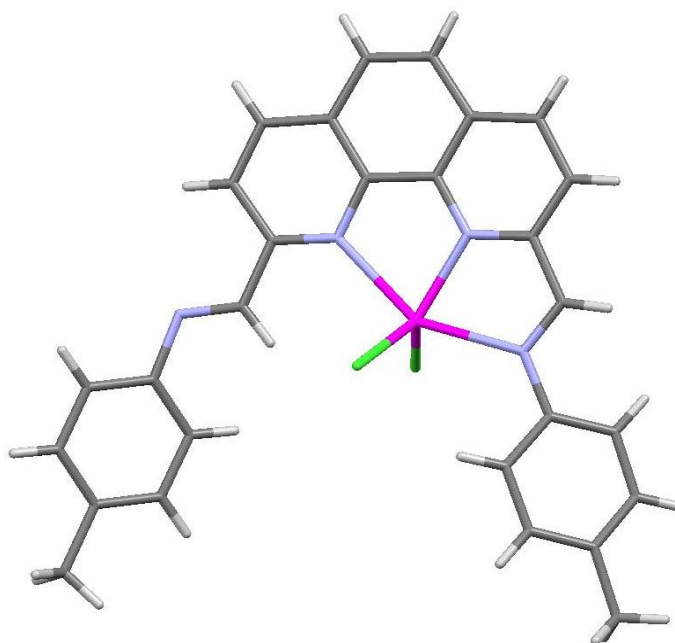
(b)



(c)



(d)



The co-ordination geometry of the two terdentate zinc complexes  $[\text{ZnCl}_2(\text{L}^2\text{Cy})]$  and  $[\text{ZnCl}_2(\text{L}^3\text{PhMe})]$  can be best described as distorted trigonal bipyramidal, where N(2),Cl(1),Cl(2) atoms make up the equatorial trigonal plane. The bond angles being close to ideal  $120^\circ$  for trigonal (Table 58.), which is the same as what was observed for the analogous  $[\text{ZnCl}_2(\text{L}^1\text{R})]$  complexes. On the other hand the copper complex exhibits a rather more distorted geometry, which is in between that of trigonal-bipyramidal and square based-pyramidal, again similar to that observed for  $[\text{CuCl}_2(\text{L}^1\text{R})]$  complexes.

The tetradentate complex  $[\text{Zn}(\text{NO}_3)(\text{H}_2\text{O})(\text{L}^2\text{PhMe})][\text{NO}_3]$ , adopts what is best described as a distorted octahedral geometry, the distortion is controlled by the bite of the tetradentate N donor set of the bipyridine ligand, which make up a distorted square equatorial plane. The bite angles of the adjacent N donors to the metal are typically  $73-75^\circ$ , which is the same for the bite angle in the terdentate zinc complexes. The ligands  $\text{H}_2\text{O}$  and O bound  $\text{NO}_3^-$  (unidentate) make up the apical positions of the octahedron,

which also give a very distorted axial bond angle [O(1)-Zn-O(2) = 149.61°] which is far from the ideal 180° bond angle of an octahedral complex.

## 7. Biological Evaluations

### 7.1. Determination of *in vitro* Toxicity of Schiff Base Complexes Against a Panel of Human Tumour Cell Lines.

The purpose of this research was to build on from earlier discoveries at Bradford University that demonstrated the particular class of Schiff base metal complex in this study showed high affinity for binding to DNA<sup>26</sup> and also because of their similar chemistry to known metallopharmaceuticals. By assessing the *in vitro* toxicity of the prepared library of complexes against human tumour cells in a chemosensitivity assay it has been possible to identify if this class of complex show any cytotoxic response.

In this section is reported the mean dose response curves and IC<sub>50</sub> values obtained for each compound, following 6 days exposure (and 1 hour exposure of selected compounds) to each of the cell lines DLD-1, H460 and HT29 (Only a handful of compounds were tested against HT29 cells due to time constraints and problems with infection of these cells). The curves were generated as explained in section 2.2.1 and each represent the mean data from 3 independent assays  $\pm$  SD unless otherwise stated.

All of the drugs tested exhibited classical dose response curves. At low drug concentrations, there was little variation from the control in terms of percentage cell survival. As the drug concentration was gradually increased, the effect on percentage cell survival became more pronounced, with survival decreasing with increasing drug concentration. At concentrations which were considerably greater than the determined IC<sub>50</sub> value, the percentage of cells surviving after 6 day drug exposure was low. The only exceptions to the classical dose response curves was compounds tested with 1 hour

exposure times, where in all but one case negligible effect on the cell population was observed in the concentration range of this study.

All compounds displayed a wide range of  $IC_{50}$  values against the three cell lines, with the majority of the compounds having lower  $IC_{50}$  values against, and thus being more toxic towards the HT29 cell lines (some exceptions observed). No complexes showed enhanced potency to that of the benchmark test compound cisplatin, but some interesting responses were observed against HT29 cells for some complexes.

## 7.1.1. Variation of Ligand 'Tail' Group

### 7.1.1.1. Cobalt<sup>II</sup>chloride Complexes of Ligand L<sup>1</sup>R

**Figure 72.** Plots show the response of DLD-1, H460, HT29 cells following 6 day drug exposure to Cobalt<sup>II</sup>chloride complexes of L<sup>1</sup>R with cisplatin and Cobalt<sup>II</sup>chloride curves shown for comparison. Each point represents the mean of three independent experiments.

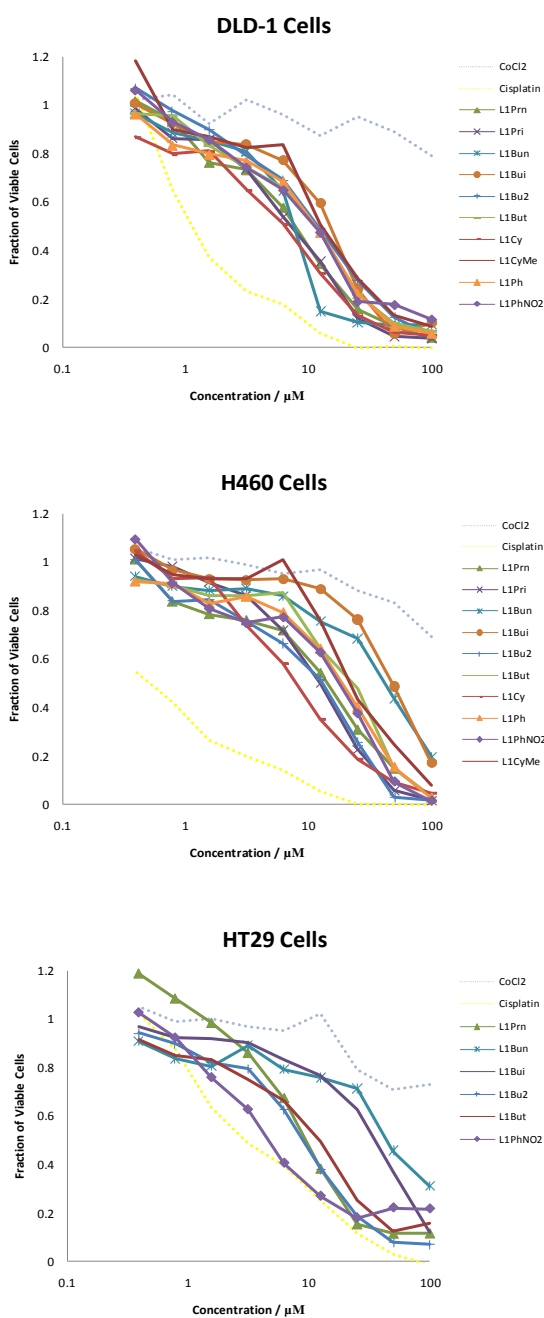




**Table 36.** Cytotoxic activity of Cobalt<sup>II</sup>chloride complexes, expressed as their mean IC<sub>50</sub> values in  $\mu\text{M}$  for three independent experiments,  $\pm$  standard deviation in brackets.

Compound	IC <sub>50</sub> $\mu\text{M}$				cLogP of Ligand
	DLD-1	H460	HT29	1Hr Exposure DLD-1	
Cisplatin	1.08 (0.05)	0.52 (0.05)	2.6 (0.6)	2.5 (0.5)	-
[CoCl <sub>2</sub> (L <sup>1</sup> Et)]	not isolated	not isolated	-	-	2.63
[CoCl <sub>2</sub> (L <sup>1</sup> Pr <sup>n</sup> )]	7.9 (1.1)	15.0 (3.8)	-	-	3.6
[CoCl <sub>2</sub> (L <sup>1</sup> Pr <sup>i</sup> )]	7.2 (0.4)	14.6 (2.3)	9.25 (1.1)	-	3.27
[CoCl <sub>2</sub> (L <sup>1</sup> Bu <sup>n</sup> )]	7.5 (1.8)	41.8 (4.5)	53.5 (22)	-	4.44
[CoCl <sub>2</sub> (L <sup>1</sup> Bu <sup>2</sup> )]	5.6 (0.4)	13.3 (1.3)	13.8 (2.5)	-	4.24
[CoCl <sub>2</sub> (L <sup>1</sup> Bu <sup>i</sup> )]	15.3 (3.1)	48.1 (10.5)	41.0 (12.8)	-	4.4
[CoCl <sub>2</sub> (L <sup>1</sup> Bu <sup>r</sup> )]	10.9 (3.7)	23.1 (3.1)	12.0 (4.1)	-	3.7
[CoCl <sub>2</sub> (L <sup>1</sup> Cy)]	6.4 (0.5)	8.0 (1.2)	-	>100	5.05
[CoCl <sub>2</sub> (L <sup>1</sup> CyMe)]	12.7 (n=1)	21.2 (n=1)	-	-	5.71
[CoCl <sub>2</sub> (L <sup>1</sup> Ph)]	11.6 (0.9)	23.0 (1.8)	-	>100	5.28
[CoCl <sub>2</sub> (L <sup>1</sup> PhMe)]	hydrolyses	hydrolyses	hydrolyses	-	6.25
[CoCl <sub>2</sub> (L <sup>1</sup> PhCl)]	insoluble	insoluble	insoluble	-	6.4
[CoCl <sub>2</sub> (L <sup>1</sup> PhNO <sub>2</sub> )]	11.4 (0.3)	16.7 (3.8)	4.9 (1.9)	-	3.68

It was possible to test nearly all but a few of the cobalt complexes prepared in this study. The troublesome ones were namely [CoCl<sub>2</sub>(L<sup>1</sup>PhMe)] which hydrolyses to precipitate free ligand on dissolution in water and could not be tested on these grounds. The toxicity data for complex [CoCl<sub>2</sub>(L<sup>1</sup>PhCl)] was unobtainable due to its insolubility in aqueous and DMSO. All complexes showed moderate toxicity toward their cell lines (Figure 72 and Table 36) with a general cell line selectivity DLD-1 > HT29  $\geq$  H460, which is roughly the inverse of cisplatin selectivity towards these three cell lines. The average toxicities towards DLD-1, H460 and HT29 cells was 9.7, 22.5 and 22.4  $\mu\text{M}$  respectively.

There was no blatant relationship observed for any of the complexes in relation to structure and activity i.e. no trend with steric bulk,<sup>191</sup> +I, -I effects,<sup>192</sup> etc since the

complexes tended to have  $IC_{50}$ 's within the same order of magnitude and the scatter and standard deviation of some mean values was quite large (this was also observed for all metal salts of ligand  $L^1$ ).

The most potent complex of this series appeared to come from the  $L^1Cy$  and  $L^1Bu^2$  ligands with  $IC_{50}$ 's of 6.4 and 5.6  $\mu M$  respectively towards DLD-1 cells, which was in the same order of magnitude as cisplatin toxicity (1.08  $\mu M$ ). More interestingly the toxicity of the complex  $[CoCl_2(L^1PhNO_2)]$  (4.9  $\mu M$ ) is merely two fold higher than that of cisplatin toward the HT29 cell line and for this complex the selectivity toward the three cell lines changes to what is typically observed for the other complexes.

None of the complexes tested showed any acute toxicity after 1 hour exposure toward DLD-1 cells. As a control experiment  $CoCl_2$  showed no toxicity in the concentration range used for this series. (This control was utilised for all metal salts and cell lines and identifies that the ligand is essential for the observed toxicities of these complexes).

### 7.1.1.2. Nickel<sup>II</sup>chloride Complexes of L<sup>1</sup>R

**Figure 73.** Plots showing the response of DLD-1, H460, HT29, cells following 6 day drug exposure to Nickel<sup>II</sup>chloride complexes of L<sup>1</sup>R with cisplatin and Nickel<sup>II</sup>chloride curves shown for comparison. Each point represents the mean of three independent experiments.

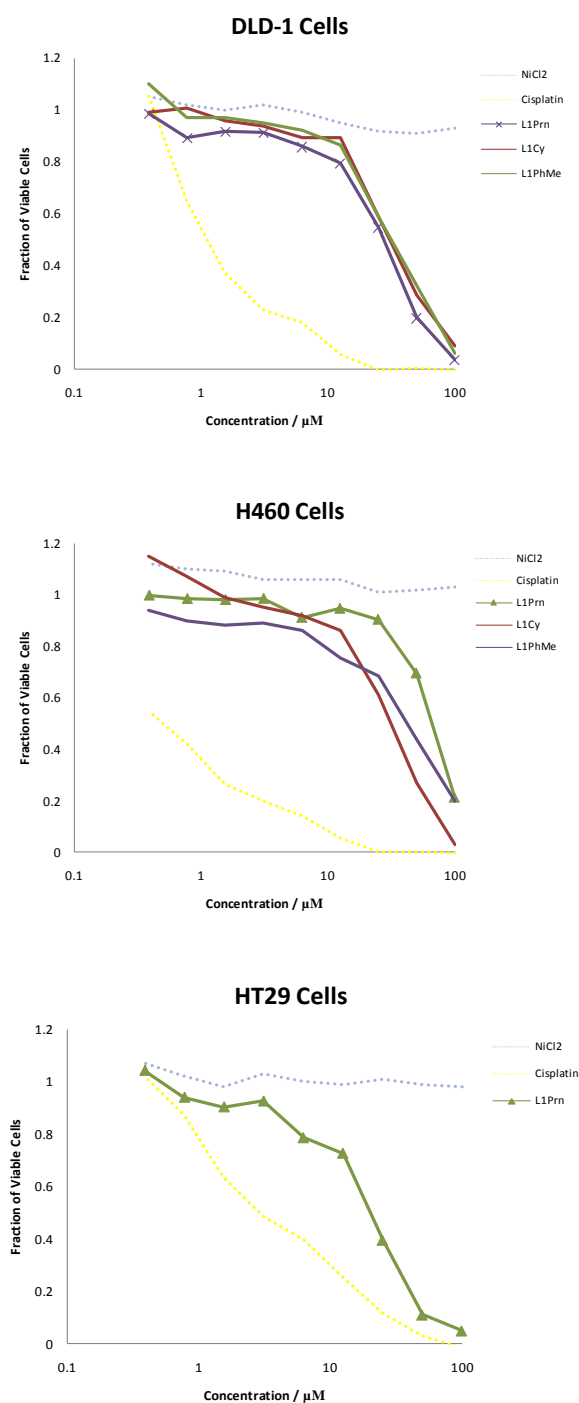


**Table 37.** Cytotoxic activity of Nickel<sup>II</sup>chloride complexes, expressed as their mean IC<sub>50</sub> values in  $\mu\text{M}$  for three independent experiments,  $\pm$  standard deviation in brackets.

Compound	IC <sub>50</sub> $\mu\text{M}$				cLogP of Ligand
	DLD-1	H460	HT29	1Hr Exposure DLD-1	
Cisplatin	1.08 (0.05)	0.52 (0.05)	2.6 (0.6)	2.5 (0.5)	-
[NiCl <sub>2</sub> (L <sup>1</sup> Pr <sup>n</sup> )]	27.2 (6.2)	70.4 (15.4)	20.1 (0.4)	>100	3.6
[NiCl <sub>2</sub> (L <sup>1</sup> Cy)]	34 (2.4)	31.9 (6.3)	-	>100	5.05
[NiCl <sub>2</sub> (L <sup>1</sup> PhMe)]	35.2 (5.3)	40.2 (6.1)	-	>100	6.25

Only a small number of Nickel complexes were tested due to the small number of Nickel complexes prepared in this study and also because of their low solubility. Looking at Figure 73 there was no obvious trend in activity with this class of ligand, virtually all toxicities were similar and within the same order of magnitude. Complexes were moderately toxic to all cell lines but were relatively distant from the values of cisplatin (at least greater than 10 fold, see Table 37). The most potent complex was that of [NiCl<sub>2</sub>(L<sup>1</sup>Pr<sup>n</sup>)] which showed an IC<sub>50</sub> of 20.1  $\mu\text{M}$  towards HT29 cells but strangely showed a much larger value of 70.4  $\mu\text{M}$  against H460 cells which seems pretty anomalous looking at the values of the related compounds toward the same cell lines. The selectivity of the complexes toward the different cell lines also cannot be easily drawn out since all IC<sub>50</sub> values are in a similar range.

Not surprisingly the Nickel complexes of this series did not show any acute toxicity toward DLD-1 cell lines.

### 7.1.1.3. Copper<sup>II</sup>chloride Complexes of L<sup>1</sup>R

**Figure 74.** Plots showing the response of DLD-1, H460, HT29, cells following 6 day drug exposure to Copper<sup>II</sup>chloride complexes of L<sup>1</sup>R with cisplatin and Copper<sup>II</sup>chloride curves shown for comparison. Each point represents the mean of three independent experiments.

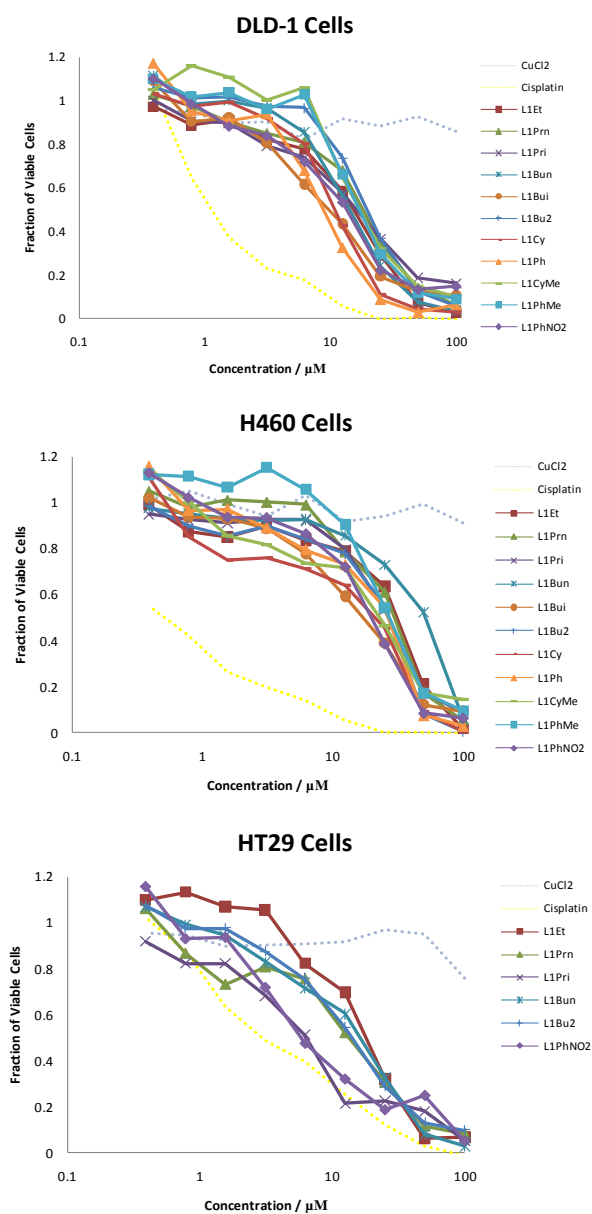


**Table 38.** Cytotoxic activity of Copper<sup>II</sup>chloride complexes, expressed as their mean IC<sub>50</sub> values in  $\mu\text{M}$  for three independent experiments,  $\pm$  standard deviation in brackets.

Compound	IC <sub>50</sub> $\mu\text{M}$				cLogP of Ligand
	DLD-1	H460	HT29	1Hr Exposure DLD-1	
Cisplatin	1.08 (0.05)	0.52 (0.05)	2.6 (0.6)	2.5 (0.5)	-
[CuCl <sub>2</sub> (L <sup>1</sup> Et)]	14.8 (4.0)	27.1 (8.1)	17.6 (2.3)	-	2.63
[CuCl <sub>2</sub> (L <sup>1</sup> Pr <sup>n</sup> )]	18.2 (2.0)	31.1 (5.3)	26.5 (2.7)	>100	3.6
[CuCl <sub>2</sub> (L <sup>1</sup> Pr <sup>i</sup> )]	16.5 (5.5)	32.6 (4.1)	7.3 (4.0)	-	3.27
[CuCl <sub>2</sub> (L <sup>1</sup> Bu <sup>n</sup> )]	11.8 (1.3)	52.7 (6.8)	16.6 (n=1)	-	4.44
[CuCl <sub>2</sub> (L <sup>1</sup> Bu <sup>2</sup> )]	19.6 (3.6)	27.1 (1.8)	19.8 (14.4)	-	4.24
[CuCl <sub>2</sub> (L <sup>1</sup> Bu <sup>i</sup> )]	9.8 (1.0)	17.3 (0.4)	-	-	4.4
[CuCl <sub>2</sub> (L <sup>1</sup> Bu <sup>t</sup> )]	not isolated	not isolated	not isolated	-	3.7
[CuCl <sub>2</sub> (L <sup>1</sup> Cy)]	10.0 (1.7)	21.8 (0.7)	-	-	5.05
<i>racemic</i> - [CuCl <sub>2</sub> (L <sup>1</sup> CyMe)]	16.7 (0.7)	22.9 (2.8)	-	-	5.71
[CuCl <sub>2</sub> (L <sup>1</sup> Ph)]	8.8 (0.4)	27 (1.5)	-	>100	5.28
[CuCl <sub>2</sub> (L <sup>1</sup> PhMe)]	16.6 (0.5)	27.2 (1.3)	-	-	6.25
[CuCl <sub>2</sub> (L <sup>1</sup> PhCl)]	insoluble	insoluble	insoluble	-	6.4
[CuCl <sub>2</sub> (L <sup>1</sup> PhNO <sub>2</sub> )]	11.9 (5.7)	24.7 (2.6)	6.2 (2.2)	-	3.68

Almost all copper complexes prepared in this series were tested against the cell panel, the exception being the [CuCl<sub>2</sub>(L<sup>1</sup>PhCl)] complex which is analogous to the [CoCl<sub>2</sub>(L<sup>1</sup>PhCl)] complex in both ligand and solubility properties. Clearly this particular ligand must provide the incorrect chemistry for this class of complex to achieve any solubility in DMSO or water.

Again no clear trend in cytotoxicity is observed within this series of complex since the IC<sub>50</sub> values are very similar for all three cell lines with a few exceptions (Figure 74 and Table 38). The most potent complexes being the aromatic complexes [CuCl<sub>2</sub>(L<sup>1</sup>Ph)] (8.8  $\mu\text{M}$ , DLD-1) and [CuCl<sub>2</sub>(L<sup>1</sup>PhNO<sub>2</sub>)] (6.2  $\mu\text{M}$ , HT29). The general order of selectivity toward the cell panel for the majority of complexes was HT29 $\approx$ DLD-1>H460, with averages of 15.7, 14.0, and 28.3  $\mu\text{M}$  respectively.

The acute toxicity of this series of complexes was  $>100\mu\text{M}$  showing the complexes are slow working, especially when compared to cisplatin ( $2.5\ \mu\text{M}$ ) after a 1 hour exposure.

#### 7.1.1.4. Zinc<sup>II</sup>chloride Complexes of L<sup>1</sup>R

**Figure 75.** Plots showing the response of DLD-1, H460, HT29, cells following 6 day drug exposure to Zinc<sup>II</sup>chloride complexes of L<sup>1</sup>R with cisplatin and Zinc<sup>II</sup>chloride curves shown for comparison. Each point represents the mean of three independent experiments.

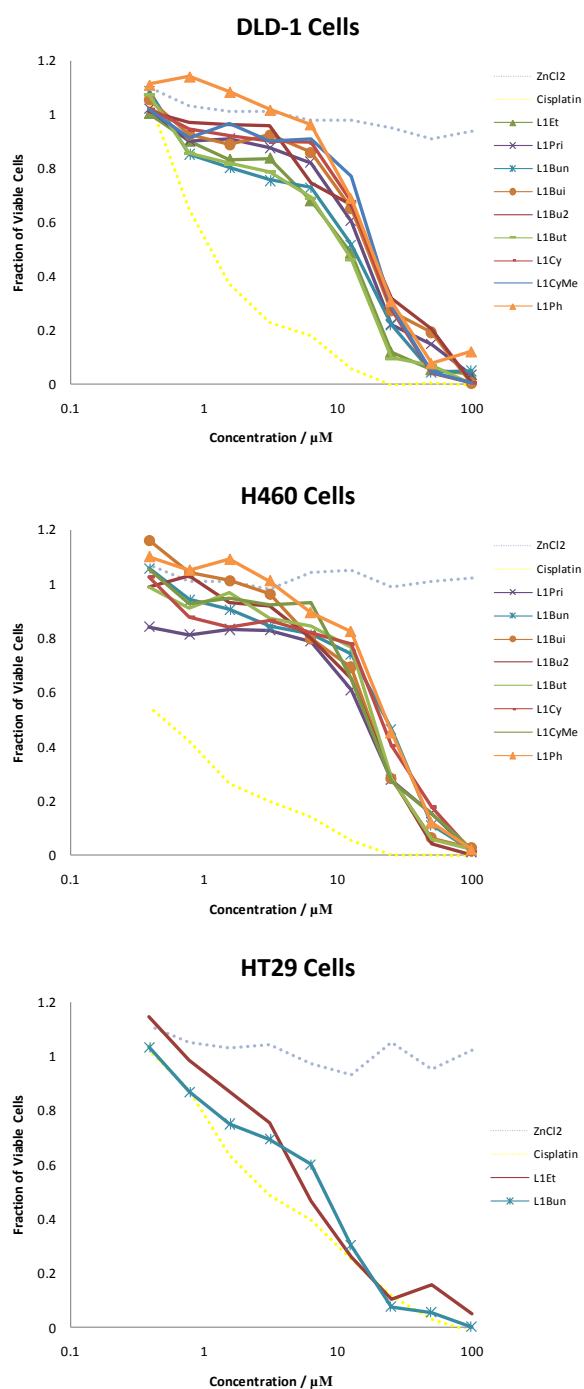




**Table 39.** Cytotoxic activity of Zinc<sup>II</sup>chloride complexes, expressed as their mean IC<sub>50</sub> values in  $\mu\text{M}$  for three independent experiments,  $\pm$  standard deviation in brackets.

Compound	IC <sub>50</sub> $\mu\text{M}$				cLogP of Ligand
	DLD-1	H460	HT29	1Hr Exposure DLD-1	
Cisplatin	1.08 (0.05)	0.52 (0.05)	2.6 (0.6)	2.5 (0.5)	
[ZnCl <sub>2</sub> (L <sup>1</sup> Et)]	11.5 (3.9)	17.6 (6.6)	6.5 (3.0)	>100	2.63
[ZnCl <sub>2</sub> (L <sup>1</sup> Pr <sup>n</sup> )]	insoluble	insoluble	insoluble	-	3.6
[ZnCl <sub>2</sub> (L <sup>1</sup> Pr <sup>i</sup> )]	15.16 (0.8)	15.8 (0.1)	-	-	3.27
[ZnCl <sub>2</sub> (L <sup>1</sup> Bu <sup>n</sup> )]	13.4 (3.6)	15.2 (2.9)	8.3 (1.7)	-	4.44
[ZnCl <sub>2</sub> (L <sup>1</sup> Bu <sup>2</sup> )]	16.4 (2.1)	16.5 (1.9)	-	-	4.24
[ZnCl <sub>2</sub> (L <sup>1</sup> Bu <sup>i</sup> )]	16.4 (0.1)	17.5 (2.3)	-	-	4.4
[ZnCl <sub>2</sub> (L <sup>1</sup> Bu <sup>t</sup> )]	11.5 (1.7)	18.3 (3.1)	-	>100	3.7
[ZnCl <sub>2</sub> (L <sup>1</sup> Cy)]	16.7 (1.2)	20.8 (2.7)	-	-	5.05
<i>racemic</i> - [ZnCl <sub>2</sub> (L <sup>1</sup> CyMe)]	18.6 (3.0)	16.3 (3.0)	-	-	5.71
[ZnCl <sub>2</sub> (L <sup>1</sup> Ph)]	17.4 (1.1)	22.7 (2.0)	-	>100	5.28
[ZnCl <sub>2</sub> (L <sup>1</sup> PhMe)]	insoluble	insoluble	insoluble	-	6.25
[ZnCl <sub>2</sub> (L <sup>1</sup> PhCl)]	insoluble	insoluble	insoluble	-	6.4
[ZnCl <sub>2</sub> (L <sup>1</sup> PhNO <sub>2</sub> )]	insoluble	insoluble	insoluble	-	3.68

All water/DMSO soluble complexes of this series were tested against DLD-1 and H460 cell lines with only two complexes tested against HT29. All but one of the aromatic complexes was insoluble in DMSO or water and so could not be tested.

From Figure 75, it is clear the mass of lines intersect the 50% population mark at similar concentrations and therefore no trend is apparent from the data observed, all complexes are moderately toxic against DLD-1 and H460 cell lines with slightly greater potency toward the HT29 cell line (average IC<sub>50</sub> for all complexes 15.2, 17.9 and 7.4  $\mu\text{M}$  respectively, see Table 39). The selectivity of the complexes toward the three cell panel is generally in the order HT29>DLD-1 $\approx$ H460. The most toxic complex appearing to be [ZnCl<sub>2</sub>(L<sup>1</sup>Et)], with its highest potency 6.5  $\mu\text{M}$  against HT29 cells which is merely 2.5

fold more than that of cisplatin (2.6  $\mu$ M). The zinc complexes of this series also showed no acute toxicity toward DLD-1 cell lines.

#### **7.1.1.5. General Observations**

There are clearly no significant differences in IC<sub>50</sub> values and no particular structure activity trends associated with the ligand observed for the dichloride metal salts. All complexes show approximately two fold selectivity towards DLD-1 cell lines than toward the H460 cell line, with the exception of nickel and zinc complexes where the values are comparable, and most complexes were more selective towards the HT29 cells. In general most IC<sub>50</sub> values against all cell lines were within the same order of magnitude and the initial presumption is that these complexes show little selectivity towards a particular cell line. Although this is only a presumption from the results obtained here and more tests against a wider array of cell lines would need to be carried out to fully identify the selectivity of this class of compound. However the limited selectivity data obtained from this screen indicates a reversal in selectivity to that shown by cisplatin. This would suggest these complexes are not working in an analogous manner to cisplatin and another mechanism must be at play.

Because these compounds show little difference in activity between ligand groups, it is most likely that the complexes (of the same metal salt) are working by a similar mechanism. Since it has been shown the ligand is essential for the activity, a control experiment to obtain the cytotoxic activity of the free ligand would have been desirable to show the metal and ligand are both required for activity but unfortunately the free ligands were insoluble in DMSO and water. Although it was not possible to obtain the IC<sub>50</sub> values of the free ligand due to their very poor solubilities, the fact there is a

difference between the different metal chloride complexes of the same ligands does suggest the metal and ligand both contribute to the toxicity observed.

### 7.1.2. Variation of Metal

**Figure 76.** Plots showing the response of DLD-1, H460, cells following 6 day drug exposure and DLD-1 cells following 1 hour exposure to Metal<sup>n+</sup>chloride complexes of L<sup>1</sup>R with cisplatin curve shown for comparison. Each point represents the mean of three independent experiments.

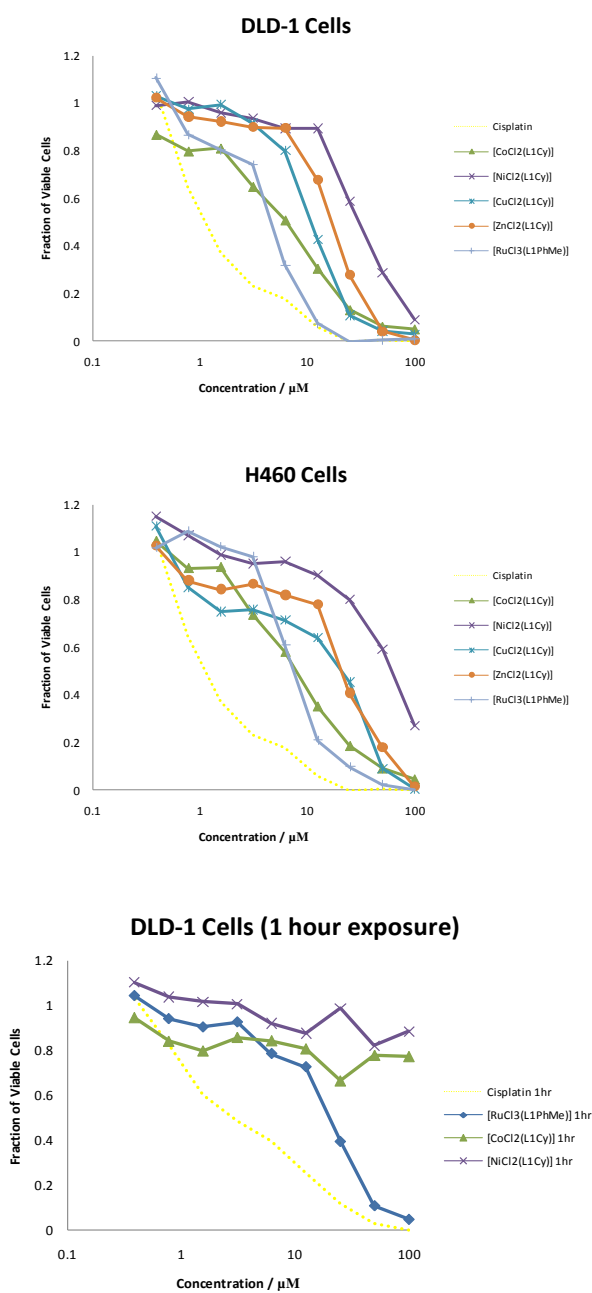


**Table 40.** Cytotoxic activity of metal<sup>n+</sup>chloride complexes of L<sup>1</sup>Cy and L1PhMe for Ru<sup>III</sup>. Values are expressed as their mean IC<sub>50</sub> values in μM for three independent experiments ± standard deviation in brackets.

Compound	IC <sub>50</sub> μM		
	DLD-1	H460	1Hr Exposure DLD-1
Cisplatin	1.08 (0.05)	0.52 (0.05)	2.5 (0.5)
[RuCl <sub>3</sub> (L <sup>1</sup> PhMe)]	4.6 (0.7)	7.5 (1.2)	20.4 (3.5)
[CoCl <sub>2</sub> (L <sup>1</sup> Cy)]	6.4 (0.5)	8.0 (1.2)	>100
[CuCl <sub>2</sub> (L <sup>1</sup> Cy)]	10.0 (1.7)	21.8 (0.7)	-
[ZnCl <sub>2</sub> (L <sup>1</sup> Cy)]	16.7 (1.2)	20.8 (2.7)	-
[NiCl <sub>2</sub> (L <sup>1</sup> Cy)]	34.0 (2.4)	31.9 (6.3)	>100

Other than changing the ligand properties, a simple approach was to change the metal centre to identify which, (if any) metal would produce the most toxic species. The metals chosen in this study were the late first row transition metals. The metals Co<sup>II</sup>, Ni<sup>II</sup>, Cu<sup>II</sup> and the non transition metal Zn<sup>II</sup> were utilised in this study and the IC<sub>50</sub> values for their dichloride complexes of ligand L<sup>1</sup>Cy are given in Table 40, along with the complex [RuCl<sub>3</sub>L<sup>1</sup>PhMe] and cisplatin for comparison. Figure 76 shows more distance between profiles than for complexes of the same metal salt. None of the complexes can better cisplatin for its cytotoxic potency against DLD-1 and H460 cell lines, though the most potent of the series was [RuCl<sub>3</sub>(L<sup>1</sup>PhMe)], being ~5 times less toxic to the DLD-1 cell line and ~14 times less toxic to the H460 cell line than cisplatin. The remaining first row complexes showed moderate toxicity to the two cell lines. The chemosensitivity data show toxicities in the order Ru<sup>III</sup> ≈ Co<sup>II</sup> > Cu<sup>II</sup> ≈ Zn<sup>II</sup> > Ni<sup>II</sup>, with Cu<sup>II</sup> and Zn<sup>II</sup> having comparable values, with their toxicities towards the H460 cell line within experimental error the same 21.8 and 20.8 μM respectively, but towards the DLD-1 cell line Cu<sup>II</sup> shows slightly higher toxicity 10.0 μM, where Zn<sup>II</sup> is 16.7 μM. Co<sup>II</sup>, was shown also to

have not too dissimilar values to the Ru<sup>III</sup> complex, being the most potent complexes of this series, their H460 cell toxicities of 7.5 and 8.0 μM for the Ru<sup>III</sup> and Co<sup>II</sup> complexes respectively, again being within experimental error of each other. The least potent metal, Ni<sup>II</sup>, was some 7.6 times less toxic than Ru<sup>III</sup> towards DLD-1 cells, and 4.3 times less toxic than Ru<sup>III</sup> and Co<sup>II</sup> towards H460 cells, though the complexes were still moderately toxic at 34.0 and 31.9 μM, against the DLD-1 and H460 cells lines respectively.

The observations for complexes [MCl<sub>2</sub>(L<sup>1</sup>Cy)] are also true for the average values of all ligands with the exception of H460 cells where Zn<sup>II</sup> shows the greatest potency for the first row transition metals (Table 41). When the HT29 average is introduced the order is reversed from DLD-1 selectivity to Zn<sup>II</sup>>Cu<sup>II</sup>>Ni<sup>II</sup>≈Co<sup>II</sup>, it must be noted however this series is an approximation from the results obtained.

**Table 41.** Average Cytotoxic activity of metal<sup>n+</sup> chloride complexes of L<sup>1</sup>R.

Compound	IC <sub>50</sub> μM		
	DLD-1	H460	HT29
Cisplatin	1.08 (0.05)	0.52 (0.05)	2.6 (0.6)
[CoCl <sub>2</sub> (L <sup>1</sup> R)]	9.7	22.5	22.4
[NiCl <sub>2</sub> (L <sup>1</sup> R)]	32	47.5	20.1
[CuCl <sub>2</sub> (L <sup>1</sup> R)]	14.0	28.3	15.7
[ZnCl <sub>2</sub> (L <sup>1</sup> R)]	15.2	17.9	7.4

Unfortunately for this series of complexes the results of a 1 hour exposure to the full panel of cell lines were not obtained and just a handful of complexes were tested for their acute toxicities against DLD-1 cell lines. In Table 40 the acute toxicities, (in the form of a 1 hour exposure), are reported for a few complexes of each metal complex. It is clear that none of the first row transition metal complexes show any acute toxicity

toward the two cell lines to which they were exposed, with none showing any cell kill in the concentration range used for this assay. However  $[\text{RuCl}_3(\text{L}^1\text{PhMe})]$  interestingly exhibited moderate potency (20.4  $\mu\text{M}$ ) in a 1 hour exposure to DLD-1 cells, which although it is 10 fold to that of cisplatin this result shows promise. It could also be a reasonable assumption that the mechanism could be associated with DNA alkylation, since those complexes that bind to DNA would remain within the cellular compartments upon washing after the 1 hour exposure, (see experimental), whereas those complexes that do not bind, are more likely be washed out in the media and have a lower concentration intracellularly. The bound complexes could then still carry out their cytotoxic effect. Therefore the acute toxicities would be controlled by the DNA binding affinities of the complexes and the cells ability to process the DNA in their presence. This is also corroborated by an observation made during the experiment. It was visually observed that after washing the cells after a 1 hour exposure to  $[\text{RuCl}_3(\text{L}^1\text{PhMe})]$  a deep red colour remained within the cellular mass which followed an intensity proportional to the concentration gradient.

The fact that the acute toxicities of the first row complexes are nowhere near the values for their longer exposure, implies that these complexes do not work via a DNA alkylating mechanism, or at least if they do, their DNA binding is particularly labile and can be processed easily by the cellular repair mechanism's, or their cell membrane permeabilities are poor. So if it is likely that these first row complexes are not operating via a DNA binding mechanism or at least a co-ordinating mechanism to produce macromolecular dysfunctions, how else can they produce their cytotoxic activity?

One explanation to this could be that they may act via a redox mechanism. The metals, could perhaps get into the cells and enter a catalytic redox cycling, which could lead to the production of reactive oxygen species and inevitably cause oxidative stress within the cellular environment. The oxidative stress could lead to all sorts of disruptions to cellular processes; one in particular would be DNA damage by the radical species produced during oxidative stress. But however, if this hypothesis were to be true, why do the redox inactive  $Zn^{II}$  complexes show comparable toxicities to the redox active complexes of  $Co^{II}$  and  $Cu^{II}$ ? The answer to this could be that either the complexes all work by the same mechanism that does not involve a redox process, or that the  $Zn^{II}$  complexes work via a different mechanism. This latter statement could be a reasonable one and is weakly supported when considering the average toxicities from Table 41 since  $Zn^{II}$  complexes show a selectivity to the three cell lines in the order  $DLD-1 \approx H460 < HT29$ , whereas the  $Co^{II}$   $Ni^{II}$  and  $Cu^{II}$  complexes seem to have a similar selectivity profile being approximately  $DLD-1 \geq HT29 > H460$  for the most of the complexes in each series. However this explanation is by no means exclusive.



### 7.1.3. Variation of Anion

**Figure 77.** Plots showing the response of DLD-1, H460, HT29, cells following 6 day drug exposure to  $\text{CoX}_2$  complexes of  $\text{L}^1\text{R}$  with cisplatin and curve shown for comparison. Each point represents the mean of three independent experiments.

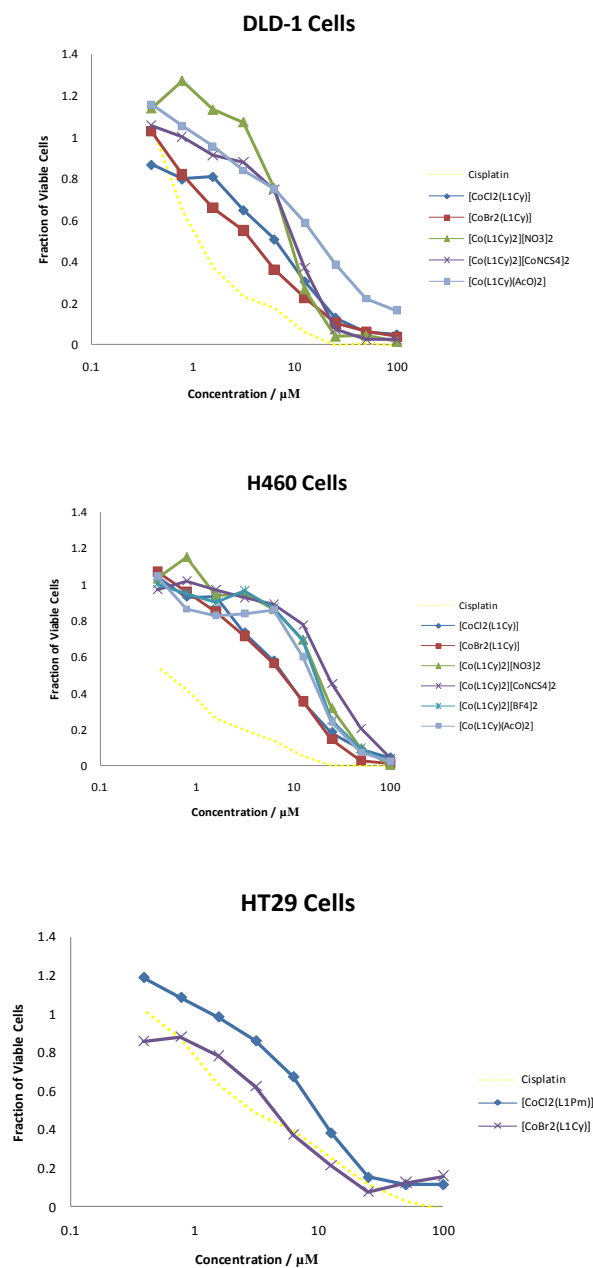


**Figure 78.** Plots showing the response of DLD-1, H460, HT29, cells following 6 day drug exposure to NiX<sub>2</sub> complexes of L<sup>1</sup>R with cisplatin and curve shown for comparison. Each point represents the mean of three independent experiments.

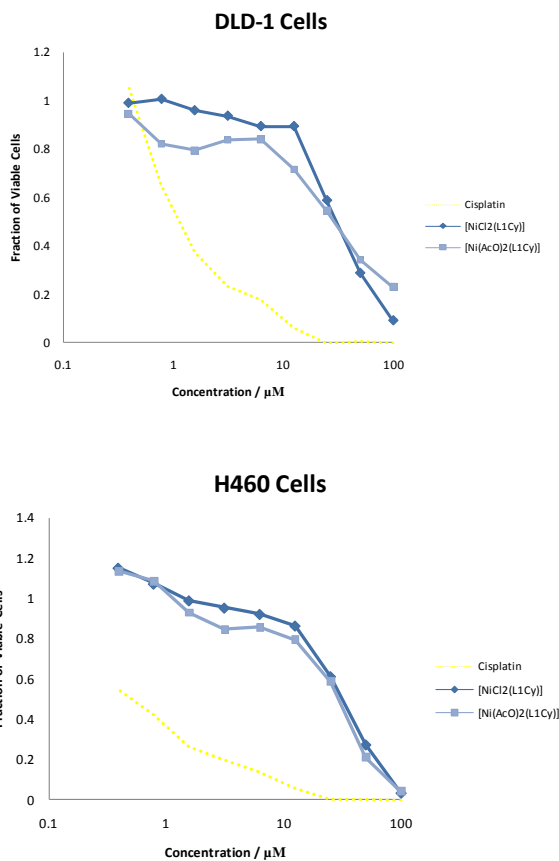


**Figure 79.** Plots showing the response of DLD-1, H460, HT29, cells following 6 day drug exposure to  $\text{CuX}_2$  complexes of  $\text{L}^1\text{R}$  with cisplatin and curve shown for comparison. Each point represents the mean of three independent experiments.

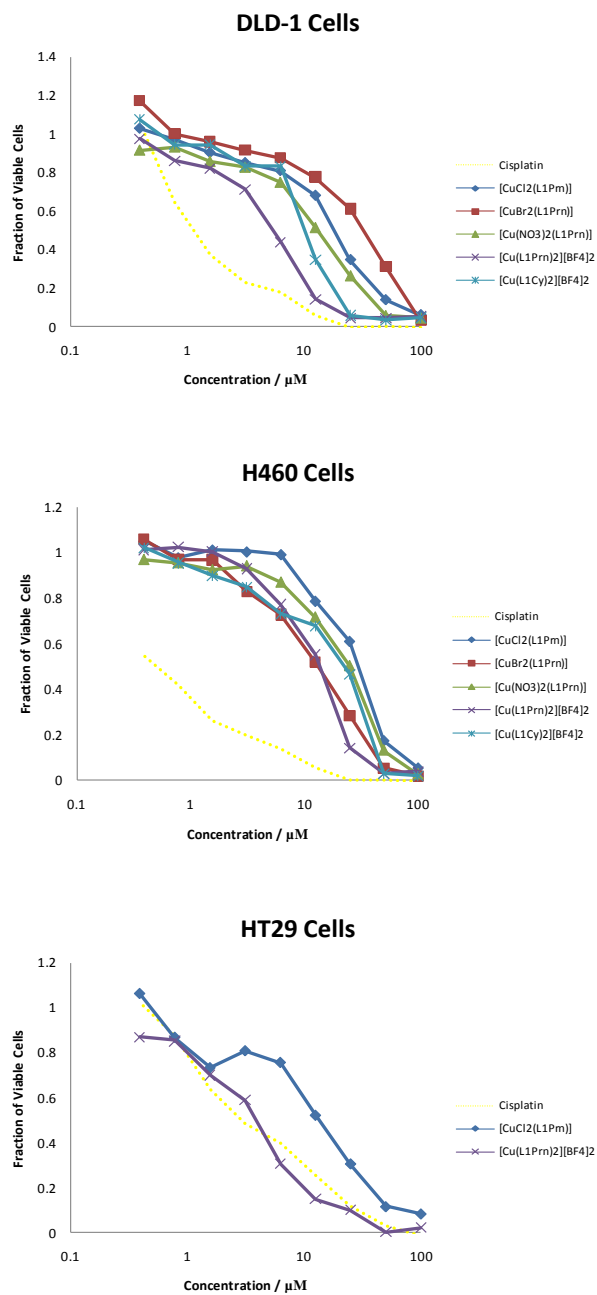


**Figure 80.** Plots showing the response of DLD-1, H460, HT29, cells following 6 day drug exposure to  $ZnX_2$  complexes of  $L^1R$  with cisplatin and curve shown for comparison. Each point represents the mean of three independent experiments.

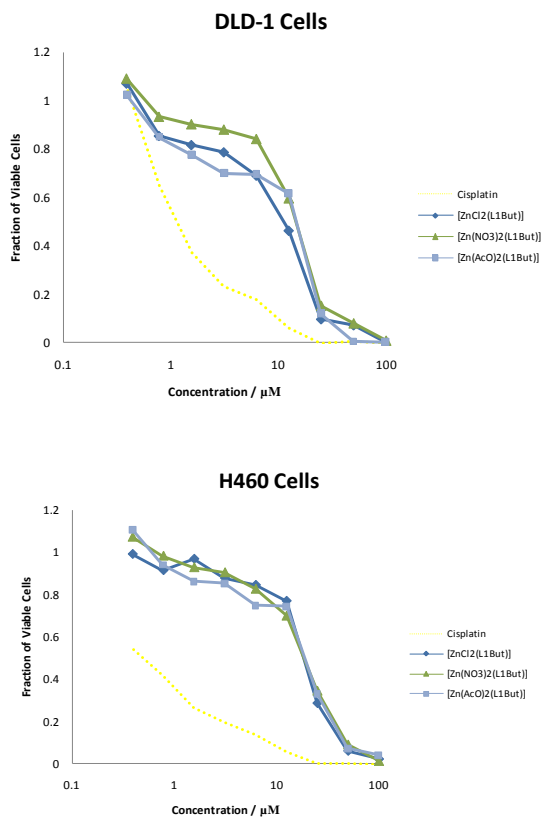


**Table 42.** Average Cytotoxic activity of MX<sub>2</sub> complexes of L<sup>1</sup>R, expressed as their mean IC<sub>50</sub> values in μM for three independent experiments ± standard deviation in brackets.

	Compound	IC <sub>50</sub> μM		
		DLD-1	H460	HT29
	Cisplatin	1.08 (0.05)	0.52 (0.05)	2.6 (0.6)
Copper	[CuCl <sub>2</sub> (L <sup>1</sup> Pr <sup>n</sup> )]	18.2 (1.8)	31.1 (5.3)	26.5 (2.7)
	[Cu(NO <sub>3</sub> ) <sub>2</sub> (L <sup>1</sup> Pr <sup>n</sup> )]	13.2 (3.0)	25.6 (7.7)	-
	[CuBr <sub>2</sub> (L <sup>1</sup> Pr <sup>n</sup> )]	16.3 (3.4)	15.2 (7.2)	-
	[Cu(L <sup>1</sup> Pr <sup>n</sup> ) <sub>2</sub> ][BF <sub>4</sub> ] <sub>2</sub>	5.4 (1.1)	13.8 (0.3)	4.0 (0.4)
	[Cu(L <sup>1</sup> Cy) <sub>2</sub> ][BF <sub>4</sub> ] <sub>2</sub>	10.0 (0.2)	22.9 (1.5)	-
Cobalt	[CoCl <sub>2</sub> (L <sup>1</sup> Cy)]	6.4 (0.5)	8.0 (1.2)	-
	[CoBr <sub>2</sub> (L <sup>1</sup> Cy)]	3.8 (0.2)	7.8 (0.3)	4.4 (0.4)
	[Co(AcO) <sub>2</sub> (L <sup>1</sup> Cy)]	16.8 (2.1)	30.3 (1.5)	-
	[Co(L <sup>1</sup> Cy) <sub>2</sub> ][Co(NCS) <sub>4</sub> ]*	9.8 (0.3)	22.5 (2.5)	-
	[Co(L <sup>1</sup> Cy) <sub>2</sub> ][NO <sub>3</sub> ] <sub>2</sub>	8.9 (0.9)	17.8 (2.0)	-
	[Co(L <sup>1</sup> Cy) <sub>2</sub> ][BF <sub>4</sub> ] <sub>2</sub>	8.4 (0.5)	16.9 (1.9)	-
Zinc	[ZnCl <sub>2</sub> (L <sup>1</sup> Bu <sup>1</sup> )]	11.5 (1.7)	18.3 (3.1)	-
	[Zn(NO <sub>3</sub> ) <sub>2</sub> (L <sup>1</sup> Bu <sup>1</sup> )]	14.7 (0.8)	18.5 (0.5)	-
	[Zn(AcO) <sub>2</sub> (L <sup>1</sup> Bu <sup>1</sup> )]	15.1 (2.5)	18.9 (1.5)	-
Nickel	[NiCl <sub>2</sub> (L <sup>1</sup> Cy)]	34.0 (2.4)	31.9 (6.3)	-
	[Ni(AcO) <sub>2</sub> (L <sup>1</sup> Cy)]	29.3 (1.8)	29.8 (1.3)	-

The third series of structural changes, involved the systematic variation of the metal salt used to prepare the complexes. The idea behind this was to incorporate a systematic variation in the anionic coordinating ligands around the metal centre, to produce complexes of the general formula [MX<sub>2</sub>(L<sup>1</sup>R)], (M = Co<sup>II</sup>, Ni<sup>II</sup>, Cu<sup>II</sup>, Zn<sup>II</sup>; R = aryl, alkyl group; X = anionic coordinating ligand), for a fixed R group. It was also possible to introduce anions of differing coordinating power and denticity, which could result in differences in coordination geometry about the metal centre. Using this concept and

based on structural reports of similar structures, several complexes with a ligand to metal stoichiometry of 2:1 were obtained with the general formula  $[M(L^1R)_2][X]_n$ , ( $M = Cu^{II}, Co^{II}$ ;  $R = \text{aryl, alky group}$ ;  $X = \text{spectator anion}$ ). The preparation of this class of compound provided an interesting addition to the structural variation of these complexes, namely coordinative saturation. Here the metals are now coordinatively saturated by the bis-terdentate pyridine Schiff base ligands, and would result in a greater chelative effect than for monodentate or bidentate ligands and so *in vivo* would provide less ability for binding to donor sites, since the metal is fully chelated and in the form of a stable complex. As mentioned in the introduction, the mechanism of cisplatin requires lability at the platinum centre, which is provided by hydrolysis, which can then facilitate DNA binding. Hydrolysis can only happen however, if there is a relatively labile ligand attached to the metal centre and in the case of cisplatin, chloride provides this prerequisite. So to back up the argument provided in the previous subsection that DNA binding is less likely to be involved in the mechanism, this class of complex could potentially provide the answer. If this class of complex could provide comparable toxicities to the cell lines as their analogous 1:1 complexes, then it could be argued that this class of complex does not deliver its toxicity through a DNA binding or for that fact any chelating mode of action.

If we look firstly at the cytotoxicity data for the complexes of type  $[CuX_2(L^1Pr^n)]$ , (where  $X = \text{acido ligand}$ ), we can observe no real difference in activity for the DLD-1 cell lines, and likewise we can also say the same is mostly true for the H460 cell line. However the bromide complex does show a lower value than the chloride and nitrate towards H460, but this value is pretty erroneous, with a standard deviation that could take it almost to within the values for the chloride and nitrate complexes. So for the

copper complexes we can conclude that for this class of compound, these particular coordinating anions have no effect on activity.

For the  $\text{Co}^{\text{II}}$  complexes of type  $[\text{CoX}_2(\text{L}^1\text{Cy})]$ , (where X = acido ligand), we can observe that the chloride and bromide have very similar  $\text{IC}_{50}$  values, which both are relatively potent with regard to the rest of the  $\text{IC}_{50}$  values observed so far. In fact the bromide complex is more active against DLD-1 cell lines than any other complex and shows an  $\text{IC}_{50}$  value 3.5 times less than cisplatin. The acetate complex however shows a marked difference in toxicity from the chloride and bromide complexes with a 2.6 fold higher  $\text{IC}_{50}$  toward DLD-1 than its analogous chloride complex and a 3.9 fold higher  $\text{IC}_{50}$  against H460. This order of activity resembles that of the spectrochemical series, which is also a good indicator for the order of stability:



Here the carboxylate ligand, which is kinetically less labile would be expected to show less activity if DNA binding was the mechanism of action for this compound class, since hydrolysis would be the activation step. However hydrolysis could also be the first step in formation of the bis complex (ligand:metal, 2:1), since the complex  $[\text{Co}(\text{L}^1\text{Cy})_2][\text{BF}_4]_2$ , was isolated by accident from an attempted aqueous ligand metathesis with  $\text{AgBF}_4$ . Which could then lead to the bis-complex being the active species *in vitro*, where a redox mechanism of action could be involved.

### 7.1.4. Variation of Ligand ‘Head’ Group

**Figure 81.** Plots A-C showing the response of DLD-1 (A), H460 (B) cells following 6 day drug exposure to Copper<sup>II</sup>chloride complexes of L<sup>1</sup>Bu<sup>i</sup> and L<sup>3</sup>Bu<sup>i</sup> with cisplatin curve shown for comparison. Each point represents the mean of three independent experiments.

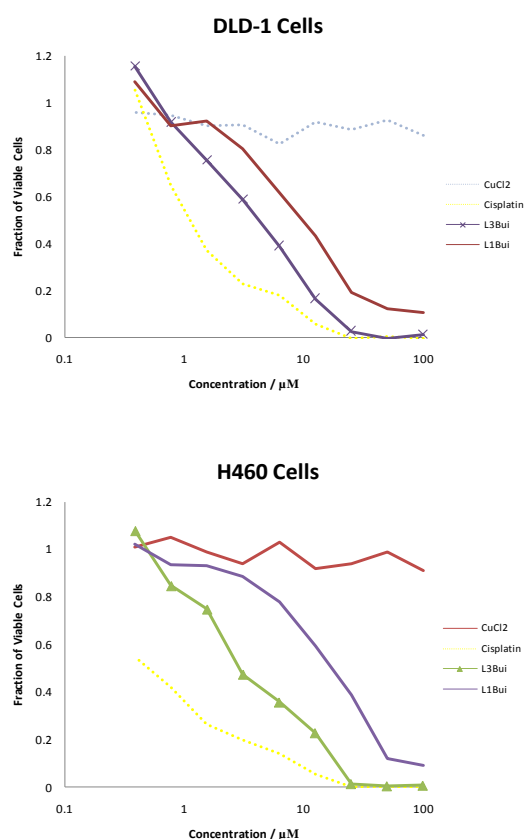


**Table 43.** Average Cytotoxic activity of Copper<sup>II</sup>chloride complexes of L<sup>1</sup>Bu<sup>i</sup> and L<sup>3</sup>Bu<sup>i</sup>, expressed as their mean IC<sub>50</sub> values in μM for three independent experiments ± standard deviation in brackets.

Compound	IC <sub>50</sub> μM		cLogP of Ligand	Selectivity Ratio DLD-1 : H460
	DLD-1	H460		
Cisplatin	1.08 (0.05)	0.52 (0.05)	-	2.07
[CuCl <sub>2</sub> (L <sup>3</sup> Bu <sup>i</sup> )]	4.3 (0.1)	2.9 (0.1)	4.26	1.5
[CuCl <sub>2</sub> (L <sup>1</sup> Bu <sup>i</sup> )]	9.8 (0.7)	17.3 (0.4)	4.4	0.6



The final series of complexes was not as comprehensive as had been hoped, owing to solubility issues of the  $L^2R$  and  $L^3R$  complexes. The  $IC_{50}$  data of only one complex of this ligand class was obtained, and even this is a maximum  $IC_{50}$  due to incomplete dissolution in DMSO to produce the stock solution prior to dilution. Therefore the  $IC_{50}$  value for this complex would actually be lower than the one stated in Table 43, but to what degree is unknown.

The concept of varying the ligand head group was for the intention that some structural and chemical features of the complexes could be systematically altered from one head group to another, (see section 1.9), and that correlations could hopefully be distinguished from the chemosensitivity assays. Because only one complex was able to be tested, this plan was not as successful. However the points raised from this single result are informative and somewhat intriguing.

Table 43, shows this lone result for  $[CuCl_2(L^3Bu^i)]$ , along with its  $L^1Bu^i$  analogue and cisplatin for comparison. Though only this single complex was able to be tested, it can be seen that its  $IC_{50}$  value is as toxic as any complex shown previously, and in fact was the most potent complex of the whole study.  $[CuCl_2(L^3Bu^i)]$ , is *Ca.* 4 fold less toxic to DLD-1 cell lines than cisplatin and *Ca.* 6 fold less toxic to H460 cell lines, these values show that this complex is not largely different from cisplatin in terms of cell line sensitivity.

The analogous  $[CuCl_2(L^1Bu^i)]$  complex is 2.3 fold less potent to the DLD-1 cell line than its  $L^3Bu^i$  analogue and 6 fold less toxic to H460 cells. Clearly the  $L^3$  complex has a more promising profile than any of the  $L^1R$  complexes. Not only does it show greater

cytotoxicity, but there is also a clear reversal in the selectivity toward the two cell lines compared to the  $L^1R$  complexes. Although the difference is not too significant, the complex  $[CuCl_2(L^3Bu^i)]$  has higher toxicity to H460 than to DLD-1. This difference in selectivity between cell lines, leads to the tentative conclusion that this complex cannot be acting by the same mechanism as with its  $L^1R$  analogues. The selectivity ratio toward H460 for  $[CuCl_2(L^3Bu^i)]$  is 1.5 and is closer to cisplatin with a ratio of 2.1 than it is to its  $L^1Bu^i$  analogue at 0.6. These figures may indicate that from the presumptions we have made so far and the facts we already know, that if  $L^1R$  complexes are not working via a DNA binding mechanism and that cisplatin does, then perhaps the H460 cell line is more chemosensitive to drugs whose mechanism of action is DNA binding than the DLD-1 cell line. It could then be argued that the  $L^3Bu^i$  complex could be working via a DNA binding mechanism owing to its selectivity toward the H460 cell line.

This conclusion bodes well with the initial rationale for altering the ligand head groups, which was to increase the planar aromatic portion and therefore enable intercalative capabilities. This could then afford a foothold to covalent binding of the metal centre and as a result lead to cellular dysfunctions and ultimately cell death. Alternatively, if this is not the case and the  $L^3Bu^i$  complex does not exert its toxicity through DNA binding, the ligand must somehow be playing a part in the increased toxicity from its  $L^1Bu^i$  analogue. From the crystal structure, the coordination geometry of the metal has slight differences between the two structures. The  $L^1Bu^i$  complex favours the distorted square based pyramid whereas the  $L^3Bu^i$  complex prefers the distorted trigonal bipyramidal geometry, however this slight difference will have little consequence on the toxicity seeing as though  $[CuCl_2L^1Bu^i]$  is a rare case of distorted square based pyramid, since the majority of the  $[CuCl_2(L^1R)]$  complexes exhibit the distorted trigonal

bipyramidal geometry, and moreover, these geometries are more likely to be a consequence of crystal packing and could possibly adopt anything in between trigonal bipyramidal and square based pyramidal in solution. Also though both ligands are shown to be terdentate from the crystal structures, the  $[\text{ZnCl}_2(\text{L}^3\text{R})]$  complexes are shown to be tetradentate at room temperature in solution by NMR spectroscopy, (see section 5.2.5). This however is proposed to be an exchange process between the vacant and coordinated Schiff base N atoms, which is too fast to be resolved on the NMR timescale at ambient temperature and so a time averaged spectrum is observed. This fluxionality between the two sites however may have an effect on the metal redox properties and as a consequence the cytotoxicity of the complex.

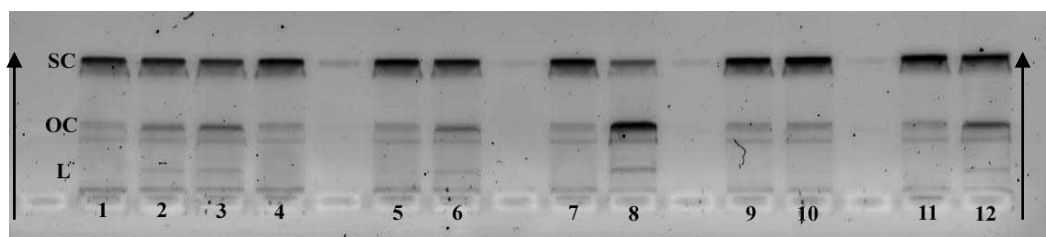
The cLogP's of the ligands are almost identical (see section 1.9, Table 6) and so lipophilicity of the ligand cannot play a part in the enhanced toxicity, however, there is clearly some difference in aqueous solubility between the two class of complex and this could be down to the effect the ligand has on hydrolysis rates at the metal. The majority of the  $\text{L}^1\text{R}$  complexes are readily water soluble and as mentioned earlier the  $\text{L}^3\text{R}$  complexes have very poor aqueous solubility, this gives an indication to the ionic nature of the two complexes (conductivity studies here could have been beneficial). From this crude observation it is possible that hydrolysis of the  $[\text{CuCl}_2(\text{L}^1\text{R})]$  complexes is instantaneous in water to give either of the aqua complexes  $[\text{CuCl}(\text{H}_2\text{O})(\text{L}^1\text{R})]^+$  or  $[\text{Cu}(\text{H}_2\text{O})_2(\text{L}^1\text{R})]^{2+}$  and also the more likely product from here would be  $[\text{Cu}(\text{L}^1\text{R})_2]^{2+}$ , and in contrast the  $[\text{CuCl}_2(\text{L}^3\text{Bu}^i)]$  could remain as the neutral dichloride complex. This likelihood leads to the suggestion that the neutral  $[\text{CuCl}_2(\text{L}^3\text{Bu}^i)]$  complex could have a greater chance of diffusion through the cell membrane where it can then carry out it's mode of action, where it could possibly bind with DNA, or have at least a better chance

of this occurring. Again at this point it would have been very beneficial to have obtained the 1 hour exposures for this compound, to see if this reasoning could be backed up by a more acute chemosensitivity.

## **7.2. DNA Damaging Assay**

After obtaining the chemosensitivity data for the majority of complexes in the compound matrix and proposing some potential mechanistic modes of action. One of the concepts was the potential for the complexes to be involved in redox cycling, which could lead to oxidative stress within the cell. This redox cycling could lead to the production of radicals and in particular the production of hydroxyl radicals in the close proximity to DNA to cause considerable damage. This damage can be monitored by a simple assay involving incubation of the compound under test, with supercoiled plasmid DNA and also  $H_2O_2$  as an oxidant, (or any possible substrates) so redox cycling can occur. After incubation for 1 hour the DNA is then subject to agarose gel electrophoresis to separate different fractions of DNA based on density of the DNA fragments. The gel can identify two types of DNA damage via this method. The highest band in the gel corresponds to undamaged supercoiled (SC) DNA. The second band observed is due to open circular (OC) DNA, which is caused by single strand breaks to the supercoiled plasmid DNA. The third band identifies that OC DNA undergoes breaking of a second strand, (called a double strand break), which gives rise to linear (L) DNA. Obviously the production of L DNA identifies quite significant DNA damage. This procedure can be used as a semi quantitative method by visual observation of the intensity of the bands produced on the gel.

**Figure 82.** DNA damaging assay of supercoiled plasmid DNA. All lanes contain Plasmid DNA. 1, DNA Control; 2, cisplatin; 3, EO9, NQO1, NADH positive control; 4, H<sub>2</sub>O<sub>2</sub> control; 5, [CuCl<sub>2</sub>(L<sup>1</sup>Pr<sup>n</sup>)]; 6, [CuCl<sub>2</sub>(L<sup>1</sup>Pr<sup>n</sup>), H<sub>2</sub>O<sub>2</sub>]; 7, [CoCl<sub>2</sub>(L<sup>1</sup>Cy)]; 8, [CoCl<sub>2</sub>(L<sup>1</sup>Cy)], H<sub>2</sub>O<sub>2</sub>; 9, [ZnCl<sub>2</sub>(L<sup>1</sup>Cy)]; 10, [ZnCl<sub>2</sub>(L<sup>1</sup>Cy)], H<sub>2</sub>O<sub>2</sub>; 11, [CuCl<sub>2</sub>(L<sup>3</sup>Bu<sup>i</sup>)]; 12, [CuCl<sub>2</sub>(L<sup>3</sup>Bu<sup>i</sup>)], H<sub>2</sub>O<sub>2</sub>. SC indicates band for supercoiled DNA; OC indicates band for open circular DNA; L indicates band for linear DNA; arrows indicate direction of mobile phase.



From Figure 82, lanes 1 and 4 identify controls for plasmid DNA alone and plasmid DNA with peroxide respectively. Lane 2 is that of cisplatin, which identifies that cisplatin alone produces significant single strand breaks, it's neighbour in lane 3 is a positive control consisting of EO9, NQO1 and NADH which also shows significant single strand breaks as was intended and some double strand breaks are also observed. All complexes incubated alone with plasmid DNA (lanes 5,7,9 and 11), produced no DNA damage on examination of the gel. However after incubation of the complexes with plasmid DNA in the presence of hydrogen peroxide, revealed DNA damage had occurred in all cases, except for the complex [ZnCl<sub>2</sub>(L<sup>1</sup>Cy)], which produced no DNA damage at all. This result is as expected as Zn<sup>II</sup> has no redox activity. The remaining three compounds [CuCl<sub>2</sub>(L<sup>1</sup>Pr<sup>n</sup>)], [CoCl<sub>2</sub>(L<sup>1</sup>Cy)] and [CuCl<sub>2</sub>(L<sup>3</sup>Bu<sup>i</sup>)] all showed relatively large amounts of single strand breaks and double strand breaks can also be observed. Both the Cu<sup>II</sup> complexes produced single strand breaks of approximately equal magnitude and are comparable to the positive control EO9 and cisplatin. The Co<sup>II</sup> complex however demonstrates greater amounts of single strand breaks due to the very

intense band of OC DNA on the gel and also a much more noticeable loss in intensity for the band of SC DNA. Also this complex provides much more damage than the control and any of the Cu<sup>II</sup> complexes, which is evident from the more intense band for L DNA, which is associated with double strand breaks.

These results show very clearly the impact of these complexes on DNA damage in the presence of an oxidant. Based on a qualitative observation it is clear that the Co<sup>II</sup> complex causes the largest amount of DNA damage, even more than cisplatin and the positive control EO9. The complex [CuCl<sub>2</sub>(L<sup>3</sup>Bu<sup>i</sup>)] seems to show the second highest DNA damage, where single and double strand breaks are clearly exhibited. The intensity of both single and double strand bands of the Cu<sup>II</sup> complex of L<sup>3</sup>Bu<sup>i</sup> also appear to be considerably greater than its L<sup>1</sup>Bu<sup>i</sup> counterpart. This observation fits well the chemosensitivity data and clearly demonstrates the enhancement the phenanthroline moiety can have on the chemistry of the metal.

## 8. Conclusions

This work was aimed at preparing a library of novel Schiff base complexes with subtle structural variations to be screened against a panel of cancer cells in a cytotoxicity assay to obtain structure activity relationships. The synthetic work in this thesis has developed improved methods and routes from the literature and characterisation work has also exposed some of the co-ordination characteristics of these complexes in the solid state and in solution.

From a synthetic point of view this thesis has been very productive and as well as successfully preparing compounds by known literature procedures, several routes and methods from the literature and previous PhD colleagues at the university have been improved to give either higher yields, better purity, or less steps and in some cases all three. The first synthesis to be improved in this thesis was the preparation of the precursor dialdehyde 2,2'-bipyridine-6,6'-dialdehyde P<sup>2</sup>. In the literature and from my predecessors, the final preparation of the dialdehyde often required two steps from 6,6'-dimethyl-2,2'-bipyridine P<sup>2b</sup> isolating the bromomethyl intermediate and oxidising with DMSO. It has been shown in this thesis that the same transformation can be done in one step using a DMSO oxidation of the preformed methyl iodide complex to give the desired dialdehyde in 71% yield. A significant improvement compared to an overall yield of 4% in one Bradford thesis.<sup>193</sup>

A further literature synthesis was developed by applying well known principles of optimising yields by taking advantage of Le Chatelier's principle regarding systems in equilibria. It has been shown how yield and purity improvements can be achieved by

removal of water and using a slight excess of amine in Schiff base ligand syntheses, particularly regarding ligands containing aliphatic tail groups.

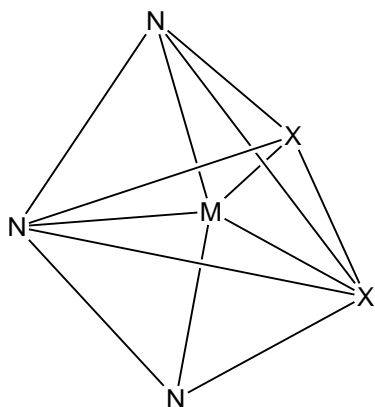
An improved and novel template synthesis of co-ordination complexes of macroacyclic Schiff base ligands has also been demonstrated. The particular class of complex prepared in this thesis is exclusively reported as being prepared via a free ligand approach in the literature, which involves a step preparing and isolating the free Schiff base ligand, followed by further reaction in the second step with a metal salt to generate the Schiff base complex which is again isolated. Although template syntheses are very common, it is the first time that the template methodology has been utilised for this class of macroacyclic complex. A plausible mechanism for this transformation has also been proposed which clearly shows the role of the metal in speeding up the Schiff base reaction and stabilising the product. This reaction is a one pot, one step synthesis with easily isolable and highly pure products. Furthermore the reaction is visually observed as being complete at time of mixing at room temperature. Altogether this approach has afforded 80 novel complexes in moderate to quantitative yield. One particular advantage of this methodology is in the preparation of Schiff base complexes where the aniline precursor is not sufficiently nucleophilic. An example of this is the Schiff base ligand  $L^1\text{PhNO}_2$ , which could not be synthesised as the free ligand, but could be generated as the complex  $[\text{MX}_2(L^1\text{PhNO}_2)]$  via the template approach. This particular methodology could be probed further by testing other poorly nucleophilic amines to see if they too can form the intact complexed ligand. This opens other routes to generate free amines by templating with a metal such as  $\text{Ba}^{\text{II}}$  and reducing the complexed ligand with borohydride for instance.



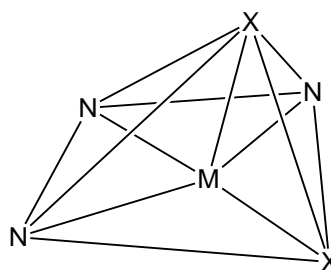
78 Schiff base complexes of late first row transition metal salts  $\text{Co}^{\text{II}}$ ,  $\text{Ni}^{\text{II}}$ ,  $\text{Cu}^{\text{II}}$ ,  $\text{Zn}^{\text{II}}$  and  $\text{Ru}^{\text{III}}$ , with differing anionic co-ordinating and non-co-ordinating counterions were successfully prepared. A comprehensive structural study has been carried out by a variety of techniques in both the solid state and in solution. Of the 78 complexes it was possible to characterise 35 of them by single crystal X-ray diffraction. It has been possible to identify the major co-ordination characteristics of this class of complex and compare the impact of the subtle structural variation.

It was evident and surprising that although the  $\text{L}^2\text{R}$  and  $\text{L}^3\text{R}$  ligands offer four donor atoms, they generally afford tridentate chelates analogous to the three donor  $\text{L}^1\text{R}$  ligand. However in one bipyridine complex  $[\text{Zn}(\text{NO}_3)(\text{H}_2\text{O})(\text{L}^1\text{PhMe})][\text{NO}_3]$ , it seems the anion dictates the denticity, where a four co-ordinate distorted octahedral complex is observed.

The co-ordination geometry typically observed for nearly all complexes (with the exception of  $\text{Ni}^{\text{II}}$  and bis complexes) is five co-ordinate and distorted somewhere between trigonal-bipyramidal or square based pyramidal.



distorted trigonal-bipyramidal



distorted square-pyramidal

Ni<sup>II</sup> complexes on the other hand showed preference for 6 co-ordinate distorted octahedral geometries. An exceptional complex was  $[\mu\text{-Cl}_2\{\text{NiCl}(\text{L}^1\text{Pr}^n)\}_2]$ , where two monomeric complexes formed a dimer through bridging chloro ligands.

Several L<sup>1</sup>R complexes were prepared with different counter ions. From their x-ray structures and vibrational spectroscopy it was possible to characterise the co-ordination modes of the majority of these ligands. One particularly interesting complex was the saline  $[\text{Co}(\text{L}^1\text{Cy})_2][\text{CoNCS}_4]$ , which was intended to be the mono ligated metal with two co-ordinated isothiocyanato anions. The x-ray crystal structure of this complex identified the bis ligated cation and a tightly bound tetra-isothiocyanato cobaltate spectator. The symmetry of this anion was also corroborated through the isothiocyanato stretching frequencies present in the infra-red and Raman spectra. Other bis complexes were prepared in this study. Copper(II) complexes generally formed monomeric species unless non-coordinating counter ions were used ( $\text{BF}_4^-$  in this study), where bis complexes were observed as expected from the literature. As for Cobalt(II) complexes, bis ligated complexes were prepared even when relatively good co-ordinating anions were used, namely  $\text{SCN}^-$  and  $\text{NO}_3^-$ . In all bis ligated complexes the cations were isostructural exhibiting a 6-co-ordinate octahedral co-ordination geometry, with counter ions as spectators.

The solution chemistry of both the diamagnetic and some paramagnetic complexes in this thesis were also studied by NMR spectroscopy. Several paramagnetic cobalt complexes of ligands L<sup>1</sup>R gave rise to isotropically shifted resonances which appeared as broad singlets. These signals were plausibly assigned on the basis of peak areas, proximity to the metal centre and comparison with spectra of similar paramagnetic

structures. Copper however only gave rise to tail group signals, these were only observed when the tails were aliphatic and their resonances retained the characteristics of diamagnetic signals. Zinc complexes were simple to characterise as these were all diamagnetic and gave ligand signals analogous to free ligand. Through NMR it became apparent that in all cases the metal and Schiff base ligand remain intact when in solution, showing  $C_2$  symmetric spectra in all cases. However it is possible that the co-ordinated anions attached to the metal are substituted with solvent molecules or at least exchanging. It is highly likely that in  $D_2O$  these complexes become aquated upon dissolution, becoming ionic which gives rise to their good aqueous solubility.

All transition metal complexes Ni, Co and Cu are paramagnetic as identified by the Evans NMR magnetic susceptibility experiments. Based on the magnetic moments and anion counts from crystal structures and based on CHN data, all metals retained the +2 oxidation state. Both  $Ni^{II}$  and  $Co^{II}$  complexes give rise to high spin magnetic moments which are slightly departed from spin only values, these values do not change with the varying ligands used within this study. Magnetic susceptibility could also be used as a tool to infer the co-ordination geometry about  $Co^{II}$ . When  $Co^{II}$  complexes of  $L^1R$  ligands contained co-ordinating anions, it was most likely that the metal centre had a co-ordination number of 5. Since the spin state of the  $Co^{II}$  centre was high spin it could be inferred that the geometry is close to trigonal bipyramidal.  $Cu^{II}$  on the other hand cannot permutate spin states and hence a magnetic moment for one unpaired electron is observed which is close to the spin only value and confirms  $Cu^{II}$  since  $Cu^I$  is diamagnetic.

Complexes of ligands  $L^2R$  and  $L^3R$  also exhibited NMR spectra of  $C_2$  symmetric complexes, indicative of symmetrical tetradentate chelates. However this was contradictory to their x-ray crystal structures, where they exhibited unsymmetrical terdentate complexes. Variable temperature NMR experiments down to  $-65^\circ\text{C}$  could not resolve any plausible fast exchange at room temperature, indicating a symmetrical coordination mode in the NMR solvent employed or an extremely low energy barrier to interconversion.

The second part of this thesis concentrated on the evaluation of these complexes as potential new anti-cancer metallopharmaceuticals. This was carried out by screening the generated complex library against a panel of cancer cell lines, firstly to obtain the cytotoxic potency of these complexes against a leading standard cytostatic, cisplatin. Secondly versus each other to form structure activity relationships and thirdly to identify if the complexes act in a similar manner to cisplatin by comparing cell line selectivities of the test compounds versus cisplatin.

The above aims were successfully achieved in this study, and a comprehensive screen of the  $L^1R$  complexes was obtained. However  $L^2R$  and  $L^3R$  complexes which suffered from poor aqueous and even DMSO solubility, did not provide the same comprehensive screen. Despite this the most promising candidate came from the  $L^3R$  series and a few promising candidates have emerged as potential leads requiring further study and development from the  $L^1R$  series.

Cytostatic figures for the complexes under test were obtained utilising the MTT assay. It was discovered that the ligand is indeed essential for activity of the metal salts against

the panel of cell lines and it was largely discovered that the variation in 'tail group' and anionic coordinating ligands played little role in providing a dramatic variation in activity of the metal salt. In general all L<sup>1</sup>R complexes displayed moderate cytotoxicity showing a trend in activity with respect to the metal in the order Ru<sup>III</sup>≈Co<sup>II</sup>>Cu<sup>II</sup>≈Zn<sup>II</sup>>Ni<sup>II</sup>, over a 6 day exposure to the three cell panel. Ru<sup>III</sup> was shown to be the most potent metal of the L<sup>1</sup>R series providing IC<sub>50</sub> values of 4.6 (0.7) and 7.5 (1.2) μM against the DLD-1 and H460 cell lines respectively, which is *Ca.* 4.6 and 15 times less potent than cisplatin to the same cell panel respectively. Ru<sup>III</sup> was discovered to be the only metal to provide an IC<sub>50</sub> value from a 1 hour exposure to the DLD-1 cell panel. The value of 20.4 (3.5) μM is a moderate figure but again *Ca.* 10 fold less potent than cisplatin for the same test.

The L<sup>2</sup>R and L<sup>3</sup>R complexes could not be screened by the same comprehension due to their low solubilities. However the lone screen that was possible from the very sparingly soluble complex [CuCl<sub>2</sub>(L<sup>3</sup>Bu<sup>i</sup>)] gave the most exciting result and most potent complex of this thesis. After a 6 day exposure, [CuCl<sub>2</sub>(L<sup>3</sup>Bu<sup>i</sup>)] gave IC<sub>50</sub> values of 4.3 (0.1) and 2.9 (0.1) μM against the DLD-1 and H460 cell lines respectively. These values are merely 4 and 6 fold more than Cisplatin to the same cell lines respectively and demonstrate the potential of this class of complex as cytostatic agents. It would be worth pursuing the phenanthroline complexes based on this discovery and more water soluble alternatives would be a good way forward. This could be achieved by trying different copper salts. Alternatively the ligand itself could be modified to be more polar and hence water soluble. An example of this could be condensation of the dialdehyde with the aniline sulphonate. It would also be worth quickly screening one complex of each of the metals Co<sup>II</sup>, Ru<sup>III</sup>, Ni<sup>II</sup> and Zn<sup>II</sup> to check if the same activity order as L<sup>1</sup>R

complexes is observed in  $L^3R$  complexes. Since  $L^3R$  complexes provided better activity than  $L^1R$  complexes, it would also be beneficial to prepare a few water soluble complexes of  $L^2R$  ligands to see if any enhanced potency is observed.

Further studies utilising a semi-quantitative DNA damaging assay, demonstrated that all first row complexes can damage DNA when in the presence of hydrogen peroxide, with the exception of  $Zn^{II}$  complexes.  $Co^{II}$  appeared to afford the greatest DNA damage with the most intense bands for double strand breaks. The  $Cu^{II}$  complex of the ligand  $L^3Bu^i$  also demonstrated a greater DNA damage as opposed to its  $L^1Bu^i$  analogue. This along with observations that co-ordinatively saturated bis complexes gave rise to similar potency as their mono ligated counterparts does indicate a DNA binding mechanism is not part of the  $L^1R$  complexes mode of action. This is also given some support by the observation of opposite cell line selectivity for  $L^1R$  complexes to that of cisplatin.

The observation that these complexes can operate via a redox pathway (exception of Zinc) does give hope to their moderate potencies, since this may not be a negative result. Indeed cisplatin is an exceptional anti-cancer metallopharmaceutical; however some drawbacks of cisplatin are related to its cytostatic potency and lack of selectivity for cancer and normal cells which leads to severe side effects during treatment. An area of opportunity of this class of redox active complex may be in their lack of potency in oxygenated cellular environments. It may be that in a reductive environment, i.e. in hypoxic tissue (relatively specific to areas of cancerous tissue), these complexes could become activated upon reduction, to give more potent species.

## 9. Further Work

It would therefore be worth identifying if potency of one  $L^1R$ ,  $L^2R$  and  $L^3R$  complex of each metal, (except Zinc) is enhanced in an anaerobic MTT assay or an assay utilising cellular spheroids which mimic hypoxic tissue.<sup>194</sup>

Clearly when progressing or carrying out further studies of these complexes any alterations to tail groups should avoid many subtle variations as was used in this study, but less and more dramatic changes should be tried instead. If any future work based on these complexes progresses, and further structure activity relationships are sought, it may be worth generating ligands with substituted head groups, since it was the difference in these substituents which provided the greatest difference in activity of the complexes.

Some experiments which were not carried out in this study due to either time, or hindsight after writing up this thesis would have been the following:

- To screen one complex of each ligand and metal against a cisplatin resistant cell line to identify if any complexes can overcome the resistance problem of cisplatin.
- To measure the 1 hour exposure MTT assay for the complex  $[CuCl_2(L^3Bu^i)]$  to identify its acute potency
- To measure DNA binding affinities for one complex of each ligand and metal and compare to cisplatin to identify if DNA binding could be a plausible mode of action for these complexes.

## 10. References

1. D. Hanahan and R. A. Weinberg, *Cell*, 2000, **100**, 57-70.
2. R. Cotran, V. Kumar and T. Collins, *Robbins Pathologic Basis of Disease*, Sixth edn., W.B. Saunders 1999.
3. F. A. Tavassoli, *Nature Clinical Practice. Oncology* 2005, **2**, 116-117.
4. C. A. Klein, *Science*, 2008, **321**, 1785–1787.
5. K. Alberts, A. Johnson, J. Lewis, M. Raff and P. Walter, *Molecular Biology of the Cell*, Fifth edn., Garland Science, 2008.
6. H. Kitano, *Nature Reviews Cancer* 2004, 227-235.
7. J. H. M. Schellens, H. L. McLeod and D. R. Newell, *Cancer Clinical Pharmacology* Oxford University Press, 2005.
8. G. L. Patrick, *An Introduction to Medicinal Chemistry*, Third edn., Oxford University Press, 2005.
9. *Report on Carcinogens*, Eleventh edn., U.S. Department of Health and Human Services, Public Health Service, National Toxicology Program, 2011.
10. R. J. B. King, *Cancer Biology*, Essex:Pearson Education Limited, 2000.
11. I.A.R.C, *Monographs*, 2010.
12. P. A. Cerutti, *Science*, 1985, 375-381.
13. A. Meister, *The Journal of Biological Chemistry*, 1994, **269**, 9397-93400.
14. D. Maxwell Parkin, F. Bray, J. Ferlay and P. Pisani, *International Journal of Cancer*, 2001, **94**, 153-156.
15. *Cancer Registration Statistics*, 2006, **MB1 No 37**.
16. F. D. Gilliland and J. M. Samet, *Cancer Survey*, 1994, **19**, 175-195.
17. I. F. Tannock and R. P. Hill, *The Basic Science of Oncology* Third edn., McGraw-Hill Professional, 1998.



18. G. D. Hall, P. M. Patel and A. S. Protheroe, *Key topics in oncology*, BIOS Scientific, Oxford, 1998.
19. J. W. Hadden, *International Journal of Immunopharmacology*, 1999, **21**, 1-14.
20. R. Ruger, *Onkologie*, 1999, **22**, 11-16.
21. P. J. Blower, *Annual Reports on Progression in Chemistry Section A*, 2001, **97**, 587-603.
22. C. S. Allardyce, A. Dorcier, C. Scolaro and P. J. Dyson, *Applied Organometallic Chemistry*, 2005, **19**, 1-10.
23. Z. Guo and P. J. Sadler, *Angew. Chem. Int. Ed.*, 1999, **38**, 1512-1531.
24. R. L. Huang, A. Wallqvist and D. G. Covell, *Biochem. Pharmacol.*, 2005, **69**, 1009-1039.
25. L. K. Johnson, C. M. Killian and M. Brookhart, *J. Am. Chem. Soc.*, 1995, **117**, 6414.
26. T. Brook, University of Bradford, 2003.
27. M. J. Cleare, P. C. Hydes, D. R. Hepburn and B. Malerbi, *Cisplatin: Current Status and New Developments*, Academic, New York, 1980.
28. P. Kopfmaier and H. Kopf, *Chemical Reviews*, 1987, **87**, 1137-1152.
29. S. Giraldi, G. Sava, G. Bertoli, G. Mestroni and G. Zaasinovich, *Cancer Research*, 1977, **37**, 2662.
30. A. C. G. Hotze, A. H. Velders, F. Ugozzoli, M. Biagini-Cingi, A. M. Manotti-Lanfredi, J. G. Haasnoot and J. Reedijk, *Inorg. Chem.*, 2000, **39**, 3838.
31. R. H. Adamson, G. P. Canellos and S. M. Sieber, *Cancer Chemotherapy Reports. Part I*, 1975, **59**, 599.
32. P. S. Schein, M. Slavic, T. Smythe, D. Hoth, F. Smith, J. S. MacDonald and P. V. Wooley, *Cancer Treatment Reports*, 1980, **64**, 1051.

33. A. J. Crowe, P. J. Smith and G. Atassi, *Chemical Biology Interactions*, 1980, **32**, 171.
34. C. V. Christodoulou, A. G. Elipoulos, L. S. Young, L. Hodgkins, D. R. Ferry and D. J. Kerr, *Br. J. Cancer*, 1998, **77**, 2088-2097.
35. H. Sun, H. Li, R. A. Weir and P. J. Sadler, *Angewante Chemie*, 1998, **37**, 1577-1579.
36. L. Y. Kuo, A. H. Liu and T. J. Marks, *Met. Ion. Biol. Syst*, 1996, **33**, 53-85.
37. B. K. Keppler, C. Friesen, H. G. Moritz, H. Vongerichten and E. Vogel, *Struct. Bonding*, 1991, **78**, 97-127.
38. T. Pieper, K. Borsky and B. K. Keppler, *Top. Biol. Inorg. Chem*, 1999, 99-116.
39. P. Kopf-Maier and H. Kopf, *Chem. Rev.*, 1987, **87**, 1137-1152.
40. S. P. Binks and M. Dobrota, *Biochemical Pharmacology*, 1990, **40**, 1329-1336.
41. S. C. Mann, P. A. Andrews and S. B. Howell, *Cancer Chemotherapy and Pharmacology*, 1990, **25**, 236-240.
42. P. A. Andrews, H. H. Huynh, S. C. Mann and E. B. Lee, *Proceedings of the American Association for Cancer Research*, 1988, **29**, 337-337.
43. D. P. Gately and S. B. Howell, *British Journal of Cancer*, 1993, **67**, 1171-1176.
44. R. E. Weiner, *Nucl. Med. Biol.*, 1996, **23**, 745-751.
45. J. H. Lundberg and C. R. Chitambar, *Cancer Research*, 1990, **50**, 6466-6470.
46. M. J. Clarke and M. Stubbs, *Met. Ion. Biol. Syst*, 1996, **32**, 727-780.
47. S. C. Srivastava, P. Richads, G. E. Meinken, S. M. Larson and Z. Grunbaum, *Radiopharmaceuticals*, Grune & Stratton, Inc., New York, 1981.
48. S. C. Srivastava, L. F. Mausner and M. J. Clarke, *Ruthenium and Other Non-Platinum Metal Complexes in Cancer Chemotherapy*, Springer-Verlag, Heidelberg, 1989.

49. F. Kratz, B. K. Keppler, L. Messori, C. Smith and E. N. Baker, *Met.-Based Drugs*, 1994, **1**, 169-173.
50. S. J. Lippard and C. A. Lepre, *Nucleic Acids and Molecular Biology*, Springer, Heidelberg, 1990.
51. M. J. Clarke, *Coordination Chemistry Reviews*, 2002, **232**, 69-93.
52. M. J. Clarke, S. Bitler, D. Rennert, M. Buchbinder and A. D. J. Kelman, *Inorg Biochem.*, 1980, **12**, 79-87.
53. M. J. Clarke, S. Bitler, D. Rennert, M. Buchbinder and A. D. J. Kelman, *Inorg. Biochem.*, 1980, **12**, 79-87.
54. D. Frasca, J. Ciampa, J. Emerson, R. S. Umans and M. J. Clarke, *J. Met.-Based Drugs*, 1996, **3**.
55. M. B. Rossi, O. E. Piro, E. E. Castellano, P. Alborés and L. M. Baraldo, *Inorg Chem.*, 2008, **47**, 2416-2417.
56. K. Wang, J. Lu and R. Li, *Coord. Chem. Rev.*, 1996, **151**, 53-88.
57. G. Speelmans, W. Sips, R. J. H. Grisel, R. Staffhorst, A. M. J. FichtingerSchepman, J. Reedijk and B. deKruijff, *Biochimica Et Biophysica Acta-Biomembranes*, 1996, **1283**, 60-66.
58. G. Speelmans, R. Staffhorst, K. Versluis, J. Reedijk and B. deKruijff, *Biochemistry*, 1997, **36**, 10545-10550.
59. P. Kopemaier and S. K. Muhlhausen, *Chemico-Biological Interactions*, 1992, **82**, 295-316.
60. H. Zeng, B. Wang, Y. Zhang and K. Wang, *Thermochim. Acta.*, 1995, **265**, 31-38.
61. J. Reedijk, *Chem. Rev.*, 1999, **99**, 2499-2510.
62. R. A. Hromas, J. A. North and C. P. Burns, *Cancer. Lett.*, 1987, **36**, 197-201.

63. J. C. Xuan and I. T. Weber, *Nucleic Acids Res*, 1992, **20**, 5457-5464.
64. J. K. Barton and S. J. Lippard, *Nucleic Acid-Metal Ion Interactions*, Wiley, New York, 1980.
65. H. S. Sheih, H. M. Berman, M. Dabrow and S. Neidle, *Nucleic Acids Research*, 1980, **8**, 85.
66. P. Horacek and J. Drobnik, *Biochim. Biophys. Acta*, 1971, **254**, 341.
67. M. Howe-Grant, K. C. Wu, W. R. Bauer and S. J. Lippard, *Biochemistry*, 1976, **15**, 4339.
68. J.-L. Butour and J.-P. Macquet, *Eur. J. Biochem.*, 1977, **78**, 455.
69. R. N. Bose, R. D. Cornelius and R. E. Viola, *Journal of the American Chemical Society*, 1986, **108**, 4403-4408.
70. M. D. Reily and L. G. Marzilli, *Journal of the American Chemical Society*, 1986, **108**, 8299-8300.
71. F. R. Hartley, *The Chemistry of Platinum and Palladium*, Wiley, New York, 1973.
72. L. G. Marzilli, T. J. Kistenmacher and G. L. Eichhorn, ed. T. J. Spiro, Wiley, New York, Editon edn., 1980, p. 179.
73. A. T. M. Marcelis and J. Reedijk, *Recueil Des Travaux Chimiques Des Pays-Bas-Journal of the Royal Netherlands Chemical Society*, 1983, **102**, 121-129.
74. S. Mansy, G. Y. H. Chu, R. E. Duncan and R. S. Tobias, *Journal of the American Chemical Society*, 1978, **100**, 607.
75. R. Bonnacorsi, A. Pullman, E. Scrocco and J. Tomasi, *Theor. Chim. Acta.*, 1972, **24**, 51.
76. A. L. Pinto and S. J. Lippard, *Proceedings of the National Academy of Sciences of the United States of America*, 1985, **82**, 4616-4619.

77. B. Rosenberg, S. Mansy and A. J. J. Thomson, *Journal of the American Chemical Society*, 1973, **95**, 1633.
78. J.-P. Macquet and T. Theophanides, *Bioinorg. Chem.*, 1975, **5**, 59.
79. J. Dehand and J. Jordanov, *J. Chem. Soc., Chem. Commun.*, 1976, 598.
80. F. J. Dijt, G. W. Canters, J. H. J. Denhartog, A. T. M. Marcelis and J. Reedijk, *Journal of the American Chemical Society*, 1984, **106**, 3644-3647.
81. H. Basch, M. Krauss, W. J. Stevens and D. Cohen, *Inorganic Chemistry*, 1986, **25**, 684-688.
82. L. A. Zwelling, S. Michaels, H. Schwartz, P. P. Dobson and K. W. Kohn, *Cancer Research*, 1981, **41**, 640-649.
83. P. Brookes and P. D. Lawlwy, *Biochem. J.*, 1961, **80**, 496.
84. A. C. M. Plooy, M. Van Dijk and P. H. M. Lohman, *Cancer Research*, 1984, **44**, 2043.
85. K. V. Shooter, R. Howes, R. K. Merrifield and A. B. Dobbins, *Chem. -Biol. Interact.*, 1972, **5**, 289.
86. A. Eastman, *Biochemistry*, 1985, **24**, 5027-5032.
87. R. B. Ciccarelli, M. J. Solomon, A. Varshavsky and S. J. Lippard, *Biochemistry*, 1985, **24**, 7533-7540.
88. L. L. Munchausen and R. O. Rahn, *Cancer Chemother. Rep., Part 1*, 1975, **59**, 643.
89. L. L. Munchausen and R. O. Rahn, *Biochim. Biophys. Acta*, 1975, **414**, 242.
90. P. J. Stone, A. D. Kelman and F. M. Sinex, *J. Mol. Biol.*, 1976, **104**, 793.
91. J.-P. Macquet and J.-L. Butour, *Biochimie*, 1978, **60**, 901.

92. R. K. Moyzis, J. M. Buckingham, L. S. Cram, M. Dani, L. L. Deaven, M. D. Jones, J. Meyne, R. L. Ratliff and J. R. Wu, *Proceedings of the National Academy of Sciences of the United States of America*, 1988, **85**, 6622-6626.
93. C. M. Counter, *Mutation Research-Reviews in Genetic Toxicology*, 1996, **366**, 45-63.
94. R. C. Allsopp, H. Vaziri, C. Patterson, S. Goldstein, E. V. Younglai, A. B. Futcher, C. W. Greider and C. B. Harley, *Proceedings of the National Academy of Sciences of the United States of America*, 1992, **89**, 10114-10118.
95. N. W. Kim, M. A. Piatyszek, K. R. Prowse, C. B. Harley, M. D. West, P. L. C. Ho, G. M. Coviello, W. E. Wright, S. L. Weinrich and J. W. Shay, *Science*, 1994, **266**, 2011-2015.
96. S. J. Lippard, Q. He and U.-M. Ohndorf, *Biochemistry*, 2000, **39**, 14426-14435.
97. T. W. Hambley, *Journal of the Chemical Society-Dalton Transactions*, 2001, 2711-2718.
98. P. Kopf-Maier, *Antitumour Bis(cyclopentadienyl)metal Complexes*, VCH Verlagsgesellschaft:, Weinheim, 1993.
99. N. Kroger, U. R. Kleeberg, K. Mross, L. Edler and D. K. Hossfeld, *Onkologie*, 2000, **23**, 60-62.
100. P. C. McGowan, O. R. Allen, L. Croll, A. L. Gott and R. J. Knox, *Organometallics*, 2004, **23**.
101. R. J. Knox and P. C. McGowan, *International Patent Application*, 2004, WO 2004/005305.
102. M. Guo, *Biochemistry*, 2000, **39**, 10023-10033.
103. G. Natta, *Makromol. Chem.*, 1957, **24**, 258.

104. C. Botteghi, A. Schionato, M. Rosini and P. Salvadori, *Journal of Molecular Catalysis*, 1990, **63**, 155.
105. C. Botteghi, S. Paganelli, A. Schionato, C. Boga and A. Fava, *Journal of Molecular Catalysis*, 1991, **66**, 7.
106. C. S. Allardyce and P. J. Dyson, *Platinum Metals Review*, 2001, **45**, 62-69.
107. M. C. Rodriguez-Arguelles, M. Belicchi Ferrari, F. Bisceglie, c. Pelizzi, G. Pelosi, S. Pinelli and M. Sassi, *Journal of Inorganic Biochemistry*, 2004, **98**, 313-321.
108. W. Friebolin, G. Schilling, M. Zoller and E. Amtmann, *Journal of Medicinal Chemistry*, 2005, **48**, 7925-7931.
109. C. Marzano, M. Pellei, F. Tisato and C. Santini, *Anticancer Agents Med Chem*, 2009, **9**, 185-211.
110. D. Magda, P. Lecane and Z. Wang, *Cancer Research*, 2008, **68**, 5318-5325.
111. M. Jung, *Arch Pharmazie*, 1997, **330**, 173-176.
112. *US Pat.*, 5,258,403, 1993.
113. I. J. Stratford, *International Journal of Radiology Oncology Biological Physics*, 1992, **22**, 529-532.
114. B. A. Teicher, *Cancer Research*, 1990, **50**, 6971-6975.
115. W. A. Denny, *Br. J. Cancer*, 1996, **74**, 32-38.
116. M. M. El-Naggar, *Cancer Letters*, 1998, **13**, 71-76.
117. I. C. Perrin, *Anti-Cancer Drug Design*, 1999, **14**, 231-241.
118. Cambridgesoft, *ChemDraw Ultra 9.0 Suite*, 2005.
119. A. Vogel, *Textbook of Practical Organic Chemistry*, Fourth edn., Longman Group Limited : London, 1978.

120. H. J. E. Loewenthal, *Guide for the Perplexed Organic Experimentalist*, Heyden London, 1978.
121. R. J. Errington, *Advanced Practical Inorganic and Metalorganic Chemistry* Blacki Academica & Professional: England, 1997.
122. J. Leonard, B. Lygo and G. Procter, *Advanced Practical Organic Chemistry*, CRC Press, 1994.
123. D. F. Evans, *J. Chem. Soc.*, 1959, 2003.
124. D. Jerchel, J. Heider and H. Wagner, *Liebigs. Ann. Chem.*, 1958, **153**, 613.
125. F. Vogtle, R. Hochberg, F. Kochendorfer, P.-M. Windscheif, M. Volkmann and M. Jansen, *Chem. Ber.*, 1990, **123**, 2181.
126. E. Breitmer and T. Rode, *Synthesis*, 1987, 574.
127. G. R. Newkome, G. E. Kiefer, N. Matsumura and W. E. Puckett, *J. Org. Chem*, 1985, **50**, 3807.
128. A. Markovac, C. L. Stevens, A. B. Ash and B. E. Hackley, *J. Org. Chem*, 1970, **35**, 841.
129. M. A. Masood and D. J. Hodgson, 1993, **32**, 4839.
130. A. Angeloff, J.-C. Daran, J. Bernadou and B. Meunier, *Eur. J. Inorg. Chem*, 2000, 1985.
131. F. Lions and K. V. Martin, *J. Am. Chem. Soc.*, 1957, 2733.
132. A. Bashall, D. E. Fenton, A. J. Leong, L. F. Lindoy, M. McPartlin and B. P. Murphy, *J. Chem. Soc.-Dalton Trans.*, 1987, 2543.
133. L. F. Lindoy and D. H. Busch, *Preparative Inorganic Reactions*, Wiley Interscience, New York, 1971.
134. W. Strober, *Current Protocols in Immunology*, Fifth edn., John Wiley & Sons, 2001.



135. T. Mosmann, *Journal of Immunological Methods*, 1983, **65**, 55-63.
136. M. I. Walton, P. J. Smith and P. Workman, *Cancer Communications*, 1991, **3**, 199-206.
137. H. L. Riley, J. F. Morley and N. A. Friend, *J. Chem. Soc.*, 1932, 1875.
138. J. March, *Advanced Organic Chemistry: reactions, mechanisms and structure*, Fourth edn., Wiley-Interscience, New York, 1992.
139. J. Fuhrop and G. Penzlin, *Organic Synthesis: Concepts, Methods, Starting Materials*, Second edn., VCH, Weinheim, 1994.
140. R. J. Fessenden and J. S. Fessenden, *Organic Chemistry*, Brooks/Cole Publishing Company: California, 1994.
141. F. Vogtle, R. Hochberg, F. Kochendorfer, P. M. Windscheif, M. Volkmann and M. Jansen, *Chemische Berichte*, 1990, **123**, 2181-2185.
142. D. H. Williams and I. Flemming, *Spectroscopic Methods in Organic Chemistry*, McGraw-Hill Book Company Europe: London, 1989.
143. T. T. Tsou and J. K. Kochi, *J. Am. Chem. Soc.*, 1979, **101**, 7547-7560.
144. E. C. Constable, A. Edwards, P. Raithby and J. Walker, *Angewante Chemie*, 1993, **32**, 1465.
145. H. Schiff, *Ann. Chim.*, 1864, **131**, 118.
146. P. W. Atkins, *Elements of Physical Chemistry*, Third edn., Oxford University Press, 1993.
147. J. Atherton and K. Carpenter, *Process Development: Physicochemical Concepts* Oxford University Press, 2000.
148. B. G. Cox, *Modern Liquid Phase Kinetics*, Oxford University Press, 1994.
149. Berkeley, *Madonna 8.3.18 for Windows.*, 2007.

150. D. L. Pavia, G. M. Lampman and G. S. Kris, *Introduction to Spectroscopy*, Second edn., Saunders College Publishing, 1996.
151. P. Guerriero, S. Tamburini and P. A. Vigato, *Coordination Chemistry Reviews*, 1995, **139**, 17-243.
152. A. A. Ismaiel, R. M. Baraka and O. S. Nasman, *Polyhedron*, 2001, **20**, 455.
153. L. F. Lindoy, *The Chemistry of Macrocyclic Ligand Complexes*, Cambridge University Press, 1989.
154. M. C. Thompson and D. H. Busch, *J. Am. Chem. Soc.*, 1962, **84**, 3744-3745.
155. E. C. Constable, *Coordination Chemistry of Macrocyclic Compounds*, Oxford University Press, Oxford, 1999.
156. V. C. Gibson, G. J. P. Britovsek, M. Bruce, B. S. Kimberley, P. J. Maddox, S. Mastroianni and S. J. McTavish, *J. Am. Chem. Soc.*, 1999, **121**, 8728-8740.
157. L. Wang, S. Wen-Hua, L. Han, H. Yang, Y. Hu and X. Jin, *Journal of Organometallic Chemistry*, 2002, **658**, 62-70.
158. M. A. Halcrow, J. M. Holland, X. Liu, J. P. Zhao, F. E. Mabbs, C. A. Kilner and M. Thornton-Pett, *J. Chem. Soc.-Dalton Trans.*, 2000, 3316-3324.
159. J. Cabral, M. F. Cabral, M. G. B. Drew, F. S. Esho and S. M. Nelson, *Journal of the Chemical Society-Chemical Communications*, 1982, 1068.
160. J. Cabral, M. F. Cabral, M. G. B. Drew, F. S. Esho and S. M. Nelson, *Journal of the Chemical Society-Chemical Communications*, 1979, 1033.
161. M. G. B. Drew, M. McCann and S. M. Nelson, *J. Chem. Soc.-Dalton Trans.*, 1981, 1869.
162. P. D. Beer, C. G. Crane and M. G. B. Drew, *J. Chem. Soc.-Dalton Trans.*, 1991, 3235.

163. J. D. Bürgi, J. M. Dunitz, J. M. Lehn and G. Wipff, *Tetrahedron*, 1974, **30**, 1563-1572.
164. S. Warren, *Chemistry of the Carbonyl Group: A programmed Approach to Organic Reaction Mechanisms*, Wiley-Blackwell, 1974.
165. K. Nakamoto, *Infrared Spectra of Inorganic and Coordination Compounds*, 1970.
166. D. F. Shriver and P. W. Atkins, *Physical Chemistry*, Third edn., Oxford University Press, 1999.
167. H. L. Schäfer and G. Gliemann, *Basic Principles of Ligand Field Theory*, Wiley Interscience, New York, 1969.
168. D. F. Shriver and P. W. Atkins, *Inorganic Chemistry*, Oxford University Press, 2001.
169. L. Sacconi, *Coord. Chem. Rev.*, 1996, **150**, 243-264.
170. J. Lisowski and J. Mazurek, *Polyhedron*, 2001, **21**, 811-816.
171. G. J. P. Britovsek, V. C. Gibson, S. K. Spitzmesser, K. P. Tellman, A. J. P. White and D. J. Williams, *J. Chem. Soc.-Dalton Trans.*, 2002, 1159-1171.
172. J. Lisowski and J. Mazurek, *Polyhedron*, 1999, **19**, 465-469.
173. E. W. Abel, N. J. Long, K. G. Orrel, A. G. Osborne, H. M. Pain and V. Sik, *Journal of the Chemical Society-Chemical Communications*, 1992, 303.
174. G. M. Sheldrick, *SHELXS97 and SHELXL97*, University of Goettingen., Germany, 1997.
175. L. J. Farrugia, *J. Applied. Cryst*, 1999, **32**, 837-838.
176. L. J. Farrugia, *J. Applied. Cryst*, 1997, **30**, 565.
177. Bruker, *SMART, SAINT and SHELXTL.*, Bruker AXS Inc., Madison, Wisconsin, USA, 2001.

178. A. W. Addison, T. N. Rao, J. Reedijk, J. van Rijn and G. C. Verschoor, *J. Chem. Soc.-Dalton Trans.*, 1984, 1349-1356.
179. A. F. Cameron, D. W. Taylor and H. R. Nutall, *J. Chem. Soc.-Dalton Trans.*, 1972, 1603.
180. A. F. Cameron, D. W. Taylor and H. R. Nutall, *J. Chem. Soc.-Dalton Trans.*, 1972, 1608.
181. A. Kovacs and Z. Varga, *Coordination Chemistry Reviews*, 2006, **250**, 710-727.
182. J.-A. van den Berg and K. R. Seddon, *Crystal Growth Design*, 2003, **3**, 643.
183. C. L. D. Gibb, E. D. Stevens and B. C. J. A. C. S. Gibb, 123, 5849; *Journal of the American Chemical Society*, 2001, **123**, 5849.
184. C. B. Aakeroy, T. A. Evans, K. R. Seddon and I. Palinko, *New Journal of Chemistry*, 1999, 145-152.
185. V. C. Gibson, S. K. Spitzmesser, A. J. P. White and D. J. Williams, *J. Chem. Soc.-Dalton Trans.*, 2003, 2718-2727.
186. A. Bondi, *J. Phys. Chem.* , **68**, 441-451.
187. J. Reedijk and J. Verbiest, *Transition. Met. Chem.*, 1978, **3**, 51-52.
188. J. C. Jansen, H. van Koningsveld, J. A. van Ooijen and J. Reedijk, *Inorg. Chem.*, 1980, **19**, 170-174.
189. G. J. Long and E. O. Schlemper, *Inorg. Chem.*, 1974, **12**.
190. G. A. van Albada, J. J. A. Kolnaar, W. J. J. Smeets, A. L. Spek and J. Reedijk, *Eur. J. Inorg. Chem*, 1998, 1337-1341.
191. R. W. Taft, *J. Am. Chem. Soc.* , 1952, **74**, 2729.
192. L. P. Hammett, *J. Am. Chem. Soc.*, 1937, **59**, 96.
193. T. Munshi, University of Bradford, 2003.

194. R. Bjerkvig, *Spheroid Culture in Cancer Research*, 1st edn., Informa Healthcare, 1991.

## 11. Appendix

### 11.1. Madonna Model for the Simulation of Reaction Profiles

The following models were used to obtain simulated reaction profiles of various Schiff base condensation reactions under various conditions. It was assumed in all cases that the forward rate constants,  $k_{1f}$  and  $k_{2f}$  of both steps was the same and vice versa for the backward rate constants  $k_{1r}$  and  $k_{2r}$ . The rate constants were estimated from a conversion time of 30 minutes (time to see 100% consumption of dialdehyde) and from the 5% residual monoimine observed at the end of reaction. The starting concentration of dialdehyde in all reactions was 74mM and hence rate constants of  $7.5 \text{ M}^{-1} \text{ min}^{-1}$  for  $k_{1f}$  and  $k_{2f}$  and  $0.025 \text{ M}^{-1} \text{ min}^{-1}$  for  $k_{1r}$  and  $k_{2r}$  were used.

#### 11.1.1. Stoichiometric Reaction



METHOD RK4

STARTTIME = 0

STOPTIME=80

DT = 0.002

k1f=7.5

K1r=0.025

k2f=7.5

k2r=0.025

k3=0

$$d/dt(\text{dialdehyde}) = -k_{1f} \cdot \text{dialdehyde} \cdot \text{RNH}_2 + k_{1r} \cdot \text{monoimine} \cdot \text{H}_2\text{O}$$

$$d/dt(\text{monoimine}) = k_{1f} \cdot \text{dialdehyde} \cdot \text{RNH}_2 - k_{1r} \cdot \text{monoimine} \cdot \text{H}_2\text{O} -$$

$$k_{2f} \cdot \text{monoimine} \cdot \text{RNH}_2 + k_{2r} \cdot \text{diimine} \cdot \text{H}_2\text{O}$$

$$d/dt(\text{diimine}) = k_{2f} \cdot \text{monoimine} \cdot \text{RNH}_2 - k_{2r} \cdot \text{diimine} \cdot \text{H}_2\text{O}$$

$$d/dt(\text{H}_2\text{O}) = k_{1f} \cdot \text{dialdehyde} \cdot \text{RNH}_2 - k_{1r} \cdot \text{monoimine} \cdot \text{H}_2\text{O} + k_{2f} \cdot \text{monoimine} \cdot \text{RNH}_2 - k_{2r} \cdot \text{diimine} \cdot \text{H}_2\text{O} - k_3 \cdot \text{H}_2\text{O}$$

$$d/dt(\text{RNH}_2) = -k_{1f} \cdot \text{dialdehyde} \cdot \text{RNH}_2 + k_{1r} \cdot \text{monoimine} \cdot \text{H}_2\text{O} -$$

$$k_{2f} \cdot \text{monoimine} \cdot \text{RNH}_2 + k_{2r} \cdot \text{diimine} \cdot \text{H}_2\text{O}$$

$$\text{init}(\text{dialdehyde}) = 0.074$$

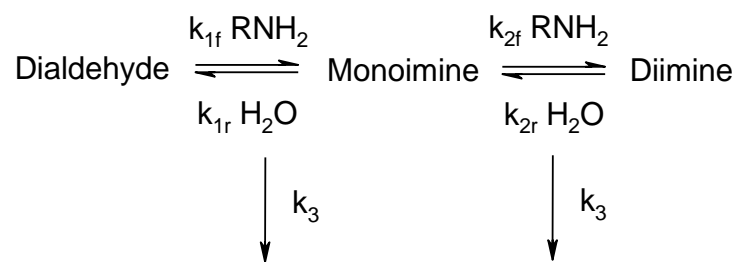
$$\text{init}(\text{monoimine}) = 0$$

$$\text{init}(\text{diimine}) = 0$$

$$\text{init}(\text{RNH}_2) = 0.148$$

$$\text{init}(\text{H}_2\text{O}) = 0$$

### 11.1.2. Stoichiometric Reaction with Simulated Molecular Sieves (Removal of Water)



METHOD RK4

STARTTIME = 0

STOPTIME=80

DT = 0.002

k1f=7.5

K1r=0.025

k2f=7.5

k2r=0.025

k3=100

$d/dt(\text{dialdehyde}) = -k1f \cdot \text{dialdehyde} \cdot \text{RNH}_2 + k1r \cdot \text{monoimine} \cdot \text{H}_2\text{O}$

$d/dt(\text{monoimine}) = k1f \cdot \text{dialdehyde} \cdot \text{RNH}_2 - k1r \cdot \text{monoimine} \cdot \text{H}_2\text{O} -$

$k2f \cdot \text{monoimine} \cdot \text{RNH}_2 + k2r \cdot \text{diimine} \cdot \text{H}_2\text{O}$

$d/dt(\text{diimine}) = k2f \cdot \text{monoimine} \cdot \text{RNH}_2 - k2r \cdot \text{diimine} \cdot \text{H}_2\text{O}$

$d/dt(\text{H}_2\text{O}) = k1f \cdot \text{dialdehyde} \cdot \text{RNH}_2 - k1r \cdot \text{monoimine} \cdot \text{H}_2\text{O} + k2f \cdot \text{monoimine} \cdot \text{RNH}_2 - k2r \cdot \text{diimine} \cdot \text{H}_2\text{O} -$

$k3 \cdot \text{H}_2\text{O}$

$d/dt(\text{RNH}_2) = -k1f \cdot \text{dialdehyde} \cdot \text{RNH}_2 + k1r \cdot \text{monoimine} \cdot \text{H}_2\text{O} -$

$k2f \cdot \text{monoimine} \cdot \text{RNH}_2 + k2r \cdot \text{diimine} \cdot \text{H}_2\text{O}$

init(dialdehyde)=0.074

init(monoimine)=0

init(diimine)=0

init(RNH2)=0.148

init(H2O)=0

### 11.1.3. 0.1eq Excess of Amine and Simulated Water Removal

METHOD RK4

STARTTIME = 0

STOPTIME=80

DT = 0.002

k1f=7.5

K1r=0.025

k2f=7.5

k2r=0.025



$$k_3=100$$

$$d/dt(\text{dialdehyde})=-k_1f*\text{dialdehyde}*\text{RNH}_2+k_1r*\text{monoimine}*\text{H}_2\text{O}$$

$$d/dt(\text{monoimine})=k_1f*\text{dialdehyde}*\text{RNH}_2-k_1r*\text{monoimine}*\text{H}_2\text{O}-$$

$$k_2f*\text{monoimine}*\text{RNH}_2+k_2r*\text{diimine}*\text{H}_2\text{O}$$

$$d/dt(\text{diimine})=k_2f*\text{monoimine}*\text{RNH}_2-k_2r*\text{diimine}*\text{H}_2\text{O}$$

$$d/dt(\text{H}_2\text{O})=k_1f*\text{dialdehyde}*\text{RNH}_2-k_1r*\text{monoimine}*\text{H}_2\text{O}+k_2f*\text{monoimine}*\text{RNH}_2-k_2r*\text{diimine}*\text{H}_2\text{O}-$$

$$k_3*\text{H}_2\text{O}$$

$$d/dt(\text{RNH}_2)=-k_1f*\text{dialdehyde}*\text{RNH}_2+k_1r*\text{monoimine}*\text{H}_2\text{O}-$$

$$k_2f*\text{monoimine}*\text{RNH}_2+k_2r*\text{diimine}*\text{H}_2\text{O}$$

$$\text{init}(\text{dialdehyde})=0.074$$

$$\text{init}(\text{monoimine})=0$$

$$\text{init}(\text{diimine})=0$$

$$\text{init}(\text{RNH}_2)=0.155$$

$$\text{init}(\text{H}_2\text{O})=0$$

11.2. Tables of Bond lengths and Angles for Cu<sup>II</sup> Complexes of Ligand L<sup>1</sup>R.

**Table 44.** Bond lengths for complexes of [CuX<sub>2</sub>(L<sup>1</sup>R)], Symmetry codes: (i) -x+1, -y, z.

N(1)—Cu	1.959 (2)	1.957 (2)	1.9265 (17)	1.9238 (16)	1.982 (4)	1.989 (3)
N(2)—Cu	2.065 (3)	2.088 (3)	2.0829 (17)	2.0905 (17)	2.108 (3)	2.137 (3)
N(3)—Cu	2.085 (3)	2.060 (2)	2.0673 (16)	2.0960 (18)	N(2i)—Cu	N(2i)—Cu
X(1)—Cu	2.3414 (10)	2.4615 (5)	2.2399 (14)	2.2054 (15)	2.3265 (8)	2.3216 (9)
X(2)—Cu	2.2839 (9)	2.4333 (4)	1.9443 (14)	1.9549 (14)	X(1i)—Cu	X(1i)—Cu
C(11)—N(2)	1.267 (4)	1.255 (4)	1.263 (3)	1.270 (2)	1.275 (4)	1.300 (3)
C(17)—N(3)	1.274 (4)	1.272 (3)	1.270 (3)	1.266 (3)	C(11i)—N(2i)	C(11i)—N(2i)

**Table 45.** Bond angles and geometrical parameters for complexes of  $[\text{CuX}_2(\text{L}^1\text{R})]$ , Symmetry codes: (i)  $-x+1, -y, z$ .

	$[\text{CuCl}_2(\text{L}^1\text{Pr}'')]$	$[\text{CuBr}_2(\text{L}^1\text{Pr}'')]$	$[\text{Cu}(\text{NO}_3)_2(\text{L}^1\text{Pr}'')]$ a	$[\text{Cu}(\text{NO}_3)_2(\text{L}^1\text{Pr}'')]$ b	$[\text{CuCl}_2(\text{L}_1\text{PhMe})]$	$[\text{CuCl}_2(\text{L}^1\text{PhCl})]$
N(1)—Cu—N(2)	77.83 (10)	78.02 (10)	79.11 (7)	78.57 (7)	77.75 (8)	77.49 (6)
N(1)—Cu—N(3)	78.01 (11)	78.12 (9)	79.10 (7)	79.19 (7)	77.75 (8)	77.49 (6)
N(2)—Cu—N(3)	155.45 (11)	155.77 (10)	156.84 (7)	157.52 (7)	155.51 (16)	154.97 (12)
N(1)—Cu—X(1)	113.80 (7)	116.18 (7)	103.84 (6)	102.62 (7)	124.73 (3)	124.99 (3)
N(1)—Cu—X(2)	135.69 (7)	131.22 (7)	171.00 (6)	167.05 (6)	124.73 (3)	124.99 (3)
N(2)—Cu—X(1)	92.70 (8)	101.20 (8)	92.21 (6)	86.25 (6)	91.63 (7)	92.63 (7)
N(2)—Cu—X(2)	97.72 (7)	95.90 (8)	99.12 (7)	100.31 (7)	91.63 (7)	92.63 (7)
N(3)—Cu—X(1)	100.98 (9)	93.04 (7)	100.55 (6)	101.83 (7)	91.63 (7)	92.63 (7)
N(3)—Cu—X(2)	96.46 (8)	96.61 (7)	101.17 (7)	100.60 (7)	91.63 (7)	92.63 (7)
X(1)—Cu—X(2)	110.42 (4)	112.497 (18)	85.00 (6)	90.14 (6)	110.53 (5)	110.01 (5)
N(2)—C(11)—C(12)	115.7 (3)	117.3 (3)	117.94 (19)	116.89 (18)	117.1 (3)	117.1 (3)
N(3)—C(17)—C(16)	116.9 (3)	116.2 (2)	117.07 (19)	117.1 (2)	117.1 (3)	117.1 (3)
N(2)—C(11)—C(12)—N(1)	1.6 (4)	5.0 (4)	1.6 (3)	2.8 (3)	0.5 (4)	0.2 (4)
N(3)—C(17)—C(16)—N(1)	4.7 (4)	1.5 (4)	2.6 (3)	2.2 (3)	0.5 (4)	0.2 (4)
$\tau$	0.33	0.41	0.24	0.16	0.51	0.50

### 11.3. Tables of Bond lengths and Angles for Ni<sup>II</sup> Complexes of Ligand L<sup>1</sup>R.

**Table 46.** Bond lengths for Ni<sup>(II)</sup> complexes of L<sup>1</sup>R, Symmetry codes: (i)  $-x+2, -y+2, -z+2$ .

	[Ni(AcO) <sub>2</sub> (L <sup>1</sup> Cy)]	[ $\mu$ -Cl <sub>2</sub> {NiCl(L <sup>1</sup> Pr <sup>n</sup> ) <sub>2</sub> } <sub>2</sub> ]	[NiCl(H <sub>2</sub> O) <sub>2</sub> (L <sup>1</sup> Et)]Cl
N(1)—Ni	1.969 (3)	1.9819 (18)	1.9909 (17)
N(2)—Ni	2.190 (3)	2.1211 (19)	2.175 (4)
N(3)—Ni	2.190 (3)	2.1222 (19)	2.133 (4)
X(1)—Ni	O(51) - 1.961 (3)	Cl(1) - 2.4159 (7)	O(1) - 2.099 (4)
X(2)—Ni	O(41) - 2.111 (3)	Cl(2) - 2.3313 (10)	Cl(1) - 2.3443 (5)
X(3)—Ni	O(42) - 2.110 (3)	Cl(1 <sup>i</sup> ) - 2.5981 (7)	O(2) - 2.097 (4)
C(11)—N(2)	1.265 (4)	1.265 (3)	1.191 (7)
C(17)—N(3)	1.258 (5)	1.268 (3)	1.352 (8)

**Table 47.** Bond angles and geometrical parameters for Ni<sup>II</sup> complexes of L<sup>1</sup>R, Symmetry codes: (i)  $-x+2, -y+2, -z+2$ .

	[Ni(AcO) <sub>2</sub> (L <sup>1</sup> Cy)]	[ $\mu$ -Cl <sub>2</sub> {NiCl(L <sup>1</sup> Pr <sup>n</sup> )} <sub>2</sub> ]	[NiCl(H <sub>2</sub> O) <sub>2</sub> (L <sup>1</sup> Et)]Cl
N(1)—Ni—N(2)	77.16 (11)	77.38 (8)	76.9 (2)
N(1)—Ni—N(3)	76.77 (11)	77.87 (8)	78.0 (2)
N(2)—Ni—N(3)	153.90 (11)	155.17 (8)	154.85 (9)
N(1)—Ni—X(1)	106.23 (12)	93.77 (5)	90.51 (19)
N(1)—Ni—X(2)	97.16 (11)	167.09 (5)	178.99 (19)
N(1)—Ni—X(3)	159.00 (11)	83.61 (5)	91.79 (19)
N(2)—Ni—X(1)	96.27 (12)	87.78 (5)	89.47 (17)
N(2)—Ni—X(2)	91.10 (11)	102.61 (5)	103.81 (15)
N(2)—Ni—X(3)	101.63 (11)	89.63 (5)	91.38 (16)
N(3)—Ni—X(1)	91.96 (13)	91.92 (5)	91.74 (15)
N(3)—Ni—X(2)	91.11 (12)	101.95 (6)	101.33 (13)
N(3)—Ni—X(3)	102.31 (11)	89.54 (5)	88.41 (16)

**Table 48.** Bond angles and geometrical parameters for Ni<sup>II</sup> complexes of L<sup>1</sup>R, continued Symmetry codes: (i)  $-x+2, -y+2, -z+2$ .

	[Ni(AcO) <sub>2</sub> (L <sup>1</sup> Cy)]	[ $\mu$ -Cl <sub>2</sub> {NiCl(L <sup>1</sup> Pr <sup>n</sup> )} <sub>2</sub> ]	[NiCl(H <sub>2</sub> O) <sub>2</sub> (L <sup>1</sup> Et)]Cl
X(1)—Ni—X(2)	156.49 (12)	99.13 (2)	88.80 (9)
X(1)—Ni—X(3)	94.76 (12)	176.66 (2)	177.67 (6)
X(2)—Ni—X(3)	61.83 (10)	89.54 (5)	88.89 (10)
N(2)—C(11)—C(12)	118.4 (3)	117.1 (2)	118.6 (5)
N(3)—C(17)—C(16)	119.0 (3)	118.1 (2)	117.7 (4)
N(2)—C(11)—C(12)—N(1)	4.0 (5)	5.0 (3)	7.1 (8)
N(3)—C(17)—C(16)—N(1)	3.2 (5)	3.3 (3)	3.1 (8)

#### 11.4. Tables of Bond lengths and Angles for Zn<sup>II</sup> Complexes of Ligand L<sup>1</sup>R.

**Table 49.** Bond lengths for complexes of [ZnX<sub>2</sub>(L<sup>1</sup>R)], Symmetry codes (i)  $-x, -y, z$ .

	[Zn(NO <sub>3</sub> ) <sub>2</sub> (L <sup>1</sup> Bu <sup>t</sup> )]	[ZnCl <sub>2</sub> (L <sup>1</sup> Bu <sup>t</sup> )].CH <sub>3</sub> CN	[ZnCl <sub>2</sub> (L <sup>1</sup> Ph)].CH <sub>3</sub> CN	[ZnCl <sub>2</sub> (L <sup>1</sup> PhMe)]	[ZnCl <sub>2</sub> (L <sup>1</sup> PhCl)]
N(1)—Zn	2.0261 (7)	2.0671 (17)	2.058 (4)	2.0499 (12)	2.080 (4)
N(2)—Zn	2.2253 (7)	2.3700 (18)	2.304 (4)	2.3405 (12)	2.324 (3)
N(3)—Zn	2.3488 (7)	2.3522 (17)	2.336 (4)	2.3416 (13)	2.324 (3)
X(1)—Zn	2.0162 (6)	2.2428 (7)	2.2437 (15)	2.2398 (4)	2.2296 (10)
X(2)—Zn	2.0251 (6)	2.2328 (7)	2.2529 (16)	2.2408 (4)	2.2296 (10)
C(11)—N(2)	1.2684 (11)	1.261 (3)	1.271 (6)	1.2750 (19)	1.281 (4)
C(17)—N(3)	1.2716 (11)	1.264 (3)	1.279 (6)	1.2705 (19)	1.281 (4)

**Table 50.** Bond angles and geometrical parameters for complexes of  $[\text{ZnX}_2(\text{L}^1\text{R})]$ , Symmetry codes (i)  $-x, -y, z$ .

	$[\text{Zn}(\text{NO}_3)_2(\text{L}^1\text{Bu}^t)]$	$[\text{ZnCl}_2(\text{L}^1\text{Bu}^t)]$	$[\text{ZnCl}_2(\text{L}^1\text{Ph})].\text{CH}_3\text{CN}$	$[\text{ZnCl}_2(\text{L}^1\text{PhMe})]$	$[\text{ZnCl}_2(\text{L}^1\text{PhCl})]$
N(1)—Zn—N(2)	76.81 (3)	73.58 (7)	74.66 (15)	74.36 (5)	73.99 (8)
N(1)—Zn—N(3)	74.63 (3)	74.15 (6)	74.36 (15)	74.28 (5)	N(1)—Cu—N(2 <sup>i</sup> )
N(2)—Zn—N(3)	151.28 (3)	147.54 (6)	149.01 (15)	148.64 (4)	147.97 (16)
N(1)—Zn—X(1)	138.09 (3)	114.32 (5)	121.68 (13)	120.76 (4)	120.65 (3)
N(1)—Zn—X(2)	130.71 (3)	123.74 (5)	118.78 (12)	120.90 (4)	N(1)—Cu—X(1 <sup>i</sup> )
N(2)—Zn—X(1)	106.85 (3)	96.91 (5)	100.36 (11)	96.77 (3)	94.35 (7)
N(2)—Zn—X(2)	100.90 (3)	98.87 (5)	94.31 (11)	99.18 (3)	101.86 (7)
N(3)—Zn—X(1)	92.55 (3)	99.32 (5)	96.30 (12)	99.05 (3)	N(2 <sup>i</sup> )—Cu—X(1)
N(3)—Zn—X(2)	99.91 (3)	96.08 (5)	99.94 (12)	96.85 (3)	N(2 <sup>i</sup> )—Cu—X(1 <sup>i</sup> )
X(1)—Zn—X(2)	90.37 (3)	121.94 (3)	119.53 (6)	118.340 (18)	118.69 (6)
N(2)—C(11)—C(12)	119.20 (8)	119.20 (19)	119.2 (5)	119.49 (13)	120.2 (3)
N(3)—C(17)—C(16)	119.55 (8)	118.98 (18)	119.4 (5)	119.64 (14)	N(2 <sup>i</sup> )—C(11 <sup>i</sup> )— C(12 <sup>i</sup> )
N(2)—C(11)—C(12)—N(1)	0.63 (12)	0.3 (3)	3.3 (7)	-2.0 (2)	
N(3)—C(17)—C(16)—N(1)	1.74 (13)	0.1 (3)	1.6 (8)	-1.7 (2)	



**11.5. Tables of Bond lengths and Angles for Co<sup>II</sup> Complexes of Ligand L<sup>1</sup>R**

**Table 51.** Bond lengths for Co<sup>II</sup> complexes with bis L<sup>1</sup>R ligands.

	[Co(L <sup>1</sup> Cy) <sub>2</sub> ][BF <sub>4</sub> ] <sub>2</sub> . CH <sub>3</sub> CN. 2H <sub>2</sub> O	[Co(L <sup>1</sup> Cy) <sub>2</sub> ][NO <sub>3</sub> ] <sub>2</sub> . CH <sub>3</sub> CN. 2H <sub>2</sub> O	[Co(L <sup>1</sup> Cy) <sub>2</sub> ] [CoNCS <sub>4</sub> ].CH <sub>3</sub> CN
N(1)—Co	1.968 (2)	1.959 (2)	1.942 (6)
N(2)—Co	2.109 (2)	2.116 (2)	2.233 (7)
N(3)—Co	2.143 (3)	2.154 (4)	2.270 (6)
N(4)—Co	1.9924 (19)	1.991 (2)	1.882 (6)
N(5)—Co	2.198 (2)	2.232 (3)	2.021 (6)
N(6)—Co	2.304 (2)	2.281 (3)	2.010 (6)
C(11)—N(2)	1.278 (4)	1.275 (4)	1.246 (8)
C(17)—N(3)	1.267 (5)	1.258 (5)	1.262 (8)
C(41)—N(5)	1.277 (3)	1.267 (4)	1.269 (9)
C(47)—N(6)	1.268 (3)	1.270 (4)	1.274 (9)

**Table 52.** Bond angles and geometrical parameters for Co<sup>II</sup> complexes with bis L<sup>1</sup>R ligands.

	[Co(L <sup>1</sup> Cy) <sub>2</sub> ][BF <sub>4</sub> ] <sub>2</sub> . CH <sub>3</sub> CN. 2H <sub>2</sub> O	[Co(L <sup>1</sup> Cy) <sub>2</sub> ][NO <sub>3</sub> ] <sub>2</sub> . CH <sub>3</sub> CN. 2H <sub>2</sub> O	[Co(L <sup>1</sup> Cy) <sub>2</sub> ] [CoNCS <sub>4</sub> ].CH <sub>3</sub> CN
N(1)—Co—N(2)	77.99 (9)	76.16 (10)	77.4 (3)
N(1)—Co—N(3)	77.29 (10)	75.87 (10)	75.4 (3)
N(1)—Co—N(4)	179.55 (8)	178.42 (10)	176.3 (3)
N(1)—Co—N(5)	103.75 (8)	102.11 (10)	102.1 (3)
N(1)—Co—N(6)	104.28 (8)	103.19 (11)	98.1 (3)
N(2)—Co—N(3)	155.07 (10)	152.03 (10)	152.8 (2)
N(2)—Co—N(4)	102.32 (9)	105.38 (10)	99.4 (3)
N(2)—Co—N(5)	86.21 (9)	88.51 (10)	87.0 (2)
N(2)—Co—N(6)	97.00 (9)	95.37 (11)	95.1 (2)
N(3)—Co—N(4)	102.42 (10)	102.58 (10)	107.7 (3)
N(3)—Co—N(5)	96.59 (10)	96.81 (9)	99.1 (2)
N(3)—Co—N(6)	92.11 (9)	91.46 (10)	88.3 (2)
N(4)—Co—N(5)	76.62 (8)	77.69 (10)	79.5 (3)
N(4)—Co—N(6)	75.37 (8)	77.08 (11)	80.3 (3)

**Table 53.** Bond angles and geometrical parameters for Co<sup>II</sup> complexes with bis L<sup>1</sup>R ligands continued.

N(5)—Co—N(6)	151.84 (8)	154.60 (11)	159.7 (3)
N(2)—C(11)—C(12)	117.5 (3)	118.3 (3)	117.8 (8)
N(3)—C(17)—C(16)	118.0 (3)	119.5 (3)	119.1 (8)
N(5)—C(41)—C(42)	117.4 (2)	117.5 (3)	117.1 (9)
N(6)—C(47)—C(46)	120.4	120.7	117.5 (8)
N(2)—C(11)—C(12)—N(1)	3.9 (4)	2.4 (4)	3.6 (12)
N(3)—C(17)—C(16)—N(1)	0.4 (4)	0.1 (4)	0.1 (12)
N(5)—C(11)—C(12)—N(4)	5.3 (4)	3.0 (4)	3.6 (11)
N(6)—C(11)—C(12)—N(4)	0.4 (4)	2.0 (5)	2.2 (11)

**Table 54.** Bond lengths for Co<sup>II</sup> complexes [Co(NCS)<sub>4</sub>]<sup>2-</sup> and [CoCl<sub>2</sub>(L<sup>1</sup>PhCl)], Symmetry codes (i)  $-x, -y+1, z$ .

[CoCl <sub>2</sub> (L <sup>1</sup> PhCl)]		[Co(NCS) <sub>4</sub> ] <sup>2-</sup>	
N(1)—Co	2.042 (8)	N(7)—Co	1.967 (8)
N(2)—Co	2.257 (7)	N(8)—Co	1.962 (8)
N(2 <sup>i</sup> )—Co	2.257 (7)	N(9)—Co	1.910 (9)
X(1)—Co	2.266 (2)	N(10)—Co	1.962 (8)
X(1 <sup>i</sup> )—Co	2.266 (2)	C—N	1.136 (10)
C(11)—N(2)	1.290 (9)	C—S	1.637 (10)
C(11 <sup>i</sup> )—N(2 <sup>i</sup> )	1.290 (9)		

**Table 55.** Bond angles and geometrical parameters for Co<sup>II</sup> complexes [Co(NCS)<sub>4</sub>]<sup>2-</sup> and [CoCl<sub>2</sub>(L<sup>1</sup>PhCl)], Symmetry codes (i)  $-x, -y+1, z$ .

[CoCl <sub>2</sub> (L <sup>1</sup> PhCl)]		[Co(NCS) <sub>4</sub> ] <sup>2-</sup>	
N(1)—Co—N(2)	75.03 (16)	N(7)—Co—N(10)	111.4 (3)
N(1)—Co—N(3)	N(1)—Co—N(2 <sup>i</sup> )	N(7)—Co—N(9)	106.8 (3)
N(2)—Co—N(3)	150.1 (3)	N(7)—Co—N(8)	108.0 (3)
N(1)—Co—X(1)	122.06 (6)	N(9)—Co—N(8)	115.8 (3)
N(1)—Co—X(2)	N(1)—Co—X(1 <sup>i</sup> )	N(10)—Co—N(9)	109.6 (3)
N(2)—Co—X(1)	93.43 (18)	N(10)—Co—N(8)	105.2 (3)
N(2)—Co—X(2)	N(2)—Co—X(1 <sup>i</sup> )		
N(3)—Co—X(1)	102.38 (18)		
N(3)—Co—X(2)	N(2 <sup>i</sup> )—Co—X(1 <sup>i</sup> )		
X(1)—Co—X(2)	115.87 (13)		
N(2)—C(11)—C(12)	118.9 (8)		
N(3)—C(17)—C(16)	N(2 <sup>i</sup> )—C(11 <sup>i</sup> )—C(12 <sup>i</sup> )		

### 11.6. Tables of Bond lengths and Angles for Complexes of Ligand L<sup>2</sup>R and L<sup>3</sup>R.

**Table 56.** Bond lengths for complexes of L<sup>2</sup>R and L<sup>3</sup>R.

	[ZnCl <sub>2</sub> (L <sup>2</sup> Cy)]	[Zn(NO <sub>3</sub> )(H <sub>2</sub> O)(L <sup>2</sup> PhMe)] [NO <sub>3</sub> ]	[ZnCl <sub>2</sub> (L <sup>3</sup> PhMe)]. 2DMF	[CuCl <sub>2</sub> (L <sup>3</sup> Bu <sup>i</sup> )].CH <sub>3</sub> CN.H <sub>2</sub> O
N(1)—M	2.259 (9)	2.235 (2)	2.284 (3)	2.0972 (13)
N(2)—M	2.072 (9)	2.1085 (18)	2.053 (3)	1.9641 (12)
N(3)—M	2.325 (9)	2.1215 (19)	2.338 (3)	2.2061 (12)
N(4)—M	-	2.326 (2)	-	-
X(1)—M	2.254 (3)	2.067 (2)	2.2296 (8)	2.4064 (4)
X(2)—M	2.240 (3)	2.0449 (15)	2.2485 (9)	2.2599 (4)
C(11)—N(1)	1.278 (14)	1.288 (3)	1.269 (4)	1.277 (2)
C(21)—N(4)	1.260 (15)	1.283 (3)	1.266 (5)	1.256 (2)

**Table 57.** Bond angles and geometrical parameters for complexes of L<sup>2</sup>R and L<sup>3</sup>R

	[ZnCl <sub>2</sub> (L <sup>2</sup> Cy)]	[Zn(NO <sub>3</sub> )(H <sub>2</sub> O)(L <sup>2</sup> PhMe)] [NO <sub>3</sub> ]	[ZnCl <sub>2</sub> (L <sup>3</sup> PhMe)]. 2DMF	[CuCl <sub>2</sub> (L <sup>3</sup> Bu <sup>i</sup> )].CH <sub>3</sub> CN.H <sub>2</sub> O
N(1)—M—N(2)	75.6 (4)	74.68 (7)	74.85 (10)	77.48 (5)
N(1)—M—N(3)	148.7 (4)	148.89 (7)	149.34 (10)	154.80 (5)
N(1)—M—N(4)	-	138.01 (7)	-	-
N(2)—M—N(3)	73.1 (4)	74.21 (8)	74.49 (11)	77.98 (5)
N(2)—M—N(4)	-	146.96 (8)	-	-
N(3)—M—N(4)	-	73.01 (7)	-	-
N(1)—M—X(1)	100.3 (3)	84.87 (9)	96.82 (7)	100.53 (4)
N(1)—M—X(2)	100.0 (3)	89.81 (7)	100.40 (6)	95.77 (4)
N(2)—M—X(1)	122.9 (3)	95.67 (8)	118.97 (7)	107.62 (4)
N(2)—M—X(2)	119.0 (3)	111.74 (6)	121.13 (7)	144.38 (4)
N(3)—M—X(1)	95.1 (3)	98.39 (8)	98.17 (6)	92.26 (3)
N(3)—M—X(2)	96.6 (2)	101.43 (7)	95.07 (7)	100.83 (3)
N(4)—M—X(1)	-	85.11 (8)	-	-

**Table 58.** Bond angles and geometrical parameters for complexes of L<sup>2</sup>R and L<sup>3</sup>R continued.

	[ZnCl <sub>2</sub> (L <sup>2</sup> Cy)]	[Zn(NO <sub>3</sub> )(H <sub>2</sub> O)(L <sup>2</sup> PhMe)] [NO <sub>3</sub> ]	[ZnCl <sub>2</sub> (L <sup>3</sup> PhMe)]. 2DMF	[CuCl <sub>2</sub> (L <sup>3</sup> Bu <sup>i</sup> )].CH <sub>3</sub> CN.H <sub>2</sub> O
N(4)—M—X(2)	-	79.00 (6)	-	-
X(1)—M—X(2)	117.80 (14)	149.61 (7)	119.85 (4)	107.995 (16)
N(1)—C(11)—C(12)	118.0 (11)	118.0 (2)	117.8 (3)	117.22 (13)
N(4)—C(21)—C(22)	121.7 (12)	117.4 (2)	121.5 (3)	121.38 (15)
N(1)—C(11)—C(12)—N(2)	0.7 (16)	4.0 (3)	3.4 (4)	1.1 (2)
N(3)—C(26)—C(16)—N(2)	0.6 (14)	1.9 (3)	0.9 (4)	1.05 (18)
N(3)—C(22)—C(21)—N(4)	161.3 (12)	1.5 (3)	173.2 (3)	170.70 (15)